RIGA TECHNICAL UNIVERSITY

Oskars Platnieks

BIODEGRADABLE POLYBUTYLENE SUCCINATE WOOD PLASTIC COMPOSITES WITH ENHANCED EXPLOITATION PROPERTIES

Doctoral Thesis

RIGA TECHNICAL UNIVERSITY

Faculty of Materials Science and Applied Chemistry
Institute of Polymer Materials

Oskars Platnieks

Doctoral Student of the Study Programme "Materials Science"

BIODEGRADABLE POLYBUTYLENE SUCCINATE WOOD PLASTIC COMPOSITES WITH ENHANCED EXPLOITATION PROPERTIES

Doctoral Thesis

Scientific supervisors
Professor Dr. sc. ing.
SERGEJS GAIDUKOVS
Professor Ph. D.
VIJAY KUMAR THAKUR

Riga 2022

Investigation, preparation, and testing of the materials was performed in the Institute of Polymer Materials of Riga Technical University.

ACKNOWLEDGEMENTS

Perfection of character is this: to live each day as if it were your last, without frenzy, without apathy, without pretence.
/*Marcus Aurelius*/

DOCTORAL THESIS PROPOSED TO RIGA TECHNICAL UNIVERSITY FOR THE PROMOTION TO THE SCIENTIFIC DEGREE OF DOCTOR OF SCIENCE

To be granted the scientific degree of Doctor of Science (Ph. D.), the present Doctoral Thesis has been submitted for the defence at the open meeting of RTU Promotion Council on September 15, 2022 at 14.30 at the Faculty of Materials Science and Applied Chemistry of Riga Technical University, Paula Valdena iela 3/7, Room 272.

SCIENTIFIC SUPERVISORS

Dr. sc. ing. Uģis Cābulis
Latvian State Institute of Wood Chemistry, Latvia

Professor Dr. Jordi Puiggalí
Universitat Politécnica de Catalunya, Spain

Professor Dr. Hom Dhakal
University of Portsmouth, United Kingdom

DECLARATION OF ACADEMIC INTEGRITY

I hereby declare that the Doctoral Thesis submitted for the review to Riga Technical University for the promotion to the scientific degree of Doctor of Science (Ph. D.) is my own. I confirm that this Doctoral Thesis had not been submitted to any other university for the promotion to a scientific degree.

Oskars Platnieks ……………………………. (signature)
Date: ………………………

The Doctoral Thesis has been written in English. It consists of an Introduction; Literature review; Materials and methods; Results and discussion; Conclusions; 58 figures; 18 tables and the total number of pages is 135. The Bibliography contains 308 titles.

ANNOTATION

Keywords: nanocellulose, biodegradation, sustainable materials, thermal and thermomechanical properties, tensile properties, chemical modification.

Poly(butylene succinate) (PBS) is a bio-based and biodegradable aliphatic polyester with good thermal and mechanical properties comparable to commodity plastics. The addition of cellulose filler reinforces the polymer matrix, thus, increasing mechanical, barrier and biodegradation properties. PBS/cellulose composites are versatile materials with potential applications in packaging, agricultural, automotive, and biomedical fields. The selection of cellulose filler from recycled cellulose to nanocellulose can be used to develop materials for specific applications.

The majority of commercially used commodity plastics are non-biodegradable. Although, production of bio-based plastics and recycling alleviates some of the environmental issues these products still often end up in landfills or nature as permanent pollution. This work uses bio-based PBS and cellulose from renewable circular resources to develop sustainable composite materials. The PBS/cellulose composites must fulfil demanding properties during materials application, while retaining high dimensional stability and mechanical properties. In addition, after the life cycle ends, it is expected that the composite will rapidly designate in the soil. This is achieved using a hydrophobic PBS matrix that offers excellent ductility and rigid cellulose particles with excellent reinforcement capabilities. Cellulose fillers have exceptional morphology that can be tailored by mechanical and chemical processing to a specific size, while surface chemistry can be adjusted with modification methods or compatibilizers. Cellulose is an excellent alternative to inorganic polymer fillers that are unsustainable and often mined in a harmful way to the environment.

The results of the work are presented into four parts:

Part 1 describes the development and investigation of PBS/recycled cellulose composites. The use of recycled cellulose from tetra pak was explored regarding including waste material into circular sustainable economy. Loading with cellulose filler up to 50 wt.% were explored, and tensile, thermomechanical, and thermal properties, including biodegradability and dimensional stability with immersion in water were tested for prepared composites.

Part 2 describes the preparation and comparison of PBS composites with varied nanocellulose and microcellulose filler ratios. The use of freeze-drying process was applied for nanocellulose processing and simplified melt mixing of PBS/nanocellulose composite was proposed. Total filler loading was fixed at 40 wt.% to compare selected fillers extensively. The section demonstrates the advantages of micro-sized filler in the direct melt mixing process.

Part 3 describes the in-depth research and optimization of PBS/nanocellulose composite preparation. The direct solvent casting is used as a reference, while the optimized process with masterbatch is proposed as an alternative. It was discovered that melt mixing significantly improved fillers ability to reinforce polymer's matrix showing much higher tensile and thermomechanical properties.

Part 4 describes the application of various modification, coating, and computerization methods for improving mechanical and thermal properties for PBS/microcellulose composites. Exceptionally high loading 70 wt.% of cellulose was used to achieve high sustainability of composite materials and test selected preparation routes.

The Doctoral Theses has been written in English; it consists of 135 pages, 58 figures, 18 tables and 308 reference sources.

ANOTĀCIJA

Bioloģiski noārdāmi polibutilēna sukcināta koka-plastmasas kompozīti ar uzlabotām ekspluatācijas īpašībām

Atslēgas vārdi: nanoceluloze, biodegradācija, ilgtspējīgi materiāli, termiskās un termomehāniskās īpašības, stiepes īpašības, ķīmiskā modifikācija.

Poli (butilēna sukcināts) (PBS) ir daļēji iegūts no atjaunojamām izejvielām un bioloģiski noārdāms alifātiskais poliesters ar labām termiskām un mehāniskām īpašībām, kuras salīdzināmas ar plaša patēriņa plastmasām. Celulozes pildvielas pievienošana veido polimēra kompozītmateriālu ar labākām mehāniskajām, barjeras un biodegradācijas īpašībām. PBS / celulozes kompozīti ir daudzpusīgi materiāli, kurus iespējams izmantot iepakojuma, lauksaimniecības, automobiļu materiāliem, kā arī biomedicīnas jomā. Pildvielas izvēle no reciklētas celulozes līdz nanocelulozei ietekmē izstrādāto materiālus īpašības un pielietojumu.

Lielākā daļa komerciāli izmantoto plaša patēriņa plastmasas nav bioloģiski noārdāmas. Lai gan plastmasas ražošana no dabas izejvielām un pārstrāde uzlabo ilgtspējīgas attīstības rādītājus, šie produkti joprojām veido pastāvīgu piesārņojumu, bieži, nonāk atkritumu poligonos vai tiek izmesti apkārtējā vidē. Šajā darbā ilgtspējīgu kompozītmateriālu izstrādei ir izmantota PBS plastmasa, kura iegūta izmantojot 50% atjaunojamu izejvielu, bet pildviela celuloze iegūta no atjaunojamiem vai atkritumu resursiem. PBS / celulozes kompozītu ekspluatācijas īpašībām jāspēj uzrādīt augsta mehānisko īpašību stabilitāte neatkarīgi no ārējās vides iedarbības. Turklāt pēc dzīves cikla beigām ir sagaidāms, ka kompozīts augsnē ātri sadalīsies. Tas tiek panākts, kombinējot hidrofobo PBS matricu, kas piedāvā izcilu plastiskumu, un celulozes daļiņas ar lieliskām stiegrojuma spējām. Celulozes pildvielām ir unikāla morfoloģija, ko var pielāgot konkrētam izmēram, veicot mehānisku un ķīmisku apstrādi, savukārt virsmas ķīmisko struktūru var pielāgot ar modifikācijas metodēm vai piedevām. Celuloze ir laba alternatīva neorganiskajām polimēru pildvielām, kuras nav ilgtspējīgas un bieži tiek iegūtas videi kaitīgā veidā.

Darba rezultāti ir izklāstīti četrās daļās:

Pirmajā daļā aprakstīta PBS / reciklētas celulozes kompozītu izstrāde. Tika pētīta atkritumu materiālu iekļautu cirkulārā un ilgtspējīgā ekonomikā. Tika pētīta celulozes iepildīšana līdz 50 wt.% un sagatavotajiem kompozītiem tika pārbaudītas stiepes, termomehāniskās un termiskās īpašības, kā arī bioloģiskā noārdīšanās un stabilitāte, izturot paraugus ūdenī.

Otrajā daļā aprakstīta PBS kompozītu izgatavošana ar dažādām nanocelulozes un mikrocelulozes pildvielu attiecībām. Vienkāršotai PBS / nanocelulozes kompozīta izgatavošanai tika izmantota liofilizēta celuloze un paraugu maisīšana veikta kausējumā. Kopējais pildvielu daudzums bija nemainīgs, lai varētu salīdzināt atlasītās pildvielas. Tika izpētītas mikro izmēra pildvielas priekšrocības tiešā kausēšanas izgatavošanas procesā.

Trešajā daļā aprakstīti padziļināti pētījumi par PBS / nanocelulozes kompozīta sagatavošanu un šī procesa optimizāciju. Paraugu atliešana no šķīduma tika izmantota kā standarts, savukārt kā alternatīva tiek piedāvāts optimizēts process ar koncentrātu. Tika atklāts, ka kausēšanas sajaukšana ievērojami uzlaboja pildvielu spēju stiegrot polimēra matricu, parādot daudz augstākas stiepes un termomehāniskās īpašības.

Ceturtajā daļā aprakstīts dažādu modifikācijas, pārklāšanas un savietošanas metožu pielietojums PBS / mikrocelulozes kompozītu mehānisko un termisko īpašību uzlabošanai. Ļoti augsts pildvielas saturs - 70 wt.% celulozes tika izmantots, lai maksimāli samazinātu polimēra ražošanas ietekmi uz vidi un pārbaudītu izvēlētos sagatavošanas ceļus.

Promocijas darbs ir uzrakstīts angļu valodā, tas sastāv no 135 lappusēm, 58 attēliem, 18 tabulām un 308 informācijas un literatūras avotiem.

TABLE OF CONTENTS

ABBREVIATIONS

AFM	Atomic-Force Microscopy
APTES	3-Aminopropyltriethoxysilane
APTMS	3-Aminopropyltrimethoxysilane
CDI	Carbodiimide
CNC	Cellulose Nanocrystal
DMA	Dynamic Mechanical Analysis
DSC	Differential Scanning Calorimetry
EST	Aliphatic Ester
FTIR	Fourier Transform Infrared Spectroscopy
HDPE	High-Density Polyethylene
LDPE	Low-Density Polyethylene
MAH	Maleic Anhydride
MCC	Microcrystalline Cellulose
NFC	Nanofibrillated Cellulose
PBAT	Poly(Butylene Adipate Terephthalate)
PBS	Poly(Butylene Succinate)
PCL	Polycaprolactone
PE	Polyethylene
PET	Poly(Ethylene Terephthalate)
PHA	Polyhydroxyamide
PHB	Polyhydroxybutyrate
PLA	Poly(Lactic Acid)
PMDI	Polymeric Diphenylmethane Diisocyanate
PP	Polypropylene
rCell	Recycled Cellulose
SEM	Scanning Electron Microscopy
TGA	Thermogravimetric Analysis
wt.%	weight percent
WPC	Wood Plastic Composite

INTRODUCTION

Accumulation of commodity plastics pollution has become a significant challenge of the 21st century. Biodegradable and bio-based polymer materials have been developed to solve sustainability issues and preserve clean unpolluted environment. As these polymers become an inseparable part of the global market, more research is needed to produce composite materials with even higher properties to adapt to increasing demand from consumers. The potential to source plastics from renewable biomass and circular raw resources like forestry and agriculture waste, byproducts and even dedicated crops, has the potential to upset many industries. Some of the most promising applications are wood-plastic composites (WPCs), packaging, automotive, agricultural, and biomedical materials. The addition of cheap cellulose-based materials can lower the cost and improve physical and barrier properties and accelerate biodegradation. Contrary to popular belief, the plastics like poly(butylene succinate) (PBS) do not degrade in normal environment and use scenarios but require immersion in the soil and contact with microorganisms. Thus, the developed materials are up to industry standards and ready for upscaled production.

The development of PBS/cellulose composite materials from sustainable feedstock is demonstrated in the Doctoral Thesis. The use of recycled cellulose, microcellulose, and nanocellulose are explored in in-depth analysis outlining the prospects of every filler. In addition, chemical modification, compatibilization and surface coating methods are investigated. Recycled cellulose shows high potential for cheap and sustainable solutions. Processing the cellulose into nanosized particles shows exceptional properties that can be applied for advanced applications while retaining the biodegradability of PBS. The dynamical mechanical properties show that cellulose reinforcement extends to elevated temperatures, and materials retain the mechanical performance and do not become soft, like neat polymer. The extensive range of studied filler loadings allows to select the optimized performance of the composites.

Within the scope of the Doctoral Thesis, the PBS/nanocellulose composite preparation method was optimized using a highly loaded masterbatch process to reduce the use of organic solvents. Masterbatch process is compatible and scalable with industrial production methods like extrusion and injection moulding. It was concluded that the process is more efficient and yields higher mechanical properties due to to high shear mixing, promoting excellent dispersion.

The biodegradation was extensively studied in composting conditions. All tested samples disintegrated in the soil within 3 months. Calorimetry and infrared spectroscopy confirmed the biodegradation process of the prepared composite materials. The water immersion was studied at room temperature to confirm the excellent dimensional stability of tested samples. While the quality of prepared materials was checked using the fracture surface produced in liquid nitrogen and examined in scanning electron microscopy.

Aim of the Doctoral Thesis

The aim is to develop biodegradable poly(butylene succinate)/cellulose composite materials with enhanced exploitation properties using sustainable resources and technologies.

Tasks of the Doctoral Thesis

1. To obtain woody-like sustainable polymer composite materials from recycled cellulose powder, microcellulose, nanocellulose, and biobased poly(butylene succinate) polymer.
2. To compare microcellulose and nanocellulose composites obtained by solution and melt blending processing technology.
3. To investigate the obtained cellulose composites' tensile, thermomechanical, thermal, and biodegradation properties.
4. To assess different modification and compatibilization methods for cellulose composites.
5. To enhance the exploitation properties of the cellulose composite materials.

Thesis statements to be defended

1. High-loading sustainable PBS/cellulose composites can be prepared by solution, melt, and masterbatch processes.
2. The masterbatch preparation is a more sustainable route for producing PBS/nanocellulose composites compared to the solution and direct melt mixing processes.
3. Chemical modification of the cellulose can significantly enhance the exploitation (thermal, tensile, thermomechanical) properties of PBS composite materials.
4. Biodegradation of PBS/cellulose composites can be controlled by the cellulose type, the chemical modification route, and the cellulose filler content.

Scientific novelty

1. Demonstration of sustainable, biodegradable composites as an alternative to fossil-based plastics for high-performance applications.
2. The proposed chemical modification routes of cellulose can adjust the exploitation properties of the PBS/cellulose composite materials.
3. The solution, melt, and masterbatch processes were developed to produce PBS/cellulose composites.

Practical significance

1. Developed sustainable poly(butylene succinate)/cellulose composite materials can be applied for biodegradable food packaging, cutlery, decks, mulch films, and many

sustainable products to replace fossil non-biodegradable polyolefins and wood-plastic composites.

2. The developed PBS/cellulose masterbatch process and cellulose modification protocols can upscale the production of these composite materials.

3. Paper, cardboard, and agricultural waste can be a sustainable source of cellulose for PBS composite preparation.

Approbation of the PhD Thesis in Scopus and Web of Science indexed articles

Literature review

1. **O. Platnieks**, S. Gaidukovs, V. K. Thakur, A. Barkane, S. Beluns. Bio-based poly (butylene succinate): Recent progress, challenges and future opportunities. European Polymer Journal, 161, (2021), 110855, doi:10.1016/j.eurpolymj.2021.110855.
Chapter 3.1.

2. **O. Platnieks**, A. Barkane, N. Ijudina, G. Gaidukova, V. K. Thakur, S. Gaidukovs. Sustainable tetra pak recycled cellulose / Poly(Butylene succinate) based woody-like composites for a circular economy. Journal of Cleaner Production, 270, (2020), 122321, doi:10.1016/j.jclepro.2020.122321.
Chapter 3.2.

3. **O. Platnieks**, S. Gaidukovs, A. Barkane, A, Sereda, G. Gaidukova, L. Grase, V. K. Thakur, I. Filipova, V. Fridrihsone, M. Skute, M. Laka. Bio-based poly(butylene succinate)/microcrystalline cellulose/nanofibrillated cellulose-based sustainable polymer composites: Thermo-mechanical and biodegradation studies. Polymers, 12(7), (2020), 1472, doi:10.3390/polym12071472.
Chapter 3.3.

4. **O. Platnieks**, A. Sereda, S. Gaidukovs, V. K. Thakur, A. Barkane, G. Gaidukova, I. Filipova, A. Ogurcovs, V. Fridrihsone. Adding value to poly (butylene succinate) and nanofibrillated cellulose-based sustainable nanocomposites by applying masterbatch process. Industrial Crops and Products, 169, (2021), 113669, doi:10.1016/j.indcrop.2021.113669.
Chapter 3.4.

5. **O. Platnieks**, S. Gaidukovs, A. Barkane, G. Gaidukova, L. Grase, V. K. Thakur, I. Filipova, V. Fridrihsone, M. Skute, M. Laka. Highly loaded cellulose/poly (butylene succinate) sustainable composites for woody-like advanced materials application. Molecules, 25(1), (2020), 121, doi:10.3390/molecules25010121.

6. S. Gaidukovs, **O. Platnieks**, G. Gaidukova, G. O. Starkova, A. Barkane, S. Beluns, V. K. Thakur. Understanding the Impact of Microcrystalline Cellulose Modification on Durability and Biodegradation of Highly Loaded Biocomposites for Woody Like Materials Applications. Journal of Polymers and the Environment, 30(4), (2022), 1435–1450, doi:10.1007/s10924-021-02291-3.

Other publications on the topic that are not included in Thesis

1. N. Neibolts, **O. Platnieks**, S. Gaidukovs, A. Barkane, V. K. Thakur, I. Filipova, G. Mihai, Z. Zelca, K. Yamaguchi, M. Enachescud, Needle-free electrospinning of nanofibrillated cellulose and graphene nanoplatelets based sustainable poly (butylene succinate) nanofibers. Materials Today Chemistry 17 (2020) 100301, doi: 10.1016/j.mtchem.2020.100301.

2. **O. Platnieks**, S. Gaidukovs, N. Neibolts, A. Barkane, G. Gaidukova, V. K. Thakur, Poly(butylene succinate) and graphene nanoplatelet–based sustainable functional nanocomposite materials: structure-properties relationship. Materials Today Chemistry 18 (2020) 10035, doi: 10.1016/j.mtchem.2020.100351.

3. G. Gaidukova, **O. Platnieks**, A. Aunins, A. Barkane, C. Ingrao, S. Gaidukovs, Spent coffee waste as a renewable source for the production of sustainable poly(butylene succinate) biocomposites from a circular economy perspective. RSC Advances 11(30) (2021) 18580-18589, doi: 10.1039/D1RA03203H.

Dissemination in international scientific conferences

1. **O. Platnieks**, S. Gaidukovs, N. Ijudina. Use of recycled cellulose filler from Tetra Pak® packaging waste for melt processing by kinetic mixer of polybutylene succinate based composites. *Baltic Polymer Symposium 2018*, Jurmala, Latvia, September 12–14.

2. **O. Platnieks**, S. Gaidukovs, N. Ijudina. Polybutylene Succinate and Recycled Cellulose Filler Composites. *Materials Science and Applied Chemistry, 2018*, Riga, Latvia, October 26.

3. **O. Platnieks**, S. Gaidukovs, V. K. Thakur, I. Filipova. Sustainable Graphene, Nanocellulose and Bio-based Polybutylene Succinate Composites. *Graphene Week, 2018*, Donostia/San Sebastian, Spain, September 10–14.

4. **O. Platnieks**, N. Neibolts, S. Gaidukovs, A. Barkane, V. K. Thakur, I. Filipova, V. Fridrihsone, M. Enachescu, Z. Zelca. Characterization of electrospun nanofibers of poly(butylene succinate) blends with nanofibrillated cellulose. *Baltic Polymer Symposium, 2019*, Vilnius, Lithuania, September 18–20.

5. **O. Platnieks**, A. Barkane, V.K. Thakur, I. Filipova, V. Fridrihsone, S. Gaidukovs. Wood-like biobased and biodegradable polybutylene succinate microcellulose composites. *The Conference on Green Chemistry and Nanotechnologies in Polymeric Materials 2019*, Riga, Latvia, October 9–11.

6. **O. Platnieks**, N. Neibolts, S.Gaidukovs, V. K. Thakur, I. Filipova. Polybutylene Succinate/Cellulose/Graphene Composites. *Materials Science and Applied Chemistry, 2019*, Riga, Latvia, October 24.

7. **O. Platnieks**, S. Gaidukovs. Nanofibrillated cellulose modification methods for potential polymer-based aerogel fabrication. *International Conference on Aerogels for Biomedical and Environmental Applications, 2020*, Santiago de Compostela, Spain, February 18–20.

8. **O. Platnieks**, A. Sereda, S. Gaidukovs. Enhanced dispersion of nanofibrillated cellulose in poly (butylene succinate) matrix via combination of solvent casting and melt blending for functional green nanocomposites. *1st International Greenering conference*, Costa da Caparica, Portugal, February 15–16, 2021.

1. LITERATURE REVIEW

1.1. Polybutylene succinate: Synthesis and Properties

1.1.1. Plastics market

Globally, bio-based plastics production has exceeded 2 million tons, with an expected 3 million tons by 2024 [1]. Overall, they contribute less than 1 % of annual plastic production, exceeding 400 million tons [2]. Around 55 % of bio-based plastics are biodegradable, of which most notable are PLA, PBAT, PBS, PCL, PHA and biodegradable starch blends [1]. PBS commercial production was pioneered by Showa Denko (Japan) under brand name Bionolle[TM] which they produced from 1993 till 2016 when production was stopped by the company, citing delay in permeation of environmental regulations on plastic shopping bags [3]. Mitsubishi Chemical Corporation (Japan) in 2003 started PBS production under the brand name GS Pla™ which was produced from fossil sources, while in 2015 bio-based (50%) PBS commercial production plant was opened in Thailand in partnership with PTT Public Company Limited (Thailand) using brand name BioPBS™ [4,5]. In the last decade, PBS production plants were built in China (Hexing Chemical and Xinfu Pharmaceutical) and Korea (Ire Chemical and SK Polymers) [5,6]. With the introduction of new technologies, the production of fully bio-based PBS is estimated to have at least 15-20% lower impact on the environment compared to petrochemical incumbents when the cradle-to-grave system was examined [7]. Crop potential for PBS production is shown in Figure 1 [1]. Corn stands out with one of the lowest feedstock requirements. At the same time, sugar beet requires relatively low land use and exceptionally low water requirements, followed by sugar cane, which grows in different climate conditions. But wheat out of all crops examined offers the worst yield.
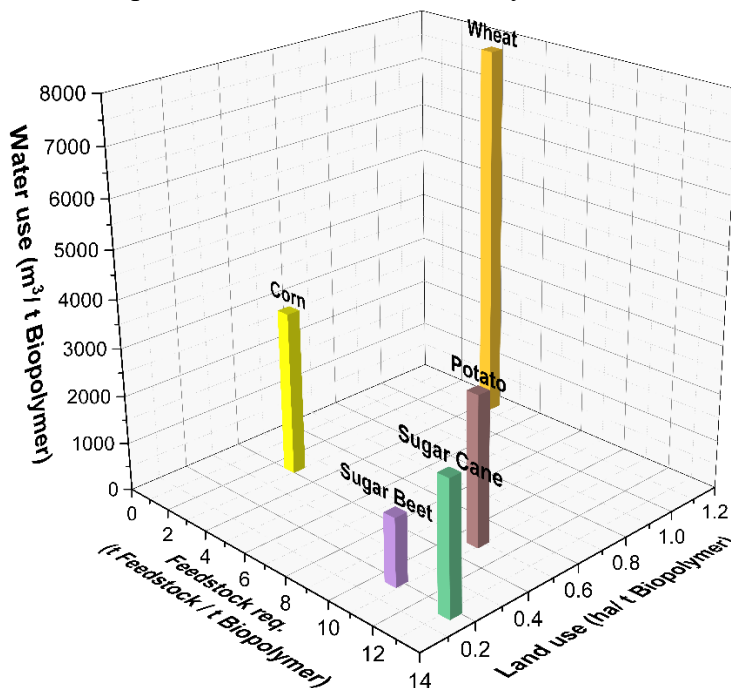

Figure 1.1. Agricultural resource requirements for 100% bio-based PBS production. Original art by author, which uses the data provided in Ref. [1].

1.1.2. Production and synthesis of succinic acid

Succinic acid (butanedioic acid) (SA) is a naturally occurring dicarboxylic acid present in foods and alcoholic beverages and forms a crucial metabolic role in anion form. It is widely considered as one of the main biorefinery building block chemicals [8,9]. Petrochemicals can be processed into SA using various routes like oxidation of butane, benzene, carbonylation of ethylene glycol and catalytic hydrogenation of maleic acid or maleic anhydride [10]. Some of these result in succinic anhydride, which is then converted to SA via hydration. These conventional routes involve harsh conditions, require large amounts of energy and are harmful to the environment. Thus, the biorefinery route has increased with rising yearly production volumes and new factories [11,12]. This has led to PBS producers investing in their succinic acid plants to secure a stable supply. Figure 1.2. shows biosynthesis routes for SA production.

Carbohydrates can be converted into succinic acid using the microbial fermentation route. In general, three main sources are considered commercially viable to produce SA from sugar (sucrose) or starch crops or sugars from lignocellulosic materials, which then can be processed with genetically modified yeasts or bacteria, a chemical process or electrodialysis [13]. Fermentation was reported as possessing the most negligible impact on the environment [13]. Still, there is a significant factor influencing the production, and it is the selection of carbohydrate sources. Escherichia coli, Actinobacillus succigogenes, Anaerobiospirillum succiniciproducens are just a few of the more commonly reported strains genetically modified for SA production [14,15]. The early literature focused on various microorganisms that used glucose as a source. This raised several concerns about the future of SA production regarding price competition with fossil sources and matched with the food industry; thus, new low-cost carbon feedstock sources and synthesis routes were the main focus in the last decade [9]. One of the proposed alternative carbon sources, i.e., glycerol, has been reported as a viable route due to relatively large production as a by-product of biofuels [16].

The global SA production has seen massive growth in the last decade, with around 15 000 metric tons produced annually in 1999 to about 30 000 metric tons in 2010. In 1999 the global SA production was only 15 000 metric tons compared to around 35 000 metric tons estimated in 2011, while a forecast of 500 000 to 700 000 metric tons was expected for 2020 [11,12]. Owning to emerging technologies, several startups and joint ventures started development and built first experimental plants, namely, BioAmber Inc., with an expected production volume of 300 000 metric tons by the end of 2020; Myriant Corp. was developing plants in various plants around the world with an anticipated capacity of 200 000 metric tons and BASF-Purac joint venture with expected 75 000 metric tons capacity and 10 000 metric tons pant by Reverdia [17-19]. Unfortunately, the costs of SA production technology proved to be much higher than expected, and BioAmber was liquidated, while other companies halted or significantly lowered their expected production capacities [12,20]. Yet, demand for SA remains high in various industries transitioning to bio-based sources and compounded annual growth rate (CAGR) of 26% during 2021-2027 has been forecasted [21]. With new advances in bio-SA technology, large-scale production is bound to happen in the near future [15].
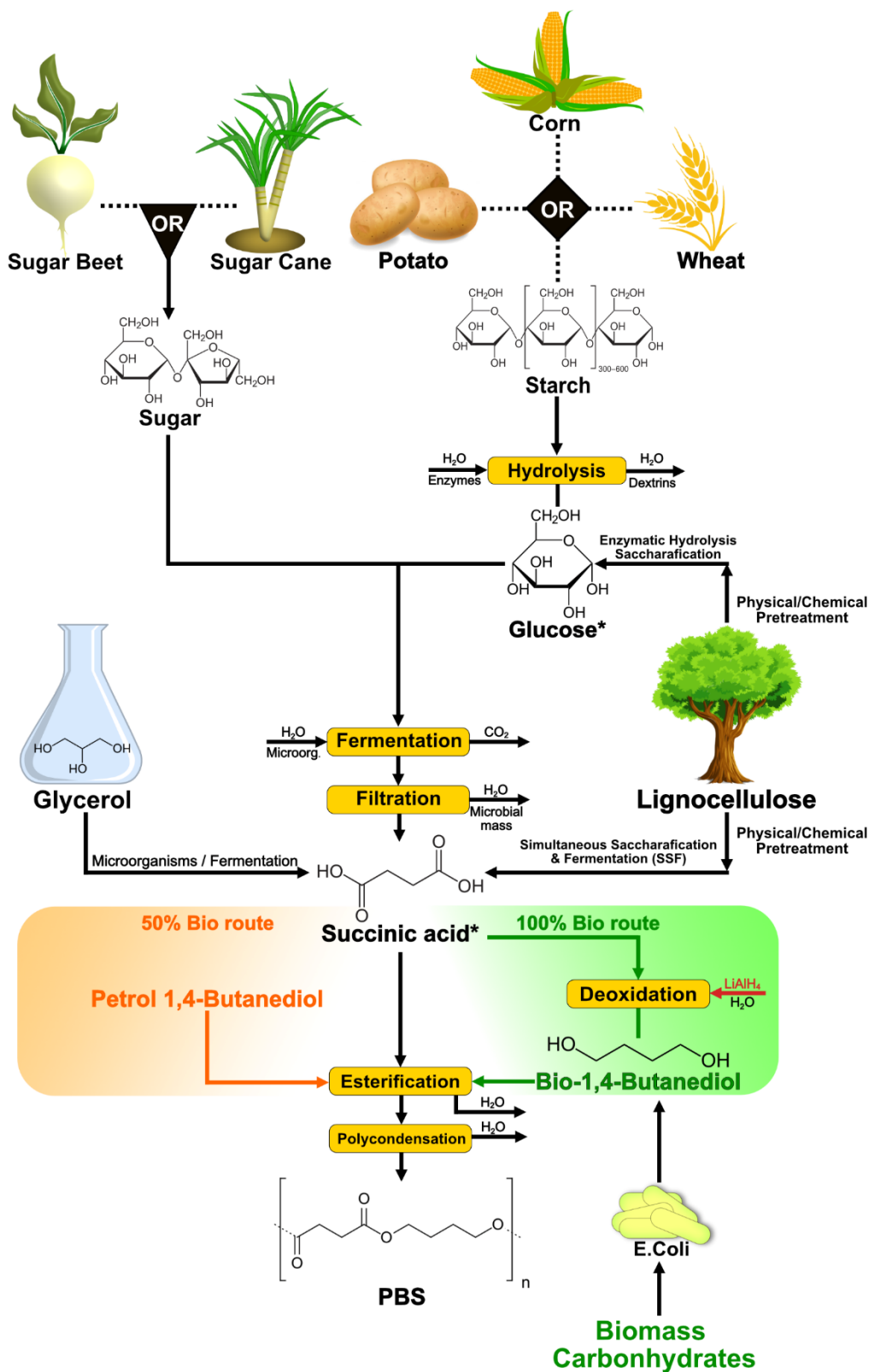
Figure 1.2. PBS production scheme.

1.1.3. Production and synthesis of 1,4-butanediol

1,4-Butanediol (Butane-1,4-diol) (BDO) is a significant volume chemical commonly used in various industries to produce polymers and polymer fibers, i.e., polyurethanes and polyesters.

While other notable products of BDO include γ-butyrolactone and tetrahydrofuran (THF). The global production of BDO is estimated at least 2 million tons and growing, with most of it coming from fossil sources [22]. The BDO can be synthesized by oxidation of butane, isomerization of propylene oxide, hydrogenation of maleic anhydride (Davy process) and reaction between formaldehyde and acetylene (Reppe process) [23]. 1,3-Butadiene acetoxylation technology is a unique procedure used by Mitsubishi that can produce either BDO or THF [24]. The petrochemical route has high energy requirements, which significantly impact the production of greenhouse gases. BDO is not naturally occurring because a new biosynthetic pathway was developed using Escherichia coli [22]. The first direct pathway commercial plant was opened by Novamont in 2016 [25]. Researchers and other large producers have proposed alternative routes of bio-BDO production and involve synthesis from bio-succinic anhydride or bio-SA [26,27].

1.1.4. Synthesis of PBS

The synthesis of PBS polymer is usually achieved with 2 step polycondensation reaction that starts with oligomer formation and is followed by a transesterification reaction of oligomers. The direct polycondensation of PBS is achievable but often leads to lower molecular weight. Some authors have demonstrated direct synthesis that yields high molecular weight PBS. Figure 1.3. shows 2 step polycondensation reaction that yields PBS polymer. The first stage of PBS synthesis is carried out with a molar excess of BDO of about 5 to 15% [10,28]. Alternatives to SA can be used like succinic anhydride [29] and succinic acid esters [30], which would result in the first reaction also being transesterification (not to be confused with the second step).
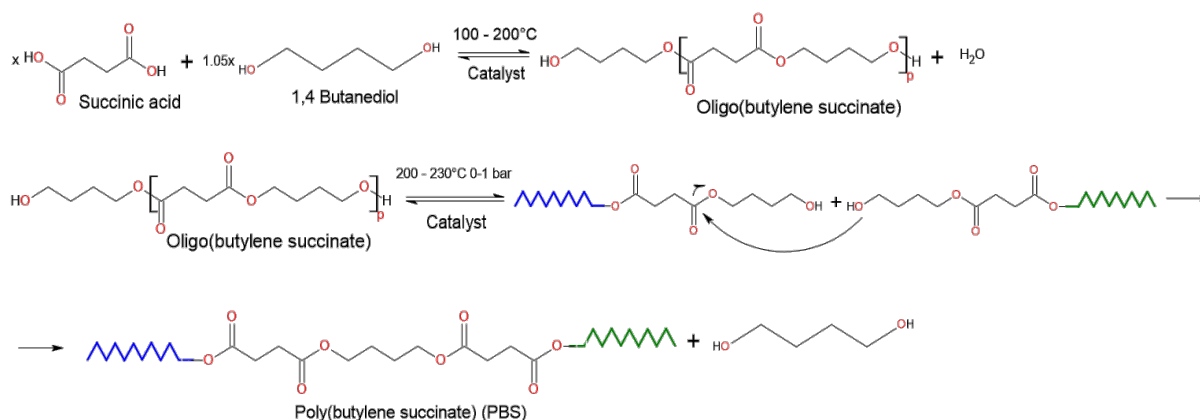
Figure 1.3. Synthesis of PBS.

Jacquel et al. explored a wide variety of metalorganic catalysts, including titanium (IV) n-butoxide (Ti(BuO)$_4$), zirconium (IV) n-butoxide, tin 2-ethylhexanoate, antinomy (III) n-butoxide, hafnium (IV) n-butoxide, bismuth neodecanoate and, in addition, metal oxide catalysts germanium (IV) oxide and antimony (III) oxide (Sb$_2$O) for PBS synthesis [28]. The authors ranked catalysts according to effectivity Ti > Ge > Zr ~ Sn > Hf > Sb > Bi with titanium-based catalysts significantly outperforming others. A unique property of Ti(BuO)$_4$ was observed regarding accelerated aging and degradation of prepared PBS and indicated that zirconium- and germanium-based catalysts produce higher stability polymers. Stannous octoate

(SnOct2), Sb$_2$O and Ti(OBu)$_4$ were compared in the different studies for their catalytic activity and authors found titanium-based catalyst was significantly better [31]. Coinciding with these studies, the use of Ti(OBu)$_4$ (n-butoxide or isopropoxide) is commonly reported in the literature and is regarded as the best metal-based catalyst [32-34]. Very high molecular weight can be achieved up to 2×10^5 g/mol [33,34]. The temperature in the first stage of synthesis is kept lower, usually starting heating slowly till water is removed from the system which is achieved by rising temperature to values between 150 to 200 °C, while in the second stage higher temperature benefits reaction, thus temperatures between 200 to 230 °C are regarded as optimal. The stage separation is imported because water can reduce the activity of metal-based catalysts. While both stages of synthesis are balanced around the boiling point (235 °C) of BDO. Microwave-assisted synthesis has been reported as an effective way to reduce reaction time and energy requirements [35,36].

A different approach to aliphatic polyester synthesis, including, PBS was demonstrated using rare-earth metal triflates [37]. The advantages of this method were milder conditions and reusable catalysts. Enzymatic synthesis of polyesters has been explored as an alternative to the conventional approach using Ti(OBu)$_4$. Candida Antarctica Lipase B (CALB) is used with relatively good yields and has potential manufacturing applications [38-41]. Relatively mild conditions are used due to limited enzymatic activity up to 150 °C. The research that compares CALB and Ti(OBu)$_4$ indicates that organometallic compounds yield lower polydispersity and higher molecular weight, but the authors noted the high potential of CALB [42]. Jiang et al. reported that relatively low temperatures around 80 °C enzymatic syntheses depend highly on solvent selection and other process optimizations [43]. The best results reported with CALB yield molecular weight from 60 000 to 73 000 g/mol with solution polymerization showing better yields than melt polymerization process [39,41,43].

To increase PBS and its copolymer molecular weight and mechanical properties, chain extension have been applied [44-46]. Jin et al. reported chain extension of PBS with the addition of maleic acid during polycondensation step to introduce double bonds for crosslinking reaction [45]. This resulted in very high M$_w$ up to 27.77×10^4, but authors found that biodegradation of these polymers was significantly affected. A study on chain extension of poly(butylene succinate-co-butylene adipate) with hexamethylene diisocyanate reported high molecular weight could be achieved while biodegradation properties are preserved [44]. The authors identified changes in crystalline structure as the main reason for good biodegradation of extended chain copolymer. Zhou et al. proposed using a chain extender with multiple epoxy groups to prepare PBS foams [46]. The authors reported that the molecular weight of PBS increased from 1.94×10^5 to 4.83×10^5 g/mol, and good cell size distribution was achieved.

1.2. Physico-chemical and mechanical properties

PBS has often been compared to PE and presented as a biodegradable alternative. Table 1.1. shows that the properties of PBS are somewhere between LDPE and HDPE. PBS is soft and flexible semi-crystalline polyester with melting temperature around 110 to 115 °C and heat deflection temperature of 95 °C. In comparison, commercial variations with additives or copolymers can be with significantly lower temperatures. The disparity between reported properties comes from confusing PBS copolymers with PBS due to manufacturer marketing and various modifications like chain extension playing a significant role in PBS properties. M_w bellow 1×10^5 g/mol is considered a low-quality polymer which is more brittle while higher molecular weight yields good PBS with excellent properties suitable for extrusion, film blowing and injection molding [10]. Xu et al. reported that PBS reaches suitable properties for film blowing when M_w is around 1.8×10^5 g/mol [10]. It has been reported that PBS melting process includes a recrystallization process observed with differential scanning calorimetry [47,48]. Crystallization occurs between 70 to 90 °C, and glass transition can be observed between -40 to -10 °C depending on manufacturer, processing, and synthesis methods [49-51]. The density is around 1.26 g/cm^3, and while melt flow rate has extensive range depending on additives [49-51]. PBS has exceptionally high thermal stability above 300 °C and, combined with low melting temperature, results in good processing properties [52,53]. As almost no degradation occurs during melt processing, recycling of PBS has been suggested as a viable option [53,54]. Tensile properties are often reported with yield strength and/or tensile strength values in the range of 20 to 60 MPa with elastic modulus around 300 MPa, and elongation (strain at break) can reach up to 560 % [49]. Flexural properties can be changed to measure for PBS owing to the material's soft nature. Manufacturers report the flexural modulus values around 650 MPa and flexural strength around 40 MPa [49-51]. While in literature, much lower flexural values are reported [55,56]. Izod impact strength values range from around 5 to 20 kJ/m^2 [57].

Table 1.1.

Comparison of the properties between PBS [50], LDPE [58], and HDPE [59].

Properties	PBS (FZ71PM)	LDPE (993I)	HDPE (DMDA-8907 NT 7)
Density (g/ cm^3)	1.260	0.923	0.952
MFR (190°C, 2.16 kg)	22	25	7
Melting Point (°C)	115	110	131
Tensile Stress at Break (MPa)	30	12	23
Tensile Strength at Yield (MPa)	40	10	27
Strain at Break (%)	170	40	1100
Flexural Modulus (MPa)	630	317	1069
Heat Deflection Temperature (°C)	95	40	73

Excellent mechanical properties attributed to high molecular weight PBS combined with thermal stability, high heat deflection temperature and good processability suitable with conventional methods have resulted in PBS being seen as a commercial biodegradable alternative to PE and PP. PBS is safe in contact with food which significantly expands applications to the food industry, while high heat deflection enables contact with hot beverages [50]. Higher density of PBS can be seen as a drawback to PBS; lower melting temperature results in reduced energy requirements for material melt-processing. In addition, when PBS is compared to biodegradable polyesters, it shows much higher ductility compared to PLA, PHA, PHB, PHV. Similarly, these polyesters have issues with limited thermal processing temperature range, which is followed by rapid degradation [60,61]. PCL with relatively low melting temperature (around 60 °C) and high price is usually suggested for specific purposes like biomedical applications [62]. Figure 1.4. shows a tensile properties comparison between commodity plastics and various degradable polyesters.
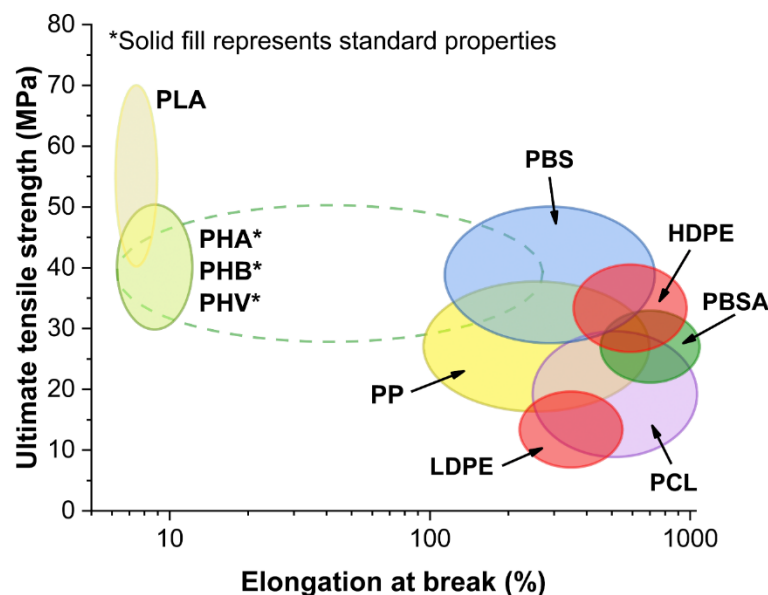
Figure 1.4. Typical tensile properties of various biodegradable polyesters and non-degradable commodity plastics LDPE, HDPE, and PP.

1.3. Crystallization process

PBS is a semicrystalline polymer with a melting temperature in the range of 114 to 116 °C. It has been reported that the equilibrium melting temperature of PBS is in the range of 127.5–146.5 °C [63,64]. The differential scanning calorimetry (DSC) curves of PBS often exhibit two endothermic peaks (Figure 1.5.), which are explained by the recrystallization process [65]. The observations are similar for ongoing isothermal and nonisothermal crystallization [66,67]. The first peak (lower temperature endotherm) is observed at a lower temperature between 90 to 110 °C, while the second peak matches the melting temperature [68]. Qiu et al. reported that two peaks are observed if crystallization temperature (Tc) ≤ 90 °C [68,69]. In addition, the authors

noted that longer crystallization time or slower cooling rate pronounce the first endotherm intensity, while the peak shifts to lower temperatures with higher cooling rates.

Wide-angle X-ray diffraction (WAXD) for PBS yields three characteristic diffraction bands at 19.5°, 21.9° and 22.6° (with variations around ± 0.2° in literature), which are assigned to (020), (021), and (110) planes, correspondingly [70-72]. The (021) plane peak is commonly revealed as a shoulder to (110) plane peak. Some authors have chosen to identify an additional weak plane (111) at around 28.7° [71,73]. The characteristic WAXD patterns are shown in Figure 1.6. The addition of fillers promotes changes in structure and peaks for planes (021) and (110) often merge and change intensities [74,75]. Yoo et al. studied the WAXD characteristic peaks for PBS samples crystallized isothermally at different temperatures and those obtained with cold crystallization and reported only one crystal structure as the characteristic bands did not change from the cooling conditions [64]. Commonly, PBS exhibits a monoclinic α crystal form [76]. Thus, the imperfect lamellae structures can be formed in the crystallization process, and they undergo recrystallization into more perfect lamellae during heating. Recrystallization seems to happen only in the region previously occupied by the originally formed crystals [65]. Reversible transition to monoclinic β crystal form can be achieved by stretching (strain) [77,78].
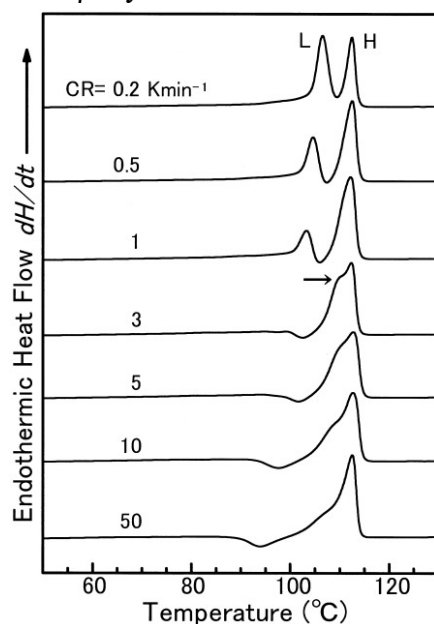
Figure 1.5. DSC curves in the heating process for the melt-crystallized samples with different cooling rates [66]. The heating rate of the DSC scans was 10 K min−1.The symbols show low (L) and high (H) temperature peaks.

24
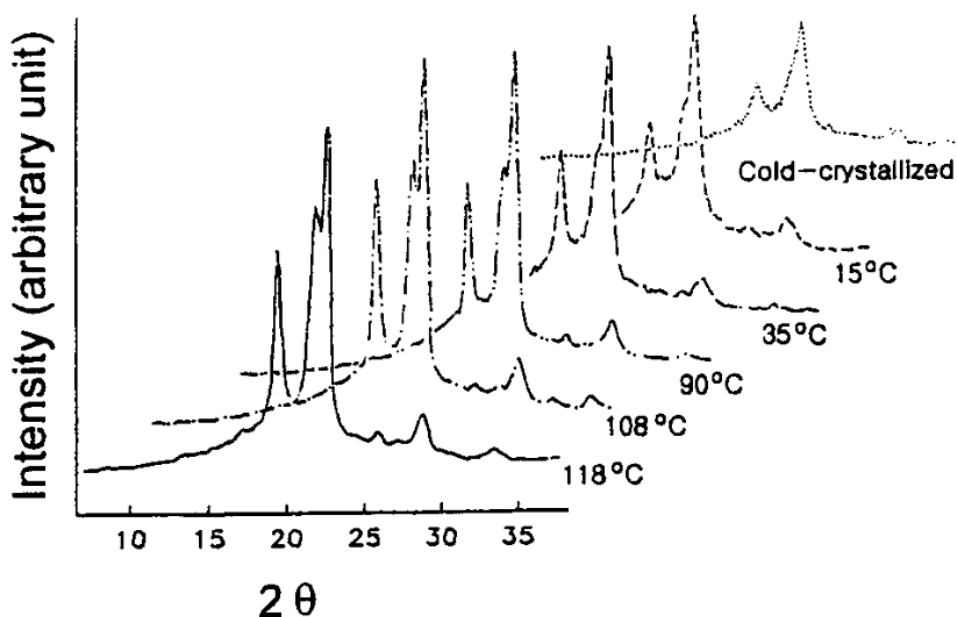
Figure 1.6. Wide-angle X-ray diffraction patterns for PBS crystallized from the melt at different temperatures and cold-crystal-lized at 10°C [64].

The distinction between crystalline and amorphous structures can also be observed in FTIR spectra in the region of 1710 to 1740 cm^{-1}, which represents C=O vibrations [79]. Yao et al. studied PBS crystalline and amorphous phase with FTIR, DSC and WAXD [80]. Authors assigned 1736, 1720 and 1714 cm^{-1} bands to mobile amorphous fraction, a rigid amorphous fraction (RAF)/intermediate phase, and crystalline phase. RAF forms semiannually with the crystalline phase and exists by attaching to it [80]. The authors' report that peak 1720 cm^{-1} represent both a rigid amorphous fraction and intermediate phase that characterizes the less ordered (perfected) structure than the crystalline region. In WAXD, crystallinity is usually calculated as relative crystallinity from WAXD peak intensities and areas. But for DSC, the theoretical melting enthalpy of 100% crystalline PBS (ΔH_m^0) is used. In literature, different values have been reported for ΔH_m^0 so far; and ΔH_m^0 are 102 [81] (DSC, density, volumetric flask method), 110.3 [80,82] (from handbooks), 110.5 [83] (calculated by the group contribution method), 200 [84] (DSC, deduced for a large crystal of infinite size) and 210 ± 10 J/g [85] (WAXD).

1.4. Biodegradability

Bacteria and fungi can degrade aliphatic polyesters, including PBS. Manufacturers recommend using composting conditions with a temperature above 30 °C, while studies on PBS biodegradation often use around 58 to 65 °C combined with high water content in the soil [86]. Kim et al. reported PBS biodegradation in natural soil at temperature 60 °C resulted in around 10 wt.% mass loss over 120 days [87]. A study using compost soil with 30 °C temperature reported around 30 wt.% loss in 180 days. The authors also noted that adding jute fibers significantly accelerated degradation [88]. While the combination of composting soil and 58 °C

resulted in PBS total degradation in around 100 days [89]. This was confirmed by analysis of evolved carbon dioxide. Similar results with composting conditions and 58 °C were reported by other authors [90]. Cho et al. studied PBS degradation in landfills and concluded that PBS degradation was relatively slow, but pretreatment methods like thermal, enzymatic, ultrasonic treatment and the application of adapted microorganisms significantly enhance decomposition speed [91]. It has been reported that PBS degrades in the marine environment, indeed, exceptional property to reduce sea pollution [86]. Unfortunately, PBS degradation was estimated to be relatively slow around 2 wt.% in reported studies [92,93].

In addition, it has been reported that CALB can be used to rapidly reduce PBS molecular weight in extrusion at 120 °C by processing material from 5 to 30 min [94]. Some authors have suggested recycling PBS, which can be achieved by improving processability with covalently grafted hydrophilic groups [54] or chain extenders [95]. Recycling biopolymers could reduce the environmental impact of their life cycle. 1.4. Polybutylene succinate: Blends and Copolymers

1.5. Blends and Copolymers

1.5.1. Blends

Polymer blends allow to combine existing materials to obtain enhanced properties that the original material does not offer. Blend preparation is often seen as a cost-effective method that does not require developing and synthesising new materials. Blends are usually divided into miscible and immiscible, with the majority of combinations being immiscible that form two or more phases in the material. Due to multiphase formation, desired properties are often not achieved, and to overcome this drawback compatibilizing agent is used to cross-link polymers. Popular cross-linking agents like maleic anhydride (MA) combine with peroxide and various diisocyanates, significantly affecting biodegradation; thus, alternatives are often explored for PBS blends.

The changes in blends can significantly affect the crystalline phase formation; thus, semi-crystalline polymers can be converted to amorphous, or the opposite can be achieved. The glass transition temperature can be changed to obtain the desired state of the material. Melt flow rate and melt strength of material affect the ability to process material for selected application; thus, such improvements are very desirable. Commonly blends are made to improve material's mechanical properties. For biodegradable polymers like PBS, desirable properties are lower cost and adjustable degradation time.

Coltelli et al. explored PBS, and plasticized whey protein (PWP) blends with loading from 30 to 50 wt.% [96]. Authors reported that when compatibilizers are used, properties like elastic modulus can be increased while tensile strength and elongation decreased. In addition, such composition improved biodegradation, and unlike other synthetic polymers, PWP is a cheap natural byproduct produced from cheese manufacturing. A study by Schmid et al. used whey protein isolate and PBS blend (70 % w/w) with varying potato pulp (0-10% w/w) addition as a filler for film preparation as an application for packaging material [97]. The addition of potato pulp increased elastic modulus, significantly decreased sample elongation, and tensile strength

was not affected, while water vapor transmission rate decreased in the sample with 2.5 wt.% loadings.

PLA and PBS blends are among the most studied biopolymer combinations due to PLA inherit brittleness that limits its application [98]. Thus, elongation at break is increased, and PBS is applied for the plastification effect. As they are immiscible, the preparation and addition compatibilizer significantly influences properties [98]. Ratsameetammajak et al. investigated the influence of three fatty acids (lauric acid, palmitic acid, and stearic acid) on poly(lactic acid) (PLA) and poly(butylene succinate) (PBS) blends [99]. PLA to PBS blends was predetermined and fixed at 90:10 weight ratio, and different ratios of each fatty acid (100:0, 100:2, and 100:4) were added to the melt blend. The authors concluded that fatty acids are a convenient and inexpensive way of plasticizing PLA/PBS blends. The addition of fatty acids enhances the plastic behavior of the films by decreasing the elastic modulus and tensile strength, fatty acid addition increased film contact angle. Still, no significant difference was observed in water vapor permeability. In a different study effect on popular cheap inorganic fillers talc, calcium carbonate and titanium dioxide were studied in PBS/PLA blends. The authors concluded that crystallinity is increased and the cost of blends can be significantly reduced [100]. Several authors have reported that blends show quite different crystallization and biodegradation performance than neat polymers [101-103]. Both PBS and PLA are suitable for applications like food packaging and biomedical scaffolds and membranes studies on blends have also reported high potential and enhanced performance [104-106].

Polycaprolactone (PCL) is a unique polymer with high potential for biomedical applications, one of the best biodegradation performances from polyesters but with a relatively low melting temperature of 60 °C and high price. Sadeghi et al. [107] report the preparation of biodegradable membranes with different compositions of PCL and poly(butylene succinate) (PBS) for wastewater purification. PCL/PBS membranes with PBS up to 30 wt.% were prepared. Blending the PCL with PBS resulted in a decrease in the elastic modulus, tensile strength, and elongation at break, but the addition of PBS to PCL increases the membrane hydrophilicity and biodegradability. 70/30 PCL/PBS blend enhanced the permeate flux and increased the rejection percentage of turbidity, chemical oxygen demand, and total dissolved solids to 100%, 66.62%, and 1.61%, respectively in comparison with the PCL membrane.

Almwli et al. reported the fabrication of novel PBS/polyvinylpyrrolidone (PVP) blends for pervaporation membrane preparation and possible application in acetone dehydration [108]. PVP up to 3 wt.% was used in the PBS blend membrane. Incorporating 3 wt.% PVP into the blend resulted in almost a 2.7-fold increased swelling, approximately 29% lower water contact angle, and about 26% higher tensile strength compared to a neat PBS membrane. PVP increased the total flux, separation factor, and pervaporation separation index of the resultant membranes by about 3, 6, and 21-fold, respectively.

Poly(butylene adipate-co-terephthalate) (PBAT) and poly(butylene succinate-co-adipate) (PBSA) are popular copolymers that are slightly cheaper than PBS and can offer similar properties to PBS in polymer blends. Thus this combination is viewed as unfavorable. Blends of PBS with PBAT showed mechanical and barrier properties changed according to polymer loading and showed good scaling [109].

Thirmizir et al. reported PBS/poly(hydroxybutyrate-co-hydroxyhexanoate) (PHBHH) that showed increased Young's modulus and flexural modulus when compared to PBS, while other mechanical properties were retained or decreased [110]. Authors reported best performance for blends with a ratio of 2 : 8 PBS/PHBHH and even better results when MA compatibilizer was used.

1.5.2. Copolymers

Synthesis of copolymers can be considered an advanced method for modification of polymer's properties. The targeted approach by adding specific units in the polymerization process allows modifying mechanical, physicochemical and thermal properties. In addition, new copolymers can have lower prices, different biodegradation speeds, and compatibility with solvents. A unique property of copolymers is relatively lower crystallinity or almost entirely amorphous structure.

The preparation of PLA-PBS copolymers aims to achieve increased elongation properties of PLA and the ability to reduce its brittleness. Srithep et al. used PLA-PBS copolymer as an additive to PLA. They reported a significant increase of elongation at break with the maximum value of 8%, and the glass transition temperature was lowered by 20 °C [111]. In other research, it was reported that copolymer could significantly alter the properties of PBS/PLA blends, and authors reported a decrease of the glass transition temperature by 30 °C [112]. In contrast, Guidotti et al. explored copolymerization of PLA with poly(butylene-co-triethylene succinate) as a scaffold for cardiovascular tissue engineering by emphasizing the elastomeric nature of prepared material [113].

Poly(butylene succinate-co-adipate) (PBSA) compared to PBS degrades significantly faster and has lower melting temperature and crystallinity [82,114]. PBSA has been proposed for the film fabrication process, especially for agriculture and packaging materials[115]. Poly(butylene succinate-co-terephthalate) (PBST) emerged as potential biodegradable alternative to poly(ethylene terephthalate) (PET) and poly(butylene terephthalate) (PBT)[116]. The relatively low amount of aromatic groups that do not form long chains of PBT can be biodegraded and possess low crystallinity, but thermal properties are more similar to PBS [116]. Zheng et al. reported that 50 mol% poly(butylene terephthalate) copolymer with PBS showed melting point around 132 °C, the modulus of 59 MPa, an elongation to break around 1300% [117]. Poly(butylene adipate-co-terephthalate) (PBAT) has had as more successful implementation aromatic groups in biodegradable polyester with good mechanical performance, ductility that is combined with superior biodegradability compared to PBST [118]. The lower cost, melting temperature and amorphous structure of PBAT make it suitable for preparing cheap polymer films, while PBS has higher stiffness, semi-crystalline structure, and good performance with processing techniques and versatility for applications.

Zeng et al. reported synthesizing poly(butylene succinate-co-diethylene glycol) copolymer and showed that most mechanical properties, crystallinity, and melting temperature decreased. The water contact angle of copolymers was from 61° to 69° compared to neat PBS with 75° and resulting in the decrease of hydrophobicity contributed to improved hydrolytic degradation [119]. As an alternative to PBS, propylene and ethylene groups have been studied in their respective polymers and even added to PBS [10]. Their implementation can diversify biorefinery

routes and increase the sustainability of copolymers while generally possessing lower properties compared to PBS.

Long chains have been implemented in PBS copolymers to obtain hydrophobic polymers. Sokołowska et al. reported poly(butylene succinate-co-dilinoleic diol) copolymers and showed that a catalyst choice block or random polymer could be obtained [120]. In further research, it was reported that the formation of PBS is more pronounced and the addition of long soft segments is limited up to 30 wt.% [121]. In addition, Sun et al. reported use of 1,2-decanediol is not only effective for enhanced elongation and can be used to control crystallization by adding branching [122].

With a wide variety of PBS copolymers, authors often try to target the biomedical field. The requirements of biomedical application often include lower molecular weight, biocompatibility, and excellent biodegradation of materials. Smola-Dmochowska et al. reported oligo (butylene succinate-co-citrate) in combination with other biopolymers has perspective for application in bioimplants with shape memory properties [123]. By adding 30 mol% of dithiodipropionic co-units to PBS, the inclusion of disulfide units was achieved, and authors reported a significant increase in fibroblasts adhesion and proliferation on copolymer scaffolds compared to PBS [124]. Wang et al. reported copolymerization with DL-malic acid units, which significantly improve hydrophilic properties due to the addition of hydroxyl groups [125]. Poly(butylene succinate-co-salicylic acid) was reported to have the ability to enhance plant growth [126].

1.6. Composites and Nanocomposites of PBS

1.6.1. Composite preparation

As discussed before PBS comes with crucial properties such as good mechanical performance, high ductility and elongation at a break that can exceed 200%, good thermal stability and processability, including, chemical resistance [127,128]. The combination of these properties makes PBS especially attractive for polymer composite preparation [129-131]. The addition of filler material can selectively increase gas barrier properties, yield higher stiffness and even reduce material costs [132]. Mochane et al. reported that PBS/natural fiber composites offer significant advantages like reducing the emission of pollutants, increasing energy recovery and biodegradability [133]. In addition, the authors outlined substantial disadvantages of the high flammability of such composites. Xiao et al. reviewed developments in fire retardancy of PBS [134]. Authors summarized that several approaches exist to improve fire retardancy, like inorganic fillers, magnesium hydroxide, expanded graphite, carbon black and organic lignin. In addition, a promising combination of ammonium polyphosphate and melamine has gained a lot of interest [134]. Most of these additives do not significantly hinder applications as they have almost no toxicity or impact on biodegradability.

The studied PBS/composites consist of inorganic fillers like various versions of carbon particles (carbon black [131,135], graphene oxide [136,137], graphene nanoplatelets [138]), silica [139] and many more. But fully bio-based composite concept with numerous variations of different natural fibers has become the focus of sustainability issues. Thus, natural lignocellulose fibers are widely used for reinforcement and cost decreasing purposes. In

addition, abundance, renewability, biodegradability, low density have played a significant role in organic filler popularity [140].

Determining optimal filler content, obtaining good dispersion in the polymer matrix and improving the interaction between composite components can be achieved by carefully choosing the right preparation technology. Figure 1.7. shows PBS composite preparation routes. Melt processing is by far the most popular choice [141-145] used to make PBS composites, while for more specific cases, solution methods are used [136,137,146], and there are some reports of in-situ polycondensation approach [139,147]. For example, twin screw extruder and an injection molding machine have been used to make PBS and padauk sawdust composites [141]. A twin-screw extruder has also been used for the preparation of PBS and hemp fibers [142], sugarcane rind fiber [143], CNC's [144,145] and other composites. Solution casting methods allow to work with specific fillers and avoid their agglomeration increase in the composites. Examples of these fillers include organically modified layered silicates (OMLS) [146] and grafting with octadecylamine-functionalized graphene oxide for creating [137]. In addition, nanocellulose fillers often agglomerate when they are dried, thus losing their nanostructured morphology. In-situ polymerization has been used to develop toughened PBS composites with chitosan nanowhiskers [147] and prepare composites with silica nanoparticles [139] and graphene oxide (GO) [148]. For industrial applications of nanofillers, both methods can be combined to prepare masterbatch with solution casting and then process it with melt extrusion. This combination allows for processing composites that melt extrusion cannot be directly made and reduces solvent usage.
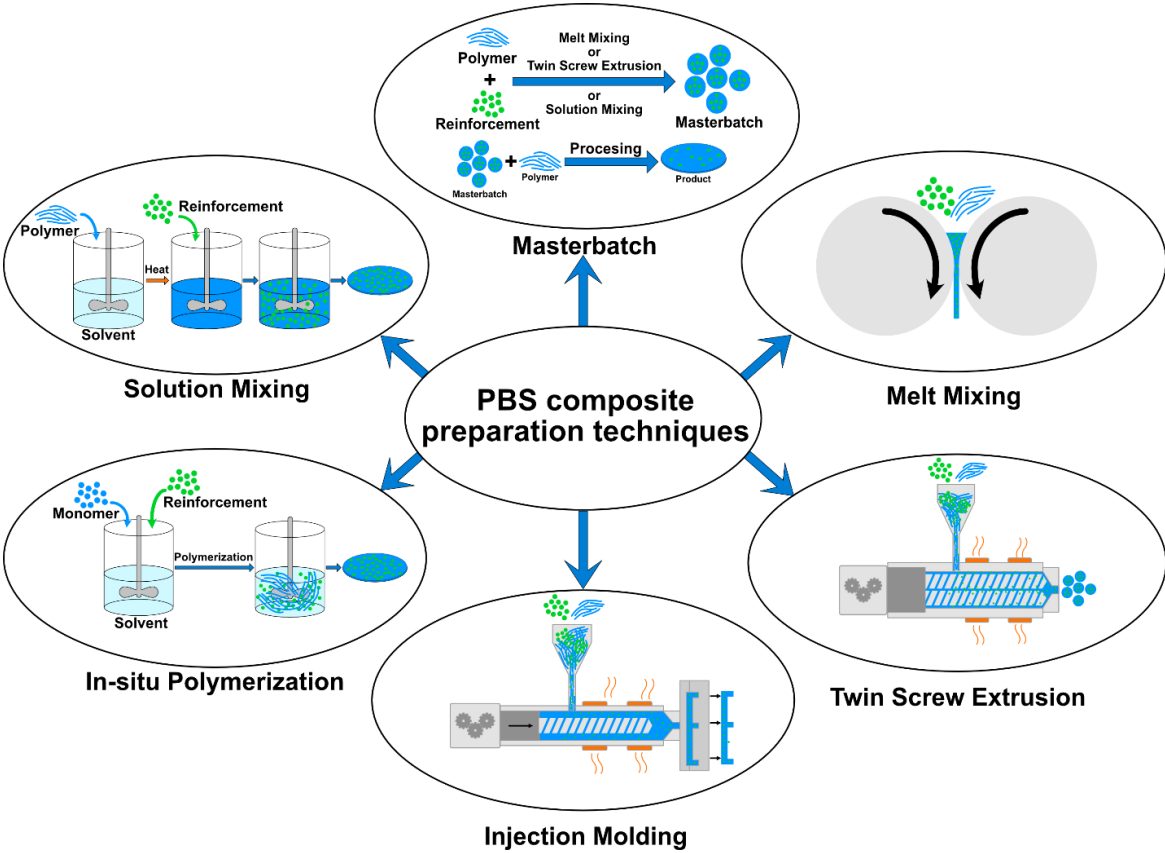
Figure 1.7. PBS composite predation techniques.

30

1.6.2. Inorganic fillers

Inorganic fillers like calcium carbonate can significantly lower the cost of the polymer as they can be used with very high loadings up to 60 wt.%. For research purposes and advanced applications fillers that increase thermal stability, conductivity or both, and mechanical properties are more appealing [137,146,149]. The addition of 5 wt.% of graphene nanosheets increased thermal stability by 35 °C and provided enhancement of 105-fold for electrical conductivity compared to PBS, and changed the crystalline structure to b-form PBS crystals that are usually observed under stress [128]. Graphene nanoplatelets have been reported to improve water and dioxygen permeability barrier properties by 38 and 35%, respectively [138]. Graphene oxide composites with the 3% loading have increased tensile strength and storage modulus by 43% and, 45%, respectively [148]. PBS nanosilver-coated carbon black (AgCB) composites with loadings up to 15 wt.% were prepared via injection molding method, and samples showed lower mechanical performance [131]. Prepared composites gained increased conductivity approximately by order and showed anti-electrostatic properties, which authors suggested for biofriendly keyboards. Antimicrobial activity was confirmed for the highest AgCB loading. Carbon black (CB) was used as filler for lightweight PBS composite foams, prepared by supercritical CO_2 foaming process [135]. The addition of CB accelerated the crystallization process, improved thermal stability, increased stiffness and electrical conductivity, and significantly enhanced compressive strength by 108%. Han et al. reported that the addition of 3.5 wt.% silica nanoparticles increased tensile strength and elongation at break from 26.6 MPa and 96% for PBS to 38.6 MPa and 515% nanocomposites [139]. In addition, filler significantly accelerated biodegradation of the PBS composites due to the reduction of the crystallinity. Stearate modified magnesium-aluminum layered double hydroxide as filler in PBS composites accelerated biodegradation under simulated marine conditions and lowered thermal stability due to the Mg and/or Al catalytic reactions [149]. PBS composite with cinnamic derivatives intercalated into ZnAl layered double hydroxides with 5 wt.% loadings showed good UV protection properties [150]. Such composites can be applied when the material is exposed to UV, thus preserving it and reducing CO_2 emission during photodegradation. Fan et al. reported tetra calcium phosphate grafted with poly(*L*-lactic acid) filler for PBS composites. Such composition could be applied as potential bone substitute material and analysis showed good biocompatibility in osteoblast attachment, spreading and proliferation on the composites [151]. Table 1.2. summarizes inorganic fillers used for PBS composites.

Table 1.2.

PBS composites with inorganic fillers.

Filler	Load	Modification	Property changed	Ref.
Silica nanoparticles	1.8, 3.5 and 5.5 wt.%	-	Tensile strength at break and elongation and biodegradability	[139]
nanosilver-coated carbon black (AgCB)	3, 5, 10, and 15%	-	Electrical conductivity and antibacterial properties	[131]
graphene nanosheets	0.5, 1, 2, 3, 5 wt.%	-	Thermal stability, electrical conductivity, mechanical properties	[128]
graphene oxide (GO)	0.1, 0.5, 1 wt.%	octadecylamine-functionalized (GOODA)	Improved tensile strength and Young's modulus, enhanced thermal stability	[137]
	0.5, 1, 3 wt.%	-	Increased storage modulus and tensile stress and higher glass transition temperature achieved	[148]
carbon black (CB)	0.5, 1, 3, 5, 10 wt.%	-	PBS composite foams: smaller cell size, a higher cell density, and more uniform cell morphology, low density, improved electrical conductivity compressive strength	[135]
graphene oxide	0.1, 0.3, 0.5, 0.7, 1 wt.%	functionalized with octadecylamine via sonochemical exfoliation method producing mono- to few-layer graphene oxide/octadecylamine	Increase in tensile strength, Young's modulus and thermal stability	[136]
Graphene nanoplatelets (GnP)	0.1, 0.5, 1, 2, wt.%	-	improve water and dioxygen permeability barrier properties	[138]
Cinnamic derivatives intercalated into ZnAl layered double hydroxides	2, 5 wt.%	LDH hybrids: cafeic, ferulic, hydroxycinnamic, cinnamic, Zn, Al-CO$_3$ (coprecipitation)	Increased viscosity, lover CO$_2$ emission during photodegradation	[150]
tetracalcium phosphate (TTCP, Ca$_4$(PO$_4$)$_2$O)	5, 10, 20, 40 wt.%	grafted with PLLA via ring-opening polymerization	good biocompatibility (osteoblast attachment), spreading and proliferation	[151]

1.6.3. Organic fillers

Plants and trees are the basis of renewable biomass, an essential resource for long-term sustainable development. Lignocellulose biomass is the most abundant natural resource; thus, it can be often obtained as a waste product (zero burden resource) or relatively cheap material. It can be used directly as stems of plants or sawdust from wood with minimal treatment, but cellulose can be purified and broken down to the nanoscale for advanced applications. PBS reinforced with lignocellulose has been widely studied [53-55,89,141-143,152-179]. Other polysaccharides like starch [180-182] or chitosan [147,183,184] are relatively popular for their unique properties, but fillers can also include protein fibers like wool [185] silk [186], etc. The resulting composite is reinforced with fibers or filled with particles, yielding a distinct set of properties. The most observed property of them has enhanced biodegradability. The variety of different PBS composites with organic-based fillers is summarized in table 1.3.

Terzopoulou et al. prepared PBS/hemp shives composites with loadings up to 70 wt.%, and all samples showed enhanced degradation in the soil but tensile strength was relatively low for compositions above 15 wt.% [142]. Sugarcane rind fibers promoted biodegradation of PBS with 5 wt.% loadings [143]. Feng et al. studied the relationship between preparation temperature and properties for PBS/sisal fiber composites [178]. The melt mixing induced degradation promoted interfacial adhesion when the temperature was increased to 200 °C yielding higher mechanical properties, but a further increase of temperature resulted in degradation and decreased performance. In addition, it was reported that steam-explosion pre-treatment resulted in increased specific fiber surface area and improved mechanical properties for PBS/sisal fiber composites. The impact of water immersion on the properties of PBS/Kenaf Bast Fibre composites with loadings from 10-40 wt.% was studied by Thirmizir et al. [179]. Authors reported optimal properties were achieved with 30 wt.% loading, while water immersion reduced mechanical properties permanently even after drying due to fiber swelling and micro-cracking-induced defects. Higher fiber content resulted in increased water absorption and a higher impact on properties after water immersion. The maximum water absorption of around 4.5% was observed at 30 wt.% loadings for PBS/burma padauk sawdust composites [141]. The reduction of crystalline regions due to the plasticization effect derived from water molecules was reported. In-depth analysis of cellulose, flax sugar cane, bamboo and hemp filler impact on PBS thermal stability and ignition was studied by Dorez et al. [177]. Authors found that fillers with higher lignin content reduced thermal stability of composites and significantly reduced flammability of composites due to the formation of char. Thus it is recommended to add lignin to composites. Ammonium polyphosphate fire retardant as an additive was examined to protect composites from the ignition, which was delayed due to the formation of char but the additive reduced long-term stability PBS [177].

To further improve composite properties, nanofillers have been applied. The increased surface and dispersion of filler yields exceptional physical properties [187]. Several authors have reported applying cellulose nanocrystals (CNCs) as unique fillers [127,144,188,189]. Ferreira et al. reviewed CNC's impact on biopolymers. They said that a significant increase could be seen for most mechanical properties, like tensile strength and Young's modulus. Still, elongation at break is usually decreased or remains close to the value of pristine PBS [127]. With better results are achieved if surface modifications are applied [127,190]. In addition, the amount of filler and size significantly affects properties [191]. But the most notable contribution to nanocomposite properties comes from the choice of preparation method [192,193]. Xu et al. reported a tensile strength increase to 88 % for PBS/chitin nanowhisker composites (CW) and up to 41 % for PBS/CNC composites with loadings from 1 to 5 wt.% [194]. CNCs showed even better properties with compatibilizer methylene diphenyl diisocyanate, while both fillers showed exceptional performance with just 1 wt.% loading. Huag et al. reported electrospun PBS/CNC nanocomposite scaffolds for tissue engineering with filler loading up to 5 wt.% [195]. CNCs increased in the in vitro degradation speed, conductivity, tensile properties, and scaffold had better cell adhesion, cell viability, and cell proliferation. Thus composites were more suitable for cell growth. Joy et al. prepared PBS composites reinforced with cellulose nanofibers (CNFs) with loadings up to 2 wt.% [145]. Tensile and flexural moduli of CNF composites

increased with an increase of filler load, owing to the nanofiber network formation in the PBS matrix. But toughness and strain at break exhibited the opposite trend. Kim et al. reported in situ polymerized PBS/CNC composites with 0.1 wt.% filler and exceptionally high tensile strength 66 MPa and elongation at break 450%, thus achieving a 1.6 fold increase for both parameters to PBS [196]. The authors of the following study further improved tensile strength to 77 MPa and elongation at break to 530% with a 0.2 wt.% loading of chitosan nanowhiskers [147]. A very high increase of toughness 3.2-fold compared to pristine PBS was reported, which is uncommon as usually decrease is observed.

Table 1.3.

PBS composites with inorganic fillers.

Filler	Load	Modification	Property changed	Ref.
chitosan nanowhiskers (CsWs)	0.05, 0.1, 0.2, 0.3 wt.%	-	Increased toughness, concurrent tensile stress, and elongation at break	[147]
padauk sawdust	10, 20 30 wt.%	-	Increased stiffness, water absorption	[141]
teakwood sawdust	10, 20, 30, 40 wt.%	APTES	lower thermal stability, tensile and flexural modulus of composites increased	[157]
almond shell flour (ASF)	30 wt.%	maleinized linseed oil	The increased glass transition temperature	[154]
wood flour	30 wt.%	Hydroxyethyl cellulose lauric acid ester sprayed on wood flour	improved mechanical properties	[168]
grape pomace (GP)	40, 50 wt.%	compatibilized with in situ manufactured maleic anhydride grafted PBS	enhanced mechanical and thermal properties improved flexural and impact properties	[156]
5 different types of industrially modified starch	40, 50, 60 wt.%	-	better strength properties and thermal stability	[158]
rice endosperm by-products	10, 20, 30 wt %	enzymatic modification	enhanced mechanical properties (tensile and flexural strength)	[160]
Filler	Load	Modification	Property changed	Ref.
CNC	0 to 7 wt.%	modified with succinic anhydride	improved thermal stability and higher Young's modulus, yield strength	[197]
starch nanocrystals	1, 3, 5, 7, 9 wt.%	L-lysine diisocya-nate (LDI) coupling agent or modification with N,N-dimethyl-4-amino-pyridine	superior tensile and barrier properties, improved elongation at break, water vapor and oxygen transmission rate values lowered, better dispersion achieved, complete wastewater treatment conditions degradation achieved	[198]
CNC	0.5, 1, 3, 5, 7 wt.%	CNCs modified with acetic anhydride, butyric anhydride and caproic anhydride	Improved thermal stability, tensile modulus improved gradually, elongation at fracture decreased	[199]

Filler	Load	Modification	Property changed	Ref.
microcrystalline cellulose, cellulose acetate, cellulose triacetate	5, 10, 15 wt.%	-	Improved enzymatic degradation encreased Young's modulus	[165]
oil palm mesocarp	30 wt.%	treatment with hydrogen peroxide under alkaline conditions	fiber surface roughness and crystallinity increment, in PBS matrix, resulted in improvement of mechanical properties	[169]
oil palm mesocarp	30 wt.%	treatment with hydrogen peroxide under alkaline conditions	enhanced tensile strength, tensile modulus and elongation at break, reduced water absorption and thickness swelling	[170]
lignin	50 wt.%	PBS matrix modified with MAH and silane addition	improvements in flexural property, tensile modulus and tensile strength	[171]
switchgrass and lignin hybrid	50 wt.% (lignin:switchgrass=1:4, 1:1)	polymeric methylene diphenyl diisocyanate (PMDI), isocyanate-terminated polybutadiene prepolymer (ITPB) and organic peroxide chemical additive	Improved impact, flexural and tensile strength, increased polymer cryslatilnty, higher storage modulus achieved	[173]
hemp fibers	15, 30, 50, 60 and 70 wt.%		PBS crystallinity decreases, degradation rate during enzymatic hydrolysis and soil burial increases	[142]
sugarcane rind fiber (SRF)	5, 10, 15 wt.%	alkali treatment	soil burial biodegradation rate accelerated	[143]
isora nanofibers (INF)	0.5, 1, 1.5, 2 parts per hundred parts of polymer resin [phr])	-	Increased tensile and flexural properties, decrease of toughness and strain-at-break	[145]
bamboo fibers	5 wt.%	modified with (3-aminopropyl) triethoxysilane and polydopamine (PDA)	improved tensile strength and modulus, flexural strength and modulus, impact strength	[200]
bamboo fibers	50 wt.%	modified with PDA coating as a bridge to graft octadecylamine (ODA) for hydrophobic surface preparation	improved interfacial adhesion, mechanical properties, particularly tensile strength, and water resistance	[159]
flaxseed fiber bundles	40 wt.%	surface modification treatment was carried out with concentrations of 10 g/L and 20 g/L sodium hydroxide (NaOH)	Increased tensile strength and flexural strength	[155]
Filler	Load	Modification	Property changed	Ref.
bamboo fibers	49 wt.%	coating fiber surface with polydopamine (PDA)	mechanical properties and thermal stability enhanced, enhanced interfacial compatibility, glass transition temperature, and crystallinity increased with DOPA loading rates	[161]
sugarcane rind fiber (SRF)	5, 10, 15 wt.%	-	increase in crystallization temperature, degree of crystallinity and maximum weight loss rate temperature, improved biodegradation	[143]

Filler	Load	Modification	Property changed	Ref.
Chemothermomechanic al pulp fiber	30 wt.%	alkali-treated and/or esterification with lauroyl chloride	Enhanced tensile and impact strengths	[162]
ramie fibers	0.5, 1 wt.%	enzymatic modification	improved compatibility between fibers and polymer matrix	[163]
ramie fibers	10, 20, 30 wt.%	treated with different agents (alkali, silane, maleic anhydride, acetic acid)	Improved tensile strength and modulus, interfacial strength	[175]
kenaf fiber	30 wt.%	PBS treated with maleic anhydride (MAH)	Improved water resistance by improved fiber-matrix interaction	[176]
cotton fiber	10-40 wt.%	Silane treated	Improvement in tensile strength, fiber-matrix compatibility improvement, significantly improved biodegradation rate	[89]
different natural fibers: hemp, flax, sugarcane and bamboo	5, 10, 15, 20, 30 wt.%	ammonium polyphosphate (APP) was used as a fire-retardant agent added	fiber reduced thermal stability regained with APP addition	[177]
steam explosion pre-treated sisal fibers	30 wt.%	-	Interfacial bonding improvement, mechanical performance increase	[178]
kenaf bast fibers	10, 20, 30, 40 wt.%	-	Increased flexural strength and modulus, decreased impact strength	[179]
Empty fruit brunch (EFB) fibers	30, 40, 50 wt.%	modified with tapioca starch	Reduced mechanical properties, enhanced water vapor permeation and reduced PBS composite cost	[201]

1.6.4. Composite modification

Improving the interfacial adhesion between polymer and filler is by far the most studied topic of PBS composite materials [89,141-143,158-179]. Similarly to most conventional polymers, the PBS is hydrophobic and is limited to intermolecular bonding, which is relatively weak to most inorganic and organic fillers that are hydrophilic. This led to structural issues like agglomeration, low-stress transfer to fibers and increased water uptake, to name a few. Various methods have been applied to eliminate these issues and even further improve the properties. This includes the use of compatibilizers, surface modifications and cross-linking agents. Following the treatment, filler's and/or polymer's surface is chemically altered, coated, or chemical bonds are formed between the components.

Lignocellulose-based fillers are commonly used for PBS, as described in the organic fillers section. This has led to the applying widely used methods like hydroxide treatment or silane-based coupling agents for cellulose surface modification [202]. Hong et al. investigated a green and effective approach to enhance interfacial adhesion between PBS and bamboo fibers [200]. Fiber modification with (3-aminopropyl) triethoxysilane and polydopamine led to increasing tensile strength by 70%, impact strength by 63%, flexural strength by 37%, and tensile strength modulus by 25%, flexural modulus by 24% and water resistance. Three types of silanes were used for cotton fiber (CF) treatment, and prepared composites with 10-40 wt.% were tested for mechanical properties and biodegradability [89]. Tensile strength without treatment showed an

increase of 15-78%, and the addition of silanes resulted in 25-118% improvement. In addition, the best of mechanical properties were reported for samples treated with (3-aminopropyl) trimethoxysilane, which slightly increased the thermal stability and biodegradation rate. Zhou et al. investigated interfacial shear strength for PBS/ramie fiber composites with various surface modifications, including maleic anhydride (MAH), acetic acid anhydride, sodium hydroxide, and silane [175]. The best interfacial shear strength was reported for untreated ramie fibers followed by alkaline treated samples, which showed high tensile modulus and strength values with 30 wt.% loadings. Thus, the authors demonstrated various components on fibers surface like wax, hemicellulose, and lignin h to enhance compatibility. While Then et al. reported oil palm mesocarp fiber surface modification with alkaline-hydrogen peroxide treatment, resulting in lignin, hemicellulose, and waxy substances removal [169]. A similar observation was reported by Azhar et al. that flaxseed fiber bundle pretreated with sodium hydroxide and introduced in PBS matrix show 84% increase in flexural strength achieved by significantly rougher surface morphology [155]. The prepared composites with 30 wt.% loadings had higher tensile, flexural and impact strength, which authors attributed to increased fiber surface roughness. Enzymatic treatment of rice endosperm [160] and ramie fiber [163] surface indicated improved properties compared to untreated composites. The authors proposed that surface can be cleaned and restructured for better interfacial adhesion, yielding better mechanical properties and lower water absorption. PBS/alkaline lignin composites with high loading of 50 wt.% were tested with two different modification routes- PBS grafting with MAH and lignin treatment with silane coupling agent [171]. Tensile and flexural properties saw a relatively good increase, while impact strength and water adsorption were decreased. The MAH grafting saw the most considerable increase for tensile strength and flexural modulus, while silane treatment showed better elongation at break and tensile modulus values. A combination of 1:4 Lignin: Switchgrass filler with 50% loading was studied with polymeric methylene diphenyl diisocyanate (PMDI) cross-linking agent and peroxide in melt processing conditions [173]. The authors reported around a 5-fold increase in tensile and flexural modulus after the addition of PMDI. PBS grafted with MAH was used as a compatibilizer for PBS/kenaf bast fiber composites and authors studied dimensional stability and water adsorption of composites [176]. Untreated composite retained better properties than the most treated samples, the us authors concluded that grafted polymer preparation process contributed to increased water uptake and decreased dimensional stability. In addition, the purification process is vital for the application of this method. In a different study the balance between mechanical and thermal properties of PBS/grape pomace composites with MAH grafted PBS was reported at a ratio of 57:40:3. Authors reported improved flexural and impact strength by 28% and 59% compared to pristine PBS [156].

Coating fiber surface to increase interfacial adhesion is another modification route. Hong et al. treated bamboo fibers (BF) with polydopamine (PDA), thus showing enhanced thermomechanical properties like storage modulus, loss modulus, thermal stability, in addition, demonstrating the better formation of an interface between filler and matrix as indicated by SEM analysis [161]. The following authors further improved PDA coating with graft octadecylamine grafting and showed even better mechanical properties and significantly lower water absorption for composites [159]. Yue et al. spray-coated wood flour with hydroxyethyl

cellulose lauric acid ester to prepare PBS composites [168]. The authors reported tensile strength, impact strength and storage modulus increase by 20-80% compared to uncoated composites and obtained the best properties with 2 wt.% coatings from wood floor mass.

The nanofillers require different modification and composite preparation strategies, usually involving more complicated chemical modification of the surface. Wu et al. reported CNC modification with succinic anhydride and preparation of composites with filler loading up to 7 wt.% [197]. Authors reported up to 57% increase in Young's modulus and up to 11% increase in yield strength with modified CNCs showing better properties as filler. In addition, the authors demonstrated that modified filler showed highly hydrophobic surface properties compared to hydrophilic CNCs. PBS/banana starch nanocrystal (SNC) composite modification routes with coupling agent L-lysine diisocyanate (LDJ) and surface treatment with lauroyl chloride were compared [198]. Water vapor transmission rate and oxygen transmission rate were lower by up to 2-fold owning well dispersed nanoparticles. Surface treatment yielded the tensile strength and elongation at break increase up to 3.8% and 51.1% compared with the neat PBS film. Coupling agent improved biodegradation speed while surface treatment delayed the microbial process. He et al. used different acid anhydrides for the improvement of CNCs dispersion in the PBS matrix [199]. To decrease hydrophilicity, the CNCs were treated with acetic anhydride, butyric anhydride and caproic anhydride. The surface energy of modified CNCs was lower than that of pure CNCs. The initial decomposition temperature of 5 wt.% modified CNCs/PBS composites was slightly higher compared to unmodified sample. Tensile tests indicated the tensile modulus improved gradually with increase of modified CNCs content, whereas the elongation at fracture decreased. CNCs modified with phthalic anhydride in melt were further squeeze treated, resulting in a significant increase in tensile strength from 35.2 MPa to 136 MPa [56]. Almond shell flour (ASF), a common agricultural waste material, was functionalized with maleinized linseed oil (MLO) particles and used as filler for PBS composites [154]. The addition of MLO contributed to a significant increase of elongation at break, achieving around a 3-fold increase compared to untreated composite and showing even slightly higher results than pristine PBS. The authors reported optimal properties for 2.5 wt.% loading of MLO with 30 wt.% loading of the filler.

1.7. Applications of PBS based Materials
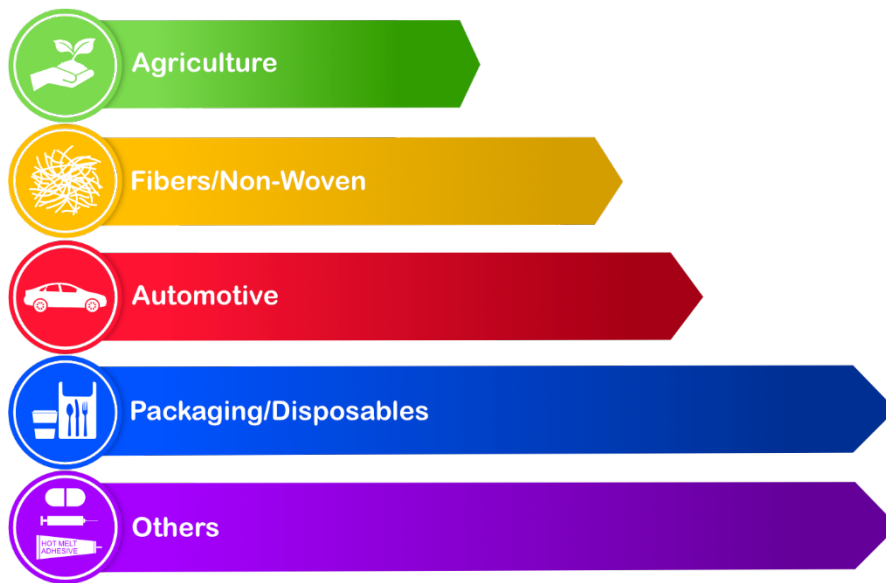
Figure 1.8. PBS applications and their relative distribution.

Short term use of light packaging materials and films is problematic for the recovery and recycling of plastics [203]. These products often end up in landfills, soil, forest, or ocean contributing to major pollution, which can be avoided with the use of bioplastics. The remains of plastics in soil can significantly reduce the yield of crops and contribute to food supply issues in the long term [204]. Once microplastics are formed, it is almost impossible to collect them from soil or water, but they will remain in this form for hundreds of years. While their impact on humans and animals is only being studied, the alarming rate of their rising content in nature has pushed for new policies and legislation [205].

New applications for bioplastics are introduced every year, resulting in a growing market size. Perspective application fields are given in Figure 1.8. Since the PBS biodegradation has been widely studied and degrades into water and carbon dioxide, it is presented as an alternative to commodity polymers like PET, PP, LDPE, and HDPE [49-51]. The manufacturers and scientists alike have presented these comparisons, which show a great feasibility for replacing commodity plastics with similar thermal and mechanical properties [49,51,206]. As seen in Figure 1.9. the manufacturers like Mitsubishi Chemicals have suggested application mainly in food packaging and agriculture industries [206]. In addition, there is great potential for biomedical applications like scaffolds for tissue recovery, drug delivery and implants [130,207,208]. While large industries like automotive are pushing for sustainable manufacturing [209].

1.7.1. Agriculture & food packaging

Figure 1.9. Proposed PBS applications by manufacturers [206,210].

Figure 1.10. Biodegradable PBS bottles [211] and cutlery [212].

Food packaging requires properties that extend the product's shelf-life and protect it during transportation and storage. Packaging must have excellent barrier properties to prevent microbial contamination and water vapor, carbon dioxide, aroma, and oxygen permeation [213,214]. The PBS mechanical, thermal, and barrier properties must be adjusted by developing modification strategies that include chemical crosslinking, blending with other polymers, and composite processing to guarantee these requirements. It is also crucial to adapt the foraging behavior for various conditions, especially toward moisture content, ultraviolet and visible light irradiation.

For example, PBS polymer materials processed into films, compost bags, or boxes are promising candidates for biodegradable packaging, particularly food packaging, cosmetics, and mulching films in agricultural applications. Mitsubishi chemical corporation has developed a line of PBS biodegradable plastics for the preparation of coated/laminated paper for applications like drinking cups and oily food wraps as they are resistant to elution to oil and vinegar [206]. It is also resistant to the permeability of sauces and oils.

The PBS grades produced are processable in LDPE machinery, have excellent printability, low heat seal temperature, and excellent heat seal strength.

Another example is futamura, a leading producer of sustainable cellulose packaging films, and Scientex, the Malaysian flexible packaging manufacturer. They selected PBS as a sealant layer to create bio-based laminated solutions with biodegradable zippers. The multi-layer construction is entirely compostable and offers excellent sealing characteristics and appearance, along with moisture and oxygen barrier properties, making it suitable for various types of dry food [210]. PBS can also be used in environmentally friendly applications, thanks to its excellent

dimensional stability and flowability. It can be formed by injection molding into cutlery and bottles that quickly decompose in the soil as shown in Figure 1.10. In addition, the excellent biodegradation properties enable applications like mulch films and pots for seedlings. This is especially important as these films are broken down by weather, ultraviolet radiation, and mechanical treatment. They do not leave permanent pollution in the soil.

1.7.2. Biomedical engineering

PBS properties include biocompatibility, biodegradability and non-cytotoxicity, making it suitable for medical applications like implantable materials, tissue engineering, drug delivery and encapsulation [130,207,208]. The benefits of using drug delivery systems based on the PBS are easy preparation, prolonged, controlled, and steady release of drugs. For biomedical applications, the PBS is emulsion polymerized as microcapsules or electrospun from solution as nanofibers. Some of the reported structures are shown in Figure 1.11.
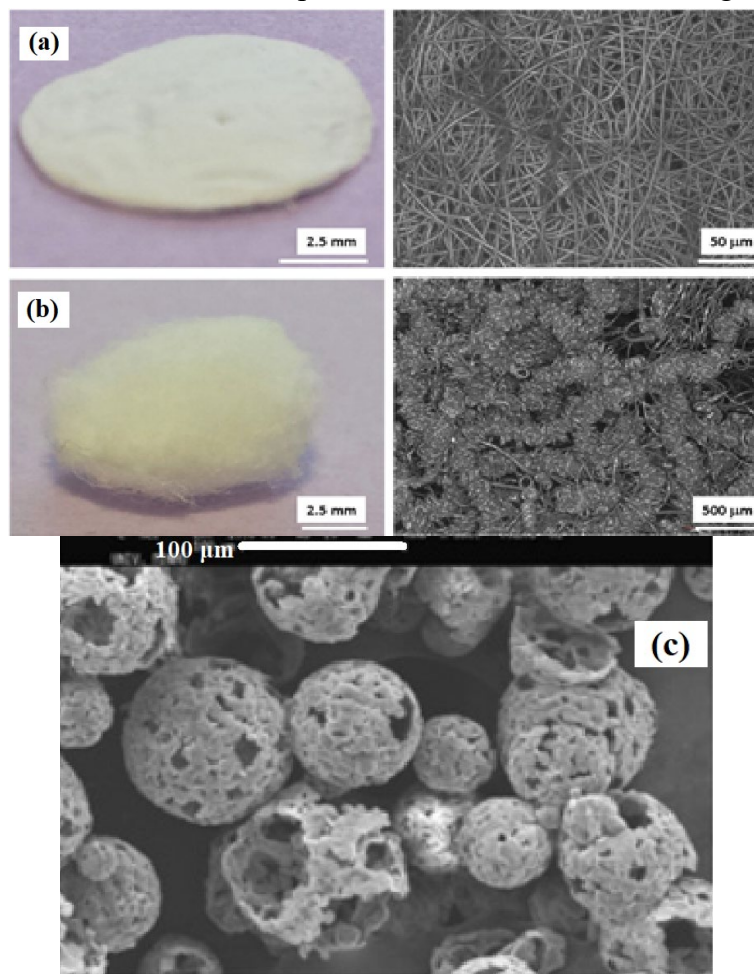
Figure 1.11. Scanning electron microscopy images of (a) electrospun scaffolds collected on conventional flat collector [208], (b) helically coiled scaffolds collected in methanol bath [208] and (c) PBS microcapsules for drug delivery [207].

1.7.3. Adhesives

PBS as a biodegradable adhesive is shown in Figure 1.12. PBS adhesives can alleviate the environmental problems caused by nondegradable hot-melt adhesives. A case study of hot melt adhesive based on PBS was reported [215]. The authors tested PBS and prepared poly(butylene-

co-isosorbide succinate) copolymer applied them between two iron plates. The use of copolymer further improves the bond strength between adhesive and metal interfaces. The suitability of PBS as a direct-melt coating on recycled paperboard for grease resistance in microwave rapid reheat and heat and hold convenience food packaging applications was researched [213]. This research demonstrates that PBS can be a viable alternative to perfluorinated and petroleum-based chemicals and polymers. Advantages include more sustainable end-of-life options owning to oil migration resistance at elevated temperatures and biodegradability.
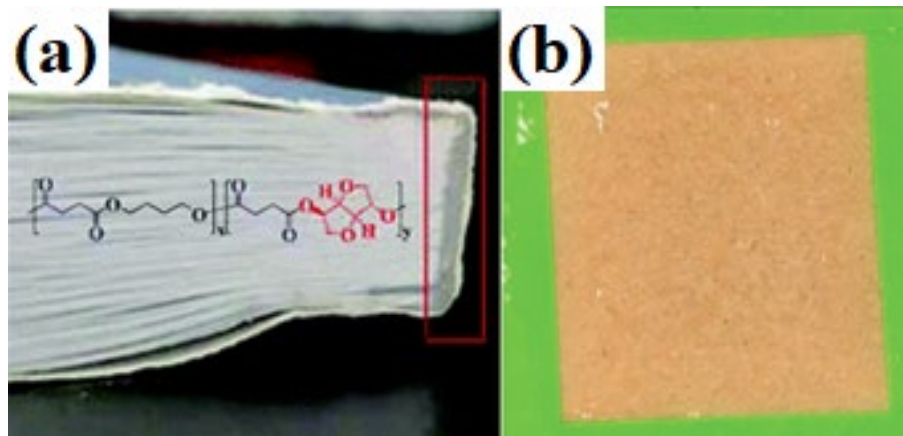
Figure 1.12. (a) PBS as hot melt adhesive [215] and (b) paperboard coated with PBS [213].

1.7.4. Automotive

There is a potential to substitute polypropylene (PP), polyethylene terephthalate (PET), and polyethylene (PE) with PBS owing to its high tensile strength and heat resistance. Now there is no clear evidence that PBS is used in the automotive market. Car producers are confronted with many inherent technical challenges with biodegradable polymers, including the need to overcome potential biodegradation, ensure the polymer material's stability when exposed to environmental factors, dealing with natural variability in fibers, and adjusting the manufacturing process for new material. However, in 2006, Mitsubishi Chemical and Faurecia (FR) offered the global auto market a sound, versatile, and lightweight biopolymer material [216]. They co-developed a bio-based plastic called BioMat that could be massed-produced and used for automotive interior parts such as door panels, trim and strip, structural instrument panels, console inserts, air ducts, and door panel inserts. Faurecia further developed BioMat, optimizing it with hemp fiber filler to produce injection molded car parts, which were expected to reach market as early as 2016 [209]. Figure 1.13. shows car panel produced from BioMat. While now, no new information on BioMat has been shared by Faurecia. The other possible applications for biopolymers in the automotive could be the engine and transmission cover in underbody panels, scuff plates, interior trims, door linings, luggage trim upholstery, and cowl side trim and seat cushions, door scuff plate, and toolbox area [217]. The composites, blends, and combination of various bio-based materials can fully substitute fossil-based materials.

Figure 1.13. Injection molded PBS/hemp custom interior panel [209].

1.7.5. Water and wastewater treatment

Durable and biodegradable membranes from PBS to efficiently filter the wastewater and reduce the wastewater pollutants are actively researched. Figure 1.14. shows membranes produced from PBS. Commonly other PBS blends with other biopolymers are proposed to control the morphology, hydrophilicity, chemical structure, crystalline structure, mechanical properties, and biodegradability of the membranes for those applications [218,219]. For example, the membranes of high thermal stability and composability were prepared using immersion precipitation technique to control macro and microvoids [218]. Authors reported that the addition of cellulose acetate could regulate macro void formation and thus change permeation properties. Sadeghi et al. prepared PBS/ polycaprolactone membranes with immersion precipitation technique and reported the best composition with weight ratio of 85:15 [219]. Furthermore, the performance of the obtained membranes was validated through the treatment of wastewater sampled from the chips and snacks factory and their efficiency was testified by high values of pure water flux, flux recovery ratio, and permeate flux and the higher rejection of pollution.
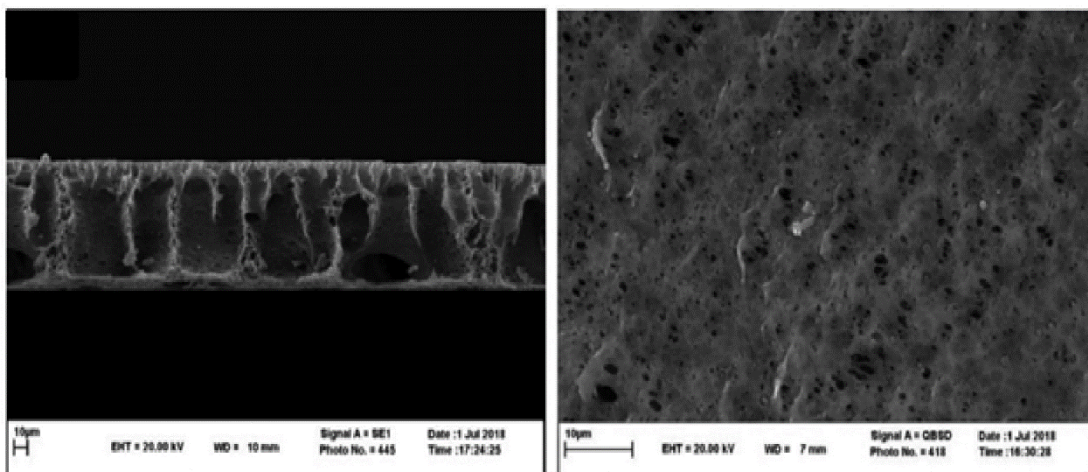

Figure 1.14. SEM cross-sectional and surface images of the PBS membranes with microvoids [219].

1.8. Techno-economic potential and challenges

When it comes to the commercialization and mass production of bio-based polymers, there are often two main drawbacks given. The limited amount of farmland and the relatively high cost of bioplastics. While the farmland question might be more complicated with various solutions such as sea farming and innovative ways to increase crop density, the initial challenge lies within the price. This raises the question of whether bioplastics can compete on price. In this regard, we can set the base line using conventional polymers like PP and PE. The bulk price for PP and PE, according to various sources, ranges from around 1.0 to 2.0 $/kg [220,221]. As PBS is still considered an emerging product with limited production, we can look at PLA and polybutylene adipate terephthalate (PBAT), which are currently two of the most produced bio-based polyesters [222]. According to various sources, bulk prices for PLA and PBAT are within a range of around 2.0 to 3.5 $/kg [222,223]. According to a 2015 European Commission report, the bulk price of PBS was 4.5 $/kg [222]. A slightly lower price estimation was provided by Wageningen University at 4.0 $/kg for PBS in 2016 [224]. Ioannidou et al. researched techno-economic risk assessment for PBS based on sugar beet pulp, glucose syrup, and corn stover feedstocks [225]. The authors assumed that PBS is produced as fully bio-based and examined production capacities of up to 120 kt/year. When production reaches 60 kt/year, the estimated production costs for PBS are around 2.6 $/kg for glucose syrup and corn stover. According to estimations, use of sugar beet pulp could offset production costs (around 4 $/kg) to a minimum selling price of 1.4 $/kg (60 kt/year or more) with sales of high-cost pectin byproduct. Thus, it can be concluded that the current price of bio-based polyesters is around two to three times higher than their conventional fossil-based counterparts. As remaining oil volumes are reduced due to increasing oil extraction costs, the price gap between bio-based and oil-based polymers is expected to narrow in the coming decades. It is widely accepted that oil prices are much more unstable than crop (feedstock) prices [226]. This opens the door for various pieces of legislation to influence consumer choices, such as tax and environmental policies aimed at closing the price gap and changing consumer preferences.
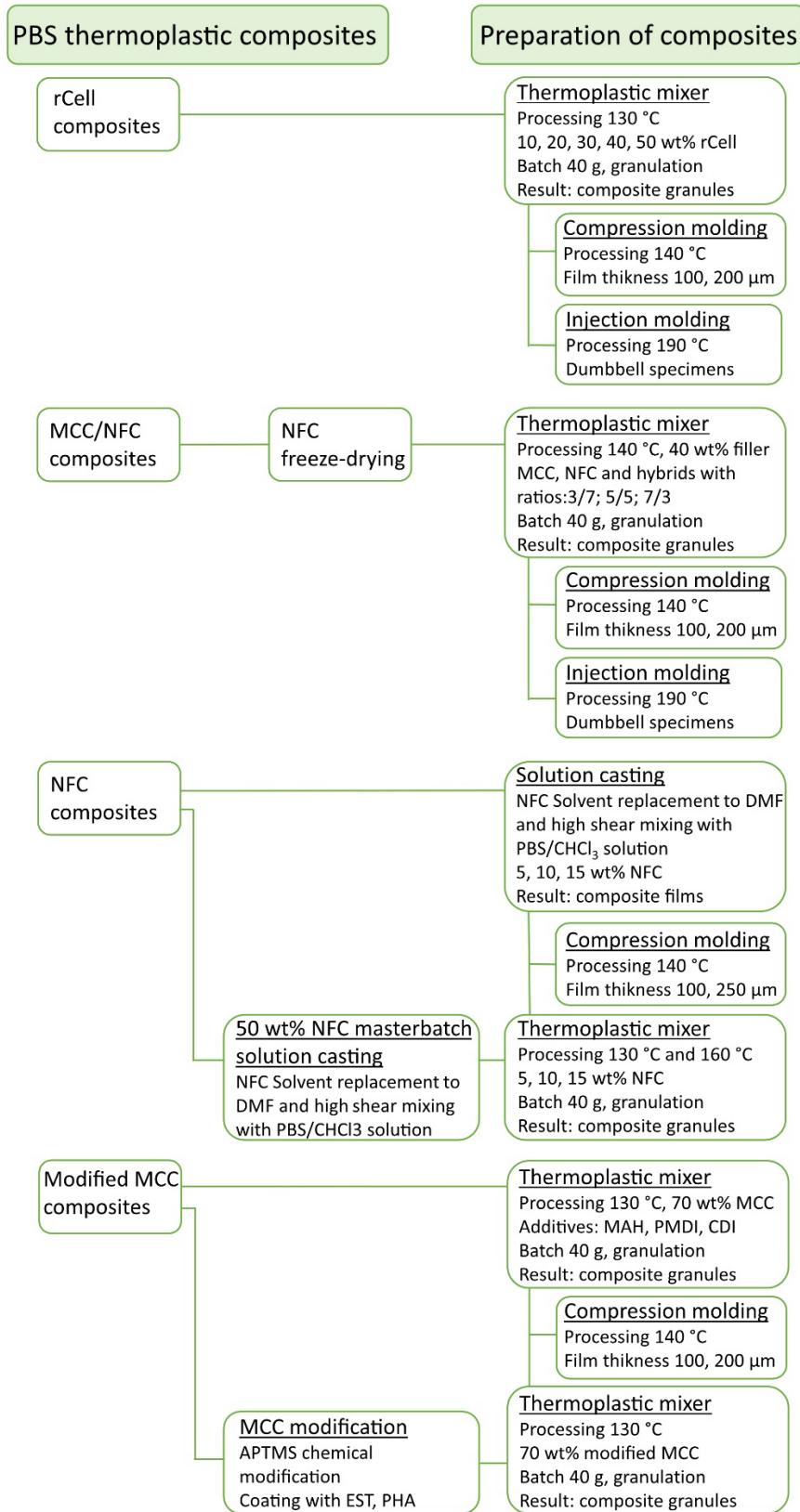
2. MATERIALS AND METHODS

Figure. 2.1. Structure of the research.

2.1. Materials

Polymer

Poly(butylene succinate) (PBS) selected was BioPBS™ grade FZ71PB® (PTT MCC Biochem Company Ltd) and, according to the producer, is bio-based (50 wt.%), the biodegradable thermoplastic polymer [50]. Bio-based content comes from bio-succinic acid used in the synthesis. Its inherent melting point is 115 °C, density − 1.26 g/cm^3, and melt flow index − 22 g/10 min (2.16 kg, 190 °C). According to the manufacturer, FZ71 is flexible semi-crystalline polyester with excellent properties suitable for cast extrusion and extrusion coating. It can be used in contact with food and hot beverages with temperatures up to 100 °C. In addition, PBS is compostable in soil, landfills and at home, while recommended temperature for compost is at least 30 °C.

Recycled cellulose

The rCell was received from the TetraPak® recycling industry company as a recycled cellulose pulp (Figure 2.2.a) that was separated from aluminium and polymer components during industrial-technological processing. Before laboratory processing, the pulp was ground with the Retsch cutting mill SM300. A sieve with 4 mm was used for the first grinding cycle, followed by the second milling with a sieve size of 250 μm (Figure 2.2.b). Mill was fed manually, and rotation speed was set for the whole process at 1500 rpm. rCell is fibre filler, characterized by average length −200 μm, average width −20 μm (Fig. 3.2.a-d).
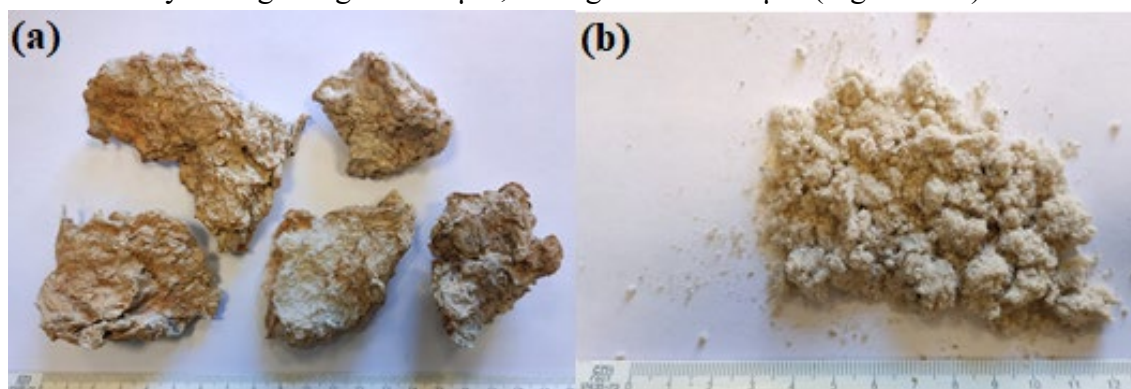
Figure. 2.2. Characteristics of raw materials: (a) received recycled cellulose from industrial plant and (b) recycled cellulose filler after grinding process.

Microcrystalline cellulose

Microcrystalline cellulose was obtained from bleached softwood kraft pulp (Metsä Botnia AB) according to the procedure reported by the authors [76]. In compliance with this method, the pulp was impregnated with a thermocatalytic degradation catalyst – weak hydrochloric acid solution (0.05%) and used modulus were 1:20. After pressing out the excess liquid, the pulp was thermally treated at a temperature of 120 ºC until a dry state. This facilitated the destruction of the amorphous part of cellulose, while the crystalline one remained almost intact. The degree of polymerization decreased and reached the so-called leveling-off degree of polymerization (LODP), which, in the case of cellulose, was ~ 250 units [77]. Then, the partially degraded pulp was ground in a ball mill "U.S. Stoneware JAR MILL 755RMV1" (USA) with variable speed.

The milling jar was made from alumina-fortified porcelain, with a capacity of 5.7 L. Cylindrical grinding media from corundum 2.1cm x 2.1cm in size were used; charging factor 1 kg/L; grinding time ~15 h. As a result, microcrystalline cellulose powder was obtained. The microstructure of the obtained microcrystalline cellulose was evaluated by SEM and shown in Figure 2.3. Average size of obtained MCC particles is 10-40 μm. Zeta potential for obtained MCC particles is about -16.9 mV.
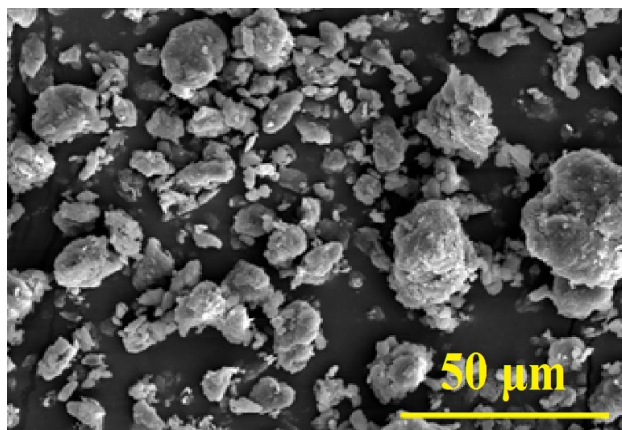
Figure 2.3. SEM image of MCC.

Nanofibrillated Cellulose

Nanofibrillated cellulose gel-like dispersion (11 wt.%) was prepared using mechanical treatment with the previously established thermo-catalytic method. NFC fabrication is like MCC preparation but involves the addition of water after the drying process and wet milling (instead of dry milling for MCC) of the cellulose for 15 h. The length of NFC was measured in a range from 200 to 550 nm with an average of 350 nm by dynamic light scattering (Malvern Nano ZS-90) as shown in Figure2.4.a, while Figure 2.3.b is AFM image and shows diameter size between 15-50 nm for nanofibrils.
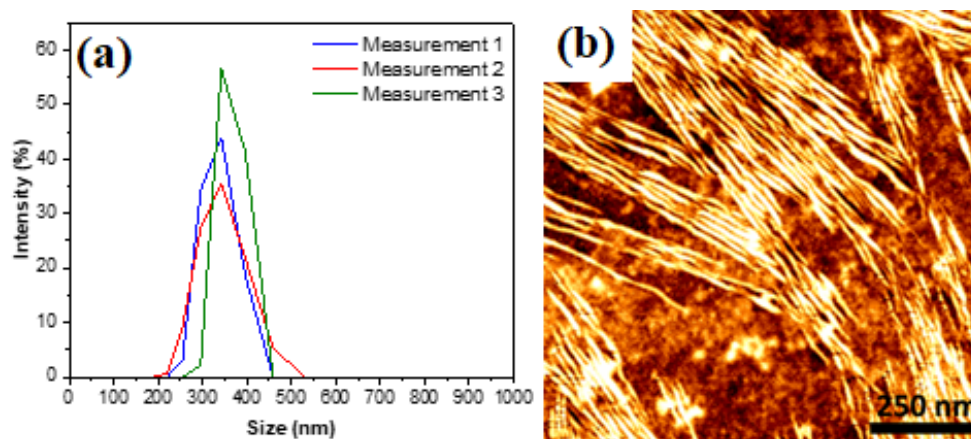
Figure 2.4. (a) Dynamic light scattering for NFC suspension and (b) AFM image of NFC.

Other chemicals

Laboratory grade hydrochloric acid, chloroform and N,N-dimethylformamide (DMF) were purchased from Merck KGaA (Darmstadt, Germany). Carbodilite® HMV-15CA was purchased from Nisshinbo Chemical Inc (Japan). Carbodilite contained a carbodiimide (CDI) group, which worked as a chain extender and hydrolysis stabilizer. Addapt® BioWet 25 L is a

solvent-free water-based, readily biodegradable surfactant based on polyhydroxy amides (PHA). Addapt® Ester 80DA is a water and solvent-soluble synthetic aliphatic ester (EST) dispersing agent. BioWet 25 L and Ester 80DA were both purchased from Adapt Chemicals B.V (Netherlands). 3-Aminopropyltrimethoxysilane (APTMS), maleic acid anhydride (MAH), and acetic acid were purchased from Sigma–Aldrich (Germany). Polymeric diphenylmethane diisocyanate IsoPMDI 92140 (PMDI) was purchased from BASF (Germany).

2.2. Testing Methods

Dynamic light scattering

Zeta potential and size of particles for MCC were determined on Zeta Sizer Nano ZS90 (Malvern, UK) for 0.05 wt.% suspension in distilled water.

Optical microscopy

The rCell particle sizes were calculated from the images of particles deposited on the glass slide, which were taken using an optical microscope Leica DMR (Leica Microsystems, Germany) at 5x, 10x magnifications. Leica Image Suite^{TM} software was applied for particles' length and width size measurements.

Differential scanning calorimetry

The Mettler DSC-1 instrument was used for calorimetric tests. Samples with a weight around 10 mg were scanned in heating and cooling modes from 30 to 150 °C in a nitrogen atmosphere. The heating and cooling rate was set to 10 °C /min, and the specimens were kept at a constant temperature for 5 min before cooling and second heating. The crystallization and melting temperatures, enthalpies, and crystallinities, respectively, were calculated from the experimental heating and cooling curves. The melting peak crystallinity of the PBS and the composites was calculated using the following equation:

$$\chi_m = \frac{\Delta H_m}{\Delta H_m^o (1 - W_{Cel})} \times 100\% \qquad (2.1)$$

where ΔH_m corresponds to the measured melting crystallization enthalpy of the specimen, ΔH_m^o is the theoretical melting enthalpy of 100% crystalline polymer (110.5 J/g for PBS [227]) and W_{Cel} is the cellulose filler weight fraction in the composition.

The crystallization peak crystallinity of the PBS and the composites was calculated using the following equation:

$$\chi_c = \frac{\Delta H_c}{\Delta H_m^o (1 - W_{Cel})} \times 100\% \qquad (2.2)$$

where ΔH_c corresponds to the measured cooling peak crystallization enthalpy of the specimen.

Thermogravimetric analysis

The thermogravimetric tests were performed on a Mettler TG50 instrument. Specimens about 10 mg in weight were heated in the air up to 800 °C. The material thermal stability was evaluated from the weight-loss heating curves. The weight loss was calculated, according to ASTM D3850, by using the Mettler original software.

Hydrostatic density testing

The density ρ was determined by weighing the material in air and ethanol on Sartorius KB BA 100 electronic scales equipped with a Sartorius YDK 01 hydrostatic density measurement kit. The density of the PBS and the composites was calculated using the following equation:

$$d_p = \frac{m_a(d_{EtOH} - 0.00120)}{0.99983(m_a - m_s)} + 0.00120 \qquad (2.3)$$

where m_a is the sample's measured mass in air atmosphere, m_s is the sample's measured mass when the sample is submerged in ethanol, d_{EtOH} is the density of ethanol, which was measured with the aerometer.

The theoretical density of the composites was calculated using the following equation:

$$d_t = d_{Cel}\varphi_{Cel} + d_{PBS}(1 - \varphi_{Cel}) \qquad (2.4)$$

where d_{Cel} is the density of cellulose 1.50 g cm^{-3} obtained from the literature [228], ϕ_{Cel} is the volume fraction of cellulose in the composite and d_{PBS} is the experimental density of PBS. At least 10 parallel samples were tested.

Vickers microhardness

The Vickers microhardness was measured on a Vickers M-17 1021 device equipped with an optical microscope lens magnification 4 times with a 0.20 kg load and a loading time of 20 s.

The Vickers microhardness of the PBS and the composites was calculated using the following equation:

$$H_V = \sin\left(\frac{\alpha}{2}\right)\frac{P \cdot g}{(d \cdot k \cdot n/1000)^2} \qquad (2.5)$$

where α is the diamond pyramid facet angle (136° from the specification of the instrument), P is the applied load, g is the standard acceleration due to gravity (9.807 m/s^2 was used), d is the average diagonal value of pyramid's indentation, k is the correction factor for the applied load (1.00 from the specification of the instrument for 0.20 kg load) and n is the correction factor for lens magnification used (1.30 from the specification of the instrument for 4 times magnification).

Fourier transform infrared spectroscopy performed in attenuated total reflectance mode

The FTIR was used to study the bonding and interactions between the components of the prepared PBS/rCell composites. FTIR spectra of composites were collected at a resolution of 4 cm^{-1} on a Nicolet 6700 (ThermoScientific, Germany) in the region of 800-4000 cm^{-1}. Sixteen measurements of every specimen were performed, and the average spectrum is shown; the measurement error was 1%.

Dielectric spectroscopy

The Novocontrol Alpha Broadband Dielectric Spectrometer was used to determine the dielectric properties. The prepared films were cut into a circular shape with a diameter of 25 mm for the measurements. The electrodes were set in parallel plate configuration, and frequencies ranging from 0.01Hz – 10 MHz were measured at ambient temperature (around 20°C).

Dynamic mechanical analysis

The force and displacement amplitudes and phase shifts were determined with the dynamic mechanical analyser Mettler DMA/SDTA861e. The specimens were tested at a temperature interval was -80...+80 °C, the applied force of 5N, elongation of 10μm, frequency of 1 Hz and heating rate of 3 deg/min, tension mode. Tested specimens were 8.50 mm in length, 4.00 mm wide and 0.15 mm thick, preconditioned in 50 % relative humidity at room temperature for 24 h.

Scanning electron microscopy

The morphology of dispersion in the polymer matrix was analysed with Phenom Desktop SEM (USA) for results section 3.1. The images were obtained using a 10 kV voltage setting. The surfaces of the PBS/rCell samples used for the measurements were fractured in liquid nitrogen. The surface coating was not applied.

The composite's fractured surfaces were examined using an SEM Hitachi Tabletop Microscope TM3000 (Japan) was used for results section 3.2. and 3.4. The composite specimens were fractured using liquid nitrogen and used as they were to obtain images in different magnifications with a voltage 10-15 kV. The surface coating was not applied.

For MCC powder sample (section 2.1.) TS Vega Tesca5136M (Czech Republic) was used with a voltage of 15 kV. The surface coating was not applied.

Tescan Mira\LMU (Czech Republic) was used to visualize the nanocomposites' surface morphology prepared with a fracture in the liquid nitrogen for results section 3.3. An acceleration voltage of 5 kV was used for image generation, while the specimens were fixed on standard aluminum pin stubs with an electrically conductive double-sided carbon tape. The surface coating was not applied.

Tensile testing

Tensile tests were performed at room temperature on a universal testing machine Tinius Olsen model 25ST (USA), equipped with a load cell of 5 kN at 0.2 mm min^{-1} crosshead speed. Dumbbells samples were dried in a vacuum oven for 12 h at 60 °C and successfully pre-conditioned overnight under the environmental conditions of measurement. 10 parallel measurements were performed for each composite at room temperature and ambient conditions.

For water immersion tests, samples were inserted in the distilled water and kept at 25 °C in the thermostat for 25 or 50 days, followed by removal from water and pre-conditioned overnight under the environmental conditions before measurement. 5 parallel measurements were performed for each sample.

Disintegration under composting conditions

The composite material's disintegration degree was studied under aerobic simulated composting conditions at 58 °C and water content at 50 wt.%. Thin films were cut into the sample shapes (25 mm × 25 mm x 0.10 mm), and 5 samples for each composition were sandwiched between sieves. Specimens were submerged at a depth of 5 cm in a commercial compost soil consisting of local Latvian swamp peat (Formoss, Latvia) and packed in plastic containers. The range of pH values from 5.7 to 6.3 was obtained from the measurements. The laboratory-scale test was used to determine disintegration, and before the measurements, specimens were vacuum dried.

For results section 3.1. after recovery, the samples were washed with distilled water and dried in a vacuum oven at 37 °C for 24 h. Disintegration times were selected to recover samples in 10 days intervals and after 50th day in 5 days intervals. The visual appearance of films was registered during disintegration.

For results section 3.2. specimens were vacuum dried for 2 h at 60 °C. The specimen's weight was measured before the test (reference abbreviated as 0 days) and on following days 10, 20, 30, 40, 50, 55, 60, 65, 70, 75. Average mass loss in percentage was calculated after measurements.

For results section 3.3. the recovery time of samples was every 10 days until degradation. Recovered samples were washed, dried in a vacuum oven at 37 °C for 4 h, weighed, and photographed. Simultaneously, disintegration was analysed with FTIR and DSC in the same manner as for pristine specimens described above.

For results section 3.4. specimens were vacuum dried for 2 hours at 60 °C. The specimen's weight was measured every 5 days for a total of 90 days, while reference was abbreviated as 0 days. Average mass loss in percentage was calculated after measurements.

Atomic-force microscope

Atomic-force microscope (AFM) Park NX10 (Park Systems Corporation, South Korea) in the tapping mode was used to analyse NFC dimensions. Samples were prepared from small drops of very dilute suspensions on the glass.

Surface wetting and energy

The contact angle of the pristine PBS and composite specimens was analysed with a Theta Lite optical tensiometer (Attension®, China) using the static sessile drop method. Five separate measurements with drops (2 μL) of each test liquid were deposited on the surface of the specimen, and the measurements were obtained in 30 s. Distilled water, glycerol and diiodomethane were selected as liquids and measurements were conducted at 20 °C. Total surface free energy (SFE) and its dispersive, polar components were calculated from contact angle values using Attension® original software via Owen, Wendt, Rabel and Kaelble method (OWRK). The Zisman model was used to calculate critical SFE values.

3. RESULTS AND DISCUSSION

The development and research of polybutylene succinate/cellulose composite materials were divided into four parts, which are reflected in the sections of the PhD thesis. The first section focuses on the use of recycled cellulose as a cheap filler derived from waste. Recycled cellulose was used after shredding without any further treatment and mixed in a range of 10 to 50 wt.% with PBS. The data from this section allowed to understand the optimal choice of the amount of filler for further research.

The second section uses smaller cellulose particles, such as microcrystalline cellulose and nanofibrillated cellulose. The particle size of MCC is about 10 times smaller than previously used recycled cellulose and is close to the size of wood flour (a popular waste product). But NFC is one of the most relevant and popular nanofibers of natural origin, which is already being produced in relatively large quantities in various pilot plants. In this section, NFC was freeze-dried from an aqueous solution, thus simplifying the composite manufacturing process. The results obtained with freeze-dried NFC did not yield the expected benefit, so in-depth studies were performed in the next section.

When considering the possibility of forming PBS/NFC composites, two methods were chosen: the solution method, widely used in the literature for sample preparation, and the masterbatch process, which is suitable as an industrial production method. Furthermore, the loading of NFC was reduced to a maximum of 15 wt.% to avoid agglomeration. The section investigated the amount of NFC that could be added to the polymer to improve the properties of the composite and how this process could be combined with the production of industrially viable thermoplastic polymer composites. The use of NFC, unlike the fillers discussed above, could increase the cost rather than reduce the cost of composite material, but it is possible to obtain unique applications and excellent properties that are not provided by micro-sized fillers.

The fourth section deals with a more complex variant of composite production, which involves adding a modifier to the polymer and cellulose system. For this section, a high loading of filler (70 wt.% MCC) was chosen to maximize the impact on the properties depending on the type of modification. Modification can make the production process more expensive and complex, so it can be justified by reducing the required mass fraction of bioplastic. As an additional benefit from the modifications, the possibility of regulating the rate of biodegradation of composite materials was observed.

3.1. Sustainable tetra pak recycled cellulose/poly (butylene succinate) based woody-like composites for a circular economy

Long term sustainability requires the elimination of waste products and their integration in the circular economy according to goals set by the European Union. Such is the case with Tetra pak one of the world's most extensively used food packaging materials. More than half of the Tetra pak packaging ends up in the landfills due to the complicated disposal that requires special processing plants. This chapter aims to investigate recycled cellulose (rCell) that has been separated from polypropylene and aluminum in the industrial processing plant as a structural

filler for functional biocomposites. Cellulose-based waste products are widely used as filler materials for the composites classified as wood-plastic composites (WPCs) and are one of the leading materials for sustainable building materials, furniture, and packaging industry. From bio-based and biodegradable polymers, poly(butylene succinate) (PBS) has comparable mechanical properties to polyethylene and polypropylene as a matrix for the composites. Thus, this study proposes a novel application route for rCell obtained during the Tetra pak recycling process and evaluation of its performance. High filler loading from 10 to 50 wt.% has been used in the melt blending process to prepare 5 compositions that contain 55 to 75 % bio-based carbon content. Life cycle inventory has been combined with excessive thermal and mechanical analysis to assess the composite's suitability for various applications, including submerging in water.

3.1.1. Material processing and composite formulations

The PBS/rCell composites were processed by melt compounding with Brabender® Mixer 50EHT thermoplastic mixer. The screw rotation speed was set to − 60 rpm, heating to – 130 °C for all zones, mixing time − 5 min. Altogether, five compositions were obtained: PBS/rCell composites 10, 20, 30, 40, 50 wt.% of rCell. The materials are characterized by the recycled component 0-50 wt.%, bio-based component 50-100 wt.% and bio-based carbon content 50-75% (see Table 3.1.). The processed composite materials were cut into pieces and compression molded with Carver CH 4386 to obtain film specimens. The processing was done at 140 °C; granules were preheated for 2 min and compressed under 3 metric ton pressure for 3 min followed by rapid cooling between thick steel plates with the total weight of 30 kg. The injection molding was performed with previously granulated composite, and the temperature was set at 190 °C for all heating zones. Dumbbell specimens were obtained from the injection molding and used for the tensile test. At the same time, films were prepared with the thickness of 0.1 mm for dynamic mechanical, denigration measurements and 1.0 mm for density, calorimetric, thermal, and dielectric properties.

Table 3.1.

The prepared PBS/rCell composites and their bio-based carbon content.

Sample	Recycled component, wt.%	Bio-based component, wt.%	Bio-based carbon content, %
PBS	-	100	50
10rCell	10	90	55
20rCell	20	80	60
30rCell	30	70	65
40rCell	40	60	70
50rCell	50	50	75

3.1.2. Life cycle inventory
Method

The life cycle inventory (LCI) study was carried out in compliance with the ISO 14040 and ISO 14044 standards, where overall guidelines were provided for conducting LCI and LCA studies.

Goal and scope

The goal of the LCI study was to carry out a cradle-to-gate for PBS/rCell composites −10 wt.% and 50 wt.% of rCell production to be further involved in an LCA for PBS/rCell composites. In the LCI stage, inputs and outputs within the system's boundary are identified and quantified [ISO 14040 and ISO 14044].

Functional unit

The functional unit (FU) for PBS/rCell composite production was one kilogram (1 kg) of composite – 10 wt.% and 50wt.% of rCell. All input and output data, which are known from the laboratory manufacture of the 10 wt.% and 50 wt.% biocomposite, were included in functional unit.

System boundary

The system boundary of PBS/rCell composites −10 wt.% and 50 wt.% of rCell production is presented in Figure 3.1. The system boundary considers all the energy and material inputs into, and environmental outputs from, at the cradle-to-gate processes associated with the laboratory manufacture of the PBS/rCell (10 wt.% and 50 wt.% of rCell) biocomposite: drying of PBS and rCell, grinding of rCell pulp, processing of PBS/rCell composite by melt compounding, compression molding (CM) or injection molding (IM) of PBS/rCell pellets. Drying of PBS and rCell and grinding of rCell pulp are the two steps involved in the raw material processing of inputs, while manufacturing of the biocomposites can be separated into melt compounding, compression, and injection molding stages. The challenge of the PBS/rCell biocomposite materials is a lack of real products and applications. The bio-based PBS composite is considered as very perspective material that will replace fossil-based analogs;

while real products are still to be developed continuously. As a result, cradle-to-grave LCI is impossible at this stage of the development.

Table 3.2. presents the LCI flows for manufacturing the two biocomposite compositions at the laboratory scale combined with the product performance analysis flowchart. For LCI analysis two compositions have been selected: 10 wt.% and 50wt.% rCell. While performed tests and structure analysis methods are also listed.

The raw-material processing in composition with 10 wt.% rCell consumes 5.2 kWh of energy (about 18 % in CM process and 16 % in IC process from total energy consumption) for the laboratory-scale manufacture. As appropriate in the case of composition with 50 wt.% rCell: 10.0 kWh (about 30 % in CM process and 27 % in the IC process from total energy consumption). Among the processes involved in the composite manufacture, is the most energy-intensive process as it consumes in composition with 10 wt.% rCell about 82 % (MC molding) and 84 (IC molding) and in composition with 50 wt.% rCell about 70% (MC molding) and 73% (IC molding) of the total energy demand. Solid waste accounts for both composite processing routs are about 5.5 % (0,06g) that can be reused. Fugitive emissions from component material processing, blend compounding, and drying were not tracked during the lab-scale manufacture. There is no significant waste during processing, while the biocomposite's waste received at IM and CM is again processed into samples for further testing.
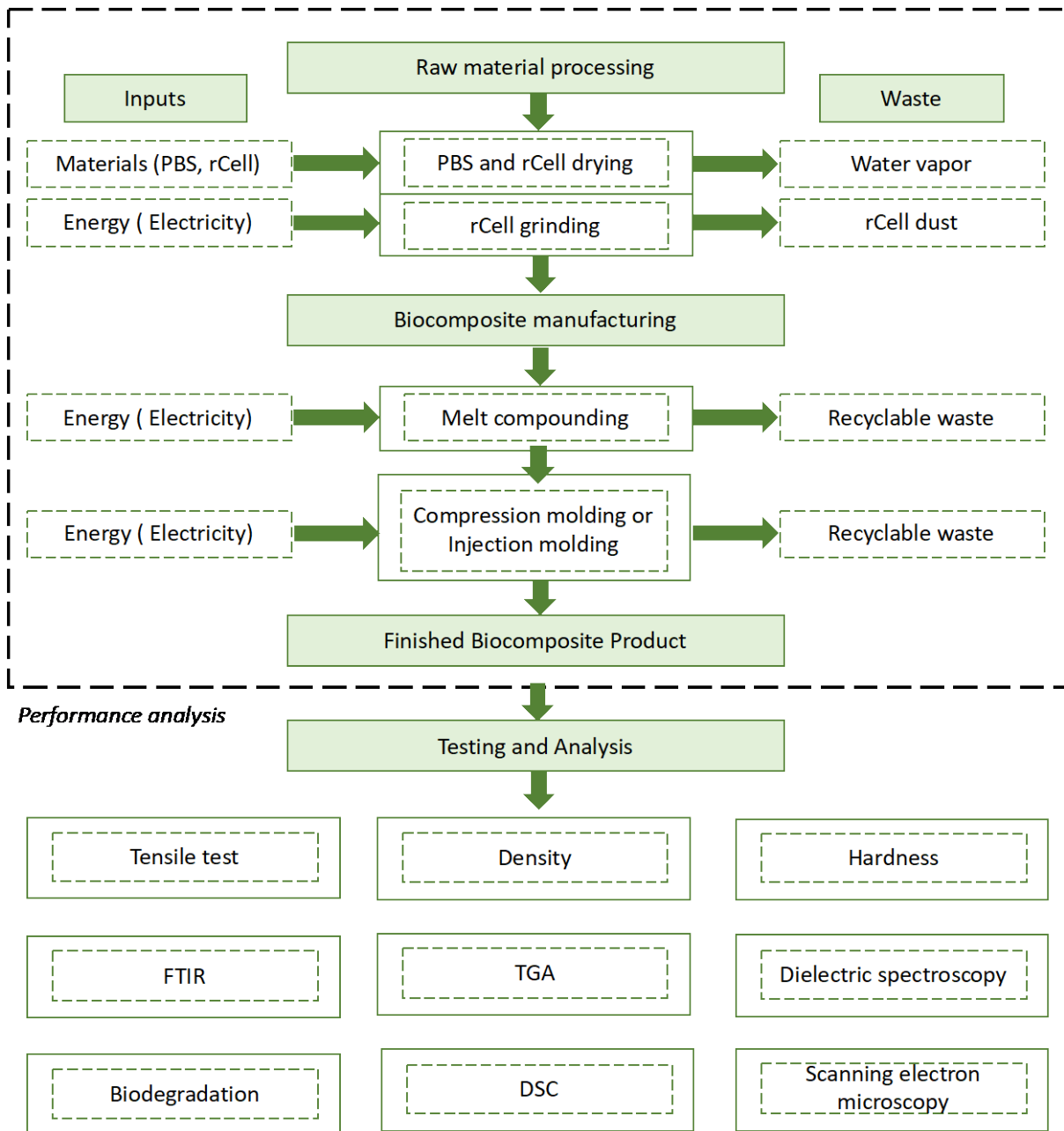
Figure 3.1. The system boundary and performance analysis flowchart of PBS/rCell composites

Table 3.2.

LCI flows for the laboratory manufacture of the 10 wt.% and 50 wt.% biocomposite's compositions.

Imput	Unit	Quantity per declared unit (1 kg of composite)	
		10 wt.%	50 wt.%
Materials			
PBS	kg	0.95	0.53
rCell (5–6 % moisture content)	kg	0.13	0.58
Electric energy			
Raw material processing			
Drying	kWh	4.00	4.00
Grinding	kWh	1.20	6.00
Total	kWh	5.20	10.00
Composite manufacturing			
Melt compounding	kWh	16.25	16.25
Compression molding (CM)	kWh	7.00	7.00
Injection molding (IM)	kWh	10.40	10.40
Total energy CM process	kWh	28.45	33.25
Total energy IM process	kWh	31.85	36.65
Emissions			
Solid waste	kg	0.06	0.06
Dust	kg	0.01	0.02
Water vapor	kg	0.01	0.03

3.1.3. Determination of the structural properties

Table 3.3.

Vickers micro hardness, the theoretical density, and the experimental density of pristine PBS and PBS/rCell composites.

W_{rCell}, wt.%	φ_{rCell}, vol.%	d_p, g/cm^3	d_t, g/cm^3	Δ, %	d_{poly}, g/cm^3	H_V, MPa
0	0	1.365	1.365	0	1.365	255±31
10	15	1.337	1.386	3.6	1.308	567±40
20	30	1.329	1.406	5.6	1.256	490±60
30	45	1.323	1.426	7.5	1.179	488±19
40	60	1.320	1.446	9.2	1.050	431±15
50	75	1.313	1.466	11.2	0.752	365±50

Figure 3.2. shows the typical example of the obtained optical microscopy (a) and SEM (b) images of rCell, measured sizes distributions of rCell (c-d), PBS/rCell composite optical microscopy (e) and SEM (f) images. As it was previously stated, the rCell are characterized by average length − 200 μm, average width − 20 μm. The microstructure of the PBS/rCell composite is shown in Fig.1(f). Table 3.3. summarizes the weight content percentage of the cellulose (W_{rCell}), volume content percentage of the cellulose (φ_{rCell}), Vickers microhardness (H_V), the theoretical density (d_t), the apparent polymer density (d_{poly}), and the experimental density (d_p) calculated according to descriptions in the methods section.

It corresponds well with the observed decrease of measured experimental composite density and calculated polymer apparent density (see Table 3.3.). The rule of mixtures was used to calculate the theoretical density of the composites and used as a reference [229]. The polymer structure can be described by the apparent density d_{poly} of the polymer. The polymer density contribution in the composite is calculated similarly as in [230] and according to the equation:

$$d_{poly} = \frac{d - d_{Cel} \cdot \varphi_{Cel}}{1 - \varphi_{Cel}} \qquad (3.1)$$

The PBS/rCell's experimental density decrease is considered from the possible agglomeration of cellulose particles and the formation of voids and defects in the composite microstructure by rCell particles addition, as observed in Fig.3.f and reported in the literature [231,232]. Similar factors have caused the gradual decrease of the polymer density. The divergence Δ of the experimental and calculated composites density values showed a substantial increase with higher contents of rCell. An increase in rCell content leads to significant depression of the apparent polymer matrix density in comparison to the initial polymer density due to the heterogeneity of the matrix structure. Value of Δ for the composition PBS/rCell 50 wt.% is almost 11%. This corresponds that the higher filler loadings develop more structural defects, voids, and heterogeneities in the composites (Figure 3.2.f), leading to the decrease in polymer material density.
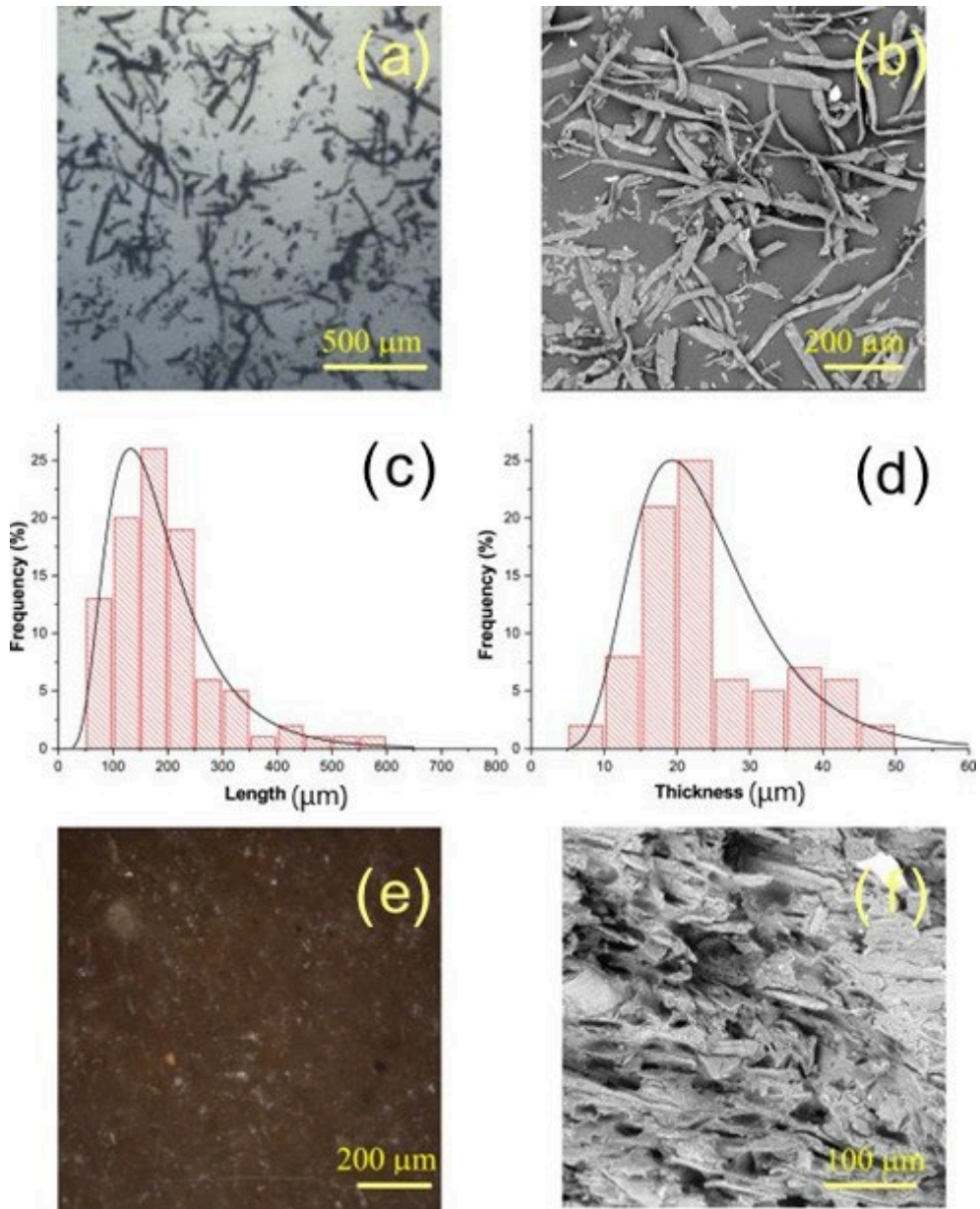
Figure 3.2. rCell particles: (a) optical microscopy image, (b) SEM image; rCell size distributions: (c) length, (d) thickness; 40rCell composite: (e) optical microscopy image, (f) SEM image.

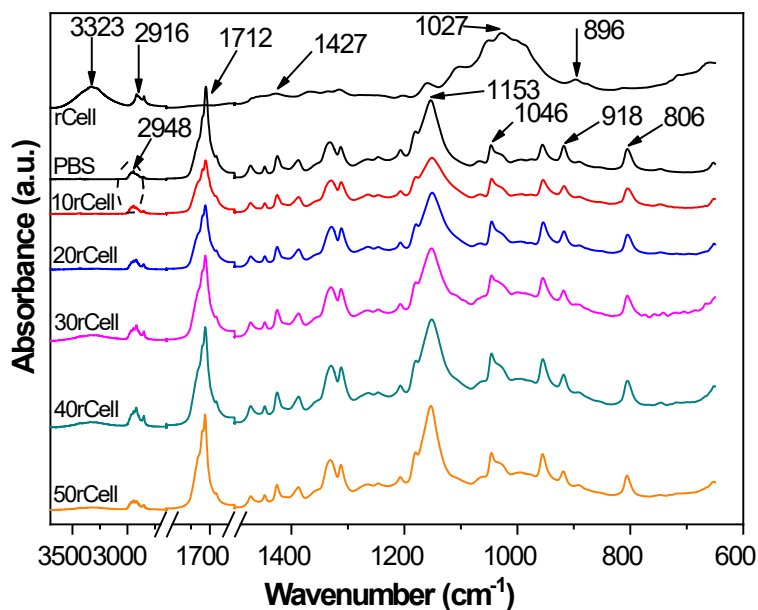### 3.1.4. Determination of filler and matrix interaction

Figure 3.3. FTIR spectra of PBS/rCell composites.

The FTIR spectra of the prepared PBS/rCell composites is shown in Figure 3.3. The characteristic spectra for aluminum and polyethylene residues in the ground tetra pak rCell filler were not observed in the obtained FTIR spectra that testify good purity of the rCell filler. FTIR spectra PBS/rCell composites of the different compositions had a similar shape. The cellulose's OH groups stretching vibration is the peak at 3323 cm^{-1} [233]. FTIR absorption band at 896 cm^{-1}, assigned to C–O–C stretching at β-(1α4)-glycoside linkages, is designed as an "amorphous" absorption band, an increase in its intensity occurring in the amorphous cellulose [234]. The presence of methylene groups in the PBS backbone is described as stretching vibration at 2948 cm^{-1} (Figure 3.4.a) [156]. While 1712 cm^{-1} region (Fig 3.4.b), also seen in this figure, is attributed to C=O stretching vibrations of the ester group in the crystalline domain, and the peak located at about 1738 cm^{-1} is C=O stretching in the amorphous region [79]. Ester group is known to work as hydrogen bond acceptor and has a lone electron pair which can form hydrogen bonding with hydroxyl group from cellulose. Cellulose mechanical properties come from its strong network of hydrogen bonding between cellulose hydroxyl groups which is hard to disrupt with molecules that lack strong polar groups. The change of the intensities for the 1712 cm^{-1} peak indicates that in lower concentration hydrogen bonding between cellulose and PBS is more unlikely to happen but in higher concentration there is a significant increase in peak intensity, indicating the presence of hydrogen bonding between filler and matrix. The peak at 1153 cm^{-1} (Figure 3.4.c) is assigned to the asymmetrical stretching vibration of the C-O-C bond, and the bands at the 1046 cm^{-1} region were assigned to O–C–C stretching vibrations [156,235]. While the bands at 918 an 806 cm^{-1} have been attributed to bending vibrations of C-OH from the carboxylic acid group [156]. The peak close to 2900 cm^{-1} was observed for cellulose with the experimental measurement at 2916 cm^{-1} and is attributed to C-H stretching vibrations, and it can clearly be differentiated from PBS backbone absorption described above [236]. FTIR absorption peak intensity at 1427 cm^{-1}, assigned to asymmetric CH$_2$ bending vibration of the

crystalline chain domains, increases by the higher cellulose content and reveals the formation of hydrogen bonding interaction between the components (Figure 3.4.a) [234]. The C-O-C and C=O bond intensity is also pronounced after cellulose filler incorporation due to the possible adsorption interactions of polymer chains with the cellulose surface (Figure 3.4.c). This increase in its intensity could reflect the trans-crystallization after the cellulose incorporation, while the overall degree of crystallinity of the composite samples, which was testified also by thermal analysis, decreases (see Table 3.4.).
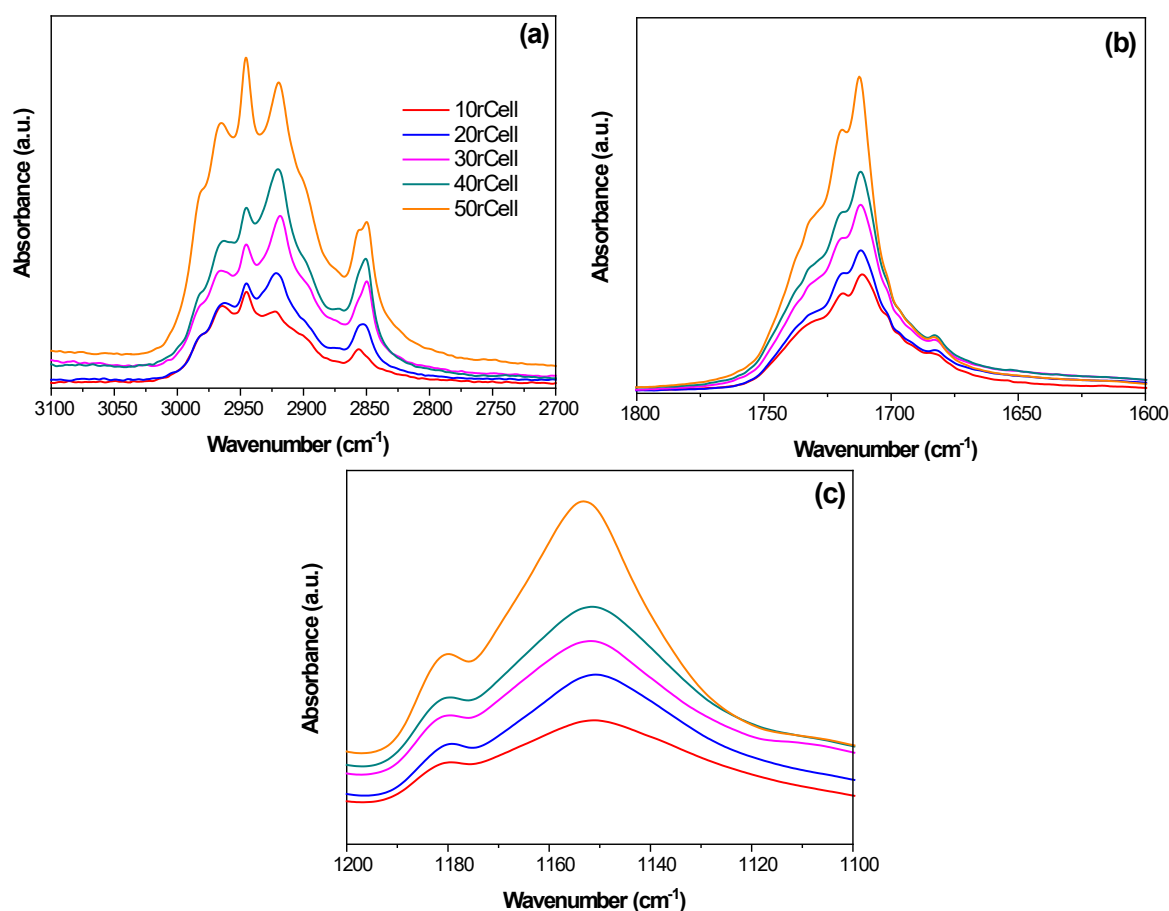
Figure 3.4. FTIR spectra of (a) CH_2, (b) C=O and (c) C-O groups for PBS/rCell composites.

3.1.5. Mechanical properties and effect of immersion in water

The mechanical and viscoelastic properties of the PBS/rCell composites are directly dependent on the developed microstructure features. The loading of 10 wt.%. of rCell into the PBS has resulted in almost a 2-fold improvement of the hardness values (see Table 3.3.). In contrast, hardness value decreases gradually with rCell loading up to 50 wt.% into the polymer. This observation well corresponds to the common forms of the defects, the voids and the heterogeneities in the polymer/cellulose composite material with high cellulose filler loadings [237]. The elasticity of the composites showed a tendency to increase significantly as higher amounts of cellulose are mixed into the PBS/rCell composite. This is in line with previous wood polymer composites studies [194,238,239]. The prepared PBS/rCell composites remarkably enhance Young's modulus E (Figure 3.5.a). The E value rises almost monotonically with the

higher rCell content. It indicates an almost 2-fold increase and the 3-fold in E for the samples containing 30 wt % and 50 wt.% of the rCell. The tensile strength at break σ decreases significantly after the rCell filler incorporation (Figure 3.5.b). The composition with the 50 wt.% of the rCell showed a 2-fold decrease of the σ value. The ductility of the composite expressed as tensile strain at break ε, decreased from 30% to 3% when rCell loading reached 50 wt.%. This observation is common for polymer composites filled with cellulose loading above 20 wt.% [240]. The immersion in water has a remarkable influence on the tensile properties of all the tested compositions. The received data indicates that the quality of cellulose-based structures is significantly impacted by moisture content [241]. It results in some decrease in the ductility, and some depression in the elasticity, while the strength of the composite remained almost unchanged after 50 days of immersion in water tests. Drop in the composite ductility can be facilitated by swelling and subsequent shrinking of the cellulose particles during the immersion and drying steps [242]. It is reported that the water absorption in the polymer composite filled with cellulose is inherently higher than that of a neat polymer because the water molecules can more readily penetrate the composites through existing voids and heterogeneities in the structure [243]. The observed high voids content in the composite sample PBS/rCell 50 wt.% can provoke the tensile properties to decrease.

Moreover, the PBS polymer hydrolysis can occur during water immersion, which can significantly accelerate the degradation of the polymer matrix and diminish the overall properties of the composite material [244]. Complete polyester degradation is possible in the water that was reported by [245]. The composite material has remained stable after 50 days water immersion test performed at room temperature of 25 °C. The test temperature is very crucial to the decomposition process. It is predicted that decomposition could be facilitated at higher temperatures, which is also confirmed by efficient material's decomposition testing at 58 °C in compost soil. The cleavage of the macromolecules could occur initially in the amorphous polymer, while the polymer crystals remained unaffected at this decomposition stage, which could contribute to the more rigid structure of the composites and some increase in tensile characteristics [246]. As well as, the polymer effectively shielded cellulose filler reinforcement, and it was not compromised, resulting in it retaining its structural load-bearing properties [247].
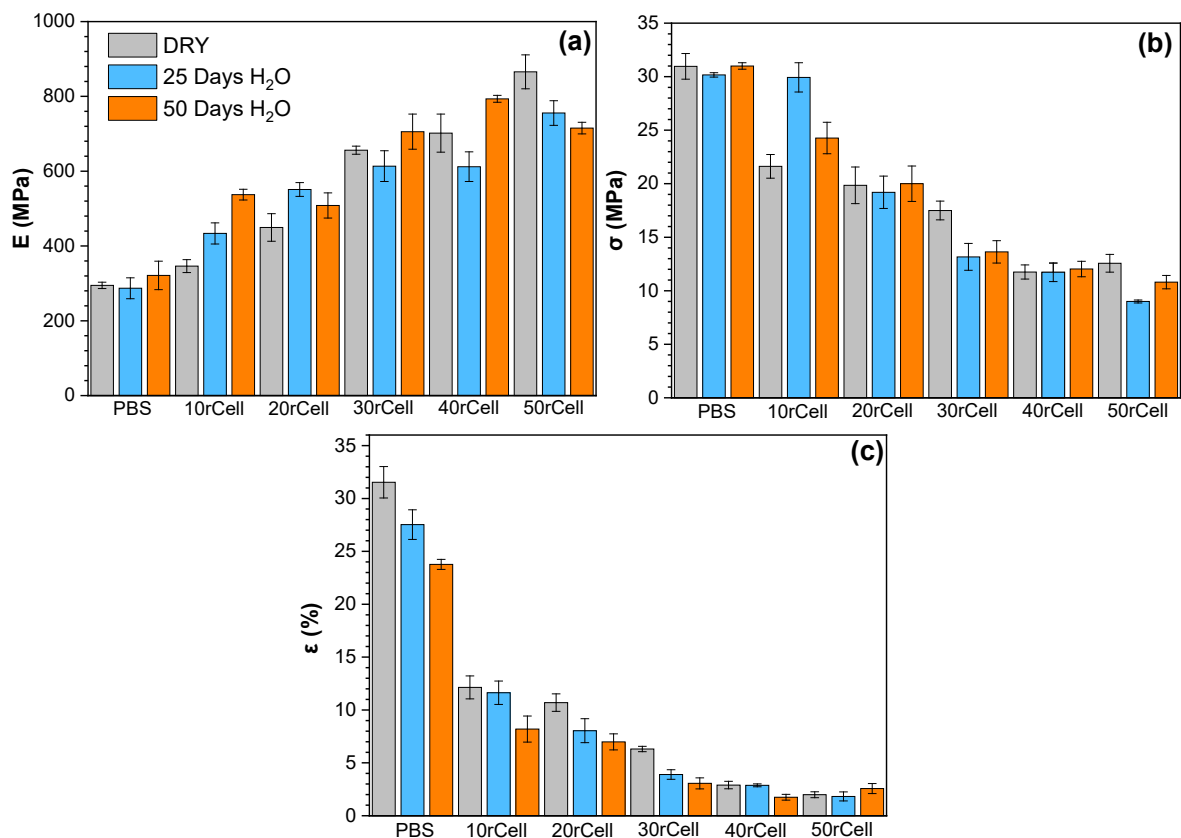
Figure 3.5. Tensile properties for PBS/rCell composites: (a) Young's modulus E; (b) tensile strength σ; (c) strain ε.

3.1.6. Crystallization behaviour of composite

Table 3.4.

Thermal properties of PBS/rCell composites

Sample	T_m, ºC	T_c, ºC	χ_m, %	χ_c, %	$T_{10\%}$, ºC	$T_{50\%}$, ºC	T_{deg}, ºC
rCell	-	-	-	-	317	484	340
PBS	114	81	65	63	366	395	397
10rCell	115	88	43	45	363	397	401
20rCell	116	89	32	36	354	395	401
30rCell	118	90	27	26	353	397	405
40rCell	117	90	18	19	344	394	402
50rCell	115	90	16	14	329	384	392

Figure 3.6. presents the DSC second heating (a) and cooling (b) of the PBS and the PBS/rCell composites. The results for the melting temperature (T_m), crystallization temperature (T_c), the crystallinity from the second heating melting peak (χ_m) and the crystallinity from the crystallization peak (χ_c) are reported in Table 3.4. A broad melting peak is identified from almost 90 ºC and reaches 125 ºC for the neat PBS. The melting temperature T_m of the PBS is

114 °C. The cellulose loading does not affect the T_m of the composite material. The presence of the cellulose particles commonly induces the nucleation of the polymer chains and the formation of the trans-crystalline phase on the cellulose surface [248]. The crystallization peak of the composites increases almost 9 °C; T_m shifts to the higher temperatures from 81 °C for the PBS to up 90 °C for the PBS/rCell 30 wt.%. The polymer composite crystallization also starts at higher temperatures than for the neat polymer. However, the crystallinity χ_m and χ_c values revealed an apparent decrease when rCell was incorporated into the PBS matrix. The addition of more than 10 wt.% of cellulose components could destroy the crystallinity of PBS polymer [249]. The strongly disrupted polymer chain mobility in the cellulose's interface significantly disrupts the crystals' growth in the PBS/rCell composite. For example, it is found that the χ_m decreased from 65% for the neat PBS to 16% for the PBS/rCell loaded with 50 wt.% of cellulose.
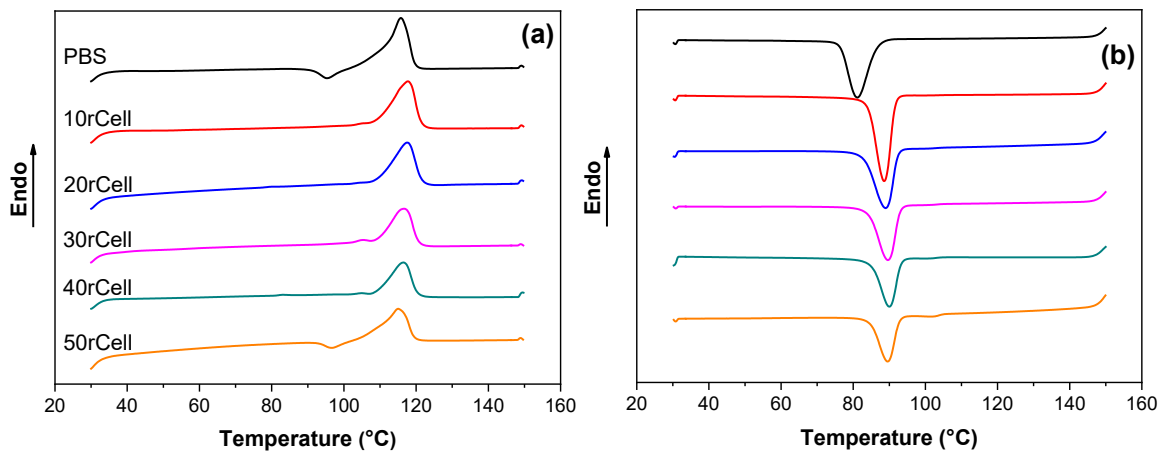

Figure 3.6. DSC curves of PBS/rCell samples: (a) second heating, (b) cooling.

3.1.7. Investigation of thermal stability

TGA was used to investigate the thermal sensitivity and degradation properties of PBS/rCell composite materials and the influence on composition with the increased filler content. Figure 3.7. showed TGA (a) and DTG (b) curves of PBS/rCell composites. Table 3.4. summarizes TGA data from which the $T_{10\%}$ represents the temperature of thermal degradation for 10% weight loss, $T_{50\%}$ represents the temperature of thermal degradation for 50% weight loss, T_{deg} represents the temperature at maximum weight loss rate. It reveals that the maximum degradation temperature for rCell is 340 °C, and the neat PBS is 398 °C. The cellulose incorporation induces lowered thermal stability for the composites [250,251]. PBS curve shows single-stage degradation. The degradation of PBS starts with small weight loss above 200 °C, which has been attributed to the degradation of oligomers present in PBS, while the main degradation of PBS starts at around 350 °C and is explained by a random cleavage of the ester bond due to the transfer of hydrogen atom from β-CH [252]. In turn, the PBS/rCell composites show similar thermal behaviour, except for PBS/rCell 50 wt.% having two-stage degradation, which is indicated in the DTG curve. The thermal degradation process of the composites is defined primarily by the PBS polymer chain degradation, while PBS/rCell 50 wt.% composite is affected by cellulose thermal degradation. With the increase of the cellulose content, it can be observed that the curves shift to lower temperatures. This is pronounced when $T_{10\%}$ is

observed for 50% rCell, which is 329 °C resulting in a 37 °C decrease compared to pristine PBS. If we take $T_{50\%}$ into consideration, 50% rCell stands out having 10 °C lower temperature compared to PBS and other composites. The thermal degradation temperature T_{deg} is 397 °C; while the PBS/rCell composites, T_{deg} remain almost unaffected from the rCell content in the composite materials. For best thermal properties and maximum cellulose loading, 30 to 40 wt.% compositions show optimum performance.
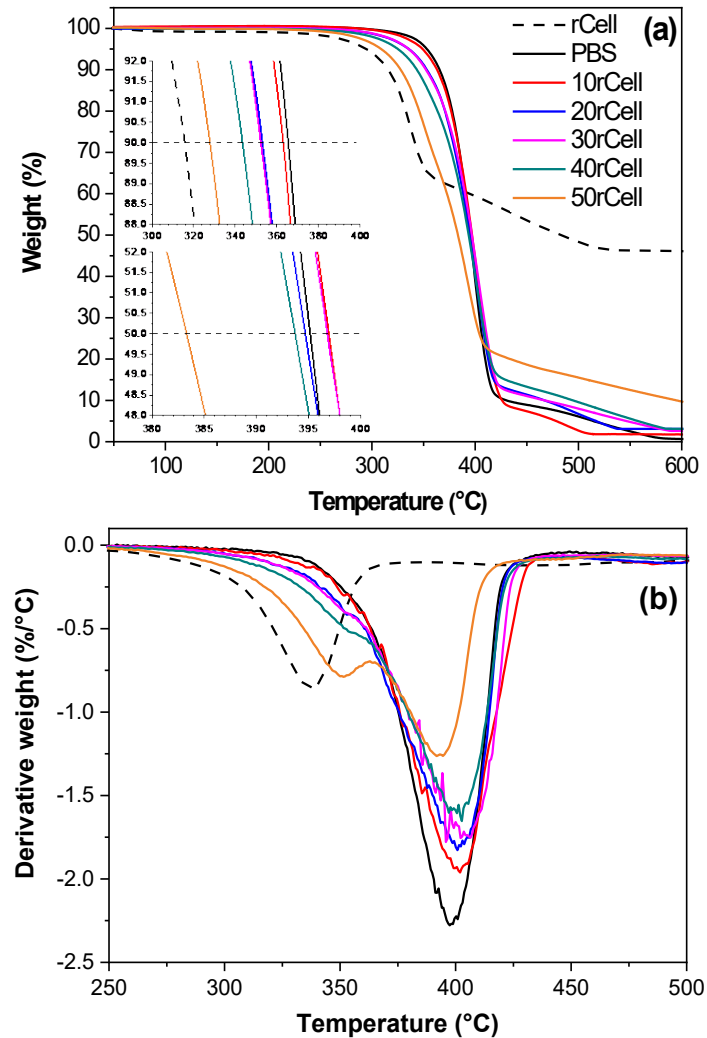
Figure 3.7. (a) TGA curves and (b) DTG of PBS/rCell composites.

3.1.8. Investigation of viscoelastic properties

Viscoelastic properties of the PBS/rCell composites were investigated by dynamic mechanical analysis. Storage modulus E', loss modulus E'' and the loss factor tanδ as a function of temperature are shown in Figure 3.8. Results show a tremendous increase in the measured viscoelastic characteristics (E', E'', tanδ) in all investigated temperature ranges. As more rCell content is loaded into the polymer, the respective improvement of composite properties to store energy reversibly, transformed energy irreversibly and to dissipate energy is to a greater extent related to the reinforcing effect of the used filler. The increase of the content of the fiber filler featured high geometrical dimensions aspect ratio improves reinforcing efficiency significantly [253]. For example, in the case of rCell loading 50 wt.%, the composites E', E'' and tanδ at

room temperature (20 °C) have increased about 3, 6 and 2-fold, accordingly. While loss modulus E'', which characterizes the dissipated energy into heat and loss, has a maximum at the temperature range of -40 to 10 °C. The relative heights of the loss factor tanδ are proportional to the energy dissipation property of the material. It shows at temperature -10 °C almost the 30% decrease in tanδ value for composites with rCell content 20-50 wt.%. Compositions 20rCell, 30rCell, 40rCell, and 50rCell show enhanced values of E', E'' in the whole measured temperature range, meaning that well-dispersed fiber network and reinforcement is established.
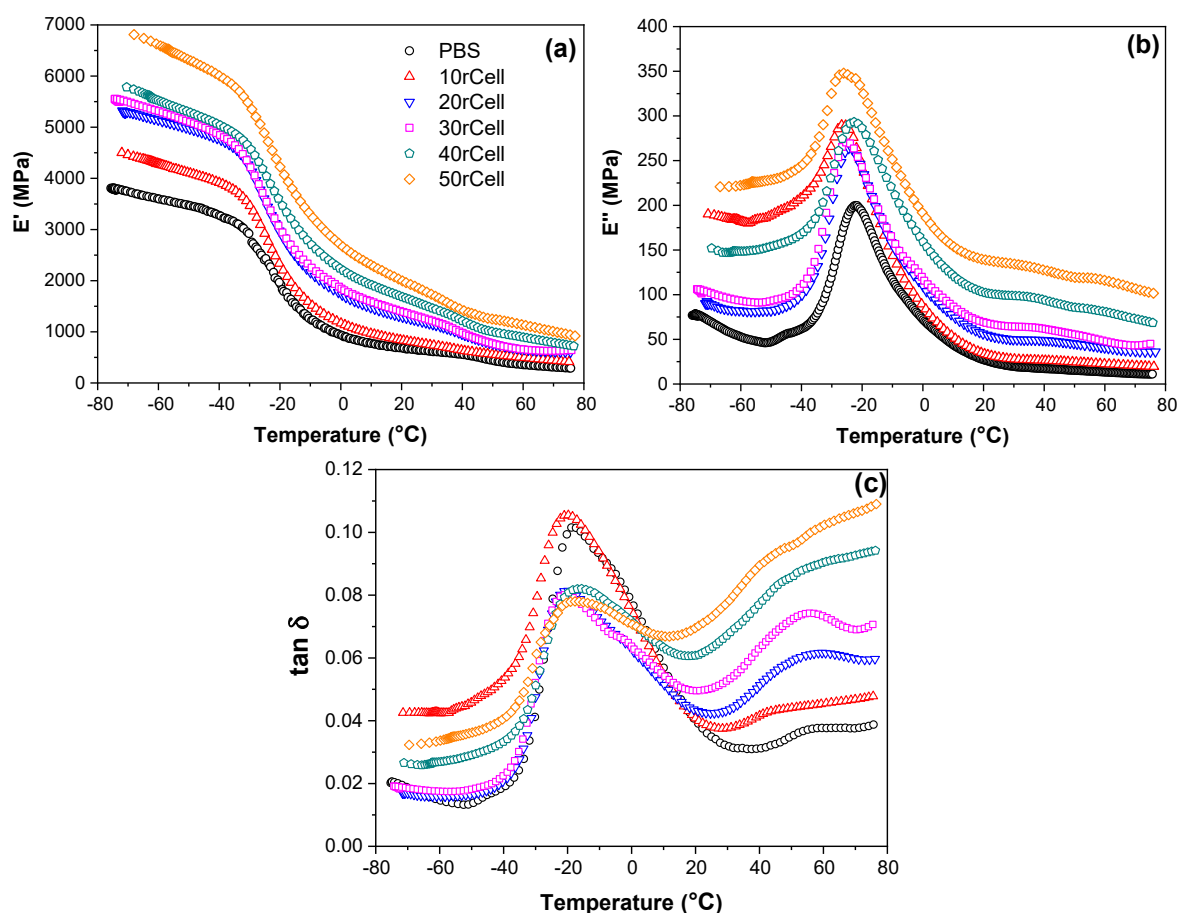
Figure 3.8. DMA curves of PBS/rCell samples: (a) storage modulus E', (b) loss modulus E'' and (c) loss factor tanδ.

3.1.9. Investigation of dielectric properties

Figure 3.9. shows the dielectric properties of the PBS/rCell composites. It was observed that the dielectric permittivity ε' (Figure 3.9.a) tended to increase starting in all frequencies range as larger content of rCell filler is loaded into PBS. It can be seen in Figure 3.9.b that the dielectric loss permittivity ε" also showed an increase after the addition of rCell. The ε' and ε" values decrease with the increasing of the applied field frequency. It corresponds to the increase of the amorphous fraction with the frozen chain mobility in the polymer matrix of the composite [254]. In turn, Figure 3.9.c shows the conductivity σ of the PBS/rCell composites. The observed σ increase with higher frequency attributes to the common electrical insulators' behavior due to the polarization of accumulated permanent dipoles and induced dipoles in the polymer chain

[255]. The observed dielectric properties of the PBS/rCell composites indirectly indicate that aluminum was separated successfully during Tetra pak recycling.

Figure 3.9. Dielectric properties for PBS/rCell composites: (a) real permittivity ε'; (b) loss permittivity ε'' and (c) conductivity σ.

3.1.10. Determination of the compositing performance

Degradation of the PBS and PBS/rCell composites under the composting conditions were used to evaluate the disintegrability in natural environments. The visual evaluation of the samples at different degradation times is shown in Figure 3.10. Considerable changes in all sample's visual appearance are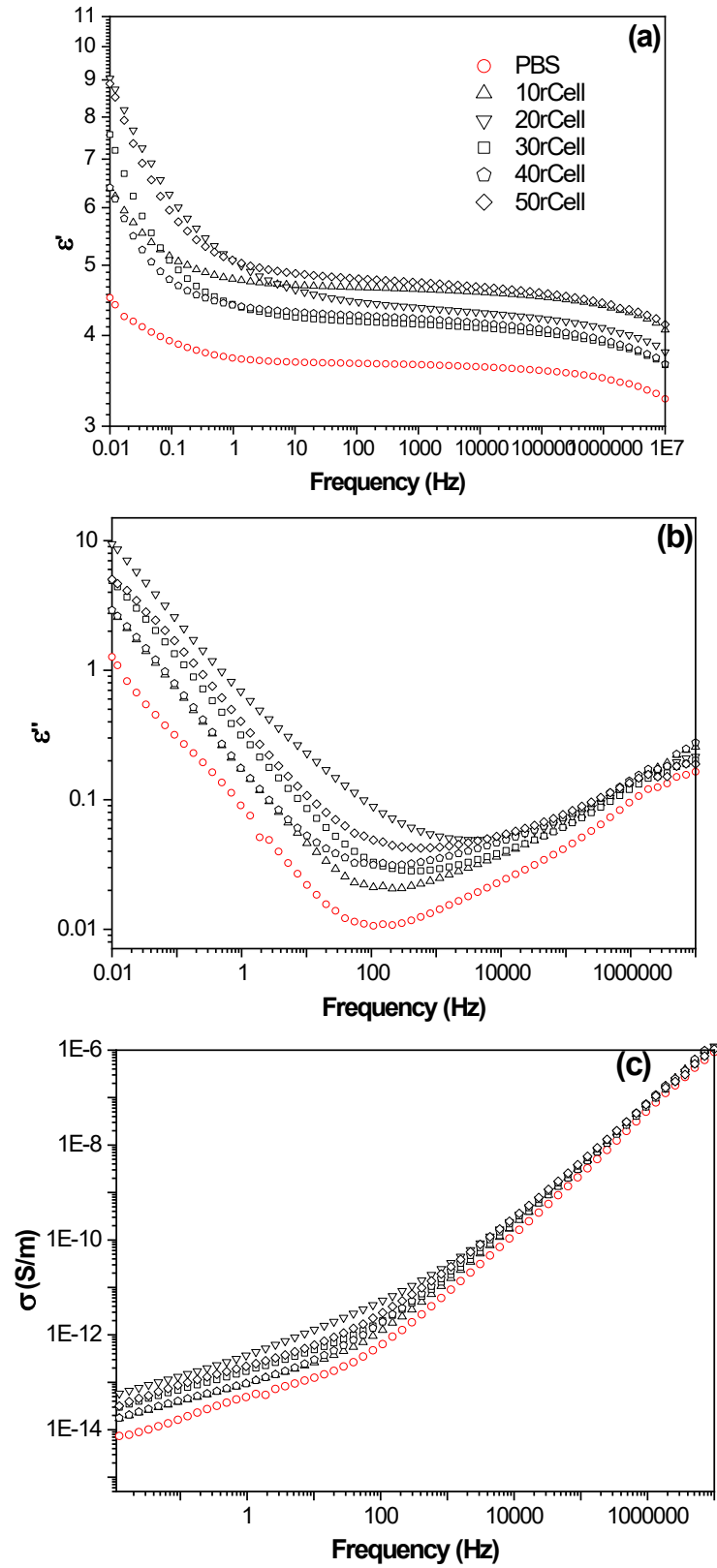 obtained already after 10 days. At the same time, the composite samples compared to the neat PBS showed evident brittleness and size reduction after 30 days. After 70 days of evaluation, all the samples were completely degraded under the composting condition at 50 °C. Figure 3.11. shows the disintegrability values (%) of the evaluated samples as a function of the burial time. A clear decrease in the degradation time is observed for the PBS/rCell composites in comparison to the neat PBS. The higher content of biodegradable cellulose in the material strongly facilitates the degradation of the PBS/rCell composites. This contribution relates to the quicken water absorption from the composting medium, resulting in an evident increase in disintegrability values for the composite samples. Similar observations were reported by [87,256]. The observed decrease in the crystallinity of the polymer matrix also could forward the degradation and disintegrability of the composite samples. Fortunati et al. indicated that the polyester hydrolysis begins in the intrinsic amorphous regions of the polymer and significantly accelerates the degradation of a polymer material [257]. Similar behavior of progressive degradation of samples after loading with the cellulose fillers was also reported by several researchers [245,257,258]. Finally, it was observed that after 70 days of the degradation test, all samples reached complete degradation. These observations testified to the possible application of the processed composite materials as biodegradable materials with disintegration times up to 70 days in controlled environmental conditions.
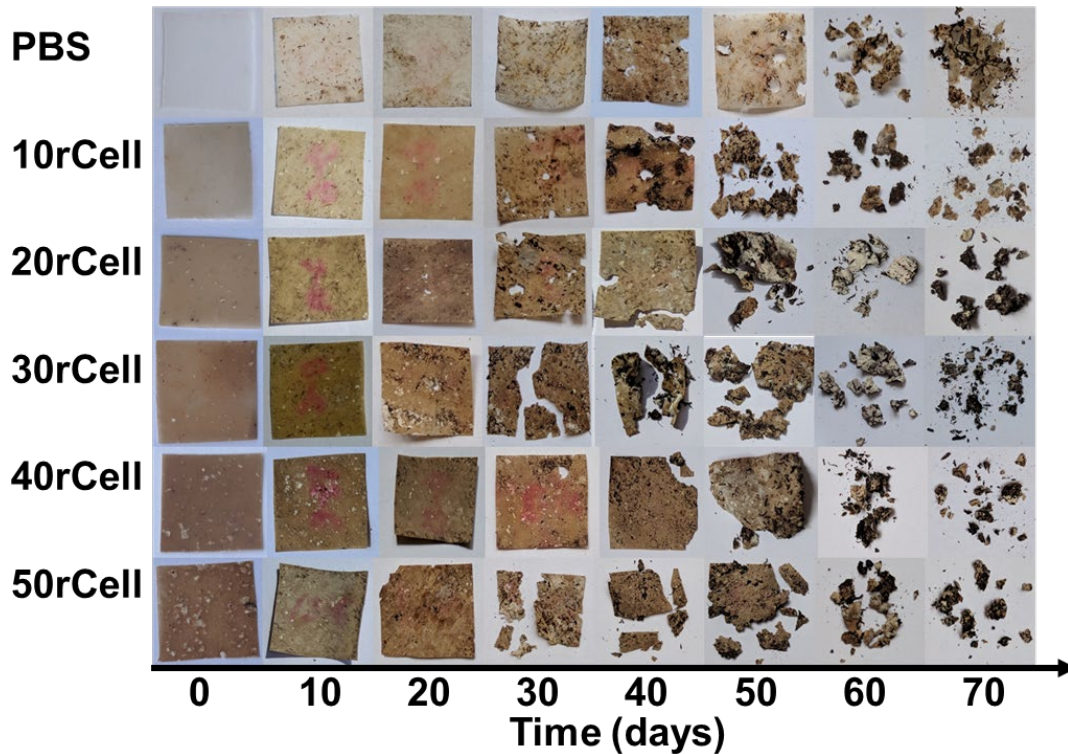

Figure 3.10. Photos of PBS/rCell composite films during biodegradation studies in soil burial test conducted in composting conditions.
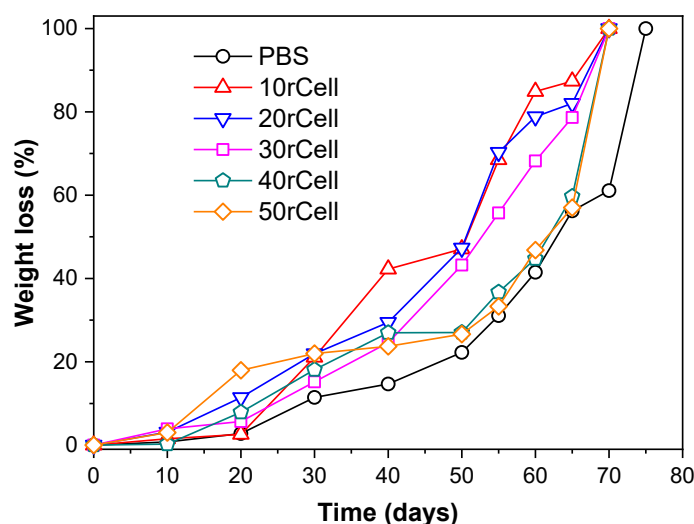
Figure 3.11. Disintegradability for PBS/rCell composites at different times.

3.1.11. Implications

The global demand for new sustainable materials and technologies is continuously rising, particularly in conjunction with the escalating demand of replacing petroleum-based products as a result of the foreseen shortage in oil feedstock and the increased ecological consciousness. Consequently, forestry resources and wood are surfacing as a viable alternative to overcome these challenges. Therefore, forest-based industries are constrained to develop high-value products and materials through innovative and sophisticated technologies. Polymer-based products have been developed as alternatives within the forest-based industries sector, using wood as the main component. Non-environmentally friendly petroleum-issued polymers (polyolefins) constitute the main component of such woody like products. For interest to the present research, the fabrication of common wood polymer composites (WPC) typically involves mixing of wood flour, petroleum-based plastic pellets and additives before processing the resulting composites into the desired final material. The forest-based industries are suffering from a significant lack in innovative development in terms of 100% green biocomposites and their sustainable fabrication processes. EU Industrial Strategy for sustainable reindustrialisation demands the implementation of the circular bioeconomy. Manufacturers of wood-plastic products such as wood-like panels and boards (see Figure 3.12.) should explore circular alternatives in order to substitute the fossil polyolefin plastics and wood flour fillers. The bio-based polymer (bioPBS synthesized from biomass) and recycled cellulose (rCELL recovered from Tetra pak waste) are 100% renewable and 100% recyclable components that could be considered for the use for manufacturing of sustainable biocomposite material. This implies that raw timber consumption could be reduced, and more sustainable forestry can be maintained. Herein, we show that using the proposed sustainable raw components and replacing fossil-based components with bio-based and recycled components can improve the final biocomposite material's thermal and mechanical properties. Summarizing, the proposed biocomposites consist of the recycled component 0-50%, the bio-based component 50-100% and the bio-based carbon content 50-75% (see Table 3.1.). By varying the PBS and rCell content in the composite, we were able to modify the structure and exploitation performance of the

composite material. The obtained biocomposites could be manufactured by extrusion, injection, and printing fabrication techniques.

Figure 3.12. Melt compounded wood polymer composites decks and sheets profiles.

3.1.12. Summary

This study investigates the performance of woody-like composites' performance consisting of the bio-based poly(butylene succinate) and 10-50 wt.% recycled cellulose obtained from the industrial Tetra pak processing plant. Based on the experimental results, the following conclusions are presented:

1. The addition of 50 wt. % of rCell into PBS leads to a 2-fold improvement of the hardness of composite compared to the neat PBS. The Young's modulus increases almost 3-fold, while tensile strength and ductility decrease correspondingly. The dynamic mechanical analysis showed that at room temperature, the storage modulus also improves by 4-fold, the loss modulus – by 6-fold, while the glass transition temperature remained almost unchanged.

2. The crystallinity of the polymer, calculated from DSC curves, significantly decreases after the incorporation of the recycled cellulose into PBS. It is resulting in a predominantly amorphous structure with higher filler loading. The increase in the crystallization temperature indicates that cellulose induces the nucleation of the polymer chains. PBS matrix effectively shields filler, enhancing the thermal stability of the rCell. Thermal stability was higher for lower rCell loadings in the PBS matrix.

3. The composting of PBS and PBS/rCell films evidenced that cellulose accelerates the degradation of PBS, resulting in decreased degradation times for the composites. The independence of the filler loading was observed and could be explained with similar degradation speeds.

4. The obtained sustainable woody-like composite material with biodegradable properties it could be suggested as an alternative for conventional fossil polymer-based wood-plastic composites. We have prolonged the Tetra pak life cycle by introducing a new application for recycled cellulose for industries like packaging, furniture and construction. The Bio-based carbon content increases from 50% up to 75% with the usage of composite materials. The research was conducted at a laboratory scale, while

the melt-blending is an industry-wide standard and could be applied for large scale production.

5. LCI investigation found that within system boundary, the difference of energy consumption between 10 and 50 wt.% was 4 kWh for 1 kg of PBS/rCell composite. The most energy-intensive process for the PBS/10rCell composite processing is 82 % for the MC molding and 84 % for the IC molding of the total energy demand; while for the PBS/rCell 50% composite – 70% for MC molding and 73% for IC molding of the total energy demand.

3.2. Bio-based poly (butylene succinate)/microcrystalline cellulose/nanofibrillated cellulose-based sustainable polymer composites: Thermo-mechanical and biodegradation studies

Biodegradable polymer composites from renewable resources are the next generation of wood-like materials and are crucial for developing various industries to meet sustainability goals. Functional applications like packaging, medicine, automotive, construction and sustainable housing are just some that would greatly benefit. Some of the existing industries like WPCs already encompass given examples but are dominated by fossil-based polymers that are unsustainable. Thus, there is a background to bring a new perspective approach for the combination of microcrystalline cellulose (MCC) and nanofibrillated cellulose (NFC) fillers in bio-based poly(butylene succinate) matrix (PBS). MCC, NFC and MCC/NFC filler total loading at 40 wt.% was used to obtain more insights for wood-like composite applications. The ability to tailor the biodegradable characteristics and the mechanical properties of PBS composites is indispensable for extended applications. Five compositions have been prepared with MCC and NFC fillers using the melt blending approach. The use of melt blending technique in combination with freeze-drying was evaluated for PBS/NFC composite preparation. Additionally, to estimate the compatibility of the components and morphology of the composite's SEM analysis was performed for fractured surfaces. The contact angle measurements testified to the developed matrix interphase. Differential scanning calorimetry evidenced the trans-crystallization of the polymer after filler incorporation. Degradation under compositing conditions was evaluated.

3.2.1. Material processing and composite formulations

PBS was dried in a vacuum for 5 hours in 80 °C according to manufacturer's recommendations. MCC and NFC in the form of powders were dried in a vacuum for 24 hours in 60 °C. The composites were prepared with Brabender® Mixer 50EHT with the blending temperature set to 140 °C and the rotation speed to 70 rpm. The pure PBS sample was processed; 5 composites were prepared with 40 wt.% of MCC, NFC and MCC/NFC combinations in the PBS matrix. The prepared compositions are summarized in Table 3.5.

Table 3.5.

The prepared PBS/cellulose compositions.

Sample	PBS, wt.%	NFC, wt.%	MCC, wt.%
PBS	100	0	0
40NFC	60	40	0
40N7/M3	60	28	12
40N5/M5	60	20	20
40N3/M7	60	12	28
40MCC	60	0	40

Carver CH 4386 hydraulic press was used to prepare thin films having a thickness of 0.1 and 0.3 mm for tests. Mini-Jector #55-1E injection moulding device was used to prepare dumbbells shaped samples for tensile tests. Compression moulding was performed at a temperature of 140 °C for 5 min and 3 metric ton of pressure, followed by rapid cooling to room temperature between thick steel plates. Injection moulding device was set at the temperature of 190 °C, and samples were cast in the steel moulds.

3.2.2. Materials and energy flows

Table 3.6. presents the materials and energy flows for the manufacture of the two types of celluloses fillers - MCC and NFC at the laboratory scale for a method that is optimized for around 50 g production but for consistency is recalculated for 1 kg of filler production. The raw-material processing steps are very similar for kraft cellulose and require treatment with diluted hydrochloric acid 20 L, filtering and washing with distilled water which is then dried for 8 hours in thermostat resulting in 224 kWh energy consumption and dry cellulose. Before milling, the cellulose for NFC preparation was suspended in water while the cellulose for MCC preparation was milled dry. Both processes require 15 hours of jar milling that require 210 kWh electric energy. After milling, MCC was ready for the composite preparation in a solid powder state, while NFC was obtained as gel and required further freeze-drying to obtain solid filler for melt processing. The freeze-drying process requires 417.6 kWh, which results in a total energy of 851.6 kWh for NFC preparation compared to 434.0 kWh for MCC preparation a difference of almost two-folds. Emissions were evaluated, and both processes resulted in very similar amounts that consisted of 0.009 kg of solid waste mainly attached to devices and lost in cleaning and a small amount of dust 0.001 kg, additionally around 20 L of acidic water is produced.

As seen in Table 2, the energy required in production for both MCC and NFC are equal and material input demand slightly more distilled water for NFC production. Thus, the wet processing of NFC is the major challenge to find sustainable routes for NFC incorporation into the polymer matrix. In our case, freeze-drying almost doubled the required energy for the production of the nanocellulose. While other methods of NFC polymer preparation often use organic solvents, which introduce other issues like toxicity and recovery of the expensive solvents [259]. Nanofillers often require much lower amounts to achieve similar properties than micro-sized fillers, so the case for lower NFC usage can make a difference [260]. To expand on this topic, a full life cycle analysis is needed that considers other factors like PBS production costs, sustainable bio-based carbon content and recycling or waste processing.

Table 3.6.

Materials and energy flow for the laboratory manufacture of the MCC and NFC.

Input	Unit	Quantity per declared unit (1 kg of composite)		
		MCC	NFC	
Materials				
Softwood kraft pulp	kg	1.010	1.010	
Hydrochloric acid 0.05 wt.%	L	20	20	
Distilled water	L	2	12	
Electric energy				
Drying	kWh	224	224	
Jar milling	kWh	210	210	
Freeze-drying	kWh	-	417.6	
Total energy	kWh	434	851.6	
Emissions				
Dust	kg	0.001	0.001	
Solid waste	kg	0.009	0.009	
Acidic water	L	20	20	

3.2.3. Thermal properties

The thermal stability along with the degradation of the composite films was assessed using thermogravimetric analysis. Figure 3.13. shows the weight loss and the derivative weight loss curves of the pristine PBS, composites, and NFC, MCC fillers. It can be observed from the differential weight loss curve that PBS, NFC and MCC all have single-stage degradation curves while composites have two-stage degradations, from which first can be attributed to cellulose filler and second to PBS matrix. NFC starts to degrade faster and has a narrower degradation peak, and it loses less of its overall weight compared to MCC, and this could be attributed to the NFC structure that includes fibrils of varied nano sizes. PBS effectively shields cellulose filler, increasing composite thermal degradation at 50% weight loss by 60 °C compared to MCC and NFC. Compared with pristine PBS, the thermal stability of composites was reduced. Weight loss curves indicate that cellulose has lower thermal stability, and both NFC and MCC are similar and shows maximum weight loss at around 320 °C, while PBS has a much higher temperature at 406 °C. The initial weight loss for the cellulose samples at around 100 °C has been attributed to the bonded water, while the cellulose carbon skeleton pyrolysis starts at around 300 °C [261]. Table 3.7. summarizes TGA data from which the $T_{5\%}$ represents the thermal degradation temperature for 5% weight loss, $T_{50\%}$ represents the temperature of thermal degradation for 50% weight loss, T_{max} represents the extreme weight loss rate temperature.

Then the thermal stability of 40NFC composite was 18 °C lower at $T_{5\%}$ compared to 40MCC and composition 40N3/M7 had the highest degradation temperature at 305 °C, proving 25 °C and 7 °C increase respectively compared to single type cellulose specimens. For the values of $T_{50\%}$ and T_{max}, all compositions showed similar values, except 40MCC sample had 10 °C lower maximum weight loss temperature compared to other composites.
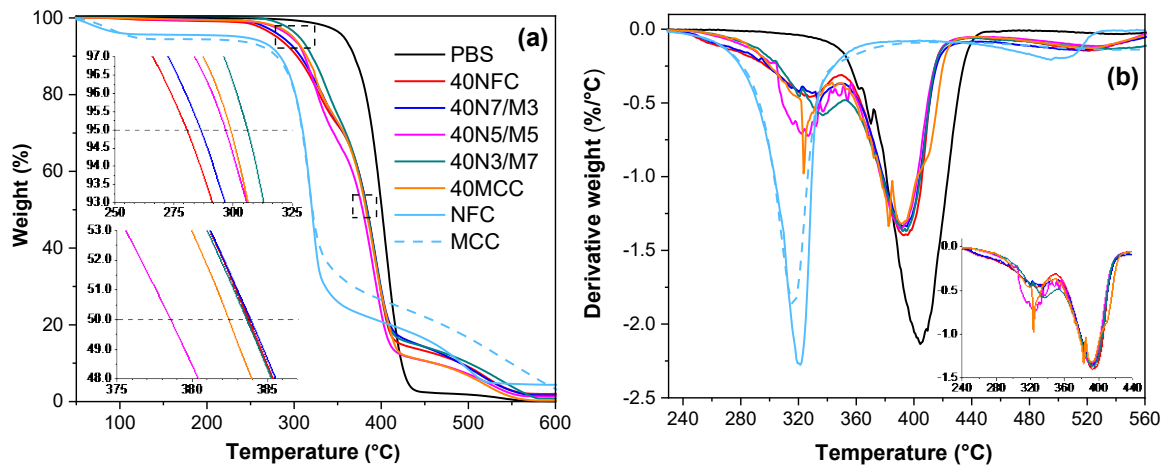
Figure 3.13. (a) Thermogravimetric analyses contours and (b) differential thermogravimetric contours of PBS, PBS/cellulose composites, NFC and MCC under air atmosphere.

Table 3.7.

Thermal properties of PBS/cellulose composites.

Sample	$T_{5\%}$, °C	$T_{50\%}$, °C	T_{max}, °C	T_m, °C	T_c, °C	H_m, J/g	H_c, J/g	χ_c, %
PBS	356	400	406	114.2	75.3	75.1	72.9	66.0
40NFC	280	384	392	114.2	81.9	31.8	35.0	52.8
40N7/M3	286	384	392	115.1	88.1	34.5	36.8	55.4
40N5/M5	296	379	392	115.8	89.0	37.7	37.2	56.1
40N3/M7	305	383	395	115.8	87.6	39.0	38.2	57.6
40MCC	298	382	383	116.5	85.2	38.8	42.6	64.2

DSC experiments were used to analyse the thermal and crystallization properties of PBS/cellulose composites. Table 3.7. displays the different thermal properties summary (e.g. crystallization temperature (T_c), melting temperature (T_m), crystallization enthalpy (H_c), melting enthalpy (H_m)), while the crystallization and melting curves are shown in Figure 3.14. Pristine PBS exhibited a sharp crystallization peak and crystallization temperatures (T_c) at 75.3 °C. The addition of NFC shifted crystallization temperature to 81.9 °C, while the addition of MCC continued to enhance the crystallization temperature to 85.2 °C, but for NFC/MCC filler compositions, even higher values were observed of which 40N5/M5 composition crystallization peak was at 89.0 °C. While the crystallinity degree χ_c decreases with the addition of cellulose fillers from 64.2% for 40.0% MCC down to 52.8% for 40.0% NFC and NFC/MCC follow the same trend with higher NFC content resulting in lower overall material's crystallinity. It has been reported that cellulose fillers structure impacts the crystallization process, while agglomeration of NFC filler lowers crystallinity [262]. Thus, the degree of crystallization χ_c increases by higher MCC content indicating heterogeneous nucleation of PBS matrix [263], while observed the different values of crystallinity for 40NFC and 40MCC composites indicate strong dependence on the structure of cellulose filler. The observed curves indicate the polymer crystal nucleation by both fillers and pronounced trans-crystallization that can be observed as splitting in the melting peak. For PBS/MCC composite, this is observed as a spilt peak or second

smaller peak [264]. The melting temperature of the composites is elevated compared to PBS and show narrower peaks, which might be the result of trans-crystallization, as a result offset to higher temperatures is observed [265].
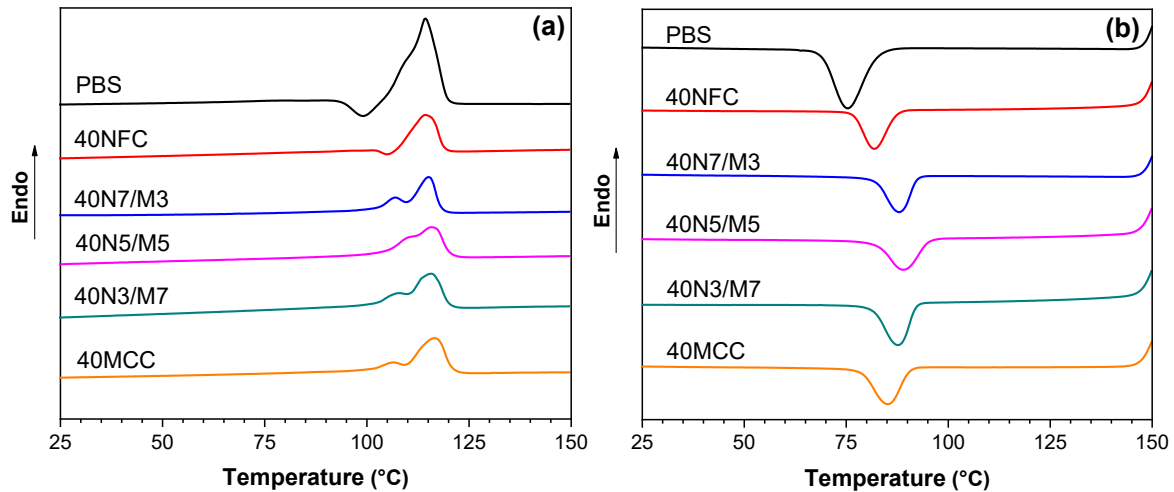

Figure 3.14. (a) Second heating melting peaks and (b) crystallization peaks of PBS and PBS/cellulose composites under the nitrogen atmosphere.

3.2.4. Thermomechanical and tensile properties

The thermo-mechanical properties of the PBS composites were studied with DMA. As evident from Figure 3.15.a, the storage modulus of the prepared composites increases significantly with the addition of cellulose fillers to the PBS matrix. The storage modulus was increased from 66 % up to 119% at 20 °C with the lowest result for 40N7/M3 composition and highest for 40MCC, which showed the best enhancement in the whole temperature range compared to PBS. Similar trends were obtained for the loss modulus peaks (Figure 3.15.b), which indicated the increase in the composite dampening properties, which saw an increase from 75 % up to 100% at 20 °C, with 40MCC having the highest observed value and 40N7/M3 lowest compared to PBS. But before the glass transition temperature, composition 40N5/M5 showed a significantly higher loss modulus than the rest of the composites. The storage and the loss modulus saw an increase in the entire temperature array, indicating a good filler dispersion and existing reinforcement network through whole composite and good load-bearing properties [266]. The loss modulus increase can be explained by the particle–particle slippage, in this case cellulose filler and polymer PBS matrix that dissipated more heat than pure PBS [267]. The glass transition values as seen in tan δ peak (Figure 3.15.c) ranges from -21 °C to -16 °C and are relatively unchanged for the composites compared to PBS value -16 °C. The absolute values of tan δ peak that characterize the energy dissipation were slightly decreased, resulting in lower energy requirement for viscoelastic deformation of the composites, indicating weak interactions between PBS matrix and NFC/MCC fillers [268]. Thus, the storage and the loss modulus increase could be explained by the rigid MCC and NFC fibres proving the enhancement and reinforcement network.
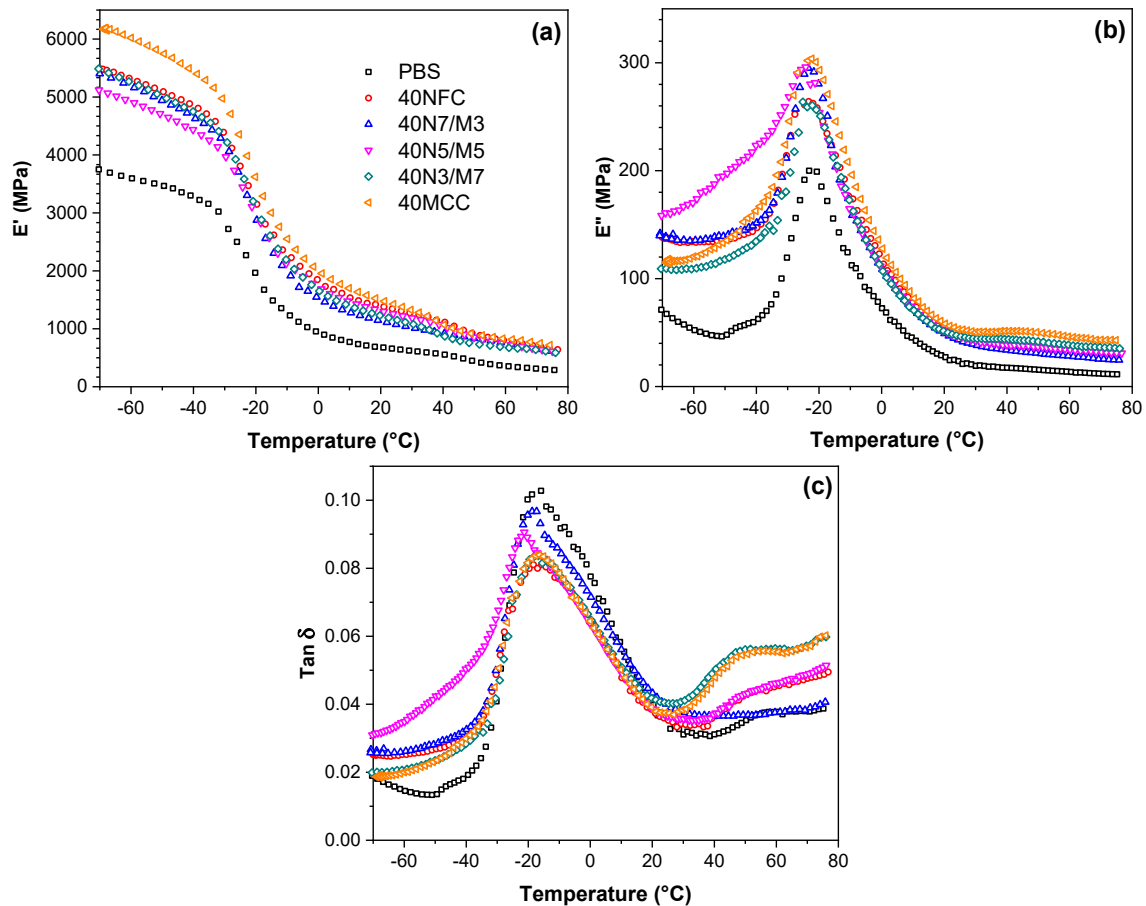
Figure 3.15. (a) The storage modulus E'; (b) the loss modulus E'' and (c) loss tangent tan δ curves of PBS and PBS/cellulose composites.

Figure 3.16. shows mechanical properties for PBS/cellulose composites tested in tension mode. The addition of the cellulose fillers to the PBS matrix causes an increase from 271 MPa to 561 MPa (107 % increase) for 40NFC with the highest value 626 MPa (131 % increase) for 40N5/M5 in Young's modulus, and this could be attributed to inherited high modulus value of cellulose. The difference between filler crystallinity with similar composition has been shown to impact Young's modulus and could explained higher values achieved with compositions that have higher MCC content [269]. Synergic effect of the fillers has been observed for 40N5/M5 composition, while 40NFC and 40N7/M3 compositions showed the lowest Young's modulus. A decrease has been observed for tensile strength from 30.9 MPa for PBS down to 22.5 MPa for 40MCC and lowest value 12.9 MPa for 40NFC, with is a similar situation for the elongation values as 40MCC has highest observed at 5.11 % and 40NFC lowest 3.18%. A decrease in tensile strength can directly be attributed to weak interactions between filler and matrix [269]. This results in stress concentrations that lead to brittle points in the composite's structure that reduce tensile strength and elongation values [270,271]. While from hybrid compositions, the highest tensile strength was observed for 40N3/M7. Thus, it can be observed that NFC shows poorer mixing with PBS matrix compared to MCC, and this could be attributed to different structures, surface area and crystallinity of cellulose, which affects the amount of available OH groups and increase chemically bound water [272]. Ductility decrease has been explained by the

increased volume of cellulose with high loading that enlarges the contact surface, which results in restricted polymer chain movements [273]. That is commonly observed as a sharp decline in elongation and has been reported for PBS/plant fibre compositions [274,275] and other polymers like polypropylene/wood composite systems [273,276].
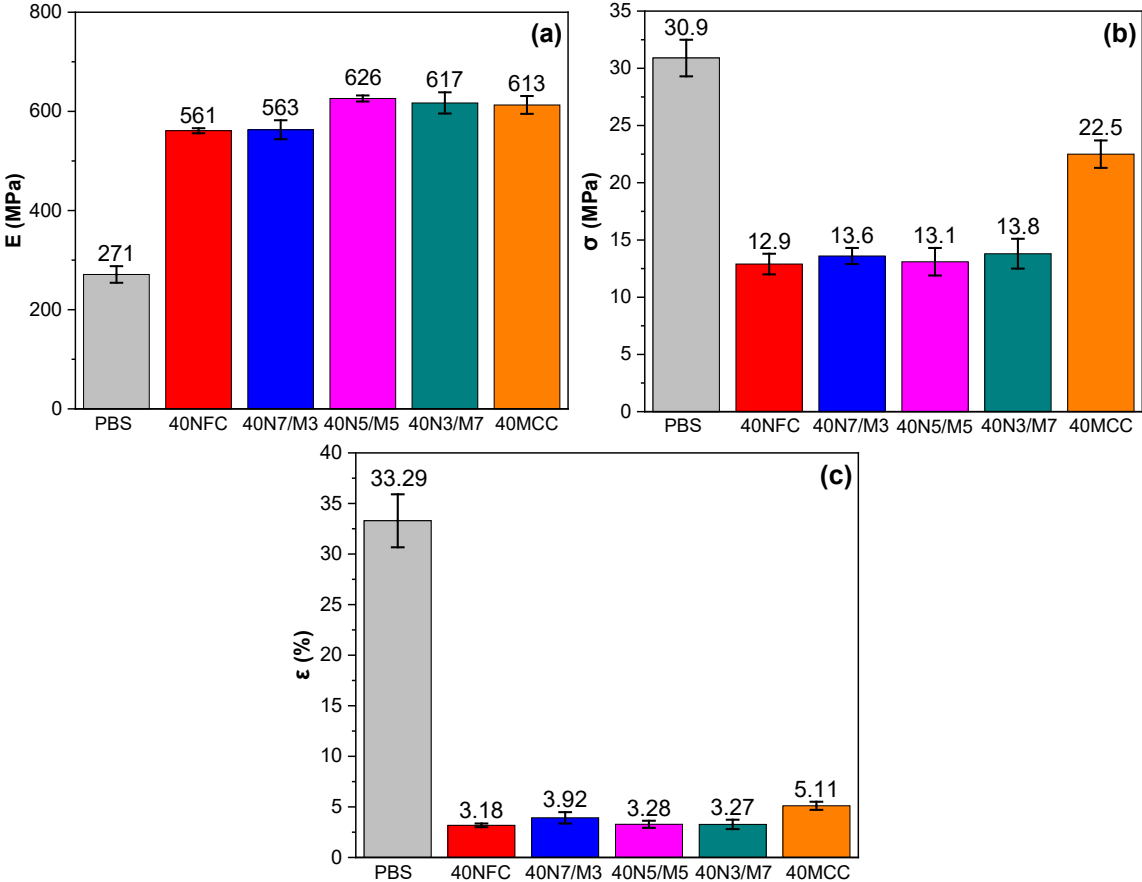
Figure 3.16. Tensile strength results of PBS and PBS/cellulose composites: (a) Elastic modulus E; (b) tensile strength σ and (c) strain ε.

3.2.5. Structure, morphology, and surface properties

The SEM images of the fracture surfaces of pristine PBS and PBS/cellulose composites are shown in Figure 3.17. SEM photographs indicate that PBS matrix coverage of MCC and NFC differ significantly. 40NFC composition has voids and a very rough fracture surface that includes micropores. The addition of MCC to NFC resulted in 40N7/M3 hybrid that has reduced the number of voids and improved filler dispersion, while surface roughness persists. It can be observed that 40N5/M5 hybrid composite has much less of previously described defects, and they have become local, but the basic structure of surface roughness is more even and smoother. 40MCC and 40N3/M7 composites have very similar fracture surfaces. There are no large voids compared to 40NFC composition, surface's structure is smooth and has now visible micropores, and blend filler is spread through matrix evenly, and there are no visible large agglomerates. Still, small voids can be observed even in these two compositions, and some smaller agglomerations with poorly covered cellulose can be observed. Tensile strength values achieved by 40N7/M3 composition show that even with very poor dispersion and compatibility

NFC can achieve acceptable results. Thus, application of for PBS/NFC blends should involve modification or grafting methods to achieve superior properties possessed by NFC.
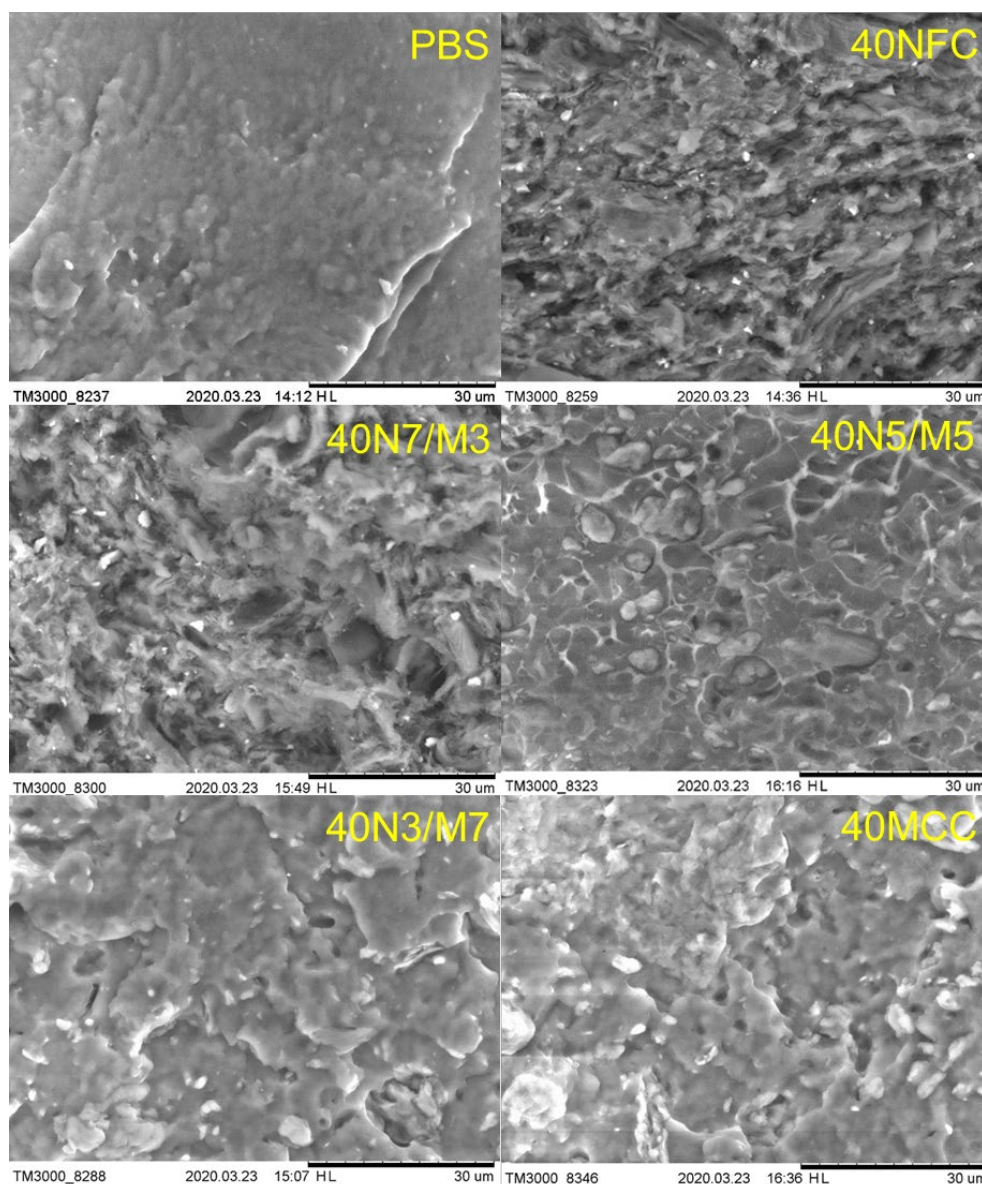
Figure 3.17. Scanning electron microscopy micrographs of PBS and composites.

The percentage weight loss in composting conditions for PBS and PBS/cellulose composites is presented in Figure 3.18. While visual specimen degradation can be observed in Figure 3.19., for the pristine PBS, it takes around 75 to 80 days to become almost indistinguishable from the soil. As seen in the case of MCC and NFC filled compositions, it takes 10 days shorter for them to degrade, resulting in total time around 65 to 70 days. We also observed that PBS/cellulose composites lose their ductility much faster, become brittle, and easily crumble with slight pressure, while pristine PBS retained mechanical toughness longer. The composition with MCC showed slightly enhanced degradation compared to NFC ones. It has been reported before that cellulose-based filler enhances the degradation of PBS in composting conditions and the weight percentage of filler determines the impact on the degradation time [89]. A hydrolysis mechanism is the first stage of PBS degradation and requires

enzymatic activity in soil and water, while degradation products are processed by bacteria and fungi [54,277]. It has been shown that the amount of water, temperature, and composition of soil influences degradation time significantly [165,278]. Other factors like crystallinity also impact the speed of degradation, and generally amorphous regions of polymers degrade faster than crystalline ones [54]. So, the result where compositions with MCC indicated faster degradation than those with more NFC could be explained by better filler distribution in the polymer matrix as observed in SEM images. Thus, better compatibility and distribution of MCC in blend allows to enhance composting properties further.
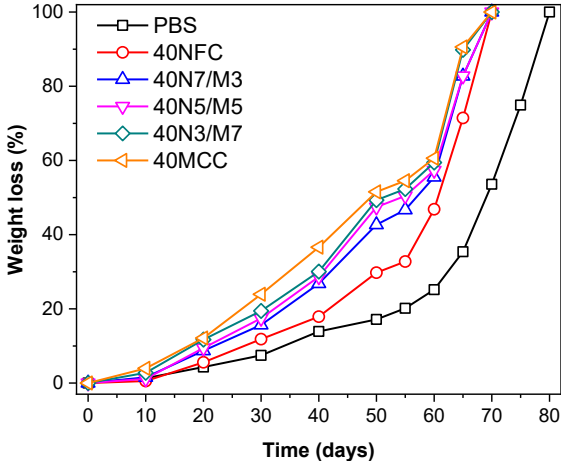

Figure 3.18. Percentage weight loss of PBS and PBS/cellulose composites in soil burial test conducted in composting conditions.
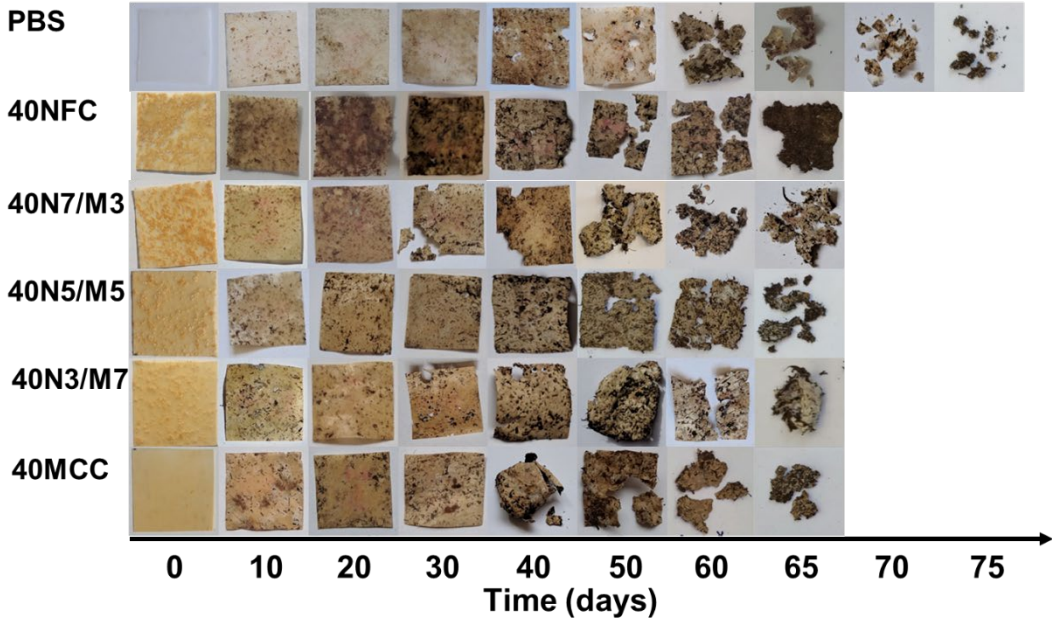

Figure 3.19. Photos of biocomposite films during biodegradation studies in soil burial test conducted in composting conditions.

Table 3.8.

Surface properties of PBS and PBS/cellulose composites.

Sample	Distilled water		OWRK			Zisman
	Θ, deg	SD	Tot, mN/m	r_s^d, mN/m	r_s^p, mN/m	γ_{cr}, mN/m
PBS	77.1	1.4	43.7	40.4	3.3	43.4
40NFC	76.4	1.0	42.3	39.0	3.3	41.9
40N7/M3	75.4	0.7	41.7	38.4	3.3	41.3
40N5/M5	73.5	1.1	41.5	37.5	4.0	39.5
40N3/M7	75.0	0.8	42.9	39.1	3.8	41.6
40MCC	76.9	1.7	42.5	39.2	3.3	42.6

Contact angle measurements were used in addition to biodegradation studies to determine surface wettability. Table 3.8. summarizes the measured contact angle (Θ) values with a standard deviation of distilled water for pristine PBS and PBS/cellulose composite films, surface free energy (SFE) calculated with the Owen, Wendt, Rabel and Kaelble (OWRK) method (total SFE of solids abbreviated as tot composed of dispersive component r_s^d and polar component r_s^p) and Zisman method (γ_{cr} critical SFE of solids) using 3 different solutions (distilled water, glycerol and diiodomethane). The contact angle values are lower for PBS/cellulose compositions compared to PBS, which means that the surface of the composites has improved wettability. Hybrid systems showed a lower contact angle value compared to single cellulose filler, with the lowest result for 1/1 composition. Zisman and OWRK methods showed that SFE decreased with the addition of cellulose, but the polar component was increased compared to PBS. Hybrid systems showed the lowest SFE, while their polar component was higher than PBS and single filler systems. All compositions show that polymer covers cellulose fillers effectively, while lower contact angle values and higher polar components indicate improved wettability, which plays a role in biodegradation. As observed in the degradation experiment in composting conditions (Figure 3.19.) PBS effectively covers cellulose filler and protects the surface from water and microorganisms, till the polymer layer is degraded.

The insights presented in this research have been combined with literature analysis to present a discussion for the selection of the filler. The MCC application in powder form makes it suitable for melt processing, showing good filler dispersion in varied concentrations even up to 70 wt.% [246]. Thus, the micro-sized cellulose fillers offer economic, environmental benefits and are suitable for conventional melt processing methods. This results in systems that can be highly loaded with microcellulose and are renewable with high bio-based carbon content, which is not always the case for bio-based polymers that are often partly oil-based. NFC is generally used in low concentrations up to 10 wt.% due to agglomeration issues that may arise [33]. Wet processing is considered standard for NFC, and film casting or freeze-drying is done by dispersing in water-soluble polymers to preserve nanostructure [144]. Some studies suggest that the nanostructure of NFC can be preserved after freeze drying [279]. Crystalline cellulose fillers are often easier to disperse in a polymer matrix, while fibrils tend to agglomerate. Very high mechanical properties and the high aspect ratio combined with nano size means that only small

NFC amounts are needed to reinforce polymer matrix and higher concentration presented diminishing affect returns or even decreased performance.

3.2.6. Summary

PBS polymer matrix can effectively shield the cellulose fillers from thermal degradation. As a result, the lower mass-loss rate was observed, and degradation occurred over a wider and upper-temperature range. The composites crystallization temperature was also increased, indicating heterogeneous nucleation of PBS stimulated by cellulose fillers. The crystallinity saw a decrease due to cellulose limiting PBS chain mobility.

The composites storage modulus increased significantly in the measured temperature range, confirming an effective filler reinforcement network. The tensile test showed that Young's modulus improved about two-fold, whereas tensile strength decreased along with elongation values. Surface wetting with water showed a slight decrease in observed contact angle values and increased polar component of the surface free energy. This was confirmed with weight loss measurements in composting conditions, where composites disintegrated 10 days faster than the pristine PBS sample. Thus, PBS/cellulose films would start to biodegrade faster, but still, have a good resistance during the product lifetime. The SEM images of the fracture surfaces displayed that MCC and NFC pose very different compatibility with PBS, which coincided with results observed in the mechanical and dynamical mechanical analysis.

Life cycle inventory for the fillers revealed an almost two-fold increase in energy consumption for NFC compared to MCC. We concluded that NFC having a higher surface area resulted in stronger hydrogen bonding, leading to large agglomerates and uneven filler distribution. Freeze-drying is not optimal processing method for unmodified NFC and wet processing is advisable. So, MCC is more suitable and economically viable in the case of unmodified cellulose filler application with melt blending for PBS composites.

3.3. Adding value to poly (butylene succinate) and nanofibrillated cellulose-based sustainable nanocomposites by applying masterbatch process

The present study highlights the beneficial effects of premixing of highly loaded poly (butylene succinate) (PBS) / nanofibrillated cellulose (NFC) nanocomposites under solution conditions and its use as a masterbatch for melt blending. The proposed masterbatch process strategy is an up-and-coming manufacturing technique for nanocomposites. This chapter demonstrates the preparation of masterbatch NFC composition with a very high loading of 50 wt.%. Research is aimed towards understanding the solution and melt processing effects on the structure and exploitation properties. The composites with NFC loadings from 5 up to 15 wt.% have been prepared by diluting the masterbatch and compared to conventional solvent casting. The masterbatch process can significantly reduce overall solvent usage and improve the NFC dispersion within the polymer matrix. SEM, DMA and tensile tests were used to evaluate composites performance. Biodegradation studies in the composting conditions were performed to underpin the weight, visual changes, calorimetric properties, while chemical changes were studied using spectroscopy. In addition, the reinforcement factor was calculated and analyzed. Obtained high-performance PBS/NFC composite materials are perspectives for films and packaging applications.

3.3.1. Material processing and composite formulations

PBS granules were dried in a vacuum furnace (J.P. Selecta) at 60 °C (5 to 20 mbar) for 8 hours before further processing. NFC gel was diluted with dimethylformamide (DMF) from 11 wt.% to around 3 wt.%. To remove water, NFC was transferred to dimethylformamide (DMF) via solvent-assisted centrifugation, which was repeated 2 times, and the high shear mixer L5M-A (Silverson Machines LTD) achieved even dispersion in the solvent (2 min, 5500 rpm). PBS solution in chloroform (5 wt.%) was prepared and mixed with NFC/DMF suspension using a high shear mixer (2 min, 5500 rpm). Five samples were cast 5, 10, 15, and 50 wt.% of NFC/PBS and a pure PBS as reference. Samples were dried in ambient conditions for 2 days and inserted in a vacuum furnace for 4 hours at 70 °C to remove the remaining solvents. The sample 50 wt.% NFC/PBS was mixed with dried PBS granules in thermoplastic mixer Brabender® Mixer 50EHT (Germany) to produce 5, 10, and 15 wt.% samples. The processing conditions were adjusted to 70 rpm for twin screws, heating in all zones was 130 °C and 5 min melt compounding followed by an additional 5 min of mixing in 160 °C.

Compression molding (Carver CH 4386) was used to obtain the specimens' films with a thickness of 0.10 mm for the biodegradation test and 0.25 mm for other tests. The compression molding heating plates were set at 140 °C, while the samples were preheated for 2 min, compressed for 3 min (3 MT pressure), cooled for 3 min between steel plates (30 kg of thermal conductive mass). To distinguish samples following abbreviations were selected 5S, 10S, 15S was used for solvent cast samples, and 5M, 10M, 15M for melt-compounded samples from masterbatch (Table 3.9). Figure 3.20. shows the visual appearance of prepared films where PBS is pure white, a masterbatch is in yellow-brown, which was obtained from cellulose, while 10 wt.% loaded samples are given as examples for composites, which all added very similar appearance of a pale brown tint to films.

Table 3.9.

The prepared PBS/NFC compositions.

Sample	PBS, wt.%	NFC, wt.%	Preparation
PBS	100	0	solution and melt
5M	95	5	solution
10M	90	10	solution
15M	85	15	solution
5S	95	5	masterbatch melt
10S	90	10	masterbatch melt
15S	85	15	masterbatch melt
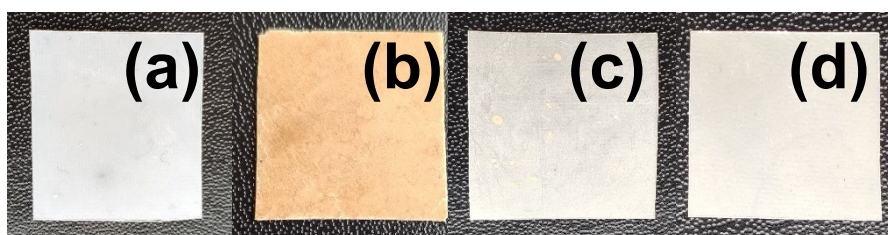
Figure 3.20. Visual appearance of prepared sample films: (a) PBS, (b) masterbatch with 50 wt.% NFC loading, (c) 10S and (d) 10M.

3.3.2. Structural properties

Figure 3.21. contains SEM images of selected specimen fracture surfaces in liquid nitrogen. The melt composite 5M shows a much better NFC distribution in the PBS matrix than 5S (Figure 3.21.a and 3.21.b). Sample, 5S, shows regions that contain almost pure polymer, while the image also shows an agglomeration for NFC. NFC shows good PBS adsorption on the fibril surface at 5 wt.% loadings. While in Figure 3.21.c 15M, the NFC is dispersed evenly, fibrils are encompassed in a polymer matrix showing no signs of being pulled out or separated from PBS. A slight agglomeration can be seen between some of the nanocellulose fibrils, but no significant defects can be observed. Unfortunately, 15S (Figure 3.21.d) SEM image indicates poor filler dispersion in matrix. Also, separation of filler and polymer matrix phases can be observed in the 15S sample. Similar SEM results were reported in the literature for PLA/NFC composites prepared by solvent casting, and the authors noted that agglomerates directly contributed to fracturing formation [280].

Figure 3.21. SEM micrographs of selected compositions obtained by a fracture in liquid nitrogen.

3.3.3. Thermal properties

The effect of NFC filler loading on the thermal properties was investigated through differential calorimetric (DSC) analysis. The results are reported in sections a and b of Figure 3.22, and su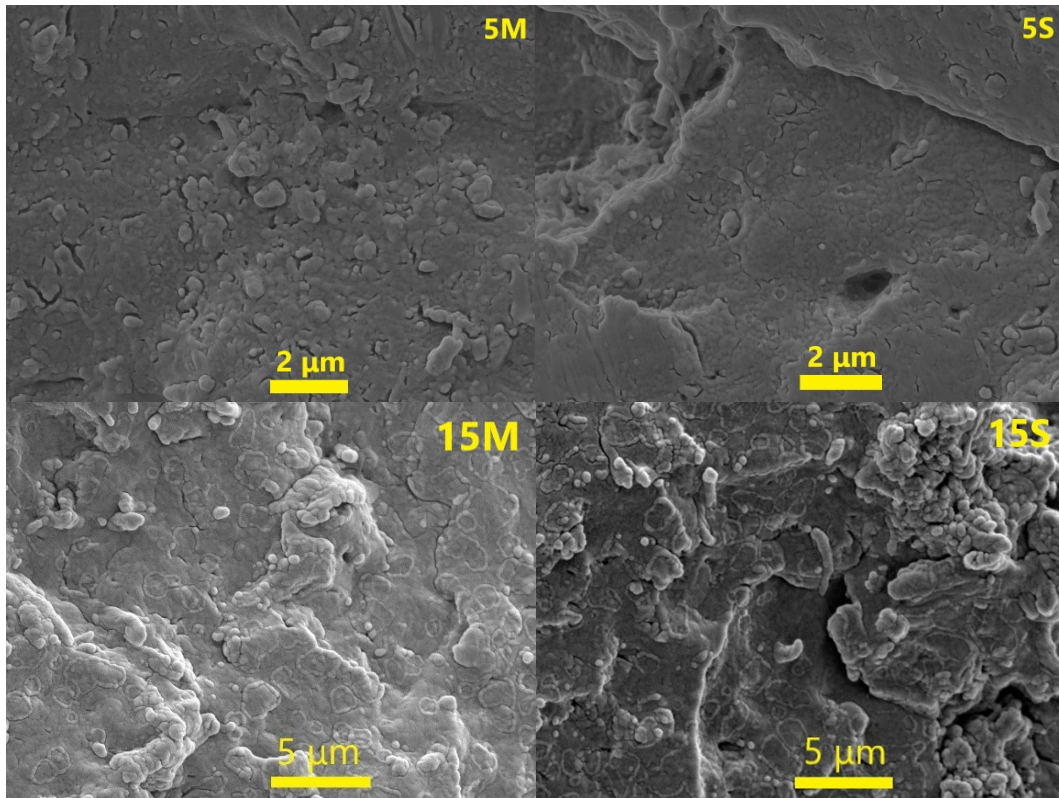mmarized in Table 3.10. The DSC second heating scan (Figure 3.22.a) clearly shows a single peak. It indicates a slight increase in melting temperature (T_m), which can be attributed to thermal lag owing to the NFC filler's low thermal conductivity. The nanocomposites' crystallization behavior indicates an increase in crystallization temperature (T_c) and crystallinity (χ_c). The NFC promotes crystallization and acts as a nucleating agent indicated by an increase in crystallization temperature by 3 to 4 °C. Rastogi et al. reported similar observations for polyhydroxybutyrate/NFC composites [281]. Crystallinity was calculated from crystallization enthalpy instead of melt enthalpy, as it has been reported before that the melting process of PBS involves recrystallization [282]. Compared to neat PBS crystallinity 66%, nanocomposites saw a slight crystallinity decrease to 54 – 58% due to the obstructed PBS chain movements in the cooling process by the NFC filler presence. Melt blended samples show lower crystallinity than solvent cast ones, and as seen above in structural analysis (SEM), filler dispersion is the main difference between the two preparation methods. Thus, an even spread filler interferes more with the crystallization process. However, it can also be concluded that the NFC samples can form a new crystalline polymer phase, which is consistent with the reported observation in literature for PLA/NC composites [280]. The increase in NFC filler up to 15% loading slightly lowers the crystallinity.
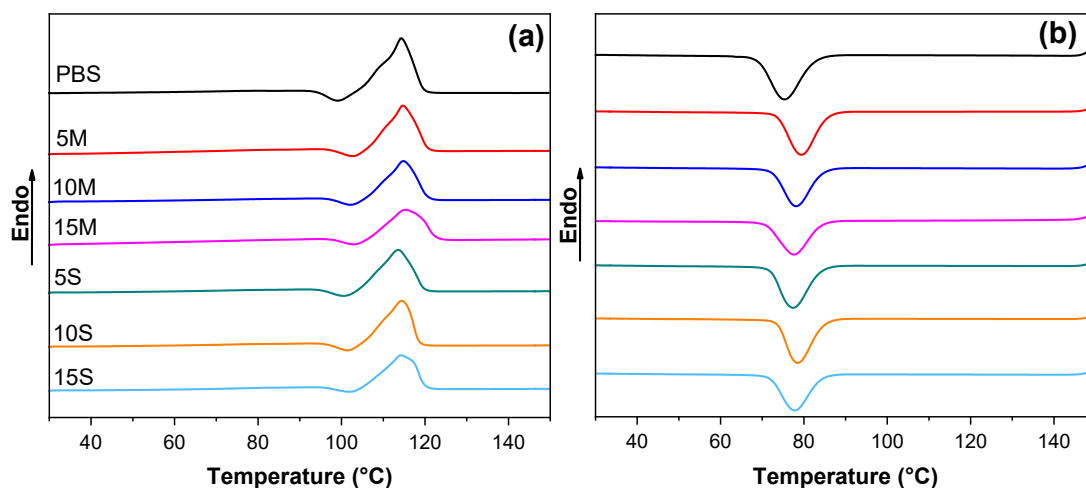
Figure 3.22. DSC (a) heating curves and (b) cooling curves of PBS and 5, 10 and 15 wt.% PBS/NFC nanocomposites fabricated using solution casting and melt compounding methods.

Table 3.10.

Thermal properties of PBS/NFC composites.

Sample	T_c, °C	ΔH_c, J/g	χ_c, %	T_m, °C	ΔH_m, J/g	$T_{5\%}$, °C	$T_{50\%}$, °C	T_{max}, °C	T_e, °C
PBS	75.0	72.9	66.0	114	75.1	357	401	404	571
5M	79.4	60.7	57.8	115	61.7	344	386	400	577
5S	77.4	60.0	57.2	114	53.1	337	382	396	577
10M	78.1	54.6	54.9	115	54.6	330	396	395	582
10S	78.5	58.1	58.4	114	59.3	338	387	400	561
15M	77.6	50.3	53.6	116	49.2	326	392	398	579
15S	77.8	54.1	57.6	114	50.9	308	389	398	583

3.3.4. Thermal degradation

The thermogravimetric analysis curves of neat PBS and nanocomposites are shown in Figure 3.23. Table 3.10. presents an overview of thermal stability parameters $T_{5\%}$, $T_{50\%}$, which indicate the weight loss at 5 and 50 wt.% correspondingly, while T_{max}, T_e show the maximum decomposition temperature and the ending decomposition temperature. A weight loss occurs faster for solvent cast samples above 120 °C losing 2-3 wt.%, which can be attributed to the remaining solvents in the composites. In contrast, the melt-processed samples and pristine PBS only saw a decrease in weight after 250 °C. $T_{5\%}$ of the nanocomposites indicate a difference in decomposition temperature from 13 up to 49 °C compared to neat PBS. The decrease has been observed much more rapidly for solvent cast samples and samples with higher NFC filler sample concentration, indeed, as the region above 300 °C is the typical decomposition temperature for cellulose [284]. The maximum decomposition temperatures and $T_{50\%}$ for the nanocomposites were within the region of 5 °C, which also contained a 10 °C difference from PBS. As seen from the measurements, the overall thermal stability was decreased by 10 to 30

°C approximately compared to neat PBS, except for the 15S sample. The decomposition ended at around 570 °C where PBS's remaining mass was around 0.07 wt.%, while the nanocomposites remained around 1 wt.% as there were no organic remains left it can be possibly attributed to inorganic char. The addition of NFC did not significantly impact the nanocomposites' application prospects, while relatively high decomposition above 250 °C indicates that recycling as a possibility remains.
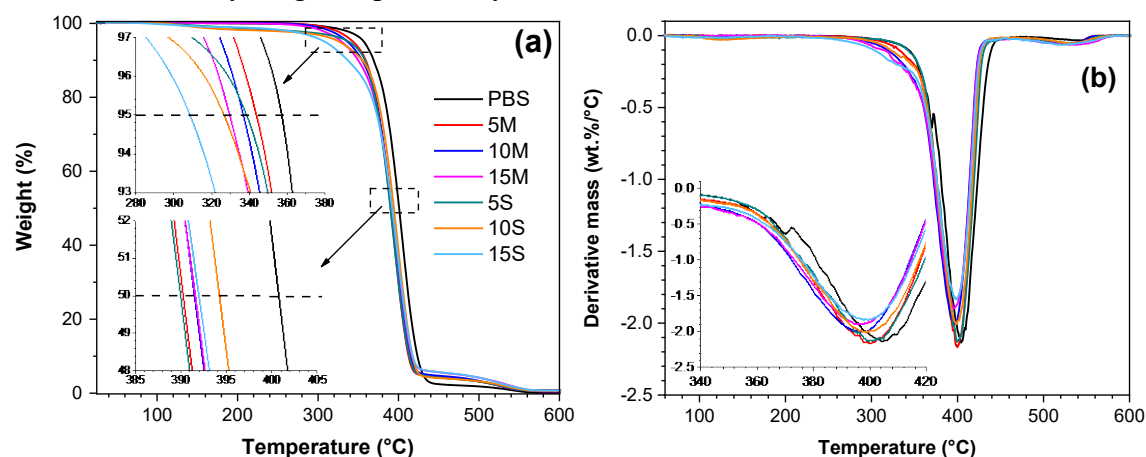

Figure 3.23. (a) TGA thermogram and (b) first derivative TGA curves of PBS and 5, 10 and 15 wt.% PBS/NFC nanocomposites fabricated using solution casting and melt compounding methods.

3.3.5. Biodegradation studies in the composting conditions
Visual and mass changes

Visual changes and mass changes of PBS and nanocomposites during the biodegradation process are presented in Figure 3.24. and Figure 3.25., respectively. Five parallel samples for each specimen were used, and two of each were removed every 10 days to register changes. Nanocomposites can be distinguished by the light brown color caused by cellulose's thermal treatment during the preparation process, which intensifies in higher NFC loading for the composites. After 10 days, changes are minimal, but small dark spots where soil particles are embedded in the surface are visible, which after 10 more days have resulted in brown discoloration spots indicating degradation on the surface. Most notable changes after 20 days are visible for the 15M specimen, which has visible macro-scale holes that slowly appear for all nanocomposites at the 30- and 40-day mark.

In comparison, the PBS sample only developed dark brown spots between 30 and 40 days and visible holes at 60 days. This indicates that cellulose filler accelerates the biodegradation process. As this process is commonly known as hydrolysis, we believe that cellulose and PBS's hydrophilic and hydrophobic nature influences water adsorption speed. Thus, once the top layer of PBS is breached, the matrix does not fully cover cellulose particles. They become local spots for more intensive biodegradation that involves the participation of microorganisms. From 30th to `50th-day, nanocomposites lose their ductility and become fragile and discolored fully. Small cracks were visible, and a notable surface roughness increase can be seen. The color changes could be linked with the amorphous phase's degradation, which leads to crystallinity changes,

as seen in Table 3.11. Finally, reaching the 70th-day, nanocomposites become inseparable from the soil, very thin and extremely fragile. Almost no distinguishable nanocomposites particles could be recovered after 90 days; thus, all remaining parts from all 5 parallel measurements were used for FTIR and DSC measurements. Although the PBS specimen was degrading slower and visually looked more intact, the film was thin and fragile and crumbled in small pieces, almost inseparable from the soil after the 80th mark. The mass changes were relatively linear after the initial 20 days and saw a slight increase with every 10 days until most of the samples were degraded at around the 60th day, where we saw a decrease in weight loss speed, which was partly impacted by the inability to separate the soil from specimens, thus contributing to measured mass. The mass changes clearly show that composites with higher cellulose content degraded faster.
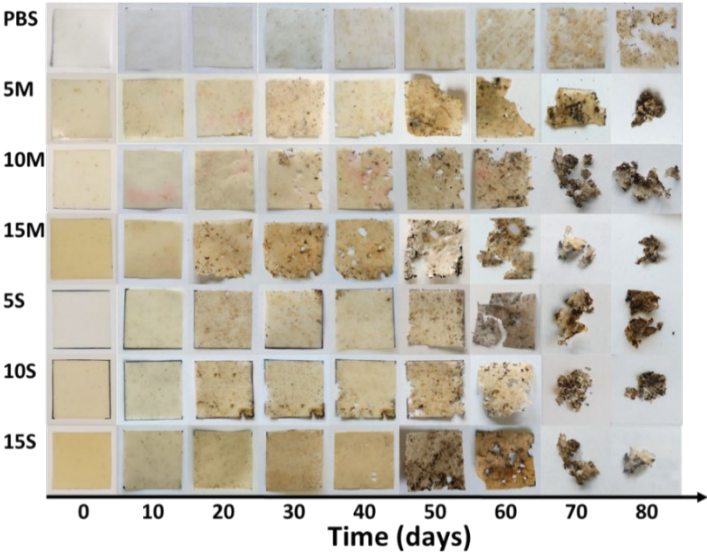

Figure 3.24. Photos of biocomposite films during biodegradation process taken every 10 days until disintegration in the compost soil.
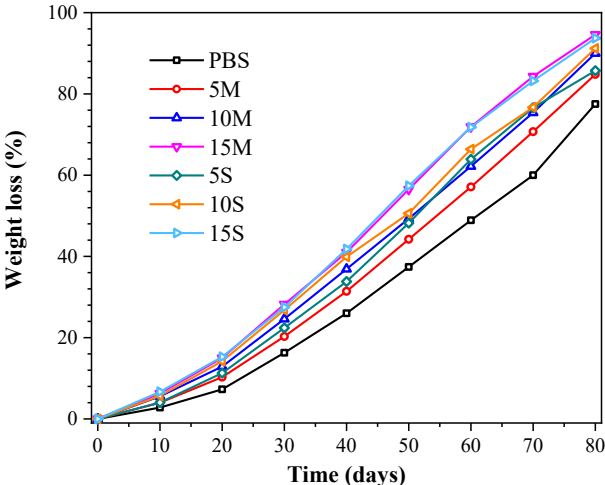

Figure 3.25. Cumulative weight loss of PBS and 5, 10 and 15 wt.% PBS/NFC nanocomposites fabricated using solution casting and melt compounding methods during the biodegradation process.

88

DSC analysis

Figure 3.26. shows DSC thermograms of pristine and biodegraded samples are compared to those buried in composting soil for 50, 70, and 90 days. Table 3.11. supplements the information with crystallization temperature at 50 and 70 days (T_{50c}, T_{70c}) and melting temperatures at 50 and 70 days (T_{50m}, T_{70m}), crystallinity at 50 and 70 days (χ_{50c}, χ_{50c}), and melting and crystallization enthalpy at 50 and 70 days (ΔH_{50m}, ΔH_{70m}, ΔH_{50c}, ΔH_{70c}). Fig. 3.26.a shows the splitting of the single melting peak into two peaks during the biodegradation process. Two melting peaks or splitting of the single peak have been reported to be a common occurrence for various PBS polymers and composites and are not unique to PBS [285]. It can be attributed to the primary and secondary crystallization of two different lamellae in PBS. The first type is more susceptible to heat that recrystallizes the perfect structure before melting and, together with the fusion process, results in the second more prominent peak [47,48]. The decrease in the melting temperature can be seen for all selected samples at 50 and 70 days with an average decrease of 4-5 °C, which indicates the rapid reduction in molecular weight for PBS [286].

Further changes are hard to distinguish due to recrystallization behavior. At 50 days, the increase in melting peak area can be observed and similarly is even more pronounced for crystallization peak; this could be explained by shorter chains being more mobile in the crystallization process, and for filled systems decrease in NFC content could result in higher PBS percentage compared to the original sample. Crystallinity changes calculated from crystallization enthalpy at 50 days show a slight decrease for 5 wt.% samples and an increase for the samples with 15 wt.% loadings, but the changes are within 2 to 5 %. Following analysis at 70 days shows a notable decrease in crystallinity, with 15M having only 8% crystalline phase. Further decomposition in the soil results in the formation of voids as visible on film structure. Then the microplastics are developed, which are hard to separate from the soil; thus, peak intensities decrease and become even undetectable at 90 days for nanocomposites with 15 wt.% loadings. There is a clear difference in the crystallization process for PBS and nanocomposites. PBS sample has much more pronounced peak broadening and a sharper decrease in crystallization temperature down to 69 °C compared to 73 - 76 °C for NFC-filled composites at 70 days. It has been reported in the literature that cellulose-based fillers accelerate PBS biodegradation and cellulose degrades faster in the soil [278]. Thus, samples with NFC filler degrade much faster around cellulose as it is much more hydrophilic than PBS, which results in films breaking apart faster (see Figure 3.25.) While remaining large pieces with lower overall degradation are analyzed, thus changing the representation of the process. PBS has much more even degradation in a volume of the measured film reflected in broader peaks and indicates a higher molecular weight difference. Owing to previous observations and knowing that biodegradation is mainly a surface process, while DSC scans reflect volume properties, the entire process cannot be captured. Further analysis with FTIR was performed.
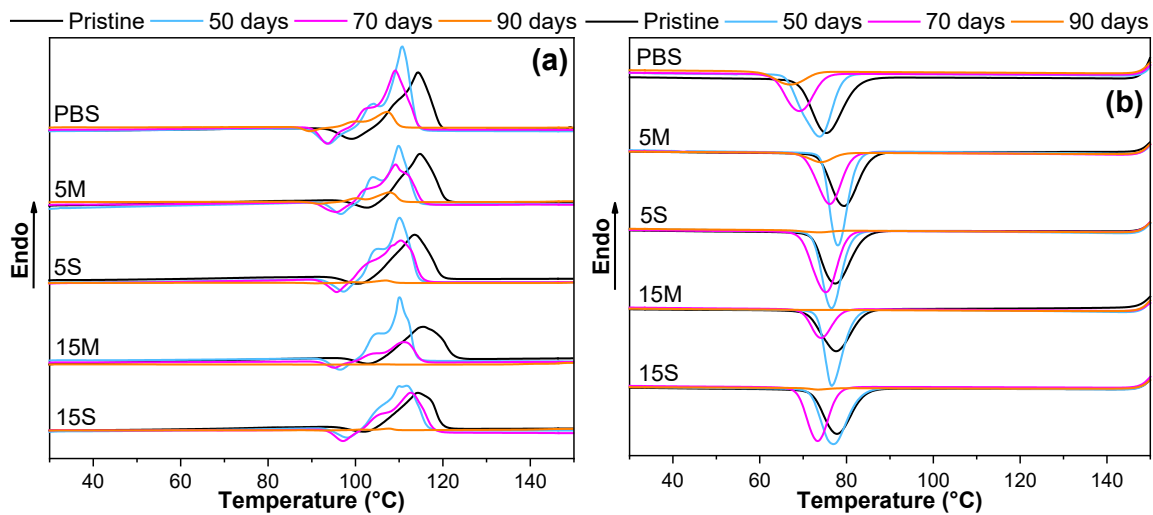
Figure 3.26. DSC (a) second heating curves and (b) cooling curves during the biodegradation process of selected samples: PBS, 5M, 5S, 15M and 15S.

Table 3.11.

Calorimetric properties of PBS/nanocellulose composites after biodegradation.

Sample	T_{50c}, °C	ΔH_{50c}, J/g	χ_{50c}, %	T_{50m}, °C	ΔH_{50m}, J/g	T_{70c}, °C	ΔH_{70c}, J/g	χ_{70c}, %	T_{70m}, °C	ΔH_{70m}, J/g
PBS	73.8	75.4	68.2	111	83.3	69.2	42.1	38.1	109	70.8
5M	78.1	69.2	66.0	110	75.3	76.1	51.3	48.9	109	55.8
5S	77.6	54.9	52.3	110	70.4	75.1	61.8	58.9	111	64.6
15M	76.7	58.9	62.7	110	62.6	74.6	7.66	8.16	111	8.70
15S	77.0	60.42	64.3	112	62.8	73.3	48.1	51.3	112	57.5

FTIR analysis

Figure 3.27. shows the FTIR-ATR spectra of PBS and selected composites before and after the biodegradability test at 50 and 90 days. The characteristic peaks of PBS can be identified 2946 cm^{-1} the stretching of the C-H bond, 1712 cm^{-1} carbonyl C=O bond from ester linkage, 1151 cm^{-1} known as C-O or C-O-C asymmetric stretching vibrations together with 1046 cm^{-1} band for symmetric stretching and are most commonly reported in PBS analysis [287,288]. The addition of bands, like 955 cm^{-1} attributed to C-O stretching of the amorphous domain, 918 cm^{-1} assigned to C-O stretching of the crystalline domain, 806 cm^{-1} for CH_2 in-plane bending, and 650 cm^{-1} for COO bending vibrations together with bands from 1000 to 1300 cm^{-1} region can be used to identify and to distinguish PBS from other polymers [287,289,290]. When biodegraded spectra are compared to pristine specimens, a significant decrease in the peaks' intensity can be observed. The most notable decrease is for 1712 cm^{-1} and 1151 cm^{-1} directly related to ester bonds cleaved in the hydrolysis process. After 50 days, a new peak can be observed in PBS spectra at the 3295 cm^{-1} signature region for OH stretching vibrations. This peak can also be

observed in the composite structure and comes from cellulose, but similarly is attributed to OH stretching vibrations. Thus, directly indicating the presence of cleavage products. Another shift is observed at 50 days and becomes more pronounced at 90 days when the partial or complete disappearance of 1712 cm^{-1} band and emergence of new peaks in the region from 1500 to 1665 cm^{-1}. It could be related to the emergence of carboxylic end groups, ketone species, and vinyl groups in the presence of microorganisms [47]. At 90 days spectra for most specimens, a broad peak from 930 to 1170 cm^{-1} with a peak around 1020 cm^{-1} emerges and can be attributed to C-O stretching vibrations of various biodegradation products.
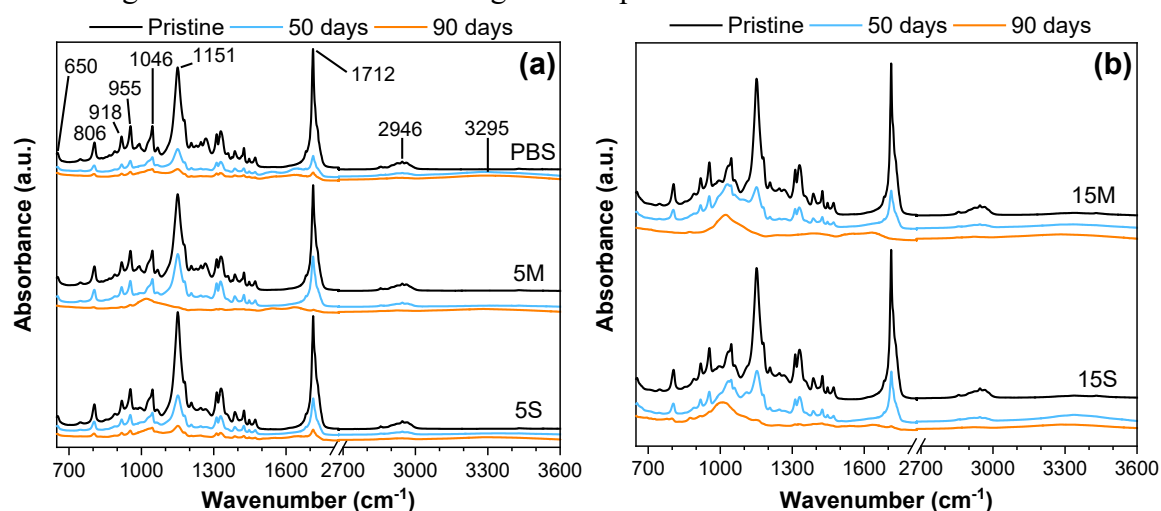

Figure 3.27. FTIR spectra representing biodegradation process of selected samples: (a) PBS, 5M, 5S and (b) 15M, 15S.

3.3.6. Mechanical properties
Tensile characteristics

The tensile modulus, ultimate strength, and elongation at break for the neat PBS and PBS /NFC nanocomposites are shown in parts a to c of Figure 3.28. Also, stress-strain graphs for selected samples are shown in Figure 3.28.d. The differences for neat PBS treatment did not reveal any notable changes. Because of the high intrinsic modulus of NFC, it acts as rigid reinforcement to the polymer matrix. The high aspect ratio of the NFC results in a large surface area for the interaction with PBS matrix; thus, two limiting factors can be considered, the effective loading at which properties peak and adhesion between polymer and matrix. The composites' elastic modulus grew progressively with increasing NFC content for melt compounded samples showing a 1.4-fold and 1.7-fold increase for 5% and 15% samples, correspondingly. However, solvent cast one's samples showed an increase of almost 1.4-folds with higher NFC loadings (Figure 3.28.a). Figure 3.28.b shows the composite's tensile strength indicating around a 10% decrease compared to neat PBS, while most samples show similar values within margin error. A slight reduction can be explained by limited adhesion between filler and matrix, which has been observed for PBS [291] and other polyester polymers like PLA [292]. The NFC filler cannot properly support stresses transferred from the polymer matrix.

However, at the same time, similar tensile strength values indicate that adhesion exists just slightly weaker when compared to polymer chain to polymer chain interaction [293]. Elongation

at break shown in Figure 28.c decreased with the increase of NFC content except for the 5S sample, which showed almost no decrease and combined with almost no increase in tensile modulus for this sample, it can be concluded that good filler dispersion was not achieved, and agglomeration occurred. As microfractures with voids and agglomerates can be seen in Figure 3.21. Such elements in structure can significantly contribute to the formation of internal stresses, thus lowering nanocomposite's mechanical performance. The decrease in elongation values was around two-fold for most samples, while 15M had a 3-fold decrease. Melt compounded samples show an almost linear increase of modulus and linear decrease in elongation values indicating good ability to scale with NFC filler content; thus, a more homogeneous filler distribution is achieved.

In comparison, solvent cast samples reached the best properties at 10 wt.% NFC. They were limited by filler dispersion that seemed to agglomerate. The elongation decreases with higher filler loading is commonly observed as stiffer particles are introduced and polymer chain movement is restricted [294]. Xu et al. reported that for PBS compositions with 1 to 5 wt.% cellulose nanocrystals, tensile strength increased by 45% from 23.3 up to 33.9 MPa, elongation decreased by 30%, while elastic modulus changes were not obtained [194]. Other authors have reported research on polypropylene/NFC composite with 6 wt. % prepared from 30 wt. % masterbatches. They reported only a 20% increase in elastic modulus, a 30% decrease in elongation, and almost no changes in tensile strength [295]. The proposed research on polypropylene composites indicates similar observations to ours but with a lower increase in elastic modulus, while PBS and CNC seem to interact differently compared to NFC.
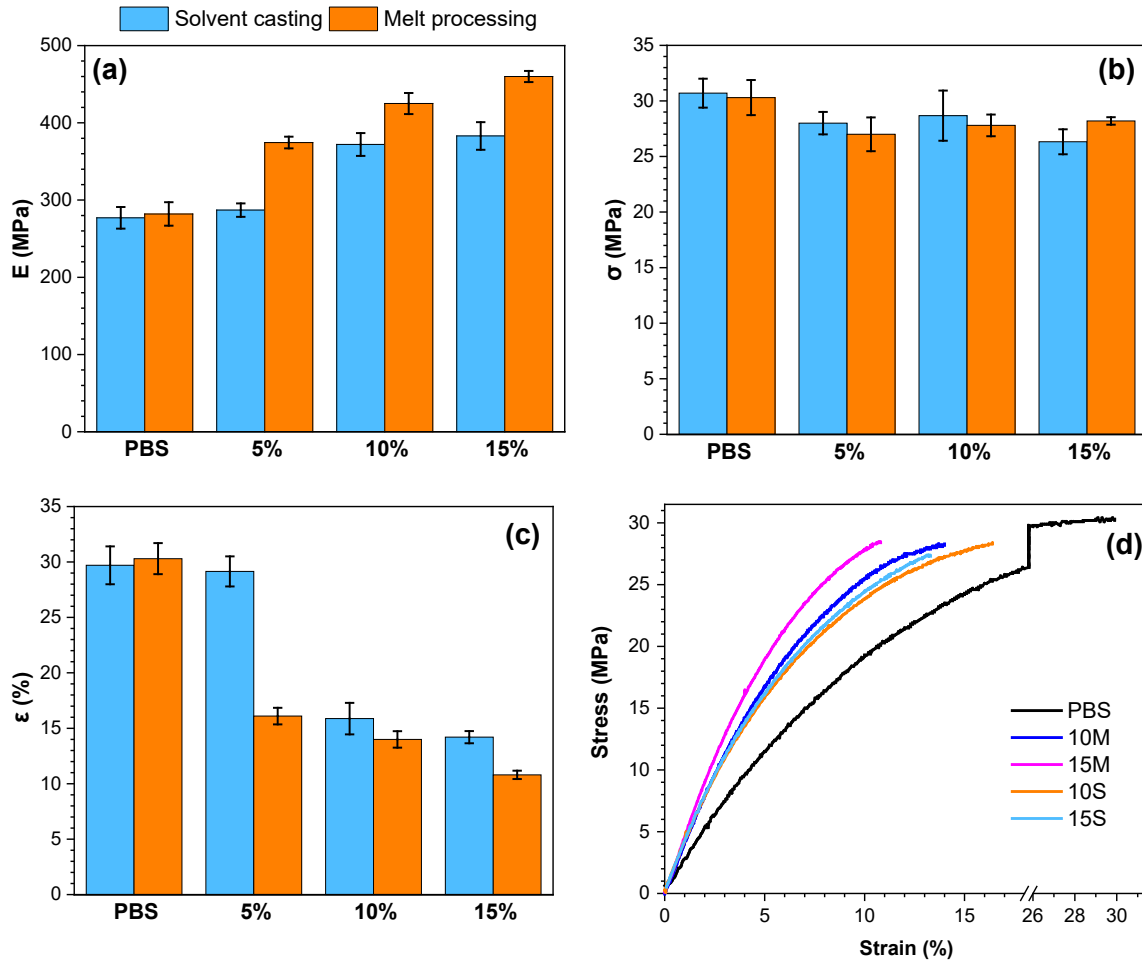
Figure 3.28. Tensile properties: (a) tensile modulus, (b) tensile strength and (c) elongation at break for PBS and 5, 10 and 15 wt.% PBS/NFC nanocomposites fabricated using solution casting and melt compounding methods. (d) Typical stress−strain curves presenting a ductile fracture in the samples: PBS, 10M, 15M, 10S and 15S.

Thermomechanical characteristics

The storage modulus E′, loss modulus E″ and tan δ of neat PBS and nanocomposites are shown in parts a to c of Figure 3.29. as a function of temperature. Storage modulus values decreased with an increase in temperature as it is commonly observed for the polymers and saw a sharp decrease in the glass transition region from -40 to +10 °C. NFC filler contributed to the material's high dimensional stability by significantly elevating values in all measured temperature ranges. The only notable exception was the 5S sample, which failed to form a reinforcement network; thus, agglomerates could not contribute to the stiffness of the composite in the viscoelastic state. The gradual increase of storage modulus values was observed with increased NFC concertation. At the same time, the melt blended samples showed higher overall values when filler loading was equally explainable by better dispersion. The drastic increase of storage modulus for 15M composite compared to 5M and 10M, which performed similarly, could be explained by NFC's ability to form a continuous filler network in high loadings instead of separate particle reinforcement [296]. The highest storage modulus values were measured to 15M sample with the 1.4-fold increase at -70 °C and 2-fold increase at +70 °C compared to

93

neat PBS. NFC hindered the polymer chains' movement, resulting in increased dampening properties, as shown in Figure 3.29.b. The increase in loss modulus values for all measured temperature ranges was observed for NFC loadings 10 and 15 wt.%. From - 70 °C up to the glass transition, 15M showed the highest increase in loss modulus but was overtaken by 15S in the viscoelastic region.

The increase of loss modulus values can be explained by a decrease in crystallinity, which changes the required energy for the segmental movements of PBS [297]. Tan δ values show the ratio between storage and loss modulus, which decreases due to stiff nanoparticles introduction into the polymer matrix, resulting in a reduced potential for energy dissipation and more elastic properties of nanocomposites than neat PBS. The glass transition temperature can be determined from the tan δ peak in Figure 3.29.c. A clear shift to lower temperatures can be observed for all nanocomposites; for example, a sample with 15% of NFC shows the glass transition at -16 °C. Besides, the neat PBS has a glass transition at -21 °C. Owing to these changes, the interaction between filler and matrix can be one explanation. Another common explanation is the restricted chain mobility that impacts segment rearrangement during phase transition [298].

Parameter C calculated from equation (3.2) describes the overall effectiveness of the filler in the composite using the storage modulus [299]:

$$C = \frac{\left(E_g'/E_v'\right)_{composite}}{\left(E_g'/E_v'\right)_{matrix}} \qquad (3.2)$$

where E_g' – glassy storage modulus measured at -60 °C and E_v' – viscoelastic storage modulus measured at 40 °C. Parameter C lower than 1 shows effectively dispersed fillers compatible with the polymer matrix, while lower the value better the reinforcement [300]. Figure 3.30.a shows graphed parameter C values which decrease within higher NFC loadings. Except for the 5S sample with a C value of 1.11, other samples showed successful reinforcement. Melt processed samples had significantly better C values than solution cast samples with the same NFC wt.%, and the best value was achieved by 15M with $C = 0.69$.

The analysis can be enhanced by calculating reinforcement efficiency factor – r, which characterizes the filler interaction with the polymer matrix [301]. An empirical relationship between composite's storage modulus (E_c') and the polymer matrix's storage modulus (E_m') can be written using Einstein's considerations for suspensions with rigid particles [299,302]:

$$E'_c = E'_m(1 + rV_f) \qquad (3.3)$$

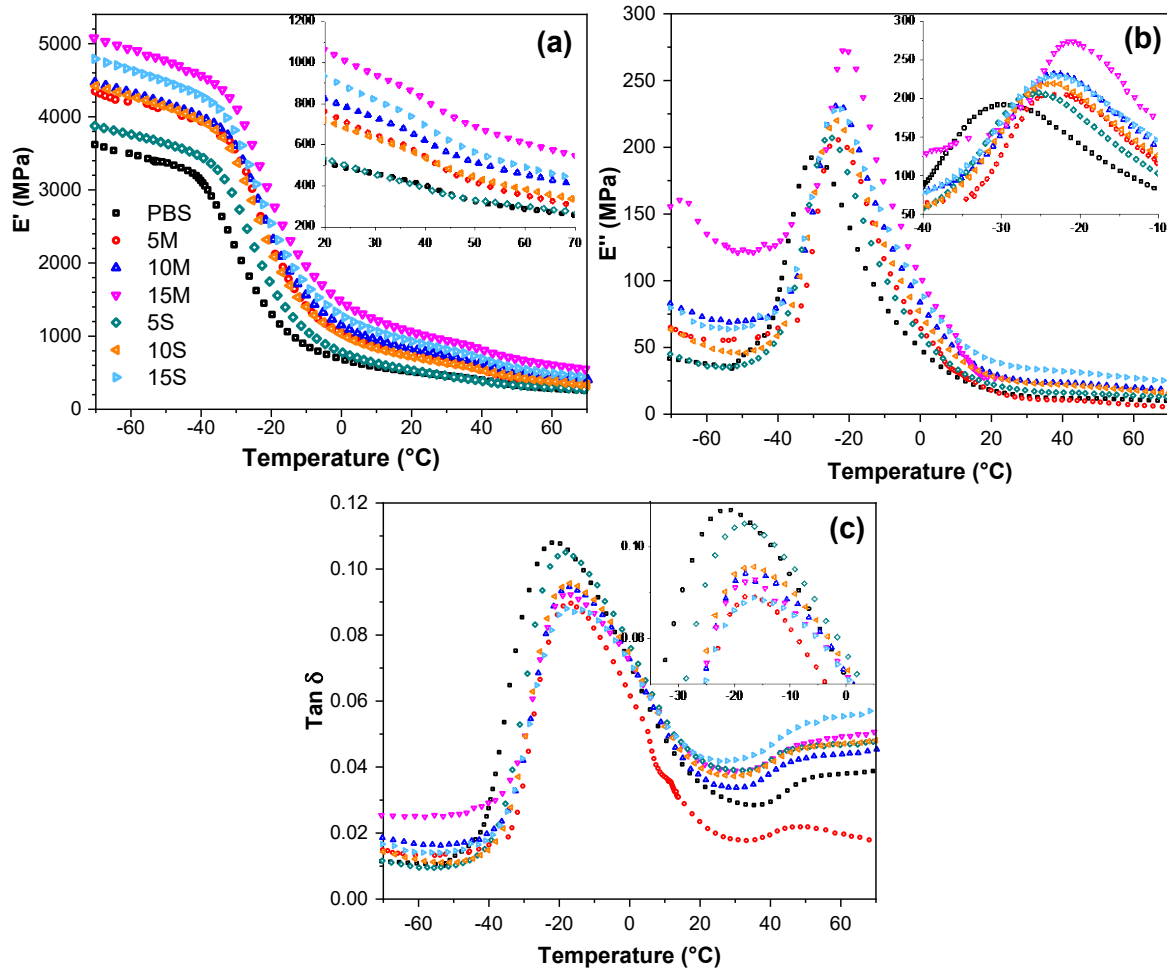where V_f – the volume fraction of filler in the composite.

Figure 3.29. Temperature dependence of (a) storage modulus, (b) loss modulus and (c) tan δ curves from DMA measurements comparing PBS and 5, 10 and 15 wt.% PBS/NFC nanocomposites fabricated using solution casting and melt compounding methods.

From equation (3.3), the ratio E_c/E_m was calculated and plotted against V_f as shown in Figure 3.30.b, where dash lines represent *r* value trend, while specific values are given in Figure 3.30.c. Calculations for E_c/E_m were performed using the storage modulus values at 25 °C. Reinforcement efficiency, unlike parameter *C*, does not directly correlate with filler loading. Melt processed samples similarly outperform solution cast ones. 5S shows similarly poor results, which indicate almost no formation of reinforcement network. In comparison, other solvent cast samples show an increase in values that are significantly lower than melt-processed samples. Masterbatch process shows great potential, with a 5M sample having the highest r-value of 10.75, which sees a decrease in higher filler loadings. Such results can be expected with the high loading of the nanofillers as agglomerates are formed. The contact surface between the filler and the polymer is affected, decreasing the mechanical performance [301]. As seen from the results, solvent cast samples had a high concentration of agglomerates even at the lowest loading. It resulted in the opposite trend of adding more NFC yields better reinforcement. Cailloux et al. reported a polyethylene glycol (PEG) carrier system for melt-processed 5 wt.% loaded PLA/NFC composite preparation [297]. However, storage modulus values compared to neat PLA showed almost no increase. The values decreased when PEG was

95

included in the composite's composition, which further illustrates NFC dispersion's importance with the correct nanocomposite preparation method.
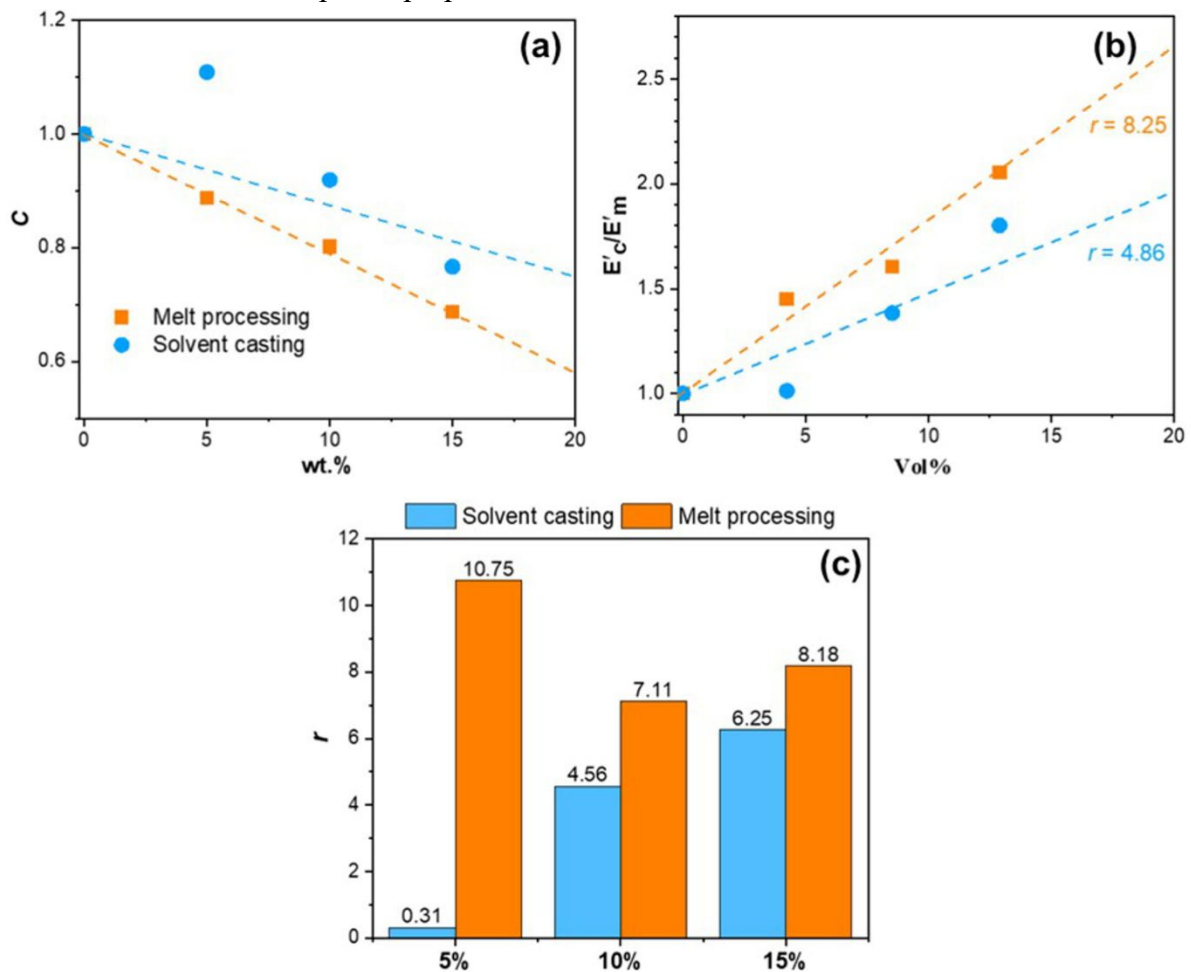
Figure 3.30. (a) C factor as a function of weight content calculated from E′ values at - 60 °C and 40 °C, (b) E′c/E′m ratio plotted with vol% at 25 °C and (c) reinforcement factor (r) with samples wt.% at 25 °C.

3.3.7. Summary

The highly loaded masterbatch process has great potential for application in industrial composite film preparation for packaging and other applications. The composites gain increased stiffness, improved biodegradability and, as described in literature, increased barrier properties. The use of nanosized cellulose did not significantly affect composites tensile strength, a common issue for polymers reinforced with cellulose and lignocellulose fibers. The research will help with the further industrialization of biodegradable cellulose nanofibrils.

Nanofibrillated cellulose was used as a filler for poly (butylene succinate). Highly loaded 50 wt.% masterbatch preparation route was compared to conventional solvent casting. The effect on the filler dispersion and loading was studied to understand these bio-based and biodegradable compositions. The nanocomposites' optimal preparation method was the masterbatch process, and reinforcement network was achieved with the lowest concentration of 5 wt.% NFC. SEM analysis indicated good filler dispersion even at a high loading of 15 wt.% for the sample prepared from masterbatch, but all solvent cast samples had visible

agglomeration. Biodegradation disintegration time was significantly reduced till 60 days, with composites showing up to 20% lower weight within the same amount of time in the soil. The observations were confirmed by FTIR and DSC measurements that showed various degradation products consisting of vinyl, hydroxyl, ketone, and carboxyl groups produced by microorganisms and hydrolysis and decreased crystallization temperature. The total degradation time of nanocomposites was determined to be around 80 days. Thermal degradation analysis showed good thermal stability for all compositions, and the lowest maximum decomposition temperature was 398 °C compared to 404 °C for neat PBS. The lowest temperature for 5 wt.% loss was 308 °C which is well above 160 °C used for masterbatch preparation. The mechanical properties increased with NFC loading; indeed, elastic modulus enhanced up to almost 1.7-fold, storage modulus up to 2-fold, and loss modulus up to 1.3-fold in room temperature. In addition, the glass transition temperature was increased by 2 to 5 °C compared to neat PBS. Reinforcement efficiency reached 10.75 for 5M showing the highest results, while the overall effectiveness of the NFC filler from parameter C = 0.69 was for the 15M sample. NFC filler's nucleating effect on PBS was observed with an almost 4 °C increase in the crystallization temperature, but polymer chain movements were restricted, and crystallinity decreased by 8 to 13%.

3.4. Highly loaded cellulose/poly (butylene succinate) sustainable composites for woody-like advanced materials application

The main goal of this study was the preparation and characterization of poly (butylene succinate) (PBS) and micro cellulose (MCC) woody-like composites with various modification methods. These composites can be applied as a sustainable woody-like composite alternative for conventional fossil polymer-based WPCs. The PBS/MCC composites were prepared using a melt blending with a very high filler loading of 70 wt.%. MCC was modified to enhance the dispersion and compatibility by means of carbodiimide (CDI), polyhydroxy amides (PHA), alkyl ester (EST), (3-Aminopropyl) trimethoxysilane (APTMS), maleic acid anhydride (MAH) and polymeric diphenylmethane diisocyanate (PMDI). Tensile tests were used to evaluate composites performance in regard to unmodified system and original polymer. Data was enhanced with DMA analysis that showed storage modulus changes depending on the temperature. FTIR was studied to examine bonding between the polymer and cellulose components in the composite. In contrast, SEM complemented results with liquid fracture surface showing significant differences between chosen modification methods. Thermal stability and biodegradability were evaluated to assess prepared composites potential applications.

3.4.1. Material processing and composite formulations

The aim was to use the high loading of MCC filler in the composite. Thereto PBS was mixed with 70% (w/w) cellulose in a thermo-kinetic mixer (Plastograph EC plus 50EHT, Brabender GmbH & Co. KG, Duisburg, Germany). Considering the previous investigations, which showed the possibility of high loadings of cellulose filler for PBS composites manufacturing, the MCC filler content was proposed to be equal to 70 wt.%. The processing temperature was set to 130 °C, and the screw speed was 70 rpm. In total, 40 g per batch were introduced in the thermo-kinetic mixer for a total mixing time of 7 min. The PBS and MCC were dried in a vacuum chamber at 40 °C for 24 hours before composite preparation.

The PBS/MCC composites were ground and compression-moulded with a Carver CH 4386 hydraulic press to obtain thin films. The plate temperature was set to 140 °C, and the material was preheated for 2 min and formed with a pressure of 3 metric tons for 3 min, followed by rapid cooling between metal plates at room temperature for 3 min. The dog-bone shape and stripes specimens were cut. These specimens were further tested for tensile, structural, dynamic-mechanical, density, calorimetric, and thermal properties.

3.4.2. Chemical modification of PBS/MCC composites

It is well known that the modification of the polymer/cellulose composites is needed to enhance the polymer and cellulose components' interface compatibility as a means to obtain high exploitation properties of the final composite material [27]. The strong interfacial adhesion and efficient stress transfer across phases of the polymer matrix and cellulose filler can be established by different modification additives during the composite processing. Based on this principle, the additives of MAH, PMDI, CDI, EST, PHA, APTMS are used to adjust the interfacial interactions through compatibilization of the components [78–85]. The used compositions and the modification procedures were selected regarding the literature data and

preliminary tryouts. Altogether, seven different PBS/MCC compositions were obtained by using different chemical modification treatments of composites to improve the compatibility between the components (Table 3.12). The obtained PBS/MCC composites and specimens were stored in sealed bags before any testing.

Table 3.12.

Obtained PBS/MCC compositions.

Sample	Description of modification
PBS	Neat polymer
70MCC	Untreated microcrystalline cellulose
70MAH	Maleic acid anhydride
70PMDI	Polymeric diphenylmethane diisocyanate
70CDI	Carbodiimide
70EST	Aliphatic ester
70PHA	Polyhydroxyamide
70APTMS	(3-Aminopropyl) trimethoxysilane

For PBS/MCC composite modification, 1 wt.% of MAH, 1.5 wt.% of PMDI and 3 wt.% of CDI were loaded during the melt processing process with a thermo-kinetic mixer [81–84]. At the same time, modified MCC was blended with PBS without any additional additive loading. The modified MCC preparation is the following. 30 g of MCC was suspended in 500 ml water, and the mixture was homogenized with ultrasound sonification for 10 minutes. Slowly 90 ml of PHA or EST were added in 2 hours, stirring and ultrasound sonification were applied sequentially for 30 min time periods [85]. The acquired modified MCC suspensions were then filtrated and dried in a vacuum. For the salinization, 50 mL of APTMS was dissolved in 250 mL distilled water and stirred, while the solution pH was stabilized to 4 by the addition of acetic acid [52]. 50 g MCC was added to the solution after pH was fixed at 4. The mixture was stirred at room temperature for 2 h, followed by filtration and drying in a vacuum. Chemical reaction and permanent surface modification of MCC has accomplished a vacuum oven at 120 °C for 2 h. The schemes that demonstrate interactions of filler or matrix with selected chemical modifications are presented in Figure 3.31.
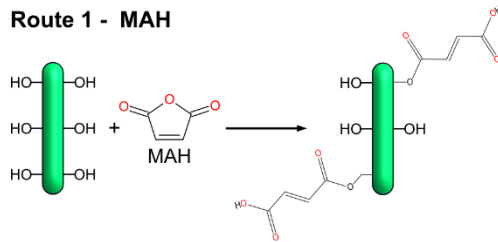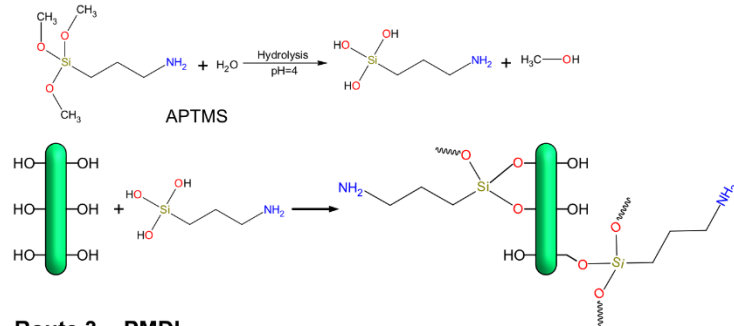
Figure 3.31. Applied chemical modifications, coatings, and chain extender.

3.4.3. Thermal properties

TGA was used to investigate the influence of the composition on the thermal sensitivity and degradation properties of PBS/MCC composite materials. Figure 3.32. showed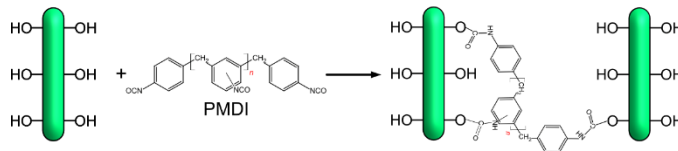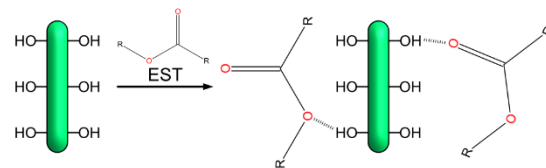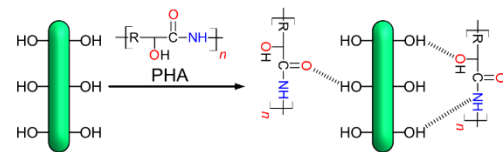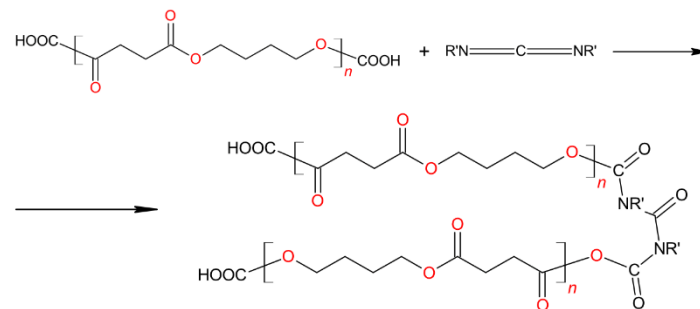 TGA (a) and DTG (b) curves of PBS/MCC composites. All PBS/MCC compositions showed a small mass loss of 2% below 100 °C, corresponding mainly to the removal of residual water [28]. The degradation mechanism and degradation temperature of neat PBS and c PBS/MCC composites differed strongly. It is assumed that MCC has lower thermal stability than neat PBS polymer [29,30]. This means that the incorporation of the MCC induced less thermal stability of PBS/MCC composites. Lee, et al. reported this for PBS/kenaf fiber composites [31]. The temperature at 5% mass loss for 70MAH composition was 240 °C and for 70EST composition was 290 °C. The rest of the composites showed a temperature at 5% mass approximately in this 240-290 temperature range. The PBS exhibited only single-stage degradation with a peak at 406 °C, whereas MCC filled composites revealed two degradation peaks in the temperature range of 301–398 °C. It indicated that the single-stage thermal degradation process was defined primarily by the PBS polymer chain degradation, while PBS/MCC composites degradation was affected by cellulose incorporation, mutual interaction between polymer matrix and fillers and filler surface modification. Roman and Winter evidenced the strict relation of cellulose surface modification and its thermal stability [32]. The temperature at 50% mass loss for PBS was 401 °C. The first stage of degradation in DTG (Figure 3.32.b) is at around 310 °C for the 70MCC sample; while for 70MAH, 70PMDI, and 70CDI composites the thermal degradation shifted to lower temperature 315 °C, then for 70EST, 70PHA and 70APTMS composites, thermal stability increased up to 340 °C. The composites loaded with chemically coupled and modified MCC revealed enhanced thermal degradation temperature at 50% mass loss up to 360 °C. This was described to the formation of crosslinked structures with the altered chains and inhibited chain release during the formation of the char in the thermal degradation process [33]. The similar behavior of thermally more stable PBS composite than neat PBS was reported by Tang et al. [34] when using grafted-nanocellulose as reinforcement.
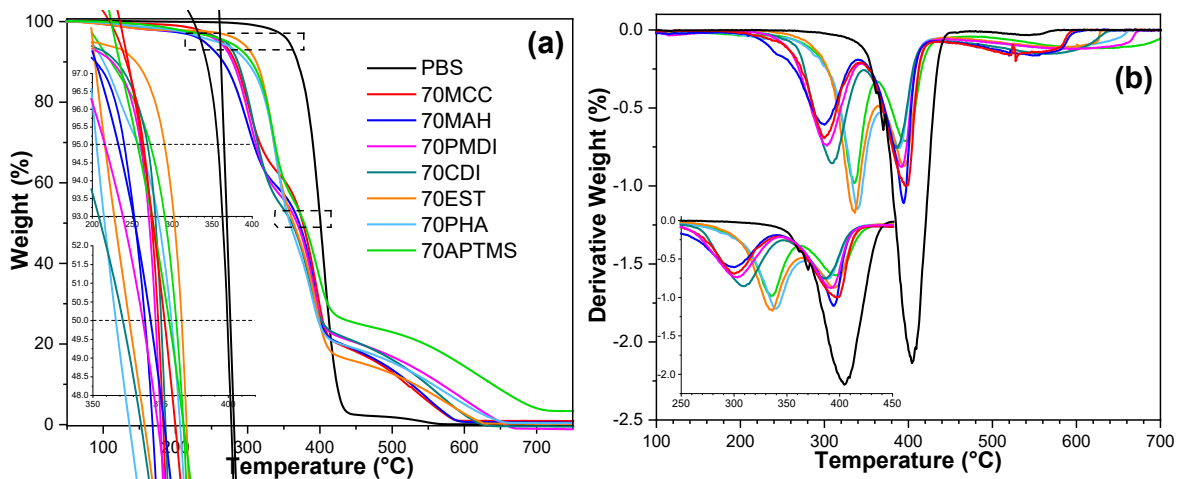

Figure 3.32. (a) TGA curves and (b) DTG of PBS/MCC composites.

The results of DSC in the form of the heating and cooling thermal curves of PBS/MCC composites are shown in Figure 3.33. The thermal curves showed a characteristic endothermic

melting transition (Figure 3.33a) and exothermic crystallization transition (Figure 3.33.b). Meaning changes in the shape of the transitions were observed. While the crystallization process shifted to the higher temperature range. The influence of the MCC usually results in either enhanced crystallization characteristics due to the nucleation effect or obstruction of polymer molecular chains, which limits the growth of polymer crystals [35]. Enhanced crystallization by means of nucleation and trans-crystallization has been reported mainly for polymer composites with cellulose and other fillers contents up to 30 wt.% [36]; while surface modification of cellulose can strongly hinder polymer chain mobility through physical adsorption and entanglement. This promoted the polymer transcrystallization process on the cellulose, which also has been ascribed by observed pronounced enhancement of the composite's mechanical and dynamic mechanical characteristics [37]. Generally, the high loading of MCC reduced crystallinity significantly [38]. This is also the case for composites with extremely high loadings – up to 50-80% of MCC. In Table 3.13. the experimental values of melt temperature (T_m), crystallization temperature (T_c), enthalpy of melting (H_m), enthalpy of crystallization (H_c), crystallinity (χ), density (d) and voids (Δ) are presented. All samples with modified MCC showed a very pronounced decrease in X compared to neat PBS and also in comparison to the 70MCC sample. X of neat PBS has been found to be about 68%. In the case of 70APTMS, 70PHA and 70EST samples χ has decreased to 52, 56, 58% correspondingly. Similar findings have also been also reported in the literature [38]. The MCC's silane treatment improved its dispersion in a polymer matrix, reduced agglomeration and suppressed the crystalline phase more strongly than PHA and EST modifications of MCC filler [39]. The chain cross-linking and/or extension mechanisms can further limit polymer chain movements and reduce crystallinity [35]. It is observed that crystallinity decreased by about 20% for compositions 70MAH, 70PMDI and 70CDI in comparison to neat PBS. Melting temperature T_m and crystallization temperature T_c of the obtained samples were modestly decreased and increased correspondingly. This means that crystallization of polymer chains with altered flexibility and mobility in the composites interfered with the crystallization process [34,36,38], which has started earlier at higher temperatures and resulted in lower crystallinity by about 30% of the final composite.
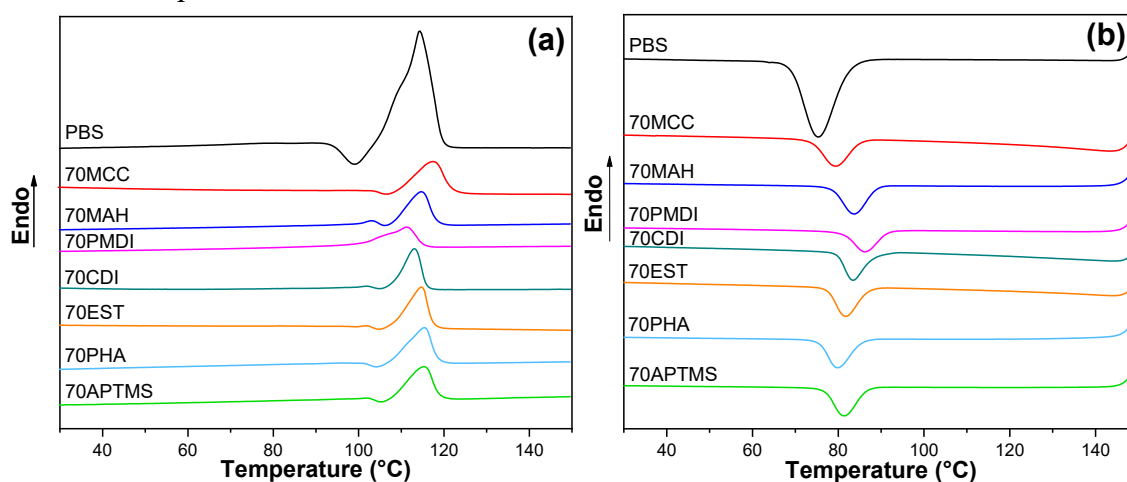

Figure 3.33. DSC curves of PBS/MCC composites: (a) heating, (b) cooling.

3.4.4. Structure and Morphology Characterization

The experimental density values d of the composites, obtained by the weighting method [40], are summarized in Table 3.13. The value of the parameter d*, defined as the apparent density of the polymer, was calculated by the equation reported elsewhere [41]. It can correspond to the decrease of the polymer density due to the pronounced drop in crystallinity observed in DSC. SEM images of the fractured surfaces of PBS/MCC composites (Figure 3.34.) evidenced the aggregates of MCC particles. According to the literature [42,43], cellulose particles had a common tendency to aggregate at high MCC loadings. The fractured surfaces of the 70MCC sample were very rough. MCC particles can be seen for 70MCC, 70MAH, 70EST, 70PHA samples. In turn, 70CDI, 70PMDI, and 70APTMS samples' surfaces looked smooth, homogeneous, and dense in different magnifications. These compositions could be characterized by enhanced compatibility between the polymer matrix and the filler. It is evidenced by the pronounced decrease of crystallinity, dense structure, and uniform dispersion of MCC particles. It also well correlates with the obtained d and χ values for the PBS/MCC composites. It is reported that the used MAH, EST, PHA, CDI, PMDI, and APTMS can wet and disperse to some extent the cellulose fillers more efficiently in the polymer matrix. MAH can also form an ester linkage between the maleic anhydride and the hydroxyl groups of the cellulose and facilitate cellulose dispersion [44]. While Espino-Pérez, et al. established that PMDI is a very effective compatibilizer, as chemical coupling can be established between the isocyanate and the hydroxyl groups on cellulose; the isocyanate and the carboxylic acid end-groups of the polyester [45]. In turn, the cellulose treatment with the silane is also reported to be the most effective among the others to improve the compatibilization and dispersion, which indicates that intramolecular and intermolecular interactions between the cellulose and the polyester are established [46].

The characteristic groups of the composites can be evaluated by FTIR spectroscopy. The representative FTIR spectra of the tested compositions are shown in Figure 3.35. and selected spectra overlays in Figure 3.36. The characteristic absorption peaks associated with components are highlighted. The absorption band between 3600 and 3100 cm^{-1} (1) corresponds to OH vibration in MCC. The band between 3000 and 2800 cm^{-1} with the absorption band at 2946 cm^{-1} (2) and the band at 1331 cm^{-1} (4) corresponded to symmetric and asymmetric CH$_2$ stretching vibration [47]. While 1712 cm^{-1} (3) C=O stretching vibrations of the ester group are usually used as one of the key bands to characterize PBS spectra [19,48–50]. At 1150 cm^{-1} (5) is an absorption band for the C-O stretching vibration of PBS. The decrease in its intensity reflects a reduction in the crystallinity of the composite material [49]. A shift of this band corresponds to the interaction between cellulose and polymer chain in the composite [51]. Finally, a band between 1050 and 1010 cm^{-1} with the maximum at 1046 cm^{-1} (6) corresponds to the stretching vibration of the O-C-C. In the 70APTMS sample's spectra, a new absorption band is observed at 1557 cm^{-1} and has been attributed to the NH scissoring bending vibration [48,50,52]. In the 70EST sample's spectra, there are decreased intensities of the ester's C=O and C-O characteristic bands at 1712 and 1150 cm^{-1} correspondingly, while the O-C-C group's band intensity increased at 1046 cm^{-1}. This could indicate the intramolecular interactions
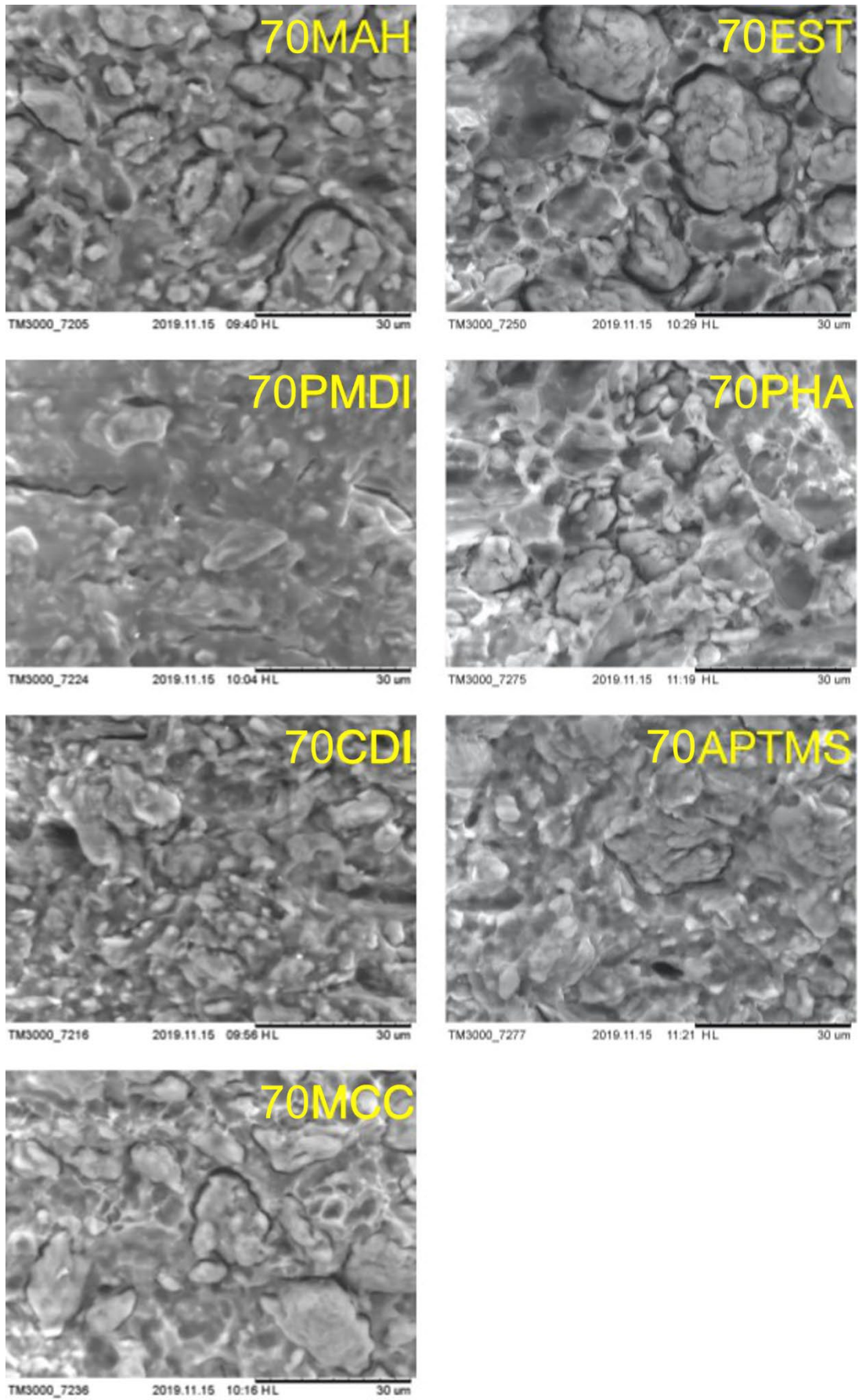
Figure 3.34. SEM micrographs of fractured surfaces of PBS/MCC composites.

between the ester chains and the cellulose surface. An absorption band at 1100 cm^{-1} could be attributed to C-O stretching vibration for the aliphatic ether linkage in the interphase of cellulose and polymer matrix. In the 70PHA sample, there is a noticeable increase of the ester's group bands intensities at 1712 and 1150 cm^{-1} that could be resulted from formed ester linkages between the cellulose and polymer. In turn, the 70CDI composition can be characterized with the new bands at 1556 and 1245 cm^{-1} that could correspond to the NH and CN, correspondingly [53]. The reaction of the carbodiimides and the carboxyl groups end-groups of the polyester macromolecules could lead to the chain extension, chain crosslinking, and the urea group linkages. The 70PMDI spectra have shown absorption bands at 1603 and 1510 cm^{-1}, which could be attributed to the C=O urethane group stretching and C=C aromatic rings, correspondingly; these linkages could be formed between the isocyanate and the hydroxyl groups on cellulose, and the isocyanate and the carboxylic acid end-groups of the polyester [45,54,55]. The 70MAH composition is characterized by the characteristic absorption bands at 1712 and 1150 cm^{-1}, which can testify to the formation of the ester linkages between the maleic anhydride and the hydroxyl groups of the cellulose [44].
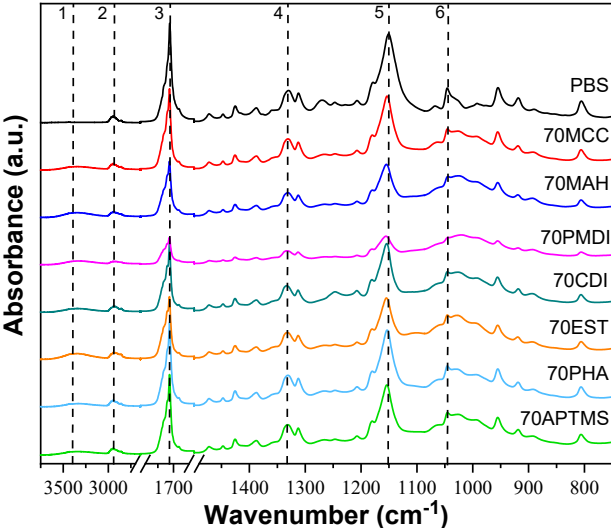
Figure 3.35. FTIR spectra of PBS/MCC composites.
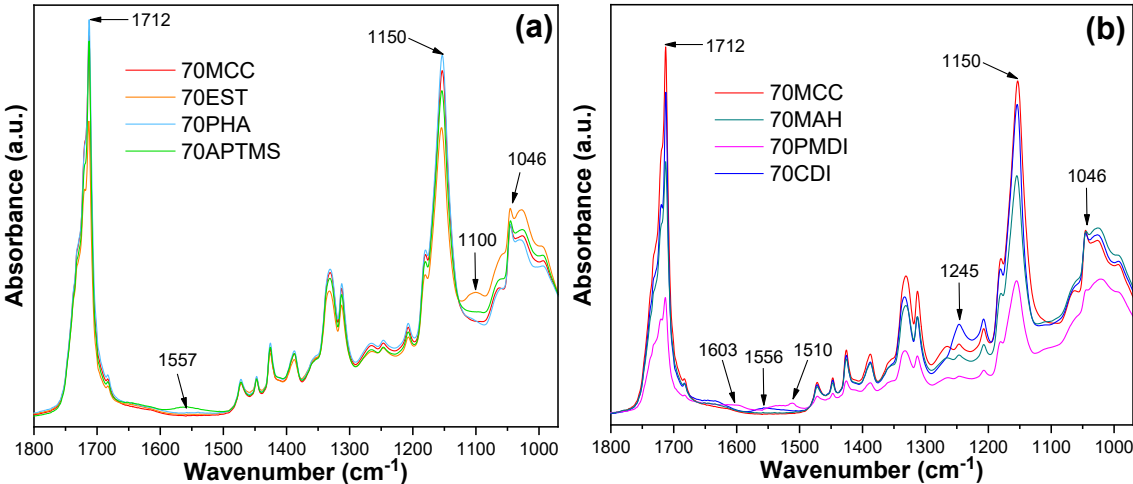
Figure 3.36. FTIR spectra of PBS/MCC composites with spectra overlays.

105

3.4.5. Thermomechanical properties

The dynamic mechanical data of the composites were measured with respect to the temperature. The viscoelasticity of PBS/MCC composite improved and rigidity dropped by with an increase of temperature. Figure 3.37. shows the temperature dependence of the storage modulus E′, loss modulus E'' and damping factor tanδ for PBS/MCC composites. PBS has three regions in the DMA curve that could be identified glassy, glass transition and rubbery regions. Glass transition region of PBS started with a sharp decrease in storage modulus that corresponded to the peak in loss modulus and tanδ graphs. Introduced 70 wt.% loading of MCC into PBS polymer can restrict overall chain mobility severely that drastically raise its viscosity [56,57]. Accordingly, MCC composites showed a less pronounced transition between the glassy and rubbery states.

MCC acted as a very effective reinforcement and increased storage and loss modulus strongly, but due to the limited incompatibility of polymer and matrix, these enhancements can be limited to some extent [10,12,58]. This can be overcome by increased crosslinks' density and enhanced intersegmental interactions for the modified samples, resulting in higher rigidity of the polymer chains in composites. This can distribute mechanical stress more evenly in the material and improve mechanical properties [59,60]. The modified compositions characterized the improved stiffness after the PHA, CDI, PMDI and APTMS treatment due to the efficient cross-linking and chain extending of the composite and polymer correspondingly [35]. The limited polymer chain flexibility leads to a strong increase in material viscoelasticity. Furthermore, the E′ and E'' increased in all temperature range for those samples. For example, there was an almost 4-fold increase in E′ for 70APTMS composition at room temperature in comparison to neat PBS. APTMS treatment provided an almost 1.6-fold increase at +70 °C and a 2-fold increase at 0 °C in E′ in comparison to the 70MCC sample. In contrast, PMDI treatment gave 2.5-fold at +70 °C and 1.7-fold increase at 0 °C. In turn, 70EST composition showed pronounced enhancement in viscoelasticity properties and a decrease in stiffness compared to 70MCC, which can be related to plasticization of the material by introducing flexible long alkyl chains of the ester surfactant molecules [61]. It also showed strong enhancements in E'', which testified that higher energy was demanded the polymer viscoelastic deformation [62].

The loss factor tanδ dependence from the temperature is shown in Figure 3.37.c. It corresponds to the efficiency of energy dissipation due to the viscoelastic deformation of the material [28,57]. The representative tanδ varied with the temperature and the composition nature. MCC did not significantly affect the glass transition temperature of the material, but it did significantly affect the magnitude of tanδ absolute values. MCC loading raised the absolute values of the energy dissipation factor significantly because the composite's viscoelastic deformation requires more energy [63]. The noticeable gain in the energy dissipation of the 70EST composite confirmed the enhancements of the composite's viscoelastic characteristics due to the long alkyl chains of ester molecules. The characteristic temperature of the tanδ peak corresponded to a glass transition of the polymer matrix. For example, its value was –15 °C for PBS, -30 °C for 70EST, -10 °C for 70MAH. The shift in tanδ temperature provided information about the strong enhancement of interactions between polymer chains and filler and polymer chains due to enhanced cross-linking correspondingly.
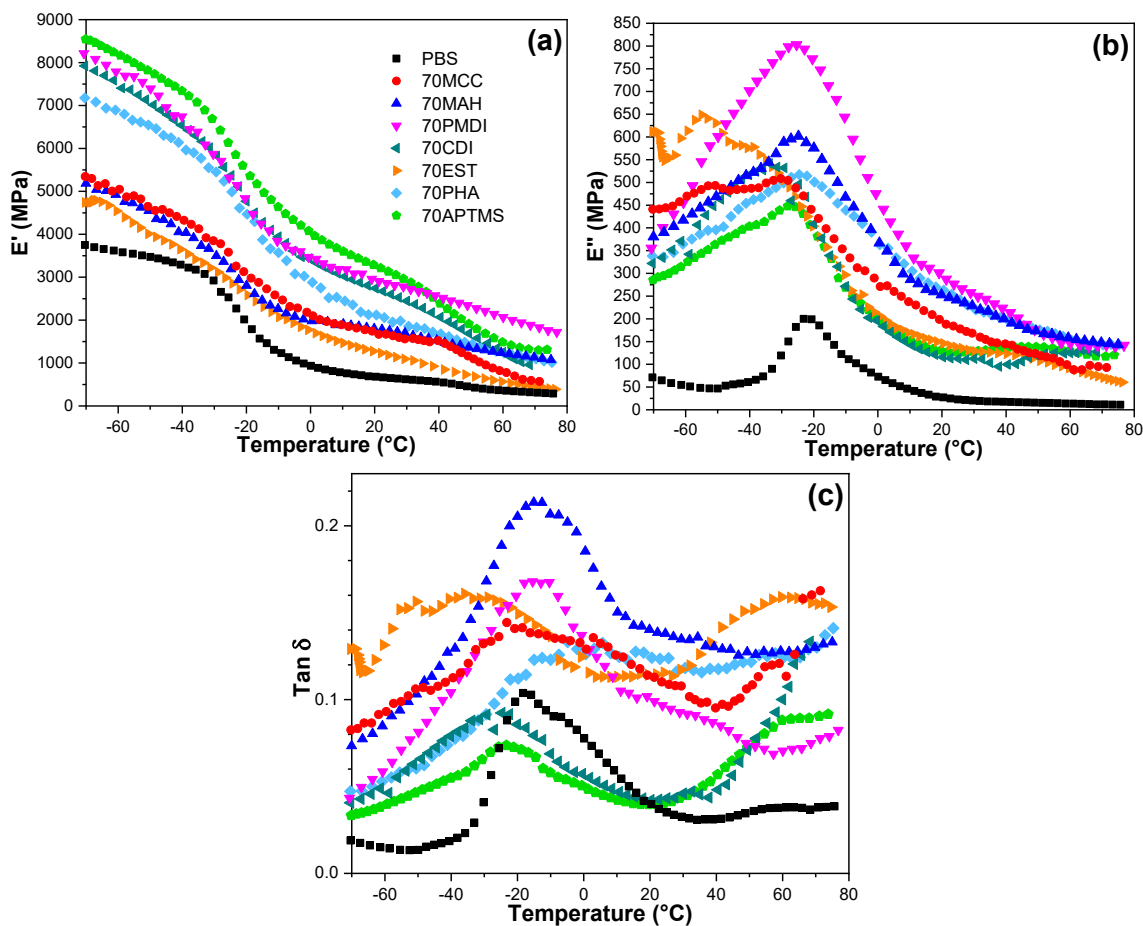
Figure 3.37. DMA curves of PBS/MCC samples: (a) storage modulus E', (b) loss modulus E''
and (c) loss factor tanδ.

Thermal and physical characteristics of PBS/MCC composites.

Sample	T_m, °C	T_c, °C	H_m, J/g	H_c, J/g	χ_c, %	d, g/cm³	d*, g/cm³
PBS	114.2	75.3	75.1	72.9	68.0	1.365	-
70MCC	117.5	79.4	21.4	19.8	64.6	1.370	0.947
70MAH	114.7	83.6	16.9	20.4	51.0	1.362	0.925
70PMDI	111.3	86.2	15.8	16.0	47.6	1.336	0.851
70CDI	113.1	83.4	15.6	16.8	47.1	1.315	0.791
70EST	114.8	81.8	19.2	18.2	57.9	1.385	0.990
70PHA	115.3	80.0	18.5	20.3	55.8	1.402	1.038
70APTMS	115.2	81.3	17.3	20.2	52.2	1.385	0.990

*calculated using the MCC density = 1.600 g/cm³ [64].

3.4.6. Mechanical properties

The tensile properties of the PBS/MCC composites were tested in tension mode. The Young's modulus E increased almost 4.5-fold for 70MCC composite in comparison to neat polymer (Figure 3.38.a). The increase in E is explained by the reinforcing effect, a common characteristic of highly loaded composite materials. As can be observed in Figure 3.38.b-c, there was a significant drop in tensile strength for some samples, and tensile strain decreased

for all samples compared to neat PBS. Generally, the addition of wood filler negatively affects the mechanical properties of the composite material. Kajaks et al. report that the increase of the wood filler amount strongly drops the strength and the ductility of the polyolefin/wood composites [65,66]. For example, for the 70MCC composite, the obtained E was 862 MPa, the σ was 9.7 MPa, but the ε value was 1.78 %. Similar results were also obtained for petrochemical polypropylene (PP) composites [66], which showed E of 510 MPa, σ of 10.9 MPa and ε of 5.09 %, and PP/wood composite filled with 50% of birch plywood sanding dust. Several authors also stressed that the mechanical properties of wood polymer composites are strongly dependent on the filler content, coupling agent and filler's modification treatment [67–69]. As expected, the additional cross-linking treatment of MCC composites increased the compatibility of the cellulose filler and the polymer matrix. As a result, the E values are increased to some extent. E values of the 70PMDI, 70CDI and 70APTMS compositions were remarkably higher than for 70MCC composite, which means improving the compatibility, stress transfer efficiency, and interfacial strength by establishing chemical bonds at the interfaces between cellulose and polymer matrix phases [27]. The E value raised 1.4-fold for 70PMDI, 1.6-fold for 70CDI and 1.1-fold for 70APTMS correspondingly. The tensile strength σ values for those samples were also significantly higher than for 70MCC composition and similar to initial neat PBS. The obtained σ values and the E values of the modified MCC composites are comparable to the polymer/wood composites reported by several authors [44,65,70].

Generally, all composites showed brittle tensile behaviour [36,58], which is also common for high rigid composites loaded with 70 wt.% of fillers. A common cause is the formation of aggregates and voids in the composite's structure and little bonding between the filler and polymer. This has been clearly evidenced by obtained SEM micrographs of the fracture surfaces for the processed composites (Figure 3.34.). This brittle behaviour can be attributed to successful chemical modification of MCC during composite preparation, which resulted in cross-linking bonding's' being developed between filler and polymer. While 70MAH, 70PHA and 70EST composites showed moderate improvement in rigidity, a strong decrease in strength and strain, which could have been affected by poor dispersion and weak bonding between components of the composite material. It is reported that the MCC interacted strongly with the polymer chains only by polar interaction with chain ester group units [43]. However, the functionalization of the filler surface leads to the enhancement of interaction strength with the developed moieties at the MCC [71]. Whether the chemical bonding of cellulose with the polymer chains through cross-linking contributed to further enhancement of material stiffness properties [58,72]. It should be noted that remarkable stiffness improvements have been generally achieved only when MCC filler is homogeneously dispersed in the polymer matrix that can promote strong interfacial interaction and suppressed polymer chain mobility [73]. Hence the tendency of particle agglomeration can be diminished by chemical treatment of its surface [74,75].
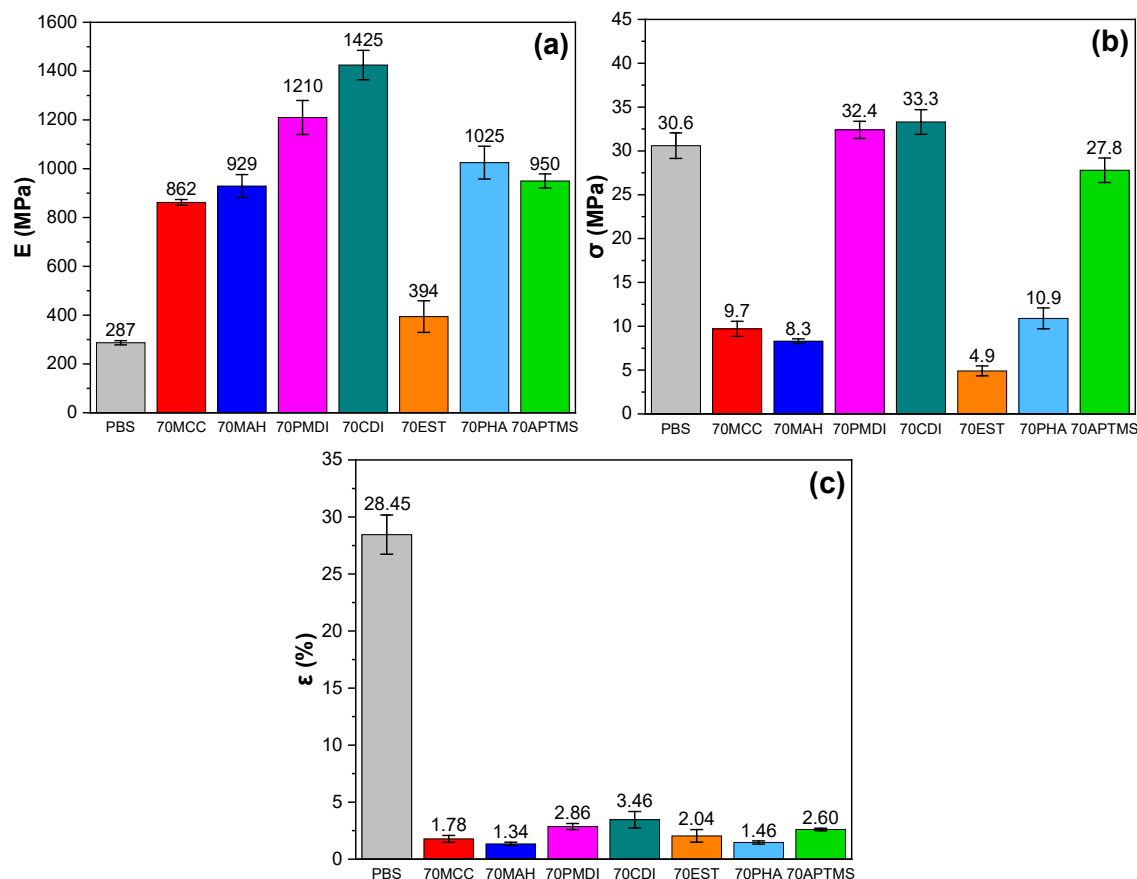
Figure 3.38. Tensile properties for PBS/MCC composites: (a) elastic modulus E; (b) strength σ; and (c) strain ε.

3.4.7. Biodegradation under composting conditions

As discussed by the authors, the polymer structure, molecular chain weight, and size can severely affect PBS biodegradation in soil [303]. The temperature, moisture, pH, and the population of active microorganisms are also essential to facilitate the material biodegradation process [304].

However, the obtained biocomposites modified by different chemical routes showed further degradation only after 30 days in compost soil. The biodegradation of the biocomposites was maintained until the complete disintegration of the material or up to 90 days, as shown in Figure 3.39. The calculated disintegration as a function of ageing time is summarized in Figure 3.40. The received results reveal that the cellulose and polymer modification chemistry significantly impact biocomposite durability due to their different hydrophobic character, as shown in Figure 3.31.
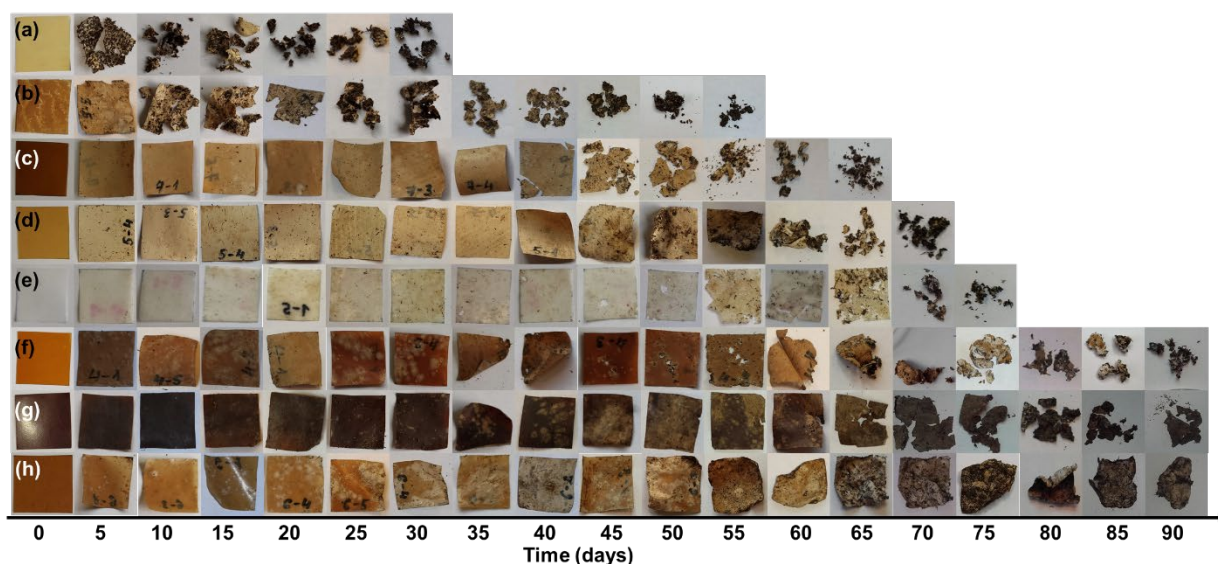
Figure 3.39. Biocomposites degradation in composting conditions: (a) 70EST, (b) 70MAH, (c) 70PHA, (d) 70MCC, (e) PBS, (f) 70APTMS, (g) 70PMDI, (h) 70CDI.
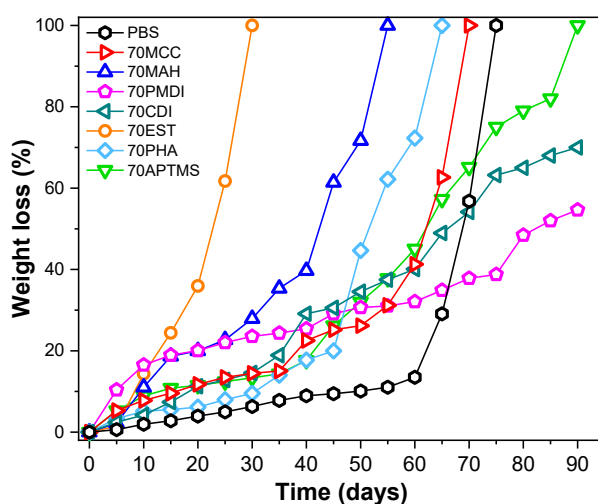
Figure 3.40. Percentage weight loss of PBS and biocomposites in soil burial test conducted in composting conditions.

PHA, APTMS, PMDI, and CDI treatment reduced composites biodegradation, which becomes even longer than the neat PBS and 70MCC composite. This shows that surface wettability does not directly translate to accelerated degradation due to the developed good adhesion between filler and matrix [305] and decreased surface area for the degradation process [306]. Biocomposites 70EST and 70MAH behavior are opposite to the previous ones. 70EST and 70MAH degrade rapidly from the 5 and 15 days, and samples cannot be separated from the soil as seen after 30 and 55 ageing days correspondingly. The total biodegradation of the obtained biocomposites corresponds to polyesters PBS and biodegradable cellulose character promoted by its hydrolysis under high humidity and bacteria conditions [303,304]. It is reported elsewhere that both low crystallinity of the polymer and high hydrophilicity of the cellulose facilitated the water wetting the composites surface, enhanced water penetration, and promoted

the attack of water molecules on the polymer chains [307]. Chemically modified biocomposites with incorporated polar functional groups of amines and carbonyls can absorb moisture through hydrogen bonds, then its biodegradation occurs rapidly [31]. While non-polar nature silane and urethane functional groups introduced into the chains slow down the sample's total deterioration until 90 days. While 70MAH, 70PHA, and 70MCC biocomposites degrade after 55, 60, and 65 days, because they showed voids, cracks, and poor adhesion between cellulose filler and polymer matrix as discussed in the previous study in SEM analysis [305] and, therefore, these samples absorb more moisture than other samples such as 70PMDI, 70APTMS, and 70CDI, which formed excellent phase contact surface. Used PMDI content does not impart the degradation properties of the biocomposites strongly. The observed results are in line with that obtained by other authors [305,306,308], that the complete deterioration of the PBS/lignocellulose biocomposites was between 60 to 100 aging days in the composting conditions.

3.4.8. Summary

The prepared PBS/MCC composites are very promising materials as a sustainable woody-like composite alternative for conventional fossil polymer-based wood-plastic composites (WPC) application. Composites were processed by melt blending, and filler content was selected at 70 wt.%. Surface chemical treatment and composition modification were performed to enhance compatibility between cellulose filler and polymer matrix as well as enhance several exploitation properties. The structure of the composites is affected strongly by the used chemical modification treatment of the MCC, which was identified with FTIR analysis.

The chemical modifications of MCC composites lead to enhanced mechanical, thermo-mechanical and thermal properties of the PBS/MCC composites. Tensile strength was enhanced around 3-fold for 70CDI, 70PMDI and 70APTES compared to unmodified composite, while elastic modulus values were enhanced for all compositions (except 70EST) 1.1 to 1.7-fold. Storage modulus demonstrated that formation of a stable reinforcement network yielded up to a 4.5-fold increase at 40 ˚C and up to a 6-fold increase at 75 ˚C for prepared modified composites compared to neat PBS. The observed changes in storage modulus values and glass transition indicated the formation of strong interfacial bonds. The ductility of the obtained composites is strongly decreased after incorporating the cellulose; nevertheless, the composites' can be applied for various construction applications, including profiles, decks, and housing of appliances, where high ductility is not compulsory.

The significant differences in biodegradation time were caused by selected modifications, which can be used for specific applications. 70EST composite degraded remarkably in 30 days, more than two times faster than neat PBS, while 70CDI and 70PMDI samples retained at least a third of their mass after 90 days. MCC promoted biodegradation as indicated by unmodified composites degradation time, which was about 10 days shorter.

4. COMPOSITE MATERIAL PROPERTIES – AN OVERVIEW

In total, the Thesis includes the preparation of 23 composites with a comparison to neat PBS. Table 4.1. summarizes the highest loadings of three cellulose fillers prepared in various ways and two of the best compatibilized compositions of MCC. From the obtained data, it is clear that the most significant changes are observable in mechanical and thermomechanical properties. Generally, the addition of cellulose fillers resulted in a stiffer material compared to PBS. The addition of cellulose fillers also increased the crystallization temperature and decreased the crystallinity. Crystallinity was significantly reduced as a result of the modifications. All cellulose fillers reduce the thermal stability of composites compared to neat PBS. However, the processing temperatures used for melt mixing at 130–160 °C are significantly lower than even the initial degradation that occurs above 250 °C. Modifications strongly shifted the glass transition temperature. But for the composites prepared only from cellulose and PBS, the melting and the glass transition temperatures remained close to the PBS value.

Table 4.1.

An overview of properties for highly loaded composites for representative fillers and preparation methods.

Properties	PBS	50rCell	40MCC	40NFC	15S	15M	70MCC	70CDI	70APTMS
T_m, °C	114	115	117	114	114	116	118	113	115
T_c, °C	75	90	85	82	78	78	79	83	81
χ_c, %	66	14	64	53	58	54	65	47	52
$T_{50\%}$, °C	401	384	382	384	389	392	377	363	380
E, MPa	271	866	613	561	383	460	862	1425	950
σ, MPa	30.9	12.6	22.5	12.9	26.3	28.2	9.72	33.3	27.8
ε, %	33.3	1.99	5.11	3.18	14.2	10.8	1.78	3.46	2.60
E', MPa (20°C)	683	2001	1495	1395	931	1060	1731	2750	3274
E'', MPa (20°C)	27	139	58	53	40	27	198	116	129
T_g, °C	-18	-18	-16	-17	-16	-17	-21	-26	-23

The biodegradation time in days for prepared composites is shown in Table 4.2. The results indicate that cellulose accelerates the degradation of composites compared to neat PBS, but the use of various compatibilizers and chemical modifications can significantly shift the degradation time in both directions, i.e., shorter or longer. Furthermore, increasing the cellulose content reduces the time it takes for the composite to degrade.

Table 4.2.

Comparison of biodegradation Time.

	PBS	PBS/rCell composites	PBS/MCC/NFC melt composites	PBS/NFC solution and masterbatch composites	PBS/70 wt.% MCC compatibilized composites
Biodegradation time in the composting conditions, days	75–85	70	65–70	80	30–90 (2 remained even after 90 days)

5. CONCLUSIONS

1. In total, 23 different types of compositions were prepared within the scope of the Tesis, with cellulose filler loading ranging from 5 to 70 wt.%. Three different types of cellulose fillers were successfully integrated into composite formulations – recycled cellulose, microcrystalline cellulose, and nanofibrillated cellulose. The compositions were studied using melt blending, masterbatch melt processing, and solution casting methods. Six different types of modification methods were tested, and their tuneable properties were determined.

2. The freeze-dried NFC powder direct melt incorporation into PBS resulted in agglomeration of cellulose filler and poor mechanical performance of the composite compared to the PBS/MCC composite. PBS/NFC composites prepared with the masterbatch process showed up to 30 % higher mechanical and thermomechanical properties at room temperature compared to those prepared with the solution method.

3. Chemical modifications of the MCC composites led to enhanced mechanical, thermo-mechanical, and thermal properties of the PBS/MCC composites. The high loading of 70 wt.% MCC demanded compatibilization between filler and matrix. Chemical modifications influenced the glass transition temperature – 10–20 °C shifts to both higher and lower temperatures. The modification of cellulose prior to melt mixing increased the thermal stability of the composite material by up to 30 °C.

4. Biodegradation under composting conditions showed that PBS degrades completely in 75 to 85 days, while the addition of cellulose accelerated biodegradation by approximately 10 days. Higher loadings of cellulose accelerated biodegradation, with the most notable difference observable at concentrations of 5 to 10 wt.%. The cellulose type only slightly influences degradation. Chemical modification strongly influenced the PBS/MCC composite biodegradation time, which ranged from 30 to 90 days with some compositions retaining part of their mass even after 90 days.

5. Biocomposites are suitable for a variety of applications, like WPCs, packaging materials, mulch films, and many more, and these composites only start to degrade when buried in the soil. The exceptional thermal stability exhibited by compositions during processing proved that PBS/cellulose composites are compatible with conventional processing methods and can be produced on an industrial scale.

REFERENCES

1. Biopolymers - facts and statistics. Availabe online: https://www.ifbb-hannover.de/en/facts-and-statistics.html (accessed on 23.03.2021.).

2. Garside, M. Global plastic production 1950-2019. Availabe online: https://www.statista.com/statistics/282732/global-production-of-plastics-since-1950/ (accessed on 23.03.2021.).

3. SDK to terminate production and sale of biodegradable plastic. Availabe online: https://www.sdk.co.jp/english/news/15030/16250.html (accessed on 23.03.2021.).

4. A friendly catalyst to help you become an environmentally friendlier brand. Availabe online: http://www.pttmcc.com/new/faq.php (accessed on 23.03.2021.).

5. Polybutylene succinate resin. Availabe online: https://fillplas.com/polybutylene-succinate-pbs-fillplas-resin/ (accessed on 23.03.2021.).

6. Rudnik, E. 10 - Compostable Polymer Materials: Definitions, Structures, and Methods of Preparation. In *Handbook of Biopolymers and Biodegradable Plastics*, Ebnesajjad, S., Ed. William Andrew Publishing: Boston, 2013, 189-211, doi:10.1016/B978-1-4557-2834-3.00010-0pp.

7. Patel, M.K.; Bechu, A.; Villegas, J.D.; Bergez-Lacoste, M.; Yeung, K.; Murphy, R.; Woods, J.; Mwabonje, O.N.; Ni, Y.; Patel, A.D., et al. Second-generation bio-based plastics are becoming a reality - Non-renewable energy and greenhouse gas (GHG) balance of succinic acid-based plastic end products made from lignocellulosic biomass. *Biofuels, Bioproducts and Biorefining* **2018**, *12*, 426-441, doi:10.1002/bbb.1849.

8. Lan, E.I.; Wei, C.T. Metabolic engineering of cyanobacteria for the photosynthetic production of succinate. *Metab. Eng.* **2016**, *38*, 483-493, doi:https://doi.org/10.1016/j.ymben.2016.10.014.

9. Wang, J.; Zhu, J.; Bennett, G.N.; San, K.Y. Succinate production from different carbon sources under anaerobic conditions by metabolic engineered Escherichia coli strains. *Metabolic Engineering* **2011**, *13*, 328-335, doi:10.1016/j.ymben.2011.03.004.

10. Xu, J.; Guo, B.H. Poly(butylene succinate) and its copolymers: research, development and industrialization. *Biotechnology Journal* **2010**, *5*, 1149-1163, doi:10.1002/biot.201000136.

11. Pinazo, J.M.; Domine, M.E.; Parvulescu, V.; Petru, F. Sustainability metrics for succinic acid production: A comparison between biomass-based and petrochemical routes. *Catalysis Today* **2015**, *239*, 17-24, doi:10.1016/j.cattod.2014.05.035.

12. Li, X.; Mupondwa, E. Empirical analysis of large-scale bio-succinic acid commercialization from a technoeconomic and innovation value chain perspective: BioAmber biorefinery case study in Canada. *Renewable and Sustainable Energy Reviews* **2021**, *137*, doi:10.1016/j.rser.2020.110587.

13. Jansen, M.L.; van Gulik, W.M. Towards large scale fermentative production of succinic acid. *Current Opinion in Biotechnology* **2014**, *30*, 190-197, doi:10.1016/j.copbio.2014.07.003.

14. Mazière, A.; Prinsen, P.; García, A.; Luque, R.; Len, C. A review of progress in (bio)catalytic routes from/to renewable succinic acid. *Biofuels, Bioproducts and Biorefining* **2017**, *11*, 908-931, doi:10.1002/bbb.1785.

15. Khairil Anwar, N.A.K.; Hassan, N.; Mohd Yusof, N.; Idris, A. High-titer bio-succinic acid production from sequential alkalic and metal salt pretreated empty fruit bunch via simultaneous saccharification and fermentation. *Industrial Crops and Products* **2021**, *166*, doi:10.1016/j.indcrop.2021.113478.

16. Zheng, T.; Xu, B.; Ji, Y.; Zhang, W.; Xin, F.; Dong, W.; Wei, P.; Ma, J.; Jiang, M. Microbial fuel cell-assisted utilization of glycerol for succinate production by mutant of

Actinobacillus succinogenes. *Biotechnol Biofuels* **2021**, *14*, 23, doi:10.1186/s13068-021-01882-5.

17. Vinoth Kumar, R.; Pakshirajan, K.; Pugazhenthi, G. Malic and Succinic Acid: Potential C4 Platform Chemicals for Polymer and Biodegradable Plastic Production. In *Platform Chemical Biorefinery*, 2016, 159-179, doi: 10.1016/b978-0-12-802980-0.00009-2pp.

18. Jian Ping, T.; Md Jahim, J.; Harun, S.; Ta Yeong, W. Overview of the Potential of Bio-Succinic Acid Production from Oil Palm Fronds. *Journal of Physical Science* **2017**, *28*, 53-72, doi:10.21315/jps2017.28.s1.4.

19. BioAmber signs take-or-pay contract for three bio-succinic acid plants. Availabe online: https://www.prnewswire.com/news-releases/bioamber-signs-take-or-pay-contract-for-three-bio-succinic-acid-plants-266099031.html (accessed on 23.04.2021.).

20. McCoy, M. Succinic acid, once a biobased chemical star, is barely being made. Availabe online: https://cen.acs.org/content/cen/articles/97/i12/Succinic-acid-once-biobased-chemical.html (accessed on 23.04.2021.).

21. Global bio succinic acid market growth survey 2021-2027 with top countries data industry size, growth factors, top leaders, development strategy, future trends, historical analysis, competitive landscape and regional forecast | with covid-19 analysis. Availabe online: https://www.wboc.com/story/43682911/global-bio-succinic-acid-market-growth-survey-2021-2027-with-top-countries-data-industry-size-growth-factors-top-leaders-development-strategy-future (accessed on 23.04.2021.).

22. Burgard, A.; Burk, M.J.; Osterhout, R.; Van Dien, S.; Yim, H. Development of a commercial scale process for production of 1,4-butanediol from sugar. *Current Opinion in Biotechnology* **2016**, *42*, 118-125, doi:10.1016/j.copbio.2016.04.016.

23. Silva, R.G.C.; Ferreira, T.F.; Borges, É.R. Identification of potential technologies for 1,4-Butanediol production using prospecting methodology. *Journal of Chemical Technology & Biotechnology* **2020**, *95*, 3057-3070, doi:https://doi.org/10.1002/jctb.6518.

24. Izawa, Y.; Yokoyama, T. *1,4-Butanediol from 1,3-Butadiene*; 2016, 159-171, doi:10.1002/9783527690121.ch10pp.

25. Sanctis, F.D. Opening of the world's first industrial scale plant for the production of butanediol via fermentation of renewable raw materials. Availabe online: https://www.novamont.com/eng/read-press-release/mater-biotech/ (accessed on 27.04.2021.).

26. Satam, C.C.; Daub, M.; Realff, M.J. Techno-economic analysis of 1,4-butanediol production by a single-step bioconversion process. *Biofuels, Bioproducts and Biorefining* **2019**, *13*, 1261-1273, doi:10.1002/bbb.2016.

27. Heisig, C.; Diedenhoven, J.; Jensen, C.; Gehrke, H.; Turek, T. Selective Hydrogenation of Biomass-Derived Succinic Acid: Reaction Network and Kinetics. *Chemical Engineering & Technology* **2020**, *43*, 484-492, doi:10.1002/ceat.201900324.

28. Jacquel, N.; Freyermouth, F.; Fenouillot, F.; Rousseau, A.; Pascault, J.P.; Fuertes, P.; Saint-Loup, R. Synthesis and properties of poly(butylene succinate): Efficiency of different transesterification catalysts. *Journal of Polymer Science Part A: Polymer Chemistry* **2011**, *49*, 5301-5312, doi:10.1002/pola.25009.

29. Simoes, S.M.; Figueiras, A.R.; Veiga, F.; Concheiro, A.; Alvarez-Lorenzo, C. Polymeric micelles for oral drug administration enabling locoregional and systemic treatments. *Expert Opinion on Drug Delivery* **2015**, *12*, 297-318, doi:10.1517/17425247.2015.960841.

30. Bechthold, I.; Bretz, K.; Kabasci, S.; Kopitzky, R.; Springer, A. Succinic Acid: A New Platform Chemical for Biobased Polymers from Renewable Resources. *Chemical Engineering & Technology* **2008**, *31*, 647-654, doi:10.1002/ceat.200800063.

31.   Ferreira, L.P.; Moreira, A.N.; Pinto, J.C.; de Souza, F.G. Synthesis of poly(butylene succinate) using metal catalysts. *Polymer Engineering & Science* **2015**, *55*, 1889-1896, doi:10.1002/pen.24029.

32.   Oishi, A.; Zhang, M.; Nakayama, K.; Masuda, T.; Taguchi, Y. Synthesis of Poly(butylene succinate) and Poly(ethylene succinate) Including Diglycollate Moiety. *Polymer Journal* **2006**, *38*, 710-715, doi:10.1295/polymj.PJ2005206.

33.   Chen, C.-H.; Peng, J.-S.; Chen, M.; Lu, H.-Y.; Tsai, C.-J.; Yang, C.-S. Synthesis and characterization of poly(butylene succinate) and its copolyesters containing minor amounts of propylene succinate. *Colloid and Polymer Science* **2010**, *288*, 731-738, doi:10.1007/s00396-010-2187-9.

34.   Garin, M.; Tighzert, L.; Vroman, I.; Marinkovic, S.; Estrine, B. The kinetics of poly(butylene succinate) synthesis and the influence of molar mass on its thermal properties. *Journal of Applied Polymer Science* **2014**, *131*, 40639, doi:10.1002/app.40639.

35.   Velmathi, S.; Nagahata, R.; Sugiyama, J.-i.; Takeuchi, K. A Rapid Eco-Friendly Synthesis of Poly(butylene succinate) by a Direct Polyesterification under Microwave Irradiation. *Macromolecular Rapid Communications* **2005**, *26*, 1163-1167, doi:10.1002/marc.200500176.

36.   Nagahata, R.; Nakamura, T.; Takeuchi, K. Microwave-assisted rapid synthesis of poly(butylene succinate): principal effect of microwave irradiation of accelerating the polycondensation reaction. *Polymer Journal* **2018**, *50*, 347-354, doi:10.1038/s41428-018-0024-z.

37.   Takasu, A.; Oishi, Y.; Iio, Y.; Inai, Y.; Hirabayashi, T. Synthesis of Aliphatic Polyesters by Direct Polyesterification of Dicarboxylic Acids with Diols under Mild Conditions Catalyzed by Reusable Rare-Earth Triflate. *Macromolecules* **2003**, *36*, 1772-1774, doi:10.1021/ma021462v.

38.   Azim, H.; Dekhterman, A.; Jiang, Z.; Gross, R.A. Candida antarctica Lipase B-Catalyzed Synthesis of Poly(butylene succinate): Shorter Chain Building Blocks Also Work. *Biomacromolecules* **2006**, *7*, 3093-3097, doi:10.1021/bm060574h.

39.   Pospiech, D.; Choińska, R.; Flugrat, D.; Sahre, K.; Jehnichen, D.; Korwitz, A.; Friedel, P.; Werner, A.; Voit, B. Enzymatic Synthesis of Poly(alkylene succinate)s: Influence of Reaction Conditions. *Processes* **2021**, *9*, doi:10.3390/pr9030411.

40.   Kondo, A.; Sugihara, S.; Kuwahara, M.; Toshima, K.; Matsumura, S. Lipase-catalyzed ring-opening polymerization of molecularly pure cyclic oligomers for use in synthesis and chemical recycling of aliphatic polyesters. *Macromolecular Bioscience* **2008**, *8*, 533-539, doi:10.1002/mabi.200700270.

41.   Ren, L.; Wang, Y.; Ge, J.; Lu, D.; Liu, Z. Enzymatic Synthesis of High-Molecular-Weight Poly(butylene succinate) and its Copolymers. *Macromolecular Chemistry and Physics* **2015**, *216*, 636-640, doi:10.1002/macp.201400550.

42.   Sokołowska, M.; Stachowska, E.; Czaplicka, M.; El Fray, M. Effect of enzymatic versus titanium dioxide/silicon dioxide catalyst on crystal structure of 'green' poly[(butylene succinate)-co-(dilinoleic succinate)] copolymers. *Polymer International* **2020**, *70*, 514-526, doi:10.1002/pi.6104.

43.   Jiang, Y.; van Ekenstein, G.O.R.A.; Woortman, A.J.J.; Loos, K. Fully Biobased Unsaturated Aliphatic Polyesters from Renewable Resources: Enzymatic Synthesis, Characterization, and Properties. *Macromolecular Chemistry and Physics* **2014**, *215*, 2185-2197, doi:10.1002/macp.201400164.

44.   Tserki, V.; Matzinos, P.; Pavlidou, E.; Panayiotou, C. Biodegradable aliphatic polyesters. Part II. Synthesis and characterization of chain extended poly(butylene

succinate-co-butylene adipate). *Polymer Degradation and Stability* **2006**, *91*, 377-384, doi:10.1016/j.polymdegradstab.2005.04.036.

45. Jin, H.-J.; Kim, D.-S.; Lee, B.-Y.; Kim, M.-N.; Lee, I.-M.; Lee, H.-S.; Yoon, J.-S. Chain extension and biodegradation of poly(butylene succinate) with maleic acid units. *Journal of Polymer Science Part B: Polymer Physics* **2000**, *38*, 2240-2246, doi: 10.1002/1099-0488(20000901)38:17<2140::AID-POLB40>3.0.CO;2-N.

46. Zhou, H.; Wang, X.; Du, Z.; Li, H.; Yu, K. Preparation and characterization of chain extended Poly(butylene succinate) foams. *Polymer Engineering & Science* **2015**, *55*, 988-994, doi:10.1002/pen.23964.

47. Phua, Y.J.; Lau, N.S.; Sudesh, K.; Chow, W.S.; Mohd Ishak, Z.A. Biodegradability studies of poly(butylene succinate)/organo-montmorillonite nanocomposites under controlled compost soil conditions: Effects of clay loading and compatibiliser. *Polymer Degradation and Stability* **2012**, *97*, 1345-1354, doi:10.1016/j.polymdegradstab.2012.05.024.

48. Lu, X.F.; Hay, J.N. Isothermal crystallization kinetics and melting behaviour of poly(ethylene terephthalate). *Polymer* **2001**, *42*, 9423-9431, doi:10.1016/S0032-3861(01)00502-X.

49. Rudnik, E. 13 - Compostable Polymer Properties and Packaging Applications. In *Plastic Films in Food Packaging*, Ebnesajjad, S., Ed. William Andrew Publishing: Oxford, 2013, 217-248, doi:10.1016/B978-1-4557-3112-1.00013-2pp.

50. BioPBS™FZ71PM Technical Data Sheet. Availabe online: http://www.pttmcc.com/new/download/BioPBS_FZ71PM_Technical_Data_Sheet_for _Extrusion_Coating1.pdf (accessed on 05.05.2021.).

51. Jiang, L.; Zhang, J. 7 - Biodegradable and Biobased Polymers. In *Applied Plastics Engineering Handbook (Second Edition)*, Kutz, M., Ed. William Andrew Publishing: 2017, 127-143, doi:10.1016/B978-0-323-39040-8.00007-9pp.

52. Bhatia, A.; Gupta, R.K.; Bhattacharya, S.N.; Choi, H.J. An investigation of melt rheology and thermal stability of poly(lactic acid)/ poly(butylene succinate) nanocomposites. *Journal of Applied Polymer Science* **2009**, *114*, 2837-2847, doi: 10.1002/app.30933.

53. Georgousopoulou, I.-N.; Vouyiouka, S.; Dole, P.; Papaspyrides, C.D. Thermo-mechanical degradation and stabilization of poly(butylene succinate). *Polymer Degradation and Stability* **2016**, *128*, 182-192, doi:10.1016/j.polymdegradstab.2016.03.012.

54. Mizuno, S.; Maeda, T.; Kanemura, C.; Hotta, A. Biodegradability, reprocessability, and mechanical properties of polybutylene succinate (PBS) photografted by hydrophilic or hydrophobic membranes. *Polymer Degradation and Stability* **2015**, *117*, 58-65, doi:10.1016/j.polymdegradstab.2015.03.015.

55. Chen, S.; Cheng, L.; Huang, H.; Zou, F.; Zhao, H.-P. Fabrication and properties of poly(butylene succinate) biocomposites reinforced by waste silkworm silk fabric. *Composites Part A: Applied Science and Manufacturing* **2017**, *95*, 125-131, doi:10.1016/j.compositesa.2017.01.004.

56. Zhang, X.; Wang, X. Polybutylene succinate/cellulose nanocrystals: Role of phthalic anhydride in squeeze oriented bionanocomposites. *Carbohydrate Polymers* **2018**, *196*, 254-261, doi:10.1016/j.carbpol.2018.04.124.

57. Zhang, Y.; Hu, Y.; Wang, J.; Tian, W.; Liew, K.M.; Zhang, Y.; Wang, B. Engineering carbon nanotubes wrapped ammonium polyphosphate for enhancing mechanical and flame retardant properties of poly(butylene succinate). *Composites Part A: Applied Science and Manufacturing* **2018**, *115*, 215-227, doi:10.1016/j.compositesa.2018.09.020.

58. DOW™ LDPE 993I Low Density Polyethylene Resin. Availabe online: https://www.dow.com/content/dam/dcc/documents/en-us/productdatasheet/400/400-00018210en-dow-ldpe-993i-tds.pdf?iframe=true (accessed on 05.05.2021.).

59. DOW™ DMDA-8907 NT 7 High Density Polyethylene Resin. Availabe online: https://www.protolabs.com/media/1011433/dow-dmda-8907-nt-7.pdf (accessed on 05.05.2021.).

60. Myung, J.; Flanagan, J.C.A.; Waymouth, R.M.; Criddle, C.S. Expanding the range of polyhydroxyalkanoates synthesized by methanotrophic bacteria through the utilization of omega-hydroxyalkanoate co-substrates. *AMB Express* **2017**, *7*, 118, doi:10.1186/s13568-017-0417-y.

61. Signori, F.; Coltelli, M.-B.; Bronco, S. Thermal degradation of poly(lactic acid) (PLA) and poly(butylene adipate-co-terephthalate) (PBAT) and their blends upon melt processing. *Polymer Degradation and Stability* **2009**, *94*, 74-82, doi: 10.1016/j.polymdegradstab.2008.10.004.

62. Bartnikowski, M.; Dargaville, T.R.; Ivanovski, S.; Hutmacher, D.W. Degradation mechanisms of polycaprolactone in the context of chemistry, geometry and environment. *Progress in Polymer Science* **2019**, *96*, 1-20, doi: 10.1016/j.progpolymsci.2019.05.004.

63. Gan, Z.; Abe, H.; Kurokawa, H.; Doi, Y. Solid-State Microstructures, Thermal Properties, and Crystallization of Biodegradable Poly(butylene succinate) (PBS) and Its Copolyesters. *Biomacromolecules* **2001**, *2*, 605-613, doi:10.1021/bm015535e.

64. Yoo, E.S.; Im, S.S. Melting behavior of poly(butylene succinate) during heating scan by DSC. *Journal of Polymer Science Part B: Polymer Physics* **1999**, *37*, 1357-1366, doi:10.1002/(SICI)1099-0488(19990701)37:13<1357::AID-POLB2>3.0.CO;2-Q.

65. Papageorgiou, D.G.; Zhuravlev, E.; Papageorgiou, G.Z.; Bikiaris, D.; Chrissafis, K.; Schick, C. Kinetics of nucleation and crystallization in poly(butylene succinate) nanocomposites. *Polymer* **2014**, *55*, 6725-6734, doi: 10.1016/j.polymer.2014.11.014.

66. Yasuniwa, M.; Satou, T. Multiple melting behavior of poly(butylene succinate). I. Thermal analysis of melt-crystallized samples. *Journal of Polymer Science Part B: Polymer Physics* **2002**, *40*, 2411-2420, doi:10.1002/polb.10298.

67. Papageorgiou, G.Z.; Achilias, D.S.; Bikiaris, D.N. Crystallization Kinetics of Biodegradable Poly(butylene succinate) under Isothermal and Non-Isothermal Conditions. *Macromolecular Chemistry and Physics* **2007**, *208*, 1250-1264, doi:10.1002/macp.200700084.

68. Qiu, Z.; Komura, M.; Ikehara, T.; Nishi, T. DSC and TMDSC study of melting behaviour of poly(butylene succinate) and poly(ethylene succinate). *Polymer* **2003**, *44*, 7781-7785, doi:10.1016/j.polymer.2003.10.045.

69. Qiu, Z.; Ikehara, T.; Nishi, T. Melting behaviour of poly(butylene succinate) in miscible blends with poly(ethylene oxide). *Polymer* **2003**, *44*, 3095-3099, doi:10.1016/S0032-3861(03)00216-7.

70. Qiu, Z.; Yang, W. Crystallization kinetics and morphology of poly(butylene succinate)/poly(vinyl phenol) blend. *Polymer* **2006**, *47*, 6429-6437, doi:10.1016/j.polymer.2006.07.001.

71. Park, J.W.; Kim, D.K.; Im, S.S. Crystallization behaviour of poly(butylene succinate) copolymers. *Polymer International* **2002**, *51*, 239-244, doi:10.1002/pi.848.

72. Yang, J.; Pan, P.; Hua, L.; Xie, Y.; Dong, T.; Zhu, B.; Inoue, Y.; Feng, X. Fractionated crystallization, polymorphic crystalline structure, and spherulite morphology of poly(butylene adipate) in its miscible blend with poly(butylene succinate). *Polymer* **2011**, *52*, 3460-3468, doi:10.1016/j.polymer.2011.05.041.

73. Wang, K.; Jiao, T.; Wang, Y.; Li, M.; Li, Q.; Shen, C. The microstructures of extrusion cast biodegradable poly(butylene succinate) films investigated by X-ray diffraction. *Materials Letters* **2013**, *92*, 334-337, doi:10.1016/j.matlet.2012.10.121.

74. Platnieks, O.; Gaidukovs, S.; Neibolts, N.; Barkane, A.; Gaidukova, G.; Thakur, V.K. Poly(butylene succinate) and graphene nanoplatelet–based sustainable functional nanocomposite materials: structure-properties relationship. *Materials Today Chemistry* **2020**, *18*, doi:10.1016/j.mtchem.2020.100351.

75. Bin, T.; Qu, J.-p.; Liu, L.-m.; Feng, Y.-h.; Hu, S.-x.; Yin, X.-c. Non-isothermal crystallization kinetics and dynamic mechanical thermal properties of poly(butylene succinate) composites reinforced with cotton stalk bast fibers. *Thermochimica Acta* **2011**, *525*, 141-149, doi:10.1016/j.tca.2011.08.003.

76. Ihn, K.J.; Yoo, E.S.; Im, S.S. Structure and Morphology of Poly(tetramethylene succinate) Crystals. *Macromolecules* **1995**, *28*, 2460-2464, doi:10.1021/ma00111a045.

77. Liu, G.; Zheng, L.; Zhang, X.; Li, C.; Jiang, S.; Wang, D. Reversible Lamellar Thickening Induced by Crystal Transition in Poly(butylene succinate). *Macromolecules* **2012**, *45*, 5487-5493, doi:10.1021/ma300530a.

78. Ichikawa, Y.; Suzuki, J.; Washiyama, J.; Moteki, Y.; Noguchi, K.; Okuyama, K. Strain-induced crystal modification in poly(tetramethylene succinate). *Polymer* **1994**, *35*, 3338-3339, doi:10.1016/0032-3861(94)90144-9.

79. Lin, N.; Yu, J.; Chang, P.R.; Li, J.; Huang, J. Poly(butylene succinate)-based biocomposites filled with polysaccharide nanocrystals: Structure and properties. *Polymer Composites* **2011**, *32*, 472-482, doi:10.1002/pc.21066.

80. Yao, S.-F.; Chen, X.-T.; Ye, H.-M. Investigation of Structure and Crystallization Behavior of Poly(butylene succinate) by Fourier Transform Infrared Spectroscopy. *The Journal of Physical Chemistry B* **2017**, *121*, 9476-9485, doi:10.1021/acs.jpcb.7b07954.

81. He, Y.; Zhu, B.; Kai, W.; Inoue, Y. Nanoscale-Confined and Fractional Crystallization of Poly(ethylene oxide) in the Interlamellar Region of Poly(butylene succinate). *Macromolecules* **2004**, *37*, 3337-3345, doi:10.1021/ma035886g.

82. Nikolic, M.S.; Djonlagic, J. Synthesis and characterization of biodegradable poly(butylene succinate-co-butylene adipate)s. *Polymer Degradation and Stability* **2001**, *74*, 263-270, doi:10.1016/S0141-3910(01)00156-2.

83. Papaspyrides, C.D.; Vouyiouka, S.; Georgousopoulou, I.-N.; Marinkovic, S.; Estrine, B.; Joly, C.; Dole, P. Feasibility of Solid-State Postpolymerization on Fossil- and Bio-Based Poly(butylene succinate) Including Polymer Upcycling Routes. *Industrial & Engineering Chemistry Research* **2016**, *55*, 5832-5842, doi:10.1021/acs.iecr.6b00588.

84. Miyata, T.; Masuko, T. Crystallization behaviour of poly(tetramethylene succinate). *Polymer* **1998**, *39*, 1399-1404, doi:10.1016/S0032-3861(97)00418-7.

85. Papageorgiou, G.Z.; Bikiaris, D.N. Crystallization and melting behavior of three biodegradable poly(alkylene succinates). A comparative study. *Polymer* **2005**, *46*, 12081-12092, doi:10.1016/j.polymer.2005.10.073.

86. Wang, G.X.; Huang, D.; Ji, J.H.; Volker, C.; Wurm, F.R. Seawater-Degradable Polymers-Fighting the Marine Plastic Pollution. *Advanced Science* **2020**, *8*, 2001121, doi:10.1002/advs.202001121.

87. Kim, H.-S.; Yang, H.-S.; Kim, H.-J. Biodegradability and mechanical properties of agro-flour-filled polybutylene succinate biocomposites. *Journal of Applied Polymer Science* **2005**, *97*, 1513-1521, doi:10.1002/app.21905.

88. Liu, L.; Yu, J.; Cheng, L.; Yang, X. Biodegradability of poly(butylene succinate) (PBS) composite reinforced with jute fibre. *Polymer Degradation and Stability* **2009**, *94*, 90-94, doi:10.1016/j.polymdegradstab.2008.10.013.

89.   Calabia, B.; Ninomiya, F.; Yagi, H.; Oishi, A.; Taguchi, K.; Kunioka, M.; Funabashi, M. Biodegradable Poly(butylene succinate) Composites Reinforced by Cotton Fiber with Silane Coupling Agent. *Polymers* **2013**, *5*, 128-141, doi:10.3390/polym5010128.

90.   Zhao, J.-H.; Wang, X.-Q.; Zeng, J.; Yang, G.; Shi, F.-H.; Yan, Q. Biodegradation of poly(butylene succinate) in compost. *Journal of Applied Polymer Science* **2005**, *97*, 2273-2278, doi:10.1002/app.22009.

91.   Cho, H.S.; Moon, H.S.; Kim, M.; Nam, K.; Kim, J.Y. Biodegradability and biodegradation rate of poly(caprolactone)-starch blend and poly(butylene succinate) biodegradable polymer under aerobic and anaerobic environment. *Waste Management* **2011**, *31*, 475-480, doi:10.1016/j.wasman.2010.10.029.

92.   Kasuya, K.-i.; Takagi, K.-i.; Ishiwatari, S.-i.; Yoshida, Y.; Doi, Y. Biodegradabilies of various aliphatic polyesters in natural waters. *Polymer Degradation and Stability* **1998**, *59*, 327-332, doi:10.1016/S0141-3910(97)00155-9.

93.   Nakayama, A.; Yamano, N.; Kawasaki, N. Biodegradation in seawater of aliphatic polyesters. *Polymer Degradation and Stability* **2019**, *166*, 290-299, doi:10.1016/j.polymdegradstab.2019.06.006.

94.   Jbilou, F.; Dole, P.; Degraeve, P.; Ladavière, C.; Joly, C. A green method for polybutylene succinate recycling: Depolymerization catalyzed by lipase B from Candida antarctica during reactive extrusion. *European Polymer Journal* **2015**, *68*, 207-215, doi:10.1016/j.eurpolymj.2015.04.039.

95.   Scaffaro, R.; Maio, A.; Sutera, F.; Gulino, E.F.; Morreale, M. Degradation and Recycling of Films Based on Biodegradable Polymers: A Short Review. *Polymers* **2019**, *11*, doi:10.3390/polym11040651.

96.   Coltelli, M.-B.; Aliotta, L.; Gigante, V.; Bellusci, M.; Cinelli, P.; Bugnicourt, E.; Schmid, M.; Staebler, A.; Lazzeri, A. Preparation and Compatibilization of PBS/Whey Protein Isolate Based Blends. *Molecules* **2020**, *25*, 3313, doi:10.3390/molecules25143313.

97.   Schmid, M.; Herbst, C.; Müller, K.; Stäbler, A.; Schlemmer, D.; Coltelli, M.-B.; Lazzeri, A. Effect of Potato Pulp Filler on the Mechanical Properties and Water Vapor Transmission Rate of Thermoplastic WPI/PBS Blends. *Polymer-Plastics Technology and Engineering* **2016**, *55*, 510-517, doi:10.1080/03602559.2015.1098690.

98.   Su, S.; Kopitzky, R.; Tolga, S.; Kabasci, S. Polylactide (PLA) and Its Blends with Poly(butylene succinate) (PBS): A Brief Review. *Polymers* **2019**, *11*, doi:10.3390/polym11071193.

99.   Ratsameetammajak, N.; Molloy, R.; Somsunan, R. Preparation and property testing of polymer blends of poly(lactic acid) and poly(butylene succinate) plasticised with long-chain fatty acids. *Plastics, Rubber and Composites* **2018**, *47*, 139-146, doi:10.1080/14658011.2018.1443875.

100.   Barletta, M.; Puopolo, M. Thermoforming of compostable PLA/PBS blends reinforced with highly hygroscopic calcium carbonate. *Journal of Manufacturing Processes* **2020**, *56*, 1185-1192, doi:10.1016/j.jmapro.2020.06.008.

101.   Srimalanon, P.; Prapagdee, B.; Sombatsompop, N. Soil Inoculation with Pseudomonas geniculata WS3 for Accelerating the Biodegradation Process of In Situ Compatibilized PBS/PLA Blends Doped with HPQM. *Journal of Polymers and the Environment* **2020**, *28*, 1138-1149, doi:10.1007/s10924-020-01670-6.

102.   Shi, K.; Bai, Z.; Su, T.; Wang, Z. Selective enzymatic degradation and porous morphology of poly(butylene succinate)/poly(lactic acid) blends. *International Journal of Biological Macromolecules* **2019**, *126*, 436-442, doi:10.1016/j.ijbiomac.2018.12.168.

103. Fenni, S.E.; Wang, J.; Haddaoui, N.; Favis, B.D.; Müller, A.J.; Cavallo, D. Crystallization and self-nucleation of PLA, PBS and PCL in their immiscible binary and ternary blends. *Thermochimica Acta* **2019**, *677*, 117-130, doi:10.1016/j.tca.2019.03.015.

104. Nazrin, A.; Sapuan, S.M.; Zuhri, M.Y.M.; Ilyas, R.A.; Syafiq, R.; Sherwani, S.F.K. Nanocellulose Reinforced Thermoplastic Starch (TPS), Polylactic Acid (PLA), and Polybutylene Succinate (PBS) for Food Packaging Applications. *Frontiers in Chemistry* **2020**, *8*, 213, doi:10.3389/fchem.2020.00213.

105. Gigante, V.; Coltelli, M.B.; Vannozzi, A.; Panariello, L.; Fusco, A.; Trombi, L.; Donnarumma, G.; Danti, S.; Lazzeri, A. Flat Die Extruded Biocompatible Poly(Lactic Acid) (PLA)/Poly(Butylene Succinate) (PBS) Based Films. *Polymers* **2019**, *11*, doi:10.3390/polym11111857.

106. Sun, Z.; Wang, L.; Zhou, J.; Fan, X.; Xie, H.; Zhang, H.; Zhang, G.; Shi, X. Influence of Polylactide (PLA) Stereocomplexation on the Microstructure of PLA/PBS Blends and the Cell Morphology of Their Microcellular Foams. *Polymers* **2020**, *12*, doi:10.3390/polym12102362.

107. Sadeghi, A.; Mousavi, S.M.; Saljoughi, E.; Kiani, S. Biodegradable membrane based on polycaprolactone/polybutylene succinate: Characterization and performance evaluation in wastewater treatment. *Journal of Applied Polymer Science* **2020**, *138*, doi:10.1002/app.50332.

108. Hashim Abed Almwli, H.; Mousavi, S.M.; Kiani, S. Preparation of poly(butylene succinate)/polyvinylpyrrolidone blend membrane for pervaporation dehydration of acetone. *Chemical Engineering Research and Design* **2021**, *165*, 361-373, doi:10.1016/j.cherd.2020.10.033.

109. de Matos Costa, A.R.; Crocitti, A.; Hecker de Carvalho, L.; Carroccio, S.C.; Cerruti, P.; Santagata, G. Properties of Biodegradable Films Based on Poly(butylene Succinate) (PBS) and Poly(butylene Adipate-co-Terephthalate) (PBAT) Blends. *Polymers* **2020**, *12*, doi:10.3390/polym12102317.

110. Ahmad Thirmizir, M.Z.; Mohd Ishak, Z.A.; Mat Taib, R.; C. Kanapathi Pillai, K.S.K.; Salim, M.S.; Hassan, A.; Abu Bakar, M.B. The effects of melt grafted maleated polybutylene succinate on the properties of poly(hydroxybutyrate-co-hydroxyhexanoate)/polybutylene succinate blends. *Journal of Vinyl and Additive Technology* **2021**, doi:10.1002/vnl.21828.

111. Srithep, Y.; Veang-in, O.; Pholharn, D.; Turng, L.-S.; Morris, J. Improving Polylactide Toughness by Plasticizing with Low Molecular Weight Polylactide-Poly(Butylene Succinate) Copolymer. *Journal of Renewable Materials* **2021**, *9*, doi:10.32604/jrm.2021.015604.

112. Supthanyakul, R.; Kaabbuathong, N.; Chirachanchai, S. Poly(l-lactide-b-butylene succinate-b-l-lactide) triblock copolymer: A multi-functional additive for PLA/PBS blend with a key performance on film clarity. *Polymer Degradation and Stability* **2017**, *142*, 160-168, doi:10.1016/j.polymdegradstab.2017.05.029.

113. Guidotti, G.; Soccio, M.; Gazzano, M.; Fusaro, L.; Boccafoschi, F.; Munari, A.; Lotti, N. New thermoplastic elastomer triblock copolymer of PLLA for cardiovascular tissue engineering: Annealing as efficient tool to tailor the solid-state properties. *Polymer* **2021**, *213*, 123336, doi:10.1016/j.polymer.2020.123336.

114. Debuissy, T.; Pollet, E.; Avérous, L. Synthesis and characterization of biobased poly(butylene succinate-ran-butylene adipate). Analysis of the composition-dependent physicochemical properties. *European Polymer Journal* **2017**, *87*, 84-98, doi:10.1016/j.eurpolymj.2016.12.012.

115. Niaounakis, M. Chapter 1 - Introduction. In *Biopolymers: Processing and Products*, Niaounakis, M., Ed. William Andrew Publishing: Oxford, 2015, 1-77, doi:10.1016/B978-0-323-26698-7.00001-5pp.

116. Li, F.; Xu, X.; Hao, Q.; Li, Q.; Yu, J.; Cao, A. Effects of comonomer sequential structure on thermal and crystallization behaviors of biodegradable poly(butylene succinate-co-butylene terephthalate)s. *Journal of Polymer Science Part B: Polymer Physics* **2006**, *44*, 1635-1644, doi:10.1002/polb.20797.

117. Zheng, C.; Zhu, G.; Shi, Y.; Liu, L.-Z.; Ren, M.; Zhang, W.; Han, L. Crystallization, structures and properties of biodegradable poly (butylene succinate-co-butylene terephthalate) with a symmetric composition. *Materials Chemistry and Physics* **2021**, *260*, 124183, doi:10.1016/j.matchemphys.2020.124183.

118. Ferreira, F.V.; Cividanes, L.S.; Gouveia, R.F.; Lona, L.M.F. An overview on properties and applications of poly(butylene adipate-co-terephthalate)-PBAT based composites. *Polymer Engineering & Science* **2019**, *59*, E7-E15, doi:10.1002/pen.24770.

119. Zeng, J.-B.; Huang, C.-L.; Jiao, L.; Lu, X.; Wang, Y.-Z.; Wang, X.-L. Synthesis and Properties of Biodegradable Poly(butylene succinate-co-diethylene glycol succinate) Copolymers. *Industrial & Engineering Chemistry Research* **2012**, *51*, 12258-12265, doi:10.1021/ie300133a.

120. Sokołowska, M.; Stachowska, E.; Czaplicka, M.; El Fray, M. Effect of enzymatic versus titanium dioxide/silicon dioxide catalyst on crystal structure of 'green' poly[(butylene succinate)-co-(dilinoleic succinate)] copolymers. *Polymer International* **2021**, *70*, 514-526, doi:10.1002/pi.6104.

121. Sonseca, A.; McClain, A.; Puskas, J.E.; El Fray, M. Kinetic studies of biocatalyzed copolyesters of poly(butylene succinate) (PBS) containing fully bio-based dilinoleic diol. *European Polymer Journal* **2019**, *116*, 515-525, doi:10.1016/j.eurpolymj.2019.04.038.

122. Sun, Z.; Jiang, Z.; Qiu, Z. Thermal, crystallization and mechanical properties of branched Poly(butylene succinate) copolymers with 1,2-decanediol being the comonomer. *Polymer* **2021**, *213*, 123197, doi:10.1016/j.polymer.2020.123197.

123. Smola-Dmochowska, A.; Śmigiel-Gac, N.; Kaczmarczyk, B.; Sobota, M.; Janeczek, H.; Karpeta-Jarząbek, P.; Kasperczyk, J.; Dobrzyński, P. Triple-Shape Memory Behavior of Modified Lactide/Glycolide Copolymers. *Polymers* **2020**, *12*, doi:10.3390/polym12122984.

124. Guidotti, G.; Soccio, M.; Gazzano, M.; Bloise, N.; Bruni, G.; Aluigi, A.; Visai, L.; Munari, A.; Lotti, N. Biocompatible PBS-based copolymer for soft tissue engineering: Introduction of disulfide bonds as winning tool to tune the final properties. *Polymer Degradation and Stability* **2020**, *182*, 109403, doi:10.1016/j.polymdegradstab.2020.109403.

125. Wang, H.; Liu, K.; Chen, X.; Wang, M. Thermal properties and enzymatic degradation of PBS copolyesters containing dl-malic acid units. *Chemosphere* **2021**, *272*, 129543, doi:10.1016/j.chemosphere.2021.129543.

126. Wang, L.; Zhang, M.; Lawson, T.; Kanwal, A.; Miao, Z. Poly(butylene succinate-co-salicylic acid) copolymers and their effect on promoting plant growth. *Royal Society Open Science* **2019**, *6*, 190504, doi:10.1098/rsos.190504.

127. Ferreira, F.V.; Dufresne, A.; Pinheiro, I.F.; Souza, D.H.S.; Gouveia, R.F.; Mei, L.H.I.; Lona, L.M.F. How do cellulose nanocrystals affect the overall properties of biodegradable polymer nanocomposites: A comprehensive review. *European Polymer Journal* **2018**, *108*, 274-285, doi:10.1016/j.eurpolymj.2018.08.045.

128. Kumari Pallathadka, P.; Koh, X.Q.; Khatta, A.; Luckachan, G.E.; Mittal, V. Characteristics of biodegradable poly(butylene succinate) nanocomposites with

thermally reduced graphene nanosheets. *Polymer Composites* **2017**, *38*, E42-E48, doi:10.1002/pc.23824.

129. Lambert, S.; Wagner, M. Environmental performance of bio-based and biodegradable plastics: the road ahead. *Chemical Society Reviews* **2017**, *46*, 6855-6871, doi:10.1039/c7cs00149e.

130. Gigli, M.; Fabbri, M.; Lotti, N.; Gamberini, R.; Rimini, B.; Munari, A. Poly(butylene succinate)-based polyesters for biomedical applications: A review. *European Polymer Journal* **2016**, *75*, 431-460, doi:10.1016/j.eurpolymj.2016.01.016.

131. Veranitisagul, C.; Wattanathana, W.; Wannapaiboon, S.; Hanlumyuang, Y.; Sukthavorn, K.; Nootsuwan, N.; Chotiwan, S.; Phuthong, W.; Jongrungruangchok, S.; Laobuthee, A. Antimicrobial, Conductive, and Mechanical Properties of AgCB/PBS Composite System. *Journal of Chemistry* **2019**, *2019*, 1-14, doi:10.1155/2019/3487529.

132. Bin, T.; Qu, J.-p.; Liu, L.-m.; Feng, Y.-h.; Hu, S.-x.; Yin, X.-c. Non-isothermal crystallization kinetics and dynamic mechanical thermal properties of poly(butylene succinate) composites reinforced with cotton stalk bast fibers. *Thermochimica Acta* **2011**, *525*, 141-149, doi:10.1016/j.tca.2011.08.003.

133. Mochane, M.J.; Magagula, S.I.; Sefadi, J.S.; Mokhena, T.C. A Review on Green Composites Based on Natural Fiber-Reinforced Polybutylene Succinate (PBS). *Polymers* **2021**, *13*, doi:10.3390/polym13081200.

134. Xiao, F.; Fontaine, G.; Bourbigot, S. Recent developments in fire retardancy of polybutylene succinate. *Polymer Degradation and Stability* **2021**, *183*, doi:10.1016/j.polymdegradstab.2020.109466.

135. Chen, Z.; Hu, J.; Ju, J.; Kuang, T. Fabrication of Poly(butylene succinate)/Carbon Black Nanocomposite Foams with Good Electrical Conductivity and High Strength by a Supercritical CO2 Foaming Process. *Polymers* **2019**, *11*, doi:10.3390/polym11111852.

136. Zainal Abidin, A.S.; Yusoh, K.; Jamari, S.S.; Abdullah, A.H.; Ismail, Z. Surface functionalization of graphene oxide with octadecylamine for improved thermal and mechanical properties in polybutylene succinate nanocomposite. *Polymer Bulletin* **2017**, *75*, 3499-3522, doi:10.1007/s00289-017-2217-6.

137. Abidin, A.S.Z.; Yusoh, K.; Jamari, S.S.; Abdullah, A.H.; Ismail, Z. Enhanced performance of alkylated graphene reinforced polybutylene succinate nanocomposite. In Proceedings of The 2nd International Conference on Functional Materials and Metallurgy (ICoFM 2016).

138. Cosquer, R.; Pruvost, S.; Gouanve, F. Improvement of Barrier Properties of Biodegradable Polybutylene Succinate/Graphene Nanoplatelets Nanocomposites Prepared by Melt Process. *Membranes* **2021**, *11*, doi:10.3390/membranes11020151.

139. Han, S.-I.; Lim, J.S.; Kim, D.K.; Kim, M.N.; Im, S.S. In situ polymerized poly(butylene succinate)/silica nanocomposites: Physical properties and biodegradation. *Polymer Degradation and Stability* **2008**, *93*, 889-895, doi:10.1016/j.polymdegradstab.2008.02.007.

140. Haghdan, S.; Smith, G.D. Natural fiber reinforced polyester composites: A literature review. *Journal of Reinforced Plastics and Composites* **2015**, *34*, 1179-1190, doi:10.1177/0731684415588938.

141. Petchwattana, N.; Sanetuntikul, J.; Sriromreun, P.; Narupai, B. Wood Plastic Composites Prepared from Biodegradable Poly(butylene succinate) and Burma Padauk Sawdust (Pterocarpus macrocarpus): Water Absorption Kinetics and Sunlight Exposure Investigations. *Journal of Bionic Engineering* **2017**, *14*, 781-790, doi:10.1016/s1672-6529(16)60443-2.

142. Terzopoulou, Z.N.; Papageorgiou, G.Z.; Papadopoulou, E.; Athanassiadou, E.; Reinders, M.; Bikiaris, D.N. Development and study of fully biodegradable composite

materials based on poly(butylene succinate) and hemp fibers or hemp shives. *Polymer Composites* **2016**, *37*, 407-421, doi:10.1002/pc.23194.

143. Huang, Z.; Qian, L.; Yin, Q.; Yu, N.; Liu, T.; Tian, D. Biodegradability studies of poly(butylene succinate) composites filled with sugarcane rind fiber. *Polymer Testing* **2018**, *66*, 319-326, doi:10.1016/j.polymertesting.2018.02.003.

144. Dufresne, A. Cellulose nanomaterials as green nanoreinforcements for polymer nanocomposites. *Philosophical Transactions of the Royal Society A* **2018**, *376*, doi:10.1098/rsta.2017.0040.

145. Joy, J.; Jose, C.; Varanasi, S.B.; Mathew P, L.; Thomas, S.; Pilla, S. Preparation and Characterization of Poly(butylene succinate) Bionanocomposites Reinforced with Cellulose Nanofiber Extracted from Helicteres isora Plant. *Journal of Renewable Materials* **2016**, *4*, 351-364, doi:10.7569/jrm.2016.634128.

146. Shih, Y.F.; Wang, T.Y.; Jeng, R.J.; Wu, J.Y.; Teng, C.C. Biodegradable nanocomposites based on poly(butylene succinate)/organoclay. *Journal of Polymers and the Environment* **2007**, *15*, 151-158, doi:10.1007/s10924-007-0055-6.

147. Kim, H.; Shin, M.S.; Jeon, H.; Koo, J.M.; Eom, Y.; Choi, S.; Shin, G.; Oh, D.X.; Hwang, S.Y.; Park, J. Highly reinforced poly(butylene succinate) nanocomposites prepared from chitosan nanowhiskers by in-situ polymerization. *International Journal of Biological Macromolecules* **2021**, *173*, 128-135, doi:10.1016/j.ijbiomac.2021.01.102.

148. Wang, X.W.; Zhang, C.A.; Wang, P.L.; Zhao, J.; Zhang, W.; Ji, J.H.; Hua, K.; Zhou, J.; Yang, X.B.; Li, X.P. Enhanced performance of biodegradable poly(butylene succinate)/graphene oxide nanocomposites via in situ polymerization. *Langmuir* **2012**, *28*, 7091-7095, doi:10.1021/la204894h.

149. Shaiju, P.; Dorian, B.B.; Senthamaraikannan, R.; Padamati, R.B. Biodegradation of Poly (Butylene Succinate) (PBS)/Stearate Modified Magnesium-Aluminium Layered Double Hydroxide Composites under Marine Conditions Prepared via Melt Compounding. *Molecules* **2020**, *25*, doi:10.3390/molecules25235766.

150. Coelho, C.; Hennous, M.; Verney, V.; Leroux, F. Functionalisation of polybutylene succinate nanocomposites: from structure to reinforcement of UV-absorbing and mechanical properties. *RSC Advances* **2012**, *2*, doi:10.1039/c2ra20579c.

151. Fan, R.R.; Zhou, L.X.; Song, W.; Li de, X.; Zhang, D.M.; Ye, R.; Zheng, Y.; Guo, G. Preparation and properties of g-TTCP/PBS nanocomposites and its in vitro biocompatibility assay. *International Journal of Biological Macromolecules* **2013**, *59*, 227-234, doi:10.1016/j.ijbiomac.2013.04.051.

152. Lu, X.; Qu, J.; Huang, J. Reactive extrusion of partially crosslinked poly (butylene succinate) via novel vane extruder: thermal, mechanical and rheological properties. *Plastics, Rubber and Composites* **2016**, *45*, 261-269, doi:10.1080/14658011.2016.1183297.

153. Wang, W.; Zhang, G.; Zhang, W.; Guo, W.; Wang, J. Processing and Thermal Behaviors of Poly (Butylene Succinate) Blends with Highly-Filled Starch and Glycerol. *Journal of Polymers and the Environment* **2013**, *21*, 46-53, doi:10.1007/s10924-012-0505-7.

154. Liminana, P.; Garcia-Sanoguera, D.; Quiles-Carrillo, L.; Balart, R.; Montanes, N. Optimization of Maleinized Linseed Oil Loading as a Biobased Compatibilizer in Poly(Butylene Succinate) Composites with Almond Shell Flour. *Materials* **2019**, *12*, doi:10.3390/ma12050685.

155. Azhar, S.W.; Xu, F.; Zhang, Y.; Qiu, Y. Fabrication and mechanical properties of flaxseed fiber bundle-reinforced polybutylene succinate composites. *Journal of Industrial Textiles* **2019**, *50*, 98-113, doi:10.1177/1528083718821876.

156. Gowman, A.; Wang, T.; Rodriguez-Uribe, A.; Mohanty, A.K.; Misra, M. Bio-poly(butylene succinate) and Its Composites with Grape Pomace: Mechanical Performance and Thermal Properties. *ACS Omega* **2018**, *3*, 15205-15216, doi:10.1021/acsomega.8b01675.

157. Hongsriphan, N.; Jeensikhong, K.; Sornnuwat, K.; Yaemyen, N. Properties of Renewable Biocomposite from Poly(butylene succinate) and Teakwood Sawdust before and after Accelerated Weathering Condition. *Journal of Bionic Engineering* **2018**, *15*, 1075-1086, doi:10.1007/s42235-018-0095-8.

158. Ayu, R.S.; Khalina, A.; Harmaen, A.S.; Zaman, K.; Jawaid, M.; Lee, C.H. Effect of Modified Tapioca Starch on Mechanical, Thermal, and Morphological Properties of PBS Blends for Food Packaging. *Polymers* **2018**, *10*, doi:10.3390/polym10111187.

159. Hong, G.; Cheng, H.; Meng, Y.; Lin, J.; Chen, Z.; Zhang, S.; Song, W. Mussel-Inspired Polydopamine as a Green, Efficient, and Stable Platform to Functionalize Bamboo Fiber with Amino-Terminated Alkyl for High Performance Poly(butylene succinate) Composites. *Polymers* **2018**, *10*, doi:10.3390/polym10040461.

160. Totaro, G.; Sisti, L.; Vannini, M.; Marchese, P.; Tassoni, A.; Lenucci, M.S.; Lamborghini, M.; Kalia, S.; Celli, A. A new route of valorization of rice endosperm by-product: Production of polymeric biocomposites. *Composites Part B: Engineering* **2018**, *139*, 195-202, doi:10.1016/j.compositesb.2017.11.055.

161. Hong, G.; Meng, Y.; Yang, Z.; Cheng, H.; Zhang, S.; Song, W. Mussel-inspired polydopamine modification of bamboo fiber and its effect on the properties of bamboo fiber/polybutylene succinate composites. *Bioresources* **2017**, *12*, 8419-8442, doi:10.15376/biores.12.4.8419-8442.

162. Xiaopeng, Y.; Pengjie, L.; Yongjian, X. Effect of Compound Surface Treatment on the Performance of Poly(butylene succinate)/Chemithermomechanical Pulp Fiber Composites. *Polymer-Plastics Technology and Engineering* **2017**, *56*, 1225-1235, doi:10.1080/03602559.2016.1266368.

163. Thakur, K.; Kalia, S. Enzymatic modification of ramie fibers and its influence on the performance of ramie-poly(butylene succinate) biocomposites. *International Journal of Plastics Technology* **2017**, *21*, 209-226, doi:10.1007/s12588-017-9178-3.

164. Nattakarn, H.; Phoorinat, D.; Mookyada, M.; Warunkarn, J. Mechanical and Thermal Properties of Eucalyptus Fiber Composites from Blend between biodegradable Poly(butylene succinate) and Recycled PET. *Journal of Metals, Materials and Minerals,* **2017**, *27*, 13-23, doi:10.14456/jmmm.2017.2.

165. Hu, X.; Su, T.; Pan, W.; Li, P.; Wang, Z. Difference in solid-state properties and enzymatic degradation of three kinds of poly(butylene succinate)/cellulose blends. *RSC Advances* **2017**, *7*, 35496-35503, doi:10.1039/c7ra04972b.

166. Boonprasertpoh, A.; Pentrakoon, D.; Junkasem, J. Effect of Crosslinking Agent and Branching Agent on Morphological and Physical Properties of Poly(Butylene succinate) Foams. *Cellular Polymers* **2017**, *36*, 333-354, doi:10.1177/026248931703600603.

167. Avolio, R.; Graziano, V.; Pereira, Y.D.; Cocca, M.; Gentile, G.; Errico, M.E.; Ambrogi, V.; Avella, M. Effect of cellulose structure and morphology on the properties of poly(butylene succinate-co-butylene adipate) biocomposites. *Carbohydrate Polymers* **2015**, *133*, 408-420, doi:10.1016/j.carbpol.2015.06.101.

168. Yue, X.; Xu, Y.; Gou, N.; Li, H. Synthesis of Cellulose-Based Macromolecular Coupling Agent and its Utilization in Poly (butylene succinate)/Wood Flour Composites. *Polymer-Plastics Technology and Engineering* **2015**, *54*, 639-646, doi:10.1080/03602559.2014.974284.

169. Then, Y.Y.; Ibrahim, N.A.; Zainuddin, N.; Chieng, B.W.; Ariffin, H.; Wan Yunus, W.M.Z. Influence of Alkaline-Peroxide Treatment of Fiber on the Mechanical

Properties of Oil Palm Mesocarp Fiber/Poly(butylene succinate)Biocomposite. *Bioresources* **2015**, *10*, 1730-1746, doi:10.15376/biores.10.1.1730-1746.

170. Then, Y.Y.; Ibrahim, N.A.; Zainuddin, N.; Ariffin, H.; Wan Yunus, W.M.Z.; Chieng, B.W. Static mechanical, interfacial, and water absorption behaviors of alkali treated oil palm mesocarp fiber reinforced poly(butylene succinate) biocomposites. *Bioresources* **2015**, *10*, 123-136, doi:10.15376/biores.10.1.123-136.

171. Liu, H.Y.; Chen, F.Q.; Guo, R.B.; Zhang, G.; Qu, J. Effect of compatibilizer on the properties of PBS/lignin composites prepared via a vane extruder. *Journal of Polymer Engineering* **2015**, *35*, 829-837, doi:10.1515/polyeng-2015-0015.

172. Morreale, M.; Liga, A.; Mistretta, M.C.; Ascione, L.; Mantia, F.P. Mechanical, Thermomechanical and Reprocessing Behavior of Green Composites from Biodegradable Polymer and Wood Flour. *Materials* **2015**, *8*, 7536-7548, doi:10.3390/ma8115406.

173. Sahoo, S.; Misra, M.; Mohanty, A.K. Biocomposites From Switchgrass and Lignin Hybrid and Poly(butylene succinate) Bioplastic: Studies on Reactive Compatibilization and Performance Evaluation. *Macromolecular Materials and Engineering* **2014**, *299*, 178–189, doi:10.1002/mame.201300038.

174. Dorez, G.; Taguet, A.; Ferry, L.; Lopez Cuesta, J.-M. Phosphorous compounds as flame retardants for polybutylene succinate/flax biocomposite: Additive versus reactive route. *Polymer Degradation and Stability* **2014**, *102*, 152-159, doi:10.1016/j.polymdegradstab.2014.01.018.

175. Zhou, M.; Yan, J.; Li, Y.; Geng, C.; He, C.; Wang, K.; Fu, Q. Interfacial strength and mechanical properties of biocomposites based on ramie fibers and poly(butylene succinate). *RSC Advances* **2013**, *3*, doi:10.1039/c3ra43713b.

176. Ahmad Thirmizir, M.Z.; Mohd Ishak, Z.A.; Mat Taib, R.; Rahim, S. Effect of water exposure on dimensional stability and mechanical properties of unpurifed and purified maleated poly(butylene succinate) compatibilised poly(butylene succinate)/kenaf bast fibre composites. *Composite Interfaces* **2013**, *20*, 469-482, doi:10.1080/15685543.2013.807163.

177. Dorez, G.; Taguet, A.; Ferry, L.; Lopez-Cuesta, J.M. Thermal and fire behavior of natural fibers/PBS biocomposites. *Polymer Degradation and Stability* **2013**, *98*, 87-95, doi:10.1016/j.polymdegradstab.2012.10.026.

178. Feng, Y.; Shen, H.; Qu, J.; Liu, B.; He, H.; Han, L. Preparation and properties of PBS/sisal-fiber composites. *Polymer Engineering & Science* **2011**, *51*, 474-481, doi:10.1002/pen.21852.

179. Thirmizir, M.Z.A.; Ishak, Z.A.M.; Taib, R.M.; Sudin, R.; Leong, Y.W. Mechanical, Water Absorption and Dimensional Stability Studies of Kenaf Bast Fibre-Filled Poly(butylene succinate) Composites. *Polymer-Plastics Technology and Engineering* **2011**, *50*, 339-348, doi:10.1080/03602559.2010.531871.

180. Zhang, S.; He, Y.; Yin, Y.; Jiang, G. Fabrication of innovative thermoplastic starch bio-elastomer to achieve high toughness poly(butylene succinate) composites. *Carbohydrate Polymers* **2019**, *206*, 827-836, doi:10.1016/j.carbpol.2018.11.036.

181. Ayu, R.S.; Khalina, A.; Harmaen, A.S.; Zaman, K.; Isma, T.; Liu, Q.; Ilyas, R.A.; Lee, C.H. Characterization Study of Empty Fruit Bunch (EFB) Fibers Reinforcement in Poly(Butylene) Succinate (PBS)/Starch/Glycerol Composite Sheet. *Polymers* **2020**, *12*, doi:10.3390/polym12071571.

182. Ohkita, T.; Lee, S.-H. Crystallization behavior of poly(butylene succinate)/corn starch biodegradable composite. *Journal of Applied Polymer Science* **2005**, *97*, 1107-1114, doi:10.1002/app.21741.

183. Costa-Pinto, A.R.; Martins, A.M.; Castelhano-Carlos, M.J.; Correlo, V.M.; Sol, P.C.; Longatto-Filho, A.; Battacharya, M.; Reis, R.L.; Neves, N.M. In vitro degradation and in vivo biocompatibility of chitosan–poly(butylene succinate) fiber mesh scaffolds. *Journal of Bioactive and Compatible Polymers* **2014**, *29*, 137-151, doi:10.1177/0883911514521919.

184. Correlo, V.M.; Pinho, E.D.; Pashkuleva, I.; Bhattacharya, M.; Neves, N.M.; Reis, R.L. Water Absorption and Degradation Characteristics of Chitosan-Based Polyesters and Hydroxyapatite Composites. *Macromolecular Bioscience* **2007**, *7*, 354-363, doi: 10.1002/mabi.200600233.

185. Guidotti, G.; Soccio, M.; Posati, T.; Sotgiu, G.; Tiboni, M.; Barbalinardo, M.; Valle, F.; Casettari, L.; Zamboni, R.; Lotti, N., et al. Regenerated wool keratin-polybutylene succinate nanofibrous mats for drug delivery and cells culture. *Polymer Degradation and Stability* **2020**, *179*, 109272, doi:10.1016/j.polymdegradstab.2020.109272.

186. Kimura, T.; Aoki, S. Application of silk composite to decorative laminate. *Advanced Composite Materials* **2007**, *16*, 349-360, doi:10.1163/156855107782325212.

187. Weijun, Y.; Elena, F.; Francesca, L.; Jose, M.K.; Luigi, T.; Debora, P. Lignocellulosic Based Bionanocomposites for Different Industrial Applications. *Current Organic Chemistry* **2018**, *22*, 1205-1221, doi:10.2174/1385272822666180515120948.

188. Ferreira, F.V.; Pinheiro, I.F.; Gouveia, R.F.; Thim, G.P.; Lona, L.M.F. Functionalized cellulose nanocrystals as reinforcement in biodegradable polymer nanocomposites. *Polymer Composites* **2018**, *39*, E9-E29, doi:10.1002/pc.24583.

189. Mariano, M.; El Kissi, N.; Dufresne, A. Cellulose nanomaterials: size and surface influence on the thermal and rheological behavior. *Polímeros* **2018**, *28*, 93-102, doi:10.1590/0104-1428.2413.

190. Pinheiro, I.F.; Ferreira, F.V.; Souza, D.H.S.; Gouveia, R.F.; Lona, L.M.F.; Morales, A.R.; Mei, L.H.I. Mechanical, rheological and degradation properties of PBAT nanocomposites reinforced by functionalized cellulose nanocrystals. *European Polymer Journal* **2017**, *97*, 356-365, doi:10.1016/j.eurpolymj.2017.10.026.

191. Chatterjee, S.; Nafezarefi, F.; Tai, N.H.; Schlagenhauf, L.; Nüesch, F.A.; Chu, B.T.T. Size and synergy effects of nanofiller hybrids including graphene nanoplatelets and carbon nanotubes in mechanical properties of epoxy composites. *Carbon* **2012**, *50*, 5380-5386, doi:10.1016/j.carbon.2012.07.021.

192. Santos, F.A.d.; Iulianelli, G.C.V.; Tavares, M.I.B. The Use of Cellulose Nanofillers in Obtaining Polymer Nanocomposites: Properties, Processing, and Applications. *Materials Sciences and Applications* **2016**, *07*, 257-294, doi:10.4236/msa.2016.75026.

193. Yu, H.-Y.; Qin, Z.-Y.; Liu, L.; Yang, X.-G.; Zhou, Y.; Yao, J.-M. Comparison of the reinforcing effects for cellulose nanocrystals obtained by sulfuric and hydrochloric acid hydrolysis on the mechanical and thermal properties of bacterial polyester. *Composites Science and Technology* **2013**, *87*, 22-28, doi:10.1016/j.compscitech.2013.07.024.

194. Xu, J.; Manepalli, P.H.; Zhu, L.; Narayan-Sarathy, S.; Alavi, S. Morphological, barrier and mechanical properties of films from poly (butylene succinate) reinforced with nanocrystalline cellulose and chitin whiskers using melt extrusion. *Journal of Polymer Research* **2019**, *26*, doi:10.1007/s10965-019-1783-8.

195. Huang, A.; Peng, X.; Geng, L.; Zhang, L.; Huang, K.; Chen, B.; Gu, Z.; Kuang, T. Electrospun poly (butylene succinate)/cellulose nanocrystals bio-nanocomposite scaffolds for tissue engineering: Preparation, characterization and in vitro evaluation. *Polymer Testing* **2018**, *71*, 101-109, doi:10.1016/j.polymertesting.2018.08.027.

196. Kim, T.; Jeon, H.; Jegal, J.; Kim, J.H.; Yang, H.; Park, J.; Oh, D.X.; Hwang, S.Y. Trans crystallization behavior and strong reinforcement effect of cellulose nanocrystals on

reinforced poly(butylene succinate) nanocomposites. *RSC Advances* **2018**, *8*, 15389-15398, doi:10.1039/c8ra01868e.

197. Wu, C.; Zhang, X.; Wang, X.; Gao, Q.; Li, X. Surface modification of cellulose nanocrystal using succinic anhydride and its effects on poly(butylene succinate) based composites. *Cellulose* **2019**, *26*, 3167-3181, doi:10.1007/s10570-019-02292-5.

198. Saeng-on, J.; Aht-Ong, D. Compatibility of banana starch nanocrystals/poly(butylene succinate) bio-nanocomposite packaging films. *Journal of Applied Polymer Science* **2018**, *135*, doi:10.1002/app.46836.

199. He, Y.; Zhu, J.; Wang, W.; Ni, H. Surface modification of cellulose nanocrystals with different acid anhydrides for improved dispersion in poly(butylene succinate). *RSC Advances* **2018**, *8*, 38305-38314, doi:10.1039/c8ra07597b.

200. Hong, G.; Cheng, H.; Zhang, S.; Rojas, O.J. Mussel-inspired reinforcement of a biodegradable aliphatic polyester with bamboo fibers. *Journal of Cleaner Production* **2021**, *296*, doi:10.1016/j.jclepro.2021.126587.

201. Ayu, R.S.; Khalina, A.; Harmaen, A.S.; Zaman, K.; Mohd Nurrazi, N.; Isma, T.; Lee, C.H. Effect of Empty Fruit Brunch reinforcement in PolyButylene-Succinate/Modified Tapioca Starch blend for Agricultural Mulch Films. *Scientific Reports* **2020**, *10*, 1166, doi:10.1038/s41598-020-58278-y.

202. Hokkanen, S.; Bhatnagar, A.; Sillanpää, M. A review on modification methods to cellulose-based adsorbents to improve adsorption capacity. *Water Research* **2016**, *91*, 156-173, doi:10.1016/j.watres.2016.01.008.

203. Qasim, U.; Osman, A.I.; Al-Muhtaseb, A.a.H.; Farrell, C.; Al-Abri, M.; Ali, M.; Vo, D.-V.N.; Jamil, F.; Rooney, D.W. Renewable cellulosic nanocomposites for food packaging to avoid fossil fuel plastic pollution: a review. *Environmental Chemistry Letters* **2021**, *19*, 613-641, doi:10.1007/s10311-020-01090-x.

204. He, D.; Luo, Y.; Lu, S.; Liu, M.; Song, Y.; Lei, L. Microplastics in soils: Analytical methods, pollution characteristics and ecological risks. *TrAC Trends in Analytical Chemistry* **2018**, *109*, 163-172, doi:10.1016/j.trac.2018.10.006.

205. Karlsson, T.M.; Vethaak, A.D.; Almroth, B.C.; Ariese, F.; van Velzen, M.; Hassellöv, M.; Leslie, H.A. Screening for microplastics in sediment, water, marine invertebrates and fish: Method development and microplastic accumulation. *Marine Pollution Bulletin* **2017**, *122*, 403-408, doi:10.1016/j.marpolbul.2017.06.081.

206. BioPBS™. Availabe online: https://www.mcpp-global.com/en/asia/products/brand/biopbstm/ (accessed on 05.05.2021.).

207. Brunner, C.T.; Baran, E.T.; Pinho, E.D.; Reis, R.L.; Neves, N.M. Performance of biodegradable microcapsules of poly(butylene succinate), poly(butylene succinate-co-adipate) and poly(butylene terephthalate-co-adipate) as drug encapsulation systems. *Colloids and Surfaces B: Biointerfaces* **2011**, *84*, 498-507, doi:10.1016/j.colsurfb.2011.02.005.

208. Sonseca, A.; Sahay, R.; Stepien, K.; Bukala, J.; Wcislek, A.; McClain, A.; Sobolewski, P.; Sui, X.; Puskas, J.E.; Kohn, J., et al. Architectured helically coiled scaffolds from elastomeric poly(butylene succinate) (PBS) copolyester via wet electrospinning. *Materials Science and Engineering: C* **2020**, *108*, 110505, doi:10.1016/j.msec.2019.110505.

209. Car interiors go green. Availabe online: https://www.plastics.gl/automotive/car-interiors-go-green/ (accessed on 05.05.2021.).

210. Supporting the Circular Economy with Compostable Packaging Solutions. Availabe online: https://packagingeurope.com/compostable-bioplastic-packaging-pbs/ (accessed on 05.05.2021.).

211. Polybutylene succinate. Availabe online: https://alchetron.com/Polybutylene-succinate (accessed on 05.05.2021.).

212. Xu, J.; Guo, B.-H. Microbial Succinic Acid, Its Polymer Poly(butylene succinate), and Applications. In *Plastics from Bacteria: Natural Functions and Applications*, Chen, G.G.-Q., Ed. Springer Berlin Heidelberg: Berlin, Heidelberg, 2010, 347-388, doi:10.1007/978-3-642-03287-5_14pp.

213. Thurber, H.; Curtzwiler, G.W. Suitability of poly(butylene succinate) as a coating for paperboard convenience food packaging. *International Journal of Biobased Plastics* **2020**, *2*, 1-12, doi:10.1080/24759651.2020.1785094.

214. Rhim, J.-W.; Park, H.-M.; Ha, C.-S. Bio-nanocomposites for food packaging applications. *Progress in Polymer Science* **2013**, *38*, 1629-1652, doi:10.1016/j.progpolymsci.2013.05.008.

215. Qu, D.; Sun, S.; Gao, H.; Bai, Y.; Tang, Y. Biodegradable copolyester poly(butylene-co-isosorbide succinate) as hot-melt adhesives. *RSC Advances* **2019**, *9*, 11476-11483, doi:10.1039/c9ra01780a.

216. Barrett, A. History of Bioplastics in the Automotive Industry. Availabe online: https://bioplasticsnews.com/2019/11/26/history-bioplastics-automotive-car-industry/ (accessed on 05.05.2021.).

217. Aaliya, B.; Sunooj, K.V.; Lackner, M. Biopolymer composites: a review. *International Journal of Biobased Plastics* **2021**, *3*, 40-84, doi:10.1080/24759651.2021.1881214.

218. Ghaffarian, V.; Mousavi, S.M.; Bahreini, M.; Afifi, M. Preparation and Characterization of Biodegradable Blend Membranes of PBS/CA. *Journal of Polymers and the Environment* **2013**, *21*, 1150-1157, doi:10.1007/s10924-012-0551-1.

219. Sadeghi, A.; Mousavi, S.M.; Saljoughi, E.; Kiani, S. Biodegradable membrane based on polycaprolactone/polybutylene succinate: Characterization and performance evaluation in wastewater treatment. *Journal of Applied Polymer Science* **2021**, *138*, 50332, doi:10.1002/app.50332.

220. Price of polypropylene worldwide from 2017 to 2022. https://www.statista.com/statistics/1171084/price-polypropylene-forecast-globally/ (accessed on 23.04.2022.).

221. HDPE prices. Historical & forecast data worldwide https://www.intratec.us/chemical-markets/hdpe-price (accessed on 23.04.2022.).

222. Bio-based and biodegradable plastics - facts and figures. Focus on food packaging in the Netherlands. https://www.wur.nl/upload_mm/1/e/7/01452551-06c5-4dc3-b278-173da53356bb_170421%20Report%20Bio-based%20Plastic%20Facts.pdf (accessed on 23.04.2022.).

223. França, D.C.; Almeida, T.G.; Abels, G.; Canedo, E.L.; Carvalho, L.H.; Wellen, R.M.R.; Haag, K.; Koschek, K. Tailoring PBAT/PLA/Babassu films for suitability of agriculture mulch application. Journal of Natural Fibers 2018, 16, 933-943, doi:10.1080/15440478.2018.1441092.

224. From the Sugar Platform to biofuels and biochemicals Final report for the European Commission Directorate-General Energy. April 2015. https://ec.europa.eu/energy/sites/ener/files/documents/EC%20Sugar%20Platform%20final%20report.pdf (accessed on 23.04.2022.).

225. Ioannidou, S.M.; Ladakis, D.; Moutousidi, E.; Dheskali, E.; Kookos, I.K.; Câmara-Salim, I.; Moreira, M.T.; Koutinas, A. Techno-economic risk assessment, life cycle analysis and life cycle costing for poly(butylene succinate) and poly(lactic acid) production using renewable resources. Sci. Total Environ. 2022, 806, 150594, doi: 10.1016/j.scitotenv.2021.150594.

226. Zhao, X.; Cornish, K.; Vodovotz, Y. Narrowing the Gap for Bioplastic Use in Food Packaging: An Update. *Environ. Sci. Technol.* **2020**, *54*, 4712-4732, doi:10.1021/acs.est.9b03755.

227. Nikolic, M.S.; Djonlagic, J. Synthesis and characterization of biodegradablepoly(butylene succinate-co-butylene adipate)s. *Polymer Degradation and Stability* **2001**, *74*, 263-270, doi:10.1016/S0141-3910(01)00156-2.

228. Eichhorn, S.J.; Baillie, C.A.; Zafeiropoulos, N.; Mwaikambo, L.Y.; Ansell, M.P.; Dufresne, A.; Entwistle, K.M.; Herrera-Framco, P.J.; Escamilla, G.C.; Groom, L., et al. Review: current international research into cellulosic fibres and composites. *Journal of materials science* **2001**, *36*, 2107-2131, doi:10.1023/A:1017512029696.

229. Maksimov, R.D.; Gaidukovs, S.; Zicans, J.; Kalnins, M.; Plume, E.; Spacek, V.; Sviglerova, P. Nanocomposites based on a styrene-acrylate copolymer and organically modified montmorillonite 1. Mechanical properties. *Mechanics of Composite Materials* **2006**, *42*, 263-272, doi:10.1007/s11029-006-0036-1.

230. Gaidukov, S.; Danilenko, I.; Gaidukova, G. Characterization of strong and crystalline polyvinyl alcohol/montmorillonite films prepared by layer-by-layer deposition method. *International Journal of Polymer Science* **2015**, *2015*, doi:10.1155/2015/123469.

231. Gaidukovs, S.; Zukulis, E.; Bochkov, I.; Vaivodiss, R.; Gaidukova, G. Enhanced mechanical, conductivity, and dielectric characteristics of ethylene vinyl acetate copolymer composite filled with carbon nanotubes. *Journal of Thermoplastic Composite Materials* **2018**, *31*, 1161-1180, doi:10.1177/0892705717734603.

232. Graupner, N.; Ziegmann, G.; Wilde, F.; Beckmann, F.; Müssig, J. Procedural influences on compression and injection moulded cellulose fibre-reinforced polylactide (PLA) composites: Influence of fibre loading, fibre length, fibre orientation and voids. *Composites Part A: Applied Science and Manufacturing* **2016**, *81*, 158-171, doi:10.1016/j.compositesa.2015.10.040.

233. Fan, M.; Dai, D.; Huang, B. 3 Fourier Transform Infrared Spectroscopy for Natural Fibres. *Fourier Transform-Materials Analysis* **2012**, 10.5772/35482, doi:10.5772/35482.

234. Ciolacu, D.; Ciolacu, F.; Popa, V.I. Amorphous cellulose – structure and characterization. *Cellulose Chemistry and Technology* **2011**, *45*, 13-21.

235. Kim, H.-S.; Kim, H.-J.; Lee, J.-W.; Choi, I.-G. Biodegradability of bio-flour filled biodegradable poly(butylene succinate) bio-composites in natural and compost soil. *Polymer Degradation and Stability* **2006**, *91*, 1117-1127, doi:10.1016/j.polymdegradstab.2005.07.002.

236. Kruer-Zerhusen, N.; Cantero-Tubilla, B.; Wilson, D.B. Characterization of cellulose crystallinity after enzymatic treatment using Fourier transform infrared spectroscopy (FTIR). *Cellulose* **2017**, *25*, 37-48, doi:10.1007/s10570-017-1542-0.

237. Dong, C.; Takagi, H. Flexural properties of cellulose nanofibre reinforced green composites. *Composites Part B: Engineering* **2014**, *58*, 418-421, doi:10.1016/j.compositesb.2013.10.032.

238. Frollini, E.; Bartolucci, N.; Sisti, L.; Celli, A. Poly(butylene succinate) reinforced with different lignocellulosic fibers. *Industrial Crops and Products* **2013**, *45*, 160-169, doi:10.1016/j.indcrop.2012.12.013.

239. Kuan, C.F.; Ma, C.C.M.; Kuan, H.C.; Wu, H.L.; Liao, Y.M. Preparation and characterization of the novel water-crosslinked cellulose reinforced poly(butylene succinate) composites. *Composites Science and Technology* **2006**, *66*, 2231-2241, doi:10.1016/j.compscitech.2005.12.011.

240. Kowalczyk, M.; Piorkowska, E.; Kulpinski, P.; Pracella, M. Mechanical and thermal properties of PLA composites with cellulose nanofibers and standard size fibers.

Composites Part A: Applied Science and Manufacturing **2011**, *42*, 1509-1514, doi:10.1016/j.compositesa.2011.07.003.

241. Crean, A. Evaluation of Various Brands of Moisture Meters in Gypsum and Wood Substrates at a Range of Moisture Contents. *Civil Engineering Journal* **2017**, *3*, 640-649, doi:10.21859/cej-03091.

242. Kuka, E.; Cirule, D.; Kajaks, J.; Andersone, I.; Andersons, B. Wood particle size influence on water resistance and mechanical properties of thermally modified wood-polypropylene composites. *International Wood Products Journal* **2018**, *9*, 90-95, doi:10.1080/20426445.2018.1493069.

243. Lee, J.M.; Mohd Ishak, Z.A.; Mat Taib, R.; Law, T.T.; Ahmad Thirmizir, M.Z. Mechanical, Thermal and Water Absorption Properties of Kenaf-Fiber-Based Polypropylene and Poly(Butylene Succinate) Composites. *Journal of Polymers and the Environment* **2013**, *21*, 293-302, doi:10.1007/s10924-012-0516-4.

244. Luzi, F.; Fortunati, E.; Jiménez, A.; Puglia, D.; Pezzolla, D.; Gigliotti, G.; Kenny, J.M.; Chiralt, A.; Torre, L. Production and characterization of PLA_PBS biodegradable blends reinforced with cellulose nanocrystals extracted from hemp fibres. *Industrial Crops and Products* **2016**, *93*, 276-289, doi:10.1016/j.indcrop.2016.01.045.

245. Kasuya, K.I.; Takagi, K.I.; Ishiwatari, S.I.; Yoshida, Y.; Doi, Y. Biodegradabilities of various aliphatic polyesters in natural waters. *Polymer Degradation and Stability* **1998**, *59*, 327-332, doi:/10.1016/S0141-3910(97)00155-9.

246. Platnieks, O.; Gaidukovs, S.; Barkane, A.; Gaidukova, G.; Grase, L.; Thakur, V.K.; Filipova, I.; Fridrihsone, V.; Skute, M.; Laka, M. Highly loaded cellulose/poly (butylene succinate) sustainable composites for woody-like advanced materials application. *Molecules* **2020**, *25*, doi:10.3390/molecules25010121.

247. Kajaks, J.A.; Bakradze, G.G.; Viksne, A.V.; Reihmane, S.A.; Kalnins, M.M.; Krutohvostov, R. The use of polyolefins-based hot melts for wood bonding. *Mechanics of Composite Materials* **2009**, *45*, 643-650, doi:10.1007/s11029-010-9120-7.

248. Bhasney, S.M.; Bhagabati, P.; Kumar, A.; Katiyar, V. Morphology and crystalline characteristics of polylactic acid [PLA]/linear low density polyethylene [LLDPE]/microcrystalline cellulose [MCC] fiber composite. *Composites Science and Technology* **2019**, *171*, 54-61, doi:10.1016/j.compscitech.2018.11.028.

249. Shi, K.; Liu, Y.; Hu, X.; Su, T.; Li, P.; Wang, Z. Preparation, characterization, and biodegradation of poly(butylene succinate)/cellulose triacetate blends. *International Journal of Biological Macromolecules* **2018**, *114*, 373-380, doi:10.1016/j.ijbiomac.2018.03.151.

250. Lizundia, E.; Vilas, J.L.; León, L.M. Crystallization, structural relaxation and thermal degradation in Poly(l-lactide)/cellulose nanocrystal renewable nanocomposites. *Carbohydrate Polymers* **2015**, *123*, 256-265, doi:10.1016/j.carbpol.2015.01.054.

251. Shen, D.K.; Gu, S. The mechanism for thermal decomposition of cellulose and its main products. *Bioresource Technology* **2009**, *100*, 6496-6504, doi:10.1016/j.biortech.2009.06.095.

252. Chrissafis, K.; Paraskevopoulos, K.M.; Bikiaris, D.N. Thermal degradation mechanism of poly(ethylene succinate) and poly(butylene succinate): Comparative study. *Thermochimica Acta* **2005**, *435*, 142-150, doi:10.1016/j.tca.2005.05.011.

253. *Green biorenewable biocomposites from knowledge to industrial applications*. 1st Edition ed.; Thakur, V.K.; Kessler, M.R., Eds.; Apple Academic Press New York, 2015, doi:10.1201/b18092p 568.

254. Schlosser, E.; Schönhals, A. Recent development in dielectric relaxation spectroscopy of polymers. *Colloid & Polymer Science* **1989**, *267*, 963-969, doi:10.1007/BF01410156.

255. Roland, C.M. Electrical and dielectric properties of rubber. *Rubber Chemistry and Technology* **2016**, *89*, 32-53, doi:10.5254/rct.15.84827.

256. Das, S. Mechanical and water swelling properties of waste paper reinforced unsaturated polyester composites. *Construction and Building Materials* **2017**, *138*, 469-478, doi:10.1016/j.conbuildmat.2017.02.041.

257. Fortunati, E.; Rinaldi, S.; Peltzer, M.; Bloise, N.; Visai, L.; Armentano, I.; Jiménez, A.; Latterini, L.; Kenny, J.M. Nano-biocomposite films with modified cellulose nanocrystals and synthesized silver nanoparticles. *Carbohydrate Polymers* **2014**, *101*, 1122-1133, doi:10.1016/j.carbpol.2013.10.055.

258. Kim, H.S.; Kim, H.J.; Lee, J.W.; Choi, I.G. Biodegradability of bio-flour filled biodegradable poly(butylene succinate) bio-composites in natural and compost soil. *Polymer Degradation and Stability* **2006**, *91*, 1117-1127, doi:10.1016/j.polymdegradstab.2005.07.002.

259. Sharma, A.; Thakur, M.; Bhattacharya, M.; Mandal, T.; Goswami, S. Commercial application of cellulose nano-composites - A review. *Biotechnology Reports* **2019**, *21*, e00316, doi:10.1016/j.btre.2019.e00316.

260. Rallini, M.; Kenny, J.M. Nanofillers in Polymers. In *Modification of Polymer Properties*, 2017, 47-86, 10.1016/b978-0-323-44353-1.00003-8pp.

261. Huang, F.-Y. Thermal Properties and Thermal Degradation of Cellulose Tri-Stearate (CTs). *Polymers* **2012**, *4*, 1012-1024, doi:10.3390/polym4021012.

262. Yuwawech, K.; Wootthikanokkhan, J.; Tanpichai, S. Effects of Two Different Cellulose Nanofiber Types on Properties of Poly(vinyl alcohol) Composite Films. *Journal of Nanomaterials* **2015**, *2015*, 1-10, doi:10.1155/2015/908689.

263. Tan, V.; Abdallah, W.; Kamal, M.R. The Effect of Cellulose Nanocrystals (CNC) on Isothermal Crystallization Kinetics of LLDPE and HDPE. *International Polymer Processing* **2018**, *33*, 371-380, doi:10.3139/217.3559.

264. Dufresne, A.; Kellerhals, M.B.; Witholt, B. Transcrystallization in Mcl-PHAs/cellulose whiskers composites. *Macromolecules* **1999**, *32*, 7396–7401, doi:10.1021/ma990564r.

265. Hristov, V.; Vasileva, S. Dynamic Mechanical and Thermal Properties of Modified Poly(propylene) Wood Fiber Composites. *Macromolecular Materials and Engineering* **2003**, *288*, 798-806, doi:10.1002/mame.200300110.

266. Qi, X.; Yang, G.; Jing, M.; Fu, Q.; Chiu, F.-C. Microfibrillated cellulose-reinforced bio-based poly(propylene carbonate) with dual shape memory and self-healing properties. *Journal of Materials Chemistry A* **2014**, *2*, 20393-20401, doi:10.1039/c4ta04954c.

267. Boparai, K.S.; Singh, R. Thermoplastic Composites for Fused Deposition Modeling Filament: Challenges and Applications. In *Reference Module in Materials Science and Materials Engineering*, Elsevier: 2018, doi:10.1016/B978-0-12-803581-8.11409-2.

268. Mathew, A.P.; Oksman, K.; Sain, M. Mechanical properties of biodegradable composites from poly lactic acid (PLA) and microcrystalline cellulose (MCC). *Journal of Applied Polymer Science* **2005**, *97*, 2014-2025, doi:10.1002/app.21779.

269. Ferreira, F.V.; Pinheiro, I.F.; Mariano, M.; Cividanes, L.S.; Costa, J.C.M.; Nascimento, N.R.; Kimura, S.P.R.; Neto, J.C.M.; Lona, L.M.F. Environmentally friendly polymer composites based on PBAT reinforced with natural fibers from the amazon forest. *Polymer Composites* **2019**, *40*, 3351-3360, doi:10.1002/pc.25196.

270. Ferreira, F.; Pinheiro, I.; de Souza, S.; Mei, L.; Lona, L. Polymer Composites Reinforced with Natural Fibers and Nanocellulose in the Automotive Industry: A Short Review. *Journal of Composites Science* **2019**, *3*, doi:10.3390/jcs3020051.

271. Siqueira, G.; Bras, J.; Follain, N.; Belbekhouche, S.; Marais, S.; Dufresne, A. Thermal and mechanical properties of bio-nanocomposites reinforced by Luffa cylindrica

cellulose nanocrystals. *Carbohydrate Polymers* **2013**, *91*, 711-717, doi:10.1016/j.carbpol.2012.08.057.

272. Tanpichai, S.; Quero, F.; Nogi, M.; Yano, H.; Young, R.J.; Lindstrom, T.; Sampson, W.W.; Eichhorn, S.J. Effective Young's modulus of bacterial and microfibrillated cellulose fibrils in fibrous networks. *Biomacromolecules* **2012**, *13*, 1340-1349, doi:10.1021/bm300042t.

273. Ichazo, M.N.; Albano, C.; Gonzalez, J.; Perera, R.; Candal, M.V. Polypropylene/wood flour composites: treatments and properties. *Composite Structures* **2001**, *54*, 207-214, doi:10.1016/S0263-8223(01)00089-7.

274. Liang, Z.; Pan, P.; Zhu, B.; Dong, T.; Inoue, Y. Mechanical and thermal properties of poly(butylene succinate)/plant fiber biodegradable composite. *Journal of Applied Polymer Science* **2010**, *115*, 3559-3567, doi:10.1002/app.29848.

275. Hee-Soo, K.; Han-Seung, Y.; Hyun-Joong, K. Biodegradability and mechanical properties of agro-flour-filled polybutylene succinate biocomposites. *Journal of Applied Polymer Science* **2005**, *97*, 1513-1521, doi:10.1002/app.21905.

276. Kajaks, J.; Kalnins, K.; Naburgs, R. Wood plastic composites (WPC) based on high-density polyethylene and birch wood plywood production residues. *International Wood Products Journal* **2017**, *9*, 15-21, doi:10.1080/20426445.2017.1410997.

277. Sakai, Y.; Isokawa, M.; Masuda, T.; Yoshioka, H.; Hayastsu, M.; Hayono, K. Usefulness of Soil p-Nitrophenyl Acetate Esterase Activity as a Tool to Monitor Biodegradation of Polybutylene Succinate (PBS) in Cultivated Soil. *Polymer Journal* **2002**, *34*, 767-774, doi:10.1295/polymj.34.767.

278. Hee-Soo, K.; Hyun-Joong, K.; Jae-Won, L.; In-Gyu, C. Biodegradability of bio-flour filled biodegradable poly(butylene succinate) bio-composites in natural and compost soil. *Polymer Degradation and Stability* **2006**, *91*, 1117-1127, doi:10.1016/j.polymdegradstab.2005.07.002.

279. Nakagaito, A.N.; Yano, H. The effect of fiber content on the mechanical and thermal expansion properties of biocomposites based on microfibrillated cellulose. *Cellulose* **2008**, *15*, 555–559, doi:10.1007/s10570-008-9212-x.

280. Josefsson, G.; Berthold, F.; Gamstedt, E.K. Stiffness contribution of cellulose nanofibrils to composite materials. *International Journal of Solids and Structures* **2014**, *51*, 945-953, doi:10.1016/j.ijsolstr.2013.11.018.

281. Rastogi, V.K.; Samyn, P. Novel processing of polyhydroxybutyrate with micro- to nanofibrillated cellulose and effect of fiber morphology on crystallization behaviour of composites. *Express Polymer Letters* **2020**, *14*, 115-133, doi:10.3144/expresspolymlett.2020.11.

282. Lv, Z.-y.; Zhang, M.C.; Zhang, Y.; Guo, B.-h.; Xu, J. Study on melting and recrystallization of poly(butylene succinate) lamellar crystals via step heating differential scanning calorimetry. *Chinese Journal of Polymer Science* **2017**, *35*, 1552-1560, doi:10.1007/s10118-017-1986-6.

283. Zaaba, N.F.; Jaafar, M.; Ismail, H. Tensile and morphological properties of nanocrystalline cellulose and nanofibrillated cellulose reinforced PLA bionanocomposites: A review. *Polymer Engineering & Science* **2020**, 10.1002/pen.25560, doi:10.1002/pen.25560.

284. Gan, P.G.; Sam, S.T.; Abdullah, M.F.b.; Omar, M.F. Thermal properties of nanocellulose-reinforced composites: A review. *Journal of Applied Polymer Science* **2019**, *137*, doi:10.1002/app.48544.

285. Ludueña, L.N.; Fortunati, E.; Morán, J.I.; Alvarez, V.A.; Cyras, V.P.; Puglia, D.; Manfredi, L.B.; Pracella, M. Preparation and characterization of polybutylene-

succinate/poly(ethylene-glycol)/cellulose nanocrystals ternary composites. *Journal of Applied Polymer Science* **2016**, *133*, 43302, doi:10.1002/app.43302.

286. Luo, Y.; Lin, Z.; Guo, G. Biodegradation Assessment of Poly (Lactic Acid) Filled with Functionalized Titania Nanoparticles (PLA/TiO2) under Compost Conditions. *Nanoscale Research Letters* **2019**, *14*, 56, doi:10.1186/s11671-019-2891-4.

287. Cai, Y.; Lv, J.; Feng, J. Spectral Characterization of Four Kinds of Biodegradable Plastics: Poly (Lactic Acid), Poly (Butylenes Adipate-Co-Terephthalate), Poly (Hydroxybutyrate-Co-Hydroxyvalerate) and Poly (Butylenes Succinate) with FTIR and Raman Spectroscopy. *Journal of Polymers and the Environment* **2012**, *21*, 108-114, doi:10.1007/s10924-012-0534-2.

288. Ostrowska, J.; Sadurski, W.; Paluch, M.; Tyński, P.; Bogusz, J. The effect of poly(butylene succinate) content on the structure and thermal and mechanical properties of its blends with polylactide. *Polymer International* **2019**, *68*, 1271-1279, doi:10.1002/pi.5814.

289. Muthuraj, R.; Misra, M.; Mohanty, A.K. Injection Molded Sustainable Biocomposites From Poly(butylene succinate) Bioplastic and Perennial Grass. *ACS Sustainable Chemistry & Engineering* **2015**, *3*, 2767-2776, doi:10.1021/acssuschemeng.5b00646.

290. Muthuraj, R.; Misra, M.; Mohanty, A.K. Hydrolytic degradation of biodegradable polyesters under simulated environmental conditions. *Journal of Applied Polymer Science* **2015**, *132*, 42189, doi:10.1002/app.42189.

291. Li, Y.D.; Fu, Q.Q.; Wang, M.; Zeng, J.B. Morphology, crystallization and rheological behavior in poly(butylene succinate)/cellulose nanocrystal nanocomposites fabricated by solution coagulation. *Carbohydrate Polymers* **2017**, *164*, 75-82, doi:10.1016/j.carbpol.2017.01.089.

292. Wang, T.; Drzal, L.T. Cellulose-nanofiber-reinforced poly(lactic acid) composites prepared by a water-based approach. *ACS Applied Materials & Interfaces* **2012**, *4*, 5079-5085, doi:10.1021/am301438g.

293. Ismaila, H.; Edyhama, M.R.; Wirjosentono, B. Bamboo fibre filled natural rubber composites: the effects of filler loading and bonding agent. *Polymer Testing* **2002**, *21*, 139-144, doi:10.1016/S0142-9418(01)00060-5.

294. Wang, X.; Tang, Y.; Zhu, X.; Zhou, Y.; Hong, X. Preparation and characterization of polylactic acid/polyaniline/nanocrystalline cellulose nanocomposite films. *International Journal of Biological Macromolecules* **2020**, *146*, 1069-1075, doi:10.1016/j.ijbiomac.2019.09.233.

295. Peng, Y.; Gallegos, S.A.; Gardner, D.J.; Han, Y.; Cai, Z. Maleic anhydride polypropylene modified cellulose nanofibril polypropylene nanocomposites with enhanced impact strength. *Polymer Composites* **2016**, *37*, 782-793, doi:10.1002/pc.23235.

296. Xu, X.; Liu, F.; Jiang, L.; Zhu, J.Y.; Haagenson, D.; Wiesenborn, D.P. Cellulose nanocrystals vs. cellulose nanofibrils: a comparative study on their microstructures and effects as polymer reinforcing agents. *ACS Applied Materials & Interfaces* **2013**, *5*, 2999-3009, doi:10.1021/am302624t.

297. Cailloux, J.; Raquez, J.M.; Lo Re, G.; Santana, O.; Bonnaud, L.; Dubois, P.; Maspoch, M.L. Melt-processing of cellulose nanofibril/polylactide bionanocomposites via a sustainable polyethylene glycol-based carrier system. *Carbohydrate Polymers* **2019**, *224*, 115188, doi:10.1016/j.carbpol.2019.115188.

298. Chen, R.-y.; Zou, W.; Zhang, H.-c.; Zhang, G.-z.; Yang, Z.-t.; Jin, G.; Qu, J.-p. Thermal behavior, dynamic mechanical properties and rheological properties of poly(butylene succinate) composites filled with nanometer calcium carbonate. *Polymer Testing* **2015**, *42*, 160-167, doi:10.1016/j.polymertesting.2015.01.015.

299.   Jyoti, J.; Singh, B.P.; Arya, A.K.; Dhakate, S.R. Dynamic mechanical properties of multiwall carbon nanotube reinforced ABS composites and their correlation with entanglement density, adhesion, reinforcement and C factor. *RSC Advances* **2016**, *6*, 3997-4006, doi:10.1039/c5ra25561a.

300.   Jyoti, J.; Babal, A.S.; Sharma, S.; Dhakate, S.R.; Singh, B.P. Significant improvement in static and dynamic mechanical properties of graphene oxide–carbon nanotube acrylonitrile butadiene styrene hybrid composites. *Journal of Materials Science* **2017**, *53*, 2520-2536, doi:10.1007/s10853-017-1592-6.

301.   Panwar, V.; Pal, K. Dynamic Mechanical Analysis of Clay–Polymer Nanocomposites. In *Clay-Polymer Nanocomposites*, 2017, 413-441, doi:10.1016/b978-0-323-46153-5.00012-4pp.

302.   Laly A. Pothan, Z.O., Sabu Thomas. Dynamic mechanical analysis of banana fiber reinforced polyester composites. *Composite science and technology* **2003**, *63*, 11.

303.   Shah, A.A.; Kato, S.; Shintani, N.; Kamini, N.R.; Nakajima-Kambe, T. Microbial degradation of aliphatic and aliphatic-aromatic co-polyesters. *Applied Microbiology and Biotechnology* **2014**, *98*, 3437-3447, doi:10.1007/s00253-014-5558-1.

304.   Eubeler, J.P.; Bernhard, M.; Knepper, T.P. Environmental biodegradation of synthetic polymers II. Biodegradation of different polymer groups. *TrAC - Trends in Analytical Chemistry* **2010**, *29*, 84-100, doi:10.1016/j.trac.2009.09.005.

305.   Platnieks, O.; Gaidukovs, S.; Barkane, A.; Gaidukova, G.; Grase, L.; Thakur, V.K.; Filipova, I.; Fridrihsone, V.; Skute, M.; Laka, M. Highly Loaded Cellulose/Poly (butylene succinate) Sustainable Composites for Woody-Like Advanced Materials Application. *Molecules* **2019**, *25*, doi:10.3390/molecules25010121.

306.   Platnieks, O.; Barkane, A.; Ijudina, N.; Gaidukova, G.; Thakur, V.K.; Gaidukovs, S. Sustainable tetra pak recycled cellulose / Poly(Butylene succinate) based woody-like composites for a circular economy. *Journal of Cleaner Production* **2020**, *270*, 122321, doi:10.1016/j.jclepro.2020.122321.

307.   Kim, H.S.; Kim, H.J. Enhanced hydrolysis resistance of biodegradable polymers and bio-composites. *Polymer Degradation and Stability* **2008**, *93*, 1544-1553, doi:10.1016/j.polymdegradstab.2008.05.004.

308.   Platnieks, O.; Gaidukovs, S.; Barkane, A.; Sereda, A.; Gaidukova, G.; Grase, L.; Thakur, V.K.; Filipova, I.; Fridrihsone, V.; Skute, M., et al. Bio-Based Poly(butylene succinate)/Microcrystalline Cellulose/Nanofibrillated Cellulose-Based Sustainable Polymer Composites: Thermo-Mechanical and Biodegradation Studies. *Polymers* **2020**, *12*, doi:10.3390/polym12071472.

Oskars Platnieks received a Master's degree in Materials Science from Riga Technical University (RTU) in 2017. His field of research is bio-based and naturally degradable materials. He has been studying these materials since his master's studies. His Tesis research was carried out at the RTU Institute of Polymer Materials, where he pursues active research. His research goal is to address sustainability issues and adapt them to the requirements of modern polymer and composite materials.